# Behaviour of Headed Stud Connectors in Composite Beams with Very Deep Profiled Sheeting

by

**Ahmed Jawad Albarram**

A thesis submitted in partial fulfillment of the requirements for the degree of Doctor of Philosophy

University of East London

School of Architecture, Computing and Engineering

December 2018

The candidate confirms that the work submitted is his own and that appropriate credit has been given where reference has been made to the work of others

# Abstract

Lack of design rules and no past research on the behaviour of composite beams with steel decks deeper than 80 mm is a major knowledge gap. Thus, this research provides fundamental information on the behaviour of headed stud connectors with narrow and very deep decks. After a series of extensive validation, a vast number of 3-D push-off tests are modelled using ABAQUS/Explicit package. Both secondary and primary composite beam systems are investigated. Critical examination is conducted on the existing design equations to assess their accuracy in predicting the shear stud capacity with the use of narrow and very deep decks.

The numerical analysis regarding the secondary composite beams showed that the shear stud capacity with narrow and very deep decks (i.e. 100 and 146 mm deep) was almost 65% of that obtained from the traditional steel decks (60-80 mm deep). The shear stud capacity was mainly affected by the concrete embedded within ribs. Reinforcing that area by a unique wire-mesh bars layout, which has not been investigated before, led the load bearing capacity to increase by 24%. For the primary composite beams, the numerical analysis indicated that the correlation between very deep decks and traditional ones regarding the shear stud capacity can not be represented through the rib deck geometry as it was believed in the past. A new concept was introduced to more accurately explain that correlation. This was through the effective cross-sectional area of concrete.

The existing design equations, when validated, did not account for narrow and very deep decks. As a result, a big discrepancy up to 50% was noticed between the predicted strengths and FE results in some cases, especially among EC4 and ANSI/AISC provisions. This necessitated to introduce more effective formulae. The developed equations regarding the secondary composite beams covered for the first time a wide range of ribbed geometries including narrow and very deep decks. For the primary composite beams, the correlation between different types of decks was established in the new equations through the effective cross-sectional area of concrete. The reliability of the new equations was proven against many previous experiments. The accuracy in results remained within ±10%. Besides the accuracy, the new equations are easy to use. This will help the designers to directly apply these equations in the practice.

## Acknowledgments

I would like to express my profound appreciation to my supervisors Dr. Jawed Qureshi and Dr. Ali Abbas for their endless support, guidance and continued encouragement throughout the whole period of this research.

Special thanks are dedicated to the University of East London for providing the comfortable environment and the computing facilities to accomplish this research.

I am indebted to the Higher Committee for Education Development in Iraq (HCED) for their financial funding and the opportunity given which allowed me to complete my PhD abroad. Without their constant help, I would not have been able to pursue a PhD in the University of East London.

My sincere gratefulness goes to my PhD colleagues Najat Al-Sheridah, Fatemeh Rostami, Jide Soyemi, Raghu Jadhav-Balaji, Hasanain Al-Naimi and Hashim Taher. I am very lucky to have such outstanding and inspiring friends in my PhD journey. Without them, I might not have come this far.

Finally, my utmost gratitude is reserved for my beloved Father (Dr. Jawad Albarram), Mother (Nida Al-Husseini), Brother (Mohammad) and Sister (Mina) for their infinite love, patience and trust in me. You are behind my all happiness and success in this life. I love you all so much and **No** one deserves my eternal acknowledgments but **You**.

# Contents

# List of Figures

# List of Tables

# Chapter 1 Introduction

# Chapter 1

# Introduction

## 1.1 Preface

Steel-concrete composite beams in multi-story buildings and bridges are widely used in the present-day constructional practice. The concept of the steel-concrete composite construction was first implemented in the early 1920s, mostly in North America and Europe. This method of construction features high strength and durability, ease of assembly and economical solution as compared with the conventional reinforced concrete members. In composite beams, the best performance of both concrete and steel is realised, as the concrete slab is mainly subjected to compression while the steel beam is subjected to tension.

Ideally, composite beams consist of an I-shape steel beam and a cast-in-situ solid concrete slab acting compositely by means of shear connectors (see Figure 1.1). However, since the 1950s, composite beams incorporating ribbed metal decking or profiled steel sheeting have become more popular than composite beams with solid slab, especially in building structures. A steel decking can be oriented perpendicular to the axis of a steel beam in case of secondary beams, or parallel in case of primary beams. A typical composite beam system containing secondary and primary composite beams is presented in Figure 1.2. Steel decking acts as a permeant formwork during concrete casting and resists tensile forces after the concrete hardens. Another benefit is that a steel decking, when used in a cellular configuration, allows the passage of electrical and mechanical services. Moreover, a profiled steel decking can reduce the need for propping. Therefore, it provides an economical solution. The shape of steel decking can be re-entrant or open trapezoidal ribs, though the latter is more common.

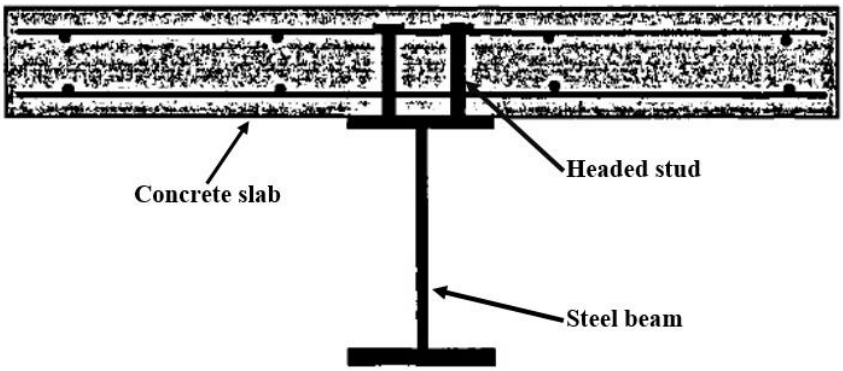


Figure 1.1 Composite beam with solid concrete slab (Wu 1998)

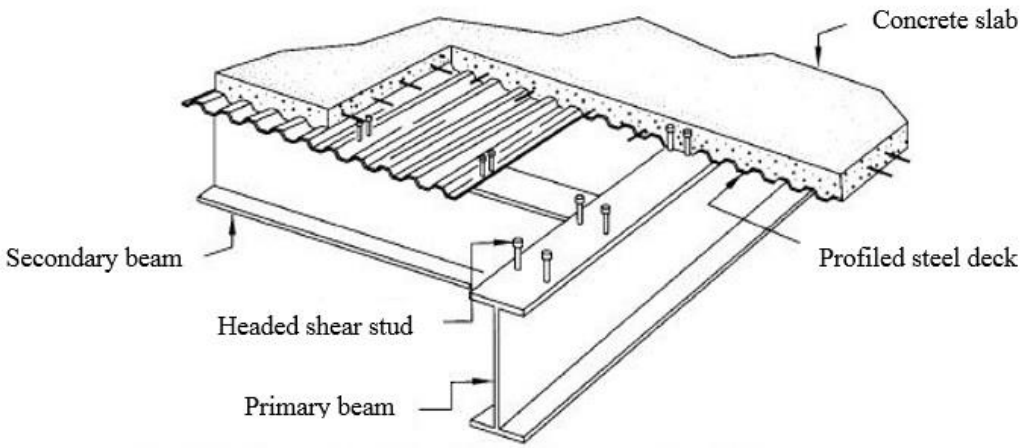


Figure 1.2 Steel-concrete composite beam system in buildings

Past research revealed that the mechanical interlock and interface friction between the concrete slab and profiled sheeting govern the shear bond strength of composite slabs (Cifuentes and Medina 2013). The frequency of embossments on the profiled decking surface, along with the shape and geometry of decking were found to profoundly influence the longitudinal shear forces transmitted through the interface between concrete and steel material. On the other hand, the mechanical composite action between the concrete slab and steel beam is achieved by stud shear connectors. The shear connectors do not only resist shear forces at the steel-concrete interface, but also prevent the tendency of vertical separation between the two materials. Several shapes have been utilised as shear connectors including channels, spirals, tee and zee sections and headed studs. The last form, however, is the most

commonly used nowadays due to their convenience in welding and capability of resisting shear forces in all directions.

In case of composite beams featuring profiled sheeting, headed stud shear connectors are welded on the top of steel beam flange through either sheeting or pre-cut holes in the sheeting. The position where headed studs are welded is likely to be in the centre of troughs. However, the inclusion of stiffeners at the bottom centre of modern troughs has caused headed studs to be placed either in a favourable or an unfavourable position or as known as strong and weak position respectively (Nie et al. 2005). The favourable position is when the concrete volume in front of a headed stud in the direction of the applied load is bigger than the concrete volume behind it. While the unfavourable position is when the concrete volume in front of a headed stud in the direction of the applied load is smaller than the concrete volume behind a headed stud. Figure 1.3 shows the different positions of headed shear studs in ribs of profiled decking.

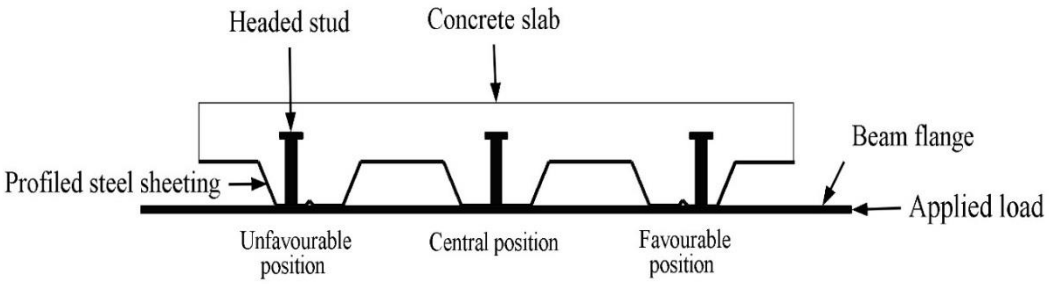


Figure 1.3 Different positions of headed studs in ribs of profiled decking

With the existence of stiffeners at the bottom of central troughs, the effect of headed studs being placed off-centre on the shear connector resistance was broadly addressed in Robinson (1988), Mottram and Johnson (1990) and Easterling et al. (1993). Other parameters studied in the past included the number and layout of headed studs within troughs, the longitudinal and transverse spacing between headed studs, the change in geometries of steel decking, etc. As a result, the existing headed stud shear strength prediction equations in some design codes (e.g. EC4 and ANSI/AISC) received criticism for being limited and not reliable in predicting the shear connector resistance in composite beams with steel decking (Jayas and Hosain 1988, Johnson and Yuan 1998a). Subsequently, many formulae and guidelines have been

recommended by researchers for better predictions such as Lawson (1992), Johnson and Yuan (1998b) and Nellinger et al. (2018).

The desire for longer slab spans has led to the development of profiled steel decking deeper than the traditional 60-80 mm deep decking (see Figure 1.4). Since 2011, Kingspan company has introduced 146 mm deep composite decking in the UK as shown in Figure 1.5. This modern steel decking has a narrow-ribbed deck, resulting in the ratio of average rib width to the rib height ($b_o/h_p$) of 0.67. The American manufacturers are not behind either with ASC Steel Deck now producing 150 mm deep decking. Using a steel decking deeper than 80 mm has some benefits, including 20-30% reduction in concrete volume and increase in the slab's span to as much as 6 m (Kingspan 2011). Research on the behaviour of composite beams with steel decking deeper than 80 mm is barely existent. Therefore, the lack of design guidelines for stud capacity remains the single most challenge in the design of the composite beams with decks deeper than 80 mm.

Figure 1.4 Deep decking in construction

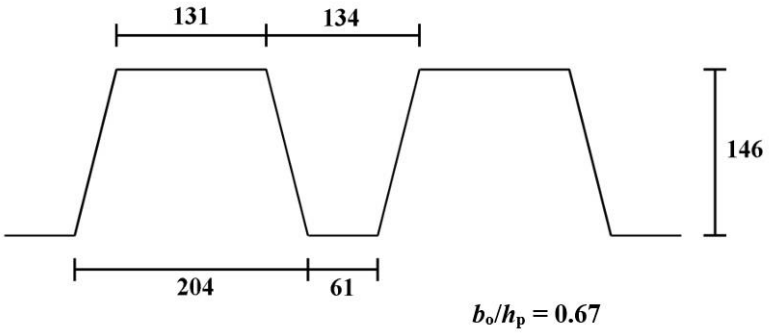


Figure 1.5 Details of 146 mm deep decking

Although Rambo-Roddenberry (2002) studied the behaviour and strength of welded stud connectors in various depths of profiled decking up to 150 mm, the shape of ribs of profiled decking more than 80 mm was rectangular, which is neither common in composite construction, nor economical. Unfortunately, both European and American design codes limit the sheeting depth to 85 and 75 mm respectively for using their stud capacity formula. The structural designers have no option but to rely on the manufacturer's specified characteristic stud strength, developed through experiments with the specific stud height and concrete strength in mind. Research is needed to establish the design stud capacity in composite beams with the sheeting depth higher than 80 mm. A generalised stud capacity formula should also be developed in the design codes for these deep decks.

The literature about secondary composite beams is only limited to decks below 100 mm deep. Thus, all existing equations in the design codes and elsewhere to predict the shear stud capacity were developed based on the geometries of common profiled sheeting (i.e. 60 and 80 mm deep), given that the ratio of average rib width to the rib height ($b_o/h_p$) was 1.5 at the very least. Considering the depth of 146 mm deep decking is almost twice as that of the common ones and the rib geometry ($b_o/h_p$) is approximately 0.67, the author feels that the applicability of the currently proposed equations is questionable. Lack of design rules and no past research on the behaviour of composite beams with decks deeper than 80 mm presents a major knowledge gap. If this knowledge gap is bridged, then this thesis will provide new insight into the literature by investigating steel decks deeper than 80 mm.

The literature also lacks information about the behaviour of primary composite beams with narrow and very deep decks. Thus, filling this knowledge gap is another motive for this thesis. It is well-known that the geometry of ribs, which is also referred to as the rib deck ratio ($b_o/h_p$), influences the performance of composite beams regarding the shear connector resistance. Based on previous studies, it is believed that the increase of the rib deck ratio ($b_o/h_p$) would lead the shear connector resistance to increase (Jayas and Hosain 1988, Gnanasambandam 1995, and Wu 1998). This theory has resulted in recognising the term "$b_o/h_p$" in several design rules establishing a direct relationship with the shear connector resistance (EC4 and ANSI/AISC 360-2016 specifications). However, all studies conducted in the past only involved wide ribbed decks ($b_o/h_p \geq 1.5$). Therefore, further studies on composite beams featuring narrow ribbed deck ($b_o/h_p < 1.5$) are needed.

Taking a 146 mm deep decking as an example, the rib deck ratio is 0.67. With this narrow geometry, the shear connector resistance would theoretically be low. However, the author is uncertain about this theory, feeling that there is a necessity to conduct inclusive tests to examine first the correlation between narrow and wide ribbed decks regarding the shear connector resistance. And second, to evaluate how accurately the design rules and other analytical methods predict the shear stud capacity in narrow and very deep decks. Another concern comes from the fact that the concrete part surrounding the shear studs is subjected to a pure shear force during the push-off tests. This suggests that the cross-sectional area of concrete mainly where the shear studs are placed could be a function of the shear connector resistance. The lack of research on this aspect requires further investigation to clarify that.

Overall, this thesis aims to investigate the behaviour of both secondary and primary composite beams. The initial focus will be on the effect of steel decks with narrow rib geometries and depths of more than 80 mm on the behaviour of headed stud connectors in terms of strength, ductility, and failure mode. The new results will be then compared to those obtained from composite beams with wide and conventional 60-80 mm deep decks. The reliability of existing design equations in predicting the shear stud capacity will be validated against the deep and narrow ribbed decks, and if necessary, new equations will be formulated to provide better correlation with test results. The novelty of this research is that the behaviour of composite beams with narrow and very deep decks is investigated for the first time. Useful information to practice, including but not limited to new design equations, is given herein. This research will be carried out by modelling 3-D push-off tests using ABAQUS/Explicit package after a series of extensive validation.

## 1.2 Objectives of the research

The research work in this thesis will be divided into four main parts as follows:

1. Investigating the behaviour of headed stud connectors in secondary composite beams with 100 and 146 mm deep decks. The shear connector resistance, ductility and failure will be presented in relation to several parameters as follows:
    i. Effect of narrow ($b_o/h_p < 1.5$) and very deep deck
    ii. Number of headed studs per rib

iii. Distribution of headed studs within ribs
iv. Effect of double wire-mesh reinforcement
v. The change in the concrete slab depth
vi. Reinforcing the concrete slab with a unique steel bars layout

2. Validating the predicted strengths obtained from the existing design equations against the FE results from numerical analysis with perpendicular steel decks. A comprehensive parametric study is accomplished aiming at covering a wide range of rib deck geometries (0.67 – 3.2), rib heights (50 – 146 mm), and other factors. The outcomes will be new separate equations that provide better predictions when headed studs are placed in:
   i. Central position
   ii. Favourable position
   iii. Unfavourable and/or staggered position

3. Examining the behaviour of headed stud connectors in primary composite beams. The effect of following parameters will be linked to the shear connector resistance, ductility and failure mode:
   i. Rib deck ratio ($b_o/h_p$), ranged from 0.67 to 2.35
   ii. Effect of the stud geometry ($h_{sc}/h_p$)
   iii. Effect of the cross-sectional area of concrete
   iv. Longitudinal stud spacings
   v. Number of headed studs
   vi. Effect of sheeting thickness

4. Comparing the results taken from numerical analysis with parallel steel decks with the existing design rules. New design equations are proposed containing two separate equations based on single and double stud layout.

## 1.3 Layout of the thesis

This thesis consists of eight chapters. The scope of this research is aligned with the behaviour of headed stud connectors in both secondary and primary composite beams applications.

**Chapter 1** gives a brief overview of the concept of steel-concrete composite beams, development of shear connection, and the inclusion of profiled steel decking into the composite constructions. This chapter also presents the objectives and contributions to be fulfilled at the completion of this research.

**Chapter 2** presents a wide range of previous studies in conjunction with the behaviour of headed studs in composite beams. The literature review includes the significant findings to date based on many experimental and analytical studies which relate to the area of interest of this thesis. At the end of this chapter, the knowledge gaps and questions are reported.

**Chapter 3** describes the methodology by which this research is carried out. In this chapter, the use of the software ABAQUS/Explicit to model 3-D finite element push tests is extensively validated against previous experiments. A suitable finite element model will eventually be selected to carry out further investigations based on the accuracy achieved in shear connector resistance, ductility, and failure mode.

**Chapter 4** presents the FE results and discussion of secondary composite beams with 100 and 146 mm deep decks. The shear connector resistance, ductility, and failure mode are investigated aligned with various parameters as mentioned in section 1.2, clause 1. The key findings and summary of this part of the research are outlined at the end of this chapter.

**Chapters 5** examines the effectiveness of some design codes and analytical methods at predicting the shear stud capacity in narrow and very deep decks oriented perpendicular to the steel beam. This chapter also includes a comprehensive parametric study resulting in new equations that account for narrow and very deep decks for the first time and fulfil the objectives given in section 1.2, clause 2.

**Chapter 6** presents the FE results and discussion of primary composite beams. The main focus is to find an accurate correlation between narrow and wide ribbed decks regarding the shear connector resistance. Besides relating the shear connector resistance, ductility and failure mode to some parameters given in section 1.2, clause 3.

**Chapter 7** checks the accuracy of some design codes and analytical methods at predicting the shear stud capacity in narrow and very deep decks oriented parallel to the steel beam. New equations are developed in this chapter that cover a wide range of steel ribbed

geometries including narrow sizes for the first time and demonstrate an accurate correlation between narrow and wide ribbed decks.

**Chapter 8** provides the summary of the conclusions derived from the present research, along with some recommendations for future work.

# Chapter 2 Literature Review

# Chapter 2

# Literature review

## 2.1 Introduction

This chapter provides critical review of previous research about composite beams. Included are experimental and numerical studies on the behaviour of headed stud connectors in composite beams with or without the profiled steel sheeting. The aim of this literature review is to present the up-to-date contribution of studies regarding composite beams and highlight the knowledge gap in this field.

## 2.2 Headed stud connector strength prediction equations

### 2.2.1 Headed stud connector embedded in solid concrete slab

The earliest form of composite beam application included solid concrete slab acting compositely with steel beam by shear connectors. Spiral and channel connectors were used extensively for both bridge and building construction before being replaced by the headed studs. The shear capacity of headed stud was first evaluated by Ollgaard et al. (1971). This was done by casting and testing 48 small-scale pushout specimens with solid concrete slabs. The variables considered were the stud diameter (16 and 19 mm), number of studs per slab, type of aggregate (Normal-weight concrete and Light-weight concrete), and the concrete properties (i.e. concrete strength, density, modulus of elasticity and split tensile strength).

Test results revealed a significant decrease in the shear connector resistance from 15 to 25% when the headed studs were embedded in the lightweight concrete. It was concluded that the shear stud capacity was primarily influenced by the compressive strength and the modulus of elasticity of the concrete. Test results also showed that the cross-sectional area of the stud was a function of the shear strength. Based on that, the following empirical equation was proposed for design purposes to determine the shear capacity of headed stud embedded in a solid concrete slab.

$$Q_n = 0.5\, A_s \sqrt{f'_c\, E_c} \qquad \text{Eq. 2.1}$$

where $A_s$ is the cross-sectional area of the shank of the headed stud ($mm^2$), $f_c'$ is the compressive strength of concrete (MPa), and $E_c$ is the modulus of elasticity (MPa).

Later on, Equation 2.1 was adopted by some design rules such as the Load and Resistance Factor Design Specifications (LRFD) developed by the American Institute of Steel Construction (1999). However, the formula was slightly modified to incorporate the tensile capacity of the stud connectors as shown below:

$$Q_n = 0.5\, A_s \sqrt{f_c' E_c} \;\leq\; A_s F_u \qquad \text{Eq. 2.2}$$

where $F_u$ is the specified minimum tensile strength of a headed stud connector (MPa).

In the latest American provisions (ANSI/AISC 360-2016), Equation 2.2 was further modified. The following equation is given to determine the nominal shear strength of one headed stud embedded in a solid concrete slab.

$$Q_n = 0.5\, A_s \sqrt{f_c' E_c} \;\leq\; R_g R_p A_s F_u \qquad \text{Eq. 2.3}$$

where $R_g$ and $R_p$ equal 1.0 and 0.75 respectively.

According to BS EN 1994-1-1:2004 Eurocode 4, the design shear resistance of headed stud embedded in a solid concrete slab is determined from the smaller of the following two equations:

$$P_{Rd} = \frac{0.8 f_u \pi d^2/4}{\gamma_v} \qquad \text{Eq. 2.4}$$

Or

$$P_{Rd} = \frac{0.29\, \alpha\, d^2 \sqrt{f_{ck} E_{cm}}}{\gamma_v} \qquad \text{Eq. 2.5}$$

$$\alpha = 0.2 \left[\frac{h_{sc}}{d} + 1\right] \qquad \text{for } 3 \leq h_{sc}/d \leq 4 \qquad \text{Eq. 2.6}$$

$$\alpha = 1 \qquad \text{for } h_{sc}/d > 4 \qquad \text{Eq. 2.7}$$

where $d$ is the diameter of the shank of the stud (mm), $h_{sc}$ is the overall nominal height of the stud (mm), $f_u$ is the specified ultimate tensile strength of headed stud but not greater than 500 MPa, $f_{ck}$ is the characteristic cylinder compressive strength of the concrete (MPa), $E_{cm}$ is the modulus of elasticity (MPa), and $\gamma_v$ is the partial factor taken as 1.25.

### 2.2.2 Headed stud connector embedded in transverse steel decking

The use of the ribbed steel decks in composite beams was found to reduce the shear capacity of headed stud if compared to those embedded in the solid slab. The correlation between the shear connector resistance in solid slab and those with composite steel decks was then demonstrated through the reduction factor method as expressed in Equation 2.8. This method was initiated by Robinson (1967) stating that the shear capacity of stud with ribbed steel decking is a function of the rib deck geometry (i.e. the ratio of the average rib width to the rib height) as shown in Figure 2.1. However, the first relative correlation was formulated by Fisher (1970) based on test results of composite beams featuring ribbed steel decks, and this is given in Equation 2.9.

$$Q_{rib} = r\,Q_{sol} \qquad \text{Eq. 2.8}$$

$$Q_{rib} = 0.36\,\frac{w}{h}\,Q_{sol} \qquad \leq Q_{sol} \qquad \text{Eq. 2.9}$$

where $Q_{rib}$ is the shear strength of stud in a rib, $Q_{sol}$ is the shear strength of stud in a solid slab, $r$ is a reduction factor which is a function of rib geometry, $w$ is the average rib width, and $h$ is the average rib height.

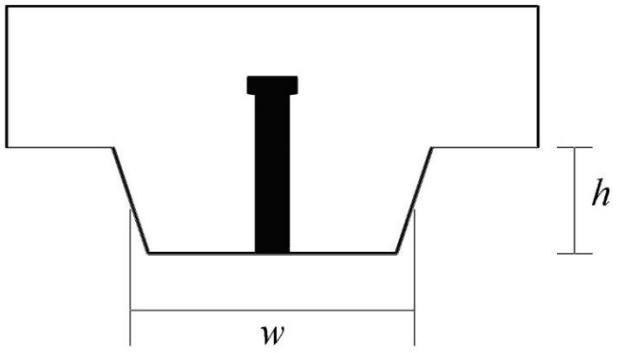


Figure 2.1 Headed stud connector in a ribbed steel decking

In fact, Equation 2.9 had then received criticism for having insufficient and uncontrolled variables. In an attempt to bridge this knowledge gap, Grant et al. (1977) carried out an experiment examining the behaviour of 17 full-scale composite beams with formed steel deck in conjunction with 58 additional tests that previously conducted by other researchers. The parametric study mainly involved the geometry of the steel deck, the diameter and height of stud connectors, the number of studs per rib, and the weight and strength of concrete. The analysis showed that the reduction factor was associated not only with the rib geometry but also with the overall height of the stud connector. As a result, an empirical reduction factor expression was proposed to determine the shear capacity of headed stud in a transverse ribbed steel decking. The shear capacity was said to be the shear strength of stud embedded in a solid slab multiplied by the following expression:

$$k_t = \frac{0.85}{\sqrt{N_r}}\left(\frac{b_o}{h_p}\right)\left(\frac{h_{sc}}{h_p}-1\right) \qquad \leq 1.0 \qquad \text{Eq. 2.10}$$

where $N_r$ is the number of studs per rib, $b_o$ is the average rib width, $h_p$ is the rib height, and $h_{sc}$ is the overall height of stud.

Equation 2.10 had received wide acceptance in the design codes of several countries such as the UK, USA, and Canada. In the revised British Standard, BS 5950: Part 3.1 (1990), the shear capacity of stud in a transverse steel decking is taken as the value calculated from Equation 2.2 multiplied by the reduction factor obtained from Equation 2.10. Except that for $N_r = 2$ and $N_r = 3$, the upper limit of the reduction factor ($k_t$) should not excess 0.8 and 0.6 respectively. Despite Equation 2.10 had been adopted for years by the American code, it is no longer in use in the latest provisions (ANSI/AISC 360-2016). The shear capacity of stud in a transverse steel decking is determined through Equation 2.3 with the factors of $R_g$ and $R_p$ given in Table 2.1.

Table 2.1 Values of $R_g$ and $R_p$ in case of a composite beam with decking oriented perpendicular to the steel beam

| **Number of headed studs per rib** | $R_g$ | $R_p$ | |
|---|---|---|---|
| | | $e_{mid\text{-}h}{}^* \geq 50$ mm | $e_{mid\text{-}h}{}^* < 50$ mm |
| 1 | 1.0 | 0.75 | 0.6 |
| 2 | 0.85 | | |
| 3 | 0.7 | | |

* $e_{mid\text{-}h}$ is the minimum distance from the centre of headed stud to mid-height of the adjacent web of rib

According to BS EN 1994-1-1:2004 Eurocode 4, the factor 0.85 in Equation 2.10 was lowered to 0.7. Therefore, the design shear connector resistance of composite beams with transverse steel decking is equal to the lesser value obtained from Equations 2.4 and 2.5 multiplied by the reduction factor given by Equation 2.11. The upper limits of $k_t$ should not exceed the values addressed in Table 2.2.

$$k_t = \frac{0.7}{\sqrt{N_r}}\left(\frac{b_o}{h_p}\right)\left(\frac{h_{sc}}{h_p}-1\right) \leq 1.0 \qquad \text{Eq. 2.11}$$

Table 2.2 Upper limits for the reduction factor $k_t$

| Number of headed studs per rib | Thickness of sheeting $t$ (mm) | Studs welded through profiled steel decking | Profiled decking with pre-holes and studs 19 mm or 22 mm in diameter |
|---|---|---|---|
| 1 | ≤ 1.0 | 0.85 | 0.75 |
| | > 1.0 | 1.0 | 0.75 |
| 2 | ≤ 1.0 | 0.70 | 0.60 |
| | > 1.0 | 0.80 | 0.60 |

### 2.2.3 Headed stud connector embedded in parallel steel decking

In primary composite beams, the profiled steel decking, if used, would be laid parallel to the steel beam. This means that the headed studs would be subjected to a pure shear similarly to those embedded in a solid slab. However, the existence of decks does not allow the headed stud to achieve its highest shear strength, causing to have less shear connector resistance. This is because the mesh reinforcement, in case of a composite beam with parallel decking, is located near to the head of studs where it is not as effective. While, the mesh reinforcement,

in case of a composite beam with a solid slab, is placed close to the root of the studs where its effectiveness is realised in confining splitting failure of the concrete slab.

Developing a relative formula to determine the shear capacity of stud in a parallel steel decking was then a natural consequence. The empirical reduction factor developed by Grant et al. (1977) was also found applicable to stud connectors with parallel decking. But in this case, the factor ($0.85/\sqrt{N_r}$) was replaced by a constant of 0.6. Therefore, the formula can be expressed as:

$$k_t = 0.6 \left(\frac{b_o}{h_p}\right)\left(\frac{h_{sc}}{h_p} - 1\right) \qquad \leq 1.0 \qquad \text{Eq. 2.12}$$

In accordance with BS EN 1994-1-1:2004 Eurocode 4, the design resistance of the headed stud connector placed in a parallel decking is calculated as the lesser value obtained from Equations 2.4 and 2.5 multiplied by the reduction factor given by Equation 2.12. As per the American provisions ANSI/AISC 360-2016, the shear capacity of stud in a parallel steel decking is determined through Equation 2.3 with the factors of $R_g$ and $R_p$ given in Table 2.3.

Table 2.3 Values of $R_g$ and $R_p$ in case of a composite beam with decking oriented parallel to the steel beam

| Condition | $R_g$ | $R_p$ |
|---|---|---|
| $b_o/h_p \geq 1.5$ | 1.0 | 0.75 |
| $b_o/h_p < 1.5$ | 0.85 | 0.75 |

## 2.3 Behaviour of headed stud connector in composite beams

### 2.3.1 General

This part presents many previous studies by other researchers in relation to the performance of headed stud in composite beams, mainly with profiled sheeting laid perpendicular or parallel to the steel beam. The existence of stiffeners at the bottom centre of some modern decks has led the headed studs to be placed off-centre. Consequently, the effect of number and layout of studs (i.e. Central, Favourable, and Unfavourable) along with the geometries of different decks were under investigation in case of composite beams with a perpendicular sheeting. On the other hand, the effect of the longitudinal and transverse stud spacings for

example, in case of composite beams with a parallel sheeting, were not either off the observation. Other parameters such as the size of concrete slab and the amount and position of steel reinforcement have also been studied.

### 2.3.2 Behaviour of headed stud connector in a perpendicular sheeting

The behavioural difference between push-out tests subjected to revised cyclic and monotonic loading was investigated by Hawkins and Mitchell (1984). The test program involved casting 10 solid slab push-out tests, 13 specimens with profiled sheeting oriented perpendicular to the steel beam, except for one, whereas the sheeting was laid parallel. Two depths of profiled sheeting were tested including 38 and 76 mm deep, whilst the average width of ribs ranged from 44 to 150 mm. The diameter of stud was 19 mm, and the longitudinal and transverse stud spacings were variable. The test results showed that the use of the revised cyclic loading resulted in a 17% lower shear connector resistance than those with monotonic loading. The shear strength of stud increased when the studs were arranged relatively away.

The push-out tests ended with four different failure modes: stud shearing, concrete pull-out, rib shearing and rib punching. In case of push-out tests failed by concrete pull-out, the shear strength and ductility of the stud was found to be less than their companions that failed by stud shearing. While rib shearing failure occurred in specimens featuring small width of the slab, rib punching failure was linked to specimens with narrow rib width. The pyramid shape cone was associated with the concrete pull-out failure, the authors proposed Equation 2.13 to calculate the shear capacity of headed stud with such failure mode.

$$V_c = 0.45 \sqrt{f'_c}\ A_c \qquad \text{Eq. 2.13}$$

Where $V_c$ is the shear capacity of headed stud due to concrete pull-out failure (N), and $A_c$ is the area of concrete pull-out failure surface ($mm^2$).

From the analysis of 110 push tests, Oehlers and Johnson (1987) proposed an equation to predict the static failure load of stud connector. The prediction equation was made to be different than those in design codes in that it avoids the need to differentiate between the normal and lightweight concrete and allows for a wide variation in the stud material strength. The prediction equation was developed from tests in which the stud heights were greater or

equal to 4$d$, the mean height of the weld collar was 0.31$d$, and the material properties varied between 430 to 640 MPa, 0.05 to 0.16, and 0.05 to 0.11 for $f_u$, ($E_c/E_s$), and ($f_{cu}/f_u$) respectively. The final form of the equation is given below:

$$P_p = K\,A\,(E_c / E_s)^{0.4} f_{cu}^{0.35} f_u^{0.65} \qquad \text{Eq. 2.14}$$

where $K = 4.1 - n^{-0.5}$, n is the number of studs subjected to similar displacements, $A$ is the cross-sectional area of stud, $E_c$ and $E_s$ is the modulus of elasticity of the concrete and steel respectively, $f_{cu}$ is the cube strength of concrete, and $f_u$ is the tensile strength stud.

In the same research, the authors found that $f_{cu}$ had a greater influence on the static strength of stud than $f_u$. The increase in $f_{cu}$ from 20 to 46 MPa brought 51% increase in the shar stud capacity, while the increase in $f_u$ from 480 to 640 MPa caused 33% increase in the shear stud capacity.

The effect of position and number of studs per rib and the studs being welded away from the centre line of the steel flange were examined by Robinson (1988). The configuration of the push-out tests with perpendicular metal deck was meant to simulate an interior and an exterior beam. For an interior beam application, the specimens were assessed with three different shapes of metal decks, the total rib heights were 76, 76, and 51 mm deep, the corresponding deck ratios ($b_o/h_p$) were 2.4, 2.0, and 2.0 mm respectively. The studs in specimens with 51 mm deep deck were 19 × 91 mm, whilst the studs in specimens with 76 mm deep deck were 19 × 116 mm. For specimens with deck ratios of 2.0, the studs were placed in a central position as single and pairs. While the studs in specimens with 2.4 deck ratio were placed in a favourable and unfavourable position as single and pairs for each.

The characteristic feature of the exterior push test beams was that the studs were placed with an edge distance of 38 and 65 mm. Test results showed that the favourable position carried an average of 23% shear connector resistance more than the unfavourable position. The difference in the shear capacity per stud between single and double studs was negligible in case of the unfavourable position. But surprisingly, the shear capacity per stud in double arrangement was 20% higher than single studs in case of both central and favourable position. It is unlikely that the stud would achieve higher shear resistance when two studs are placed in a rib as compared to the one stud per rib. The discrepancy herein could be attributed to the

test arrangement for having only one studded rib which is unlikely to give the real behaviour of headed stud. Finally, the change in the edge distance gave only 10% higher shear capacity in favour of 65 mm.

Jayas and Hosain (1988) studied the behaviour of headed stud in composite beams with parallel and perpendicular metal decks. Eighteen push-out specimens were performed in which 5 tests had solid slabs, 5 tests with parallel metal decks (explained later), and 8 tests with perpendicular metal decks. The rib heights in specimens with perpendicular metal decks were 38 and 76 mm. The shallow deck featured two rib ratios: 1.59 and 2.42. The studs used were 16 × 76 mm and 19 × 127 mm for shallow and deep deck respectively. The studs' layout was in pairs except for one test with deep deck where single studs were arranged. Test results indicated a drastic reduction in the shear capacity of stud when perpendicular metal deck was included. The shear capacity of stud in terms of wide and narrow deck geometry was respectively 60% and 42% of the shear strength obtained from solid slabs. The shear capacity per stud of pairs was 38% less than single studs. Stud pull-out failure was predominant among specimens with perpendicular metal deck.

The same authors verified Equation 2.13 proposed by Hawkins and Mitchell (1984). The predicted values underestimated the shear capacity of stud with a 38 mm deep deck and overestimated the shear capacity of stud with a 76 mm deep deck. Two separate empirical equations were then proposed using the linear regression analysis (least square fit).

For a 38 mm deep deck, $V_c = 0.61\ \lambda \sqrt{f'_c}\ A_c$ Eq. 2.15

For a 76 mm deep deck, $V_c = 0.35\ \lambda \sqrt{f'_c}\ A_c$ Eq. 2.16

$\lambda = 1.0$ for normal-density concrete

0.85 for semi low-density concrete

0.75 for structural low-density concrete

In a separate research, Jayas and Hosain (1989) verified Equations 2.15 and 2.16 by testing 4 full-size composite beams and 2 push-off specimens. Specimens were performed with profiled steel decking oriented perpendicular to the steel beam axis. The partial shear connection, deck geometry and longitudinal stud spacings were the main parameters. Test

results exhibited that the major mode of failure was concrete pull-out, while one push-off specimen and one beam failed by a combination of stud shearing failure and concrete pull-out. Good agreement was noticed between the shear stud capacities obtained from push-off specimens and the predicted strengths achieved from Equations 2.15 and 2.16. Moreover, the predicted strengths of the flexural capacity calculated from these equations were fairly close to those obtained from the experiments.

Lloyd and Wright (1990) carried out an experiment by performing 42 push-out tests with headed studs welded through-deck. The parameters were mainly made of the change in the slab width and the amount and position of the steel reinforcement. In all specimens, the slab thickness was 115 mm, and the studs used were 19 × 100 mm. The slab width ranged from 450 to 1350 mm, and the steel reinforcement was located in different heights from the upper surface of the steel deck. Tests results showed that the shear capacity of stud with profiled decking was dependent on the stud height and the geometry of decking. However, the change in the amount and position of the steel reinforcement had a negligible effect on the shear connector resistance.

The failure mode was mainly concrete cone. This failure was characterised as the concrete part starts to split and ride over the steel sheeting and leave wedge-shape cones of concrete around the studs by the end of the test. Rib shearing failure was observed when the slab width was short. To avoid such failure, the authors recommended the width of the slab to be at least 200 mm wider than the lowest width investigated. The authors developed an equation based on the wedge-shape cone method to determine the shear capacity of single studs and pairs. The formula was said to be more precise than the pyramid-shaped cone method developed by Hawkins and Mitchell (1984). The formula is given below:

$$Q_k = (A_c \sqrt{f_{cu}})^{0.34} \qquad \text{Eq. 2.17}$$

where $A_c$ is the area of the concrete cone (mm), and $f_{cu}$ is the compressive concrete strength (MPa).

The unfavourable side can be 35% weaker than the favourable side. This was concluded by Mottram and Johnson (1990) through conducting 35 push tests using through-deck welded studs. The headed studs were placed in three different types of steel decks with normal and

lightweight concrete. The stud's diameter was 19 mm, and the height of stud after welding was either 95 mm or 120 mm. The authors noticed that the shear capacity per stud for two studs per rib was 30% less than those ribs with one stud. Also, placing two favourable studs in line appeared to be stronger than staggered position (i.e. placing two studs diagonally apart in the favourable and unfavourable position). The authors recommended the studs to be on the favourable side if the central position is not possible.

The same authors found that the reduction factor formula (Equation 2.10) proposed by Grant et al. (1977) was unsafe and should be replaced by Equation 2.18 which was later modified and published by Lawson (1992). The latter formula was seen to provide more consistent and safe predictions when used by both Eurocode 4 and BS 5950: Part 3.1 drafts. The reason for better predictions was that the variable of stud position within trough (i.e. Central, Favourable, and Unfavourable) was considered.

$$k = \frac{0.75r}{N^{0.5}}\left(\frac{h_{sc}}{h_{sc}+h_p}\right) \qquad \leq 1.0 \qquad \text{Eq. 2.18}$$

where $r$ depends on the position of stud in the trough.

For favourable or central position ($e \geq b_o/2$), $r$ is the lesser of $b_o/h_p$ and 2.0.

For unfavourable position ($e < b_o/2$), $r$ is the lesser of $b_o/h_p$, $[(e/h_p)+1]$, and 2.0.

The position of studs within ribs was also studied by Easterling et al. (1993). The test program involved a total of eight push-out specimens, four with studs in the favourable position and four with studs in the unfavourable position. The test setup was vertical having two studded ribs with 19 × 125 mm stud connectors. The rib height was 76 mm, and the rib ratio was 2.0. The test was supplemented by an additional load (normal load) subjected to both slab surfaces along with the applied shear load. The normal load was approximately 10% of the expected shear load. This was meant to prevent the premature separation between the slab and metal deck and simulate the gravity load placed on a slab in a composite beam test. Test results showed that the unfavourable position was 28% weaker than the favourable position.

Rib punching was the failure mode in all of the unfavourable position tests. Prior to reaching the maximum applied shear load, the steel deck adjacent to the stud was remarkably bulged out and a small wedge of concrete was crushed between the stud and the deck web. It was

then concluded that the shear capacity of stud placed in an unfavourable side is rather affected by the strength of steel deck than the concrete strength. The authors found that the equations used in the American Institute of Steel Construction until 1999 (i.e. results obtained from Equation 2.2 multiplied by Equation 2.10) gave over-predicted shear capacity for one stud per rib. The poor accuracy was attributed to the fact that Equation 2.10 was developed from tests with only stud pairs. Thus, the authors suggested that the stud reduction factor for one stud per rib should not exceed 0.75.

Johnson and Yuan (1998a) carried out a research to verify the existing design rules for stud shear connector in profiled sheeting. The analysis involved 34 new push tests besides 269 push tests from previous research. The study found that the existing design methods given by Lawson (1992) and Eurocode 4 provided low accuracy, especially for studs placed off-centre and rib geometry ($b_o/h_p$) of 1.75. For push tests with perpendicular profiled sheeting, five failure modes were specified including stud shearing, rib punching, rib punching with stud shearing, rib punching with concrete pull-out, and concrete pull-out. For each failure mode, a theoretical model was developed to determine the shear capacity of stud with perpendicular profiled sheeting, and this part was published in a separate research (Johnson and Yuan 1998b). The predicted strengths were with a mean error of 2% and coefficient of variation of 10%. The theoretical models for transverse sheeting are discussed in detail in section 5.5 herein.

Composite edge beams with transverse steel decking are more susceptible to experience a rib shearing failure. This failure generates in narrow concrete flanges where longitudinal shear forces to be transferred to the stud connectors across the slab's width are limited. The failure mode was classified as a brittle in the literature causing a significant reduction in the strength and ductility of stud connector and should be avoided whenever possible. Patrick (2000) proposed a new reinforcing component consisting of "A waveform piece of welded-wire fabric made from cold-reduced, ribbed wire with a nominal diameter of 6 mm and a nominal yield stress of 500 MPa". The new reinforcing component was tested on both re-entrant and trapezoidal steel decking. The use of such novel fabrication resulted in stronger and more ductile stud connector when compared to the conventional tests. The author suggested that the negative moment region of continuous beams could be improved if this unique reinforcement was employed.

The strength and ductility of headed stud in push-out tests were then well-known for being remarkably less than the results obtained from full-scale composite beams. It is believed that the deficiency of headed studs in push-off tests is because of the push test method develops extra uplift effects in the concrete slab and force transfer method which are different to those in full-scale beams. This trend would result in premature failure in concrete which in turn reflect on the strength and ductility of shear connection in push-off tests. Some studies have been conducted to modify the standard setup of the push-off test in different codes. One of those was done by Bradford et al. (2006). The new test arrangement was a horizontal push test with the size of 1400 mm long and 1200 mm wide. The horizontal shear load was coupled with a normal load of 10% of the total shear load. With this new test arrangement, the strength and ductility of stud considerably developed.

Hicks (2007) studied the strength and ductility of headed stud welded in profiled steel sheeting. Two full-scale composite beams were performed. The profiled sheeting had a rib height of 60 mm and a rib ratio of 2.5. The headed studs were 19 × 95 mm and arranged in different layouts including central, favourable, and unfavourable, and as a single and pairs. Test results obtained from both composite beams exhibited excellent ductility which was significantly higher than the 6-mm limit defined in Eurocode 4 and BS 5950-3.1 for partial shear connection. Also, the resistance of stud pairs in the favourable position was underestimated by BS 5950-3.1. It was further concluded that the critical cross-section should correspond to the point load positions when a beam is subjected to concentrated loads. The author found that the load-slip curves achieved from beam tests were higher and/or different than the push tests. The poor performance exhibited by push tests was attributed to “the absence of the curvature and normal force that exist in beam tests”.

The same research performed six push-off tests. Results showed that the shear connector resistance of single stud was higher than double studs per rib. While the highest strength was obtained from the favourable stud, the lowest slip capacity was recorded from the unfavourable stud. The nominal resistance predicted by the BS 5950-3.1 and ANSI/AISC 360-05 were on the safe side for single studs, but the predictions were unconservative for double favourable studs. On the other hand, the Eurocode predictions were overly conservative, especially for single studs. The author proposed an interim modification on Equation 2.10 which is recommended by BS 5950-3.1. He stated that the resistance of double

studs is proportional to ($1/\sqrt{N_r}$) is too high and that for $N_r = 2$ the factor of $0.85/\sqrt{2} = 0.6$ should be reduced to 0.37 to give the following expression:

$$k = 0.37\left(\frac{b_o}{h_p}\right)\left(\frac{h_{sc}}{h_p}-1\right) \qquad \text{but } k \leq 0.75 \text{ for } N_r = 2 \qquad \text{Eq. 2.19}$$

Ernst et al. (2010) used the wave reinforcing components and spiral stud enhancing device to develop the strength and ductility of headed stud with steel decking. The study included testing two full-scale secondary beams, one being internal and the other being edge beam. Both beams were divided into two halves where one side was conventionally reinforced according to the design rules of EC4 and the connections on the other side had the wave reinforcing component and stud enhancing device. The latter is a ring-shaped device put around studs to confine the concrete, reduce bending of stud, and minimise the effects of localised failure.

For the internal beam, it was shown that the use of the wave reinforcing successfully contained the propagation of the horizontal stud pull-out cracks and assured a continuous load transfer. The wave reinforcing was also seen effective at suppressing the rib shearing effects in case of the edge beam. In the rib where the spiral enhancing device was used, the concrete in the vicinity of stud remained virtually undamaged. The use of both novel elements increased the shear capacity of stud by an average of 27% as compared to the connection part that did not include these elements. Despite the significance outcomes, the novel reinforcing elements were only tested on pre-cut holes 80 mm deep decking placed perpendicular to the steel beam.

Smith and Couchman (2010) investigated the effect of mesh position, slab depth, number of studs per rib, and transverse spacing of pair studs on the headed stud in transverse steel sheeting. The study consisted of performing 27 push tests subjected to a vertical shear load as well as a normal load of 12% of the vertical load applied horizontally to the slab surfaces. The slab depth was either 140 or 225 mm. Single, double, and triple studs were used, the transverse stud spacings ranged from 75 to 140 mm. The mesh reinforcement was either rested on the sheeting surface (bottom position) or located 25 mm from the top surface of slab (top position). Headed studs of 19 × 100 mm were used and positioned in the favourable side. Studs were welded through 60 mm deep decking with rib geometry ($b_o/h_p$) of 2.5.

Test results revealed that the shear capacity of stud increased by 23% and 33% when the slab depth was increased to 225 for single and double studs respectively. However, it was not certain whether this improvement was caused by the slab depth itself or due to an experimental error. Thus, further study was recommended in this aspect. The top mesh position provided sufficient ductility in the headed stud, yet it caused a decrease in the shear connector resistance by 20% as compared to the bottom mesh position. The change in the transverse stud spacings appeared to have a small effect on the shear resistance. Moreover, placing three studs per rib caused a further decrease in the shear resistance per connector.

The most recent study on the behaviour of headed stud with perpendicular steel decking was done by Nellinger et al. (2017). Twenty push-out tests with stud connectors placed centrally in the ribs of 58 and 80 mm deep decking were performed. The parameters were made of stud diameter (19 and 22 mm), number of studs per rib, single or double layers of reinforcement, welding procedure, and transverse normal load ranged from 3.8 to 17.5% of the total shear load and applied concentrically and eccentrically of 380 mm. Test results showed that the load-slip behaviour was influenced by the embedment depth of stud in the concrete above the sheeting. For push tests with studs that satisfied the minimum embedment depth of 2$d$, which is required by the EC4, the double curvature deformation of stud and large slip capacity were observed. While single curvature deformation of stud and small slip capacity were witnessed for tests that did not satisfy such limit.

The same research showed that the shear resistance of stud improved with higher concentric transverse loads and a second layer of reinforcement. However, the eccentric transverse load application (to reflect negative moments in the slab) gave a slight effect on the load-slip behaviour. The predicted strengths from the current design provisions of EC4 were compared with the test results, which were shown to be unconservative in some cases. In 2018, Nellinger et al. developed new approaches to the shear connector resistance for more accurate predictions. The equations were based on simple mechanical models which are discussed in detail in section 5.7 herein.

### 2.3.3 Behaviour of headed stud connector in a parallel sheeting

Ribbed steel decking, if included in the primary/girder composite beam system, runs parallel to the steel beam. This system was first introduced for high-rise buildings in 1971 by Colaco

(1972) in the USA before it gained gradual acceptance in Canada and Europe. Most of the research in relation to the composite beams with parallel metal decks back to the 1980s and 1990s. It should be noted that studies on such topic are limited.

Kullman and Hosain (1985) studied the shear capacity of stud with the help of three full-scale primary beams. Headed stud pairs of 19 × 100 mm or 19 × 125 mm were used and welded directly to the steel beam through pre-cut holes in 76 mm deep decking. Three different types of slab reinforcement were considered including no transverse reinforcement, transverse reinforcement, and transverse and bent bars reinforcement. Test results indicated that the additional transverse reinforcement did not increase the ultimate strength of stud. However, the bent transverse bars contributed to a 24% increase in the ultimate capacity besides improving the ductility of studs. The authors suggested that the shear stud capacity is largely influenced by the ribbed deck configuration and the placement of transverse reinforcement.

In 1986, Chan et al. carried out a study on 42 horizontal push-off tests with parallel steel decking. The test parameters considered the effects of longitudinal stud spacings, configuration and method of installation of stud, amount and placement of transverse reinforcement, and open panel length on the failure mechanism and shear capacity of stud. The open panel is a solid slab extension to the longitudinal direction of steel beam, and it was set to guarantee the distribution of longitudinal shear forces during the test. The diameter of stud was either 13 or 19 mm arranged in one line, pairs, or staggered configuration. The metal deck was a 38 mm deep. Test results showed that the increase in the open panel length from 508 mm to 711 mm caused 10% decrease in the shear stud capacity due to the increase in the prying effect. Welding the studs through the metal deck gave more shear connector resistance than the direct installation (pre-cut holes in metal decking).

Moreover, the study showed that the shear stud capacity was not affected by increasing the transverse reinforcement if the reinforcement was located near the head of studs. However, the amount of the transverse reinforcement, when placed directly on the metal deck, had more effect on the sensitivity of the shear stud capacity. The failure mechanism appeared to be highly affected by the studs' configuration. A longitudinal splitting failure of concrete was generally observed in specimens with studs arranged in one line. For specimens containing studs arranged in pairs or staggered manner, stud shearing occurred with studs placed

relatively far apart (6*d* or 8*d*) whilst concrete shearing occurred with studs placed relatively close (4*d*).

Robinson (1988) also counted the edge distance of the stud in a parallel metal deck. Eight push-off tests were performed incorporating 76 mm deep decking with a rib ratio of 2.4. Single studs per connection of 19 × 116 mm were used in all tests. In three tests, the stud connectors were centrally welded, while the remaining tests had the studs welded 38 mm away from the edge of the steel flange. Test results showed no sign of effect on the shear stud capacity caused by the edge distance. The normalised average shear strengths per stud were in a difference of barely 1%. No explanation was given by the author for this observation. But perhaps the effect of such parameter would have been realised if the edge distance had been larger than the one investigated. The failure mode in all tests was seen to be stud shearing.

In the experimental study conducted by Jayas and Hosian (1988), five out of eighteen push-off tests had metal deck oriented parallel to the steel beam. The rib height was 38 mm with a wide rib ratio of 4.2. The headed studs were 16 × 76 mm arranged in pairs with a transverse spacing of 76 mm. The variable was only the longitudinal stud spacings including 102, 152, and 305 mm. Similar to Chan et al. (1986), the failure mechanism was governed by the longitudinal stud spacing. Longitudinal shearing of concrete occurred in specimens when studs were placed at a close distance (i.e. 102 mm). While stud shearing occurred in specimens with widely spaced studs. The concrete-related failures led to a reduction in the shear stud capacity by 14% compared to those failed by stud shearing.

The influence of transverse and longitudinal stud spacings, amount of transverse reinforcement, and deck geometry on the behaviour of headed stud were studied by Gnanasambandam (1995). The study involved testing 104 push-out specimens, among which 4 had solid slabs and the remaining with wide ribbed metal deck oriented parallel to the steel beam. The transverse stud spacings ranged from 3*d* to 5*d*, whilst the longitudinal spacings ranged from 3*d* to 8*d*. Two metal decks were used including 38 and 76 mm deep deck. The deck geometry used was wide in which the rib ratio ($b_o/h_p$) ranged from 1.58 to 4.97. All tests had two studs per row arranged either in one line or staggered manner, except for only four tests containing single studs per row. Headed studs used were either 16 × 76 mm or 19 × 125 mm.

Test results showed that the shear stud capacity was more sensitive to the transverse reinforcement in case of solid concrete slabs. The transverse reinforcement had an insignificant effect on the shear resistance among tests with metal decks. The maximum stud capacity was realised when the transverse stud spacing ranged from 3*d* to 4*d* beyond which the shear strength decreased. The shear connector resistance increased when the longitudinal stud spacing, and rib ratio were increased. Tests with closely spaced studs (less than 5*d*) were more susceptible to end with concrete-related failures. While stud-related failures were mostly seen in tests with widely spaced studs. Evaluation of the push-off test results showed that the shear connector resistance formulae in both CSA (1994) and EC4 gave inconsistent results. The author proposed a new formula using a regression analysis method for more accurate predictions of the shear stud capacity arranged in two rows with parallel metal deck. The formula is given below:

$$q_u = (11\ s_l\ d - 0.82\ s_l^2)\ \sqrt{f_c} + 0.36\ (b_o/h_p)\ d\ h_{sc}\ \sqrt{f_c} \qquad \text{Eq. 2.20}$$

where $s_l$ is the longitudinal stud spacing ($3d \geq s_l \leq 8d$)

Wu (1998) investigated the behaviour of headed stud in composite beams with parallel wide ribbed metal deck. The experimental study involved 60 push-out specimens and 4 full-scale composite beams with 76 mm deep deck. The metal deck was utilised with some improvisations to provide different rib ratios including 1.58, 2.33, and 3.32. All tests contained two studs per row of 19 × 125 mm arranged in one line. The transverse stud spacings ranged from 4*d* to 6*d*, whilst the longitudinal spacings ranged from 3*d* to 8*d*. An increase of 17% in the shear stud capacity was achieved when the longitudinal stud spacing was raised from 3*d* to 8*d*. Similarly, the ultimate load per stud increased by 20% as the rib ratio was increased from 1.58 to 3.32. However, the change in the transverse stud spacings from 4*d* to 6*d* gave only 7.6% increase in the stud capacity.

It was then concluded that the longitudinal stud spacing, and deck geometry were a main function of the shear stud capacity. The study also observed that both CSA (1994) and EC4 lack the accuracy of the shear connector resistance in parallel metal deck. The comparison between the predicted and observed strengths showed that the coefficient of variation was 33% and 61% for CSA and EC4 respectively. The author reached a simplified equation after a long series of regression analysis examination to predict the shear stud capacity arranged

in two rows with parallel metal deck. The equation is expressed below and was recommended for design purposes.

$$q_u = [0.264\ (s_l/d) + 0.821\ (b_o/h_p) + 3.12]\ d\ h_{sc}\ \sqrt{f_c} \qquad \text{Eq. 2.21}$$

where $3 \leq s_l/d \leq 8$

Out of 34 push tests done by Johnson and Yuan (1998a), 18 tests contained metal deck placed parallel to the steel beam. This part of study intended to investigate the effects of rib geometry, stud positions, and concrete density. Five types of decking were used, the rib heights varied from 46 to 80 mm and the rib ratio varied from 1.75 to 3.2. The stud connectors were arranged in either two rows or staggered. The diameter of stud was 19 mm, but the height was either 95 or 125 mm. The transverse stud spacings ranged from 2.8*d* to 5.3*d*. Test results showed that the staggered arrangement gave relatively high shear connector resistance than in-line stud placement. No reduction in the shear stud capacity nor in ductility was observed when the longitudinal spacing dropped below 5.8*d*. The failure modes observed were splitting concrete and concrete pull-out failure. Due to the low accuracy obtained from EC4, Johnson and Yuan (1998b) developed a theoretical model for each failure mode to determine the shear connector resistance in parallel steel deck. This part is discussed in detail in section 7.5 herein.

## 2.4 Previous numerical modelling studies on composite beams

Finite element modelling has gained wide acceptance in the last twenty years. Experiments require intensive test facilities that are costly and time-consuming. Therefore, finite element modelling can provide an alternative solution if validated properly. Modelling a composite beam especially with a metal deck can be difficult. The non-linear definition of materials, suitable constraints and contact interactions, boundary conditions and load application should be accurately modelled to capture the real behaviour of headed stud in composite beams. Several numerical studies have been made on such topic with different methods and parameters.

Kim et al. (2001) did one of the earliest numerical studies on the behaviour of through-deck welded shear connectors. Three push-out tests were done first through experiment. Headed

studs of 13 × 65 mm were used and welded through unembossed 40 mm deep sheeting. The failure modes were concrete pull-out, stud shearing and local concrete crushing around the stud's foot. The finite element analysis consisted of linear and nonlinear two-dimensional models and a linear three-dimensional model using the LUSUS FE program. In terms of a two-dimensional model, plane stress elements were used to model the steel beam, concrete slab, and stud, whilst the profiled steel sheeting was modelled using bar elements. The stud was assumed to be a rectangular cross-section. The bottom element of stud was given half stiffness to simulate any possible stud yielding before failure. While zero stiffness was given to the concrete elements behind the stud to simulate the separation between these components.

In case of a three-dimensional model, shell elements were used to simulate the steel beam and the profiled sheeting, whilst beam elements were used for the stud. The concrete part was simulated by volume elements. Results taken from the 3-D linear FE model showed better agreement with the load-slip curve obtained from the experiment especially in the early stages of loading. However, both 2-D and 3-D FE analysis resulted in an elastic load-slip curve rather than the expected nonlinear curve. The failure mode in the FE analysis was mainly the concrete failure. The studs did not yield despite the non-linear properties were defined. Furthermore, the stud shearing and the separation of the profiled sheeting from the concrete were not captured.

A finite element model using ABAQUS software was developed by Lam and El-lobody (2005) to simulate the load-slip behaviour of headed stud. The scope of the study, however, was limited to push-off tests with solid concrete slabs. The finite element model was first validated against experiments involving the change in the concrete strength from 20 to 50 MPa. Headed studs used were 19 × 100 mm. The failure modes were stud shearing, conical concrete, and a combined failure of concrete and stud yielding. In the FE analysis, both linear and nonlinear properties were considered for all components. The elastic-plastic method that uses the Mises yield surface was used to simulate the concrete part. All failure modes were accurately predicted by the FE model. The shear stud capacity obtained from the FE was in a very good correlation with the experimental results. Despite the load-slip curve obtained from the FE model was nonlinear, the softening behaviour beyond the ultimate load was not captured.

The same research carried out a parametric study on the effect of the stud's diameter varied from 13 to 22 mm with various concrete strength ranged from 25 to 40 MPa. The FE results were then compared to the predicted strengths calculated by BS 5950, EC4 and AISC (1999). For tests with stud's diameter up to 19 mm, the FE results were very well predicted by the EC4 formulae, while overestimated by both BS 5950 and AISC. On the other hand, all design codes appeared to overestimate the shear capacity of the 22-mm diameter headed stud. The authors recommended further experiments on a 22-mm diameter headed stud to verify the results.

Ellobody and Young (2006) were first to use ABAQUS to model the headed stud connector in transverse profiled sheeting. The nonlinear material properties of the steel beam, headed stud, profiled sheeting, concrete slab and reinforcement bars were defined. The concrete part was presented using the Drucker Prager model. This model is suitable for materials that exhibit long-term inelastic deformations. The FE analysis was verified against the experimental results achieved by Lloyd and Wright (1990) and Kim et al. (2001). Good agreement in the shear stud capacity was achieved between the FE results and experiments for most tests. The mean value of $P_{Test}/P_{FE}$ was 0.99 with a coefficient of variation of 4.9%. The FE model was successfully able to predict the failure mode same as in experiments. The load-slip curve was also in a good agreement with experiment. Nevertheless, the FE model was not capable of depicting the separation of the profiled sheeting from the concrete neither the softening behaviour of the load-slip curve.

A parametric study was conducted in the same research containing 44 one studded rib push-out tests. Test parameters included the change in the wide rib geometry, diameter and height of headed stud, slab dimensions and concrete strength. The maximum rib height and stud dimension investigated were 76 mm and 19 × 127 mm respectively. The FE results were compared to the predicted strengths obtained from BS5950, EC4 and AISC (1999). The comparison revealed that both BS 5950 and AISC provisions gave over-predicted strengths with a maximum shear connector resistance difference of 25% and 27% respectively. However, the design rules in EC4 was generally conservative with a maximum shear connector resistance difference of 11% in some cases.

A three-dimensional finite element model was developed by Mirza and Uy (2009) to investigate the behaviour of headed stud in composite beams for both solid and profiled slabs

at elevated temperature. The study considered the load-slip relationship and ultimate shear stud capacity for push tests with ABAQUS. The comparison between the FE results and experimental tests under both ambient and elevated temperatures showed good agreement. The maximum discrepancy in results was at 10% and the failure mode was accurately predicted. Shear connection fracture was the dominant failure mode for the solid slabs, whilst concrete crushing failure occurred in the profiled slabs.

At ambient temperatures, the shear connector resistance in push tests with solid slab was higher than that of a profiled slab. However, the shear connector resistance in a solid slab was more sensitive to the elevated temperatures. The FE analysis showed that push tests with solid and profiled slabs can attain 40% and 60% of their ultimate load at elevated temperatures compared to ambient temperatures. It was also noticed that solid slabs can withstand fire for only 30 minutes before the failure happens while profiled slabs can withstand fire for more than 3 hours. The better performance of the profiled slabs was because the steel sheeting worked as a protective layer for the headed stud during fire. This study aimed to enrich the understanding of the behaviour of composite beams under fire exposure. But the topic is beyond the scope of the research herein.

A new three-dimensional finite element model was developed by Qureshi et al. (2011a) to study the behaviour of headed stud in push tests with perpendicular profiled sheeting. ABAQUS/Explicit was employed to simulate the nonlinear behaviour of the push test and complex contact interactions. All steel components were simulated using the elastic-plastic model and the concrete slab was simulated by the Concrete Damage Plasticity method (CPD). The FE model was verified against experimental push tests. A close agreement was achieved between the FE results and experiments. The mean average of $P_{Exp.}/P_{FE}$ was 1.04 with a corresponding coefficient of variation of 4%. This unique FE model was successfully able to simulate the post-failure behaviour of push tests, the separation between the steel deck and concrete slab and the concrete failure formation. This was important to precisely determine the shear stud capacity, slip, and failure modes.

An extensive parametric study was conducted in the same research to investigate the effect of double studs placed in favourable and staggered positions with different transverse spacings and concrete strengths. The test involved 64 push tests incorporating 60 mm Multideck with a rib ratio of 2.5. Headed studs of 19 × 100 mm were used and placed at

transverse spacings ranging from 40 to 400 mm. It was found that the shear resistance of favourable and staggered studs were respectively 94% and 86% of the strength of single stud when the transverse spacing was 200 mm or farther. The resistance of staggered pairs was generally less than the double studs in a favourable position.

Using the same FE model, Qureshi et al. (2011b) studied the effect of sheeting thickness and stud's position on the strength and ductility of headed stud. The numerical study involved 240 push tests with 60 mm Multideck placed perpendicular to the steel beam. Parameters were made of the difference of sheeting thicknesses, stud's layout, concrete strength and transverse spacings. The FE results showed that the resistance of stud in the unfavourable side was more sensitive to the sheeting thickness than the favourable and central positions. The shear connector resistance of the unfavourable stud increased by 30% when the sheeting thickness was increased from 0.9 to 2.0 mm. It was found that the resistance of the unfavourable stud was more affected by the strength and thickness of profiled sheeting than the concrete strength. The ductility of the unfavourable stud was 2-4 times higher than the favourable stud.

Also, the study found the change in the sheeting thickness and transverse spacing had an insignificant effect on the ductility of the favourable stud. But it did so for the unfavourable stud. The concrete cone failure was associated with the favourable and central stud, whilst rib punching and concrete crushing in front of the stud was the failure mode of the unfavourable stud. Strength prediction equations for unfavourable and central studs were proposed using a linear regression analysis method. Equation 2.22 is to predict the shear stud capacity of unfavourable single or double studs. While Equations 2.23 and 2.24 are to predict the shear connector resistance of single and double studs placed in the central position respectively.

$$P_{U\text{-}EQ} = \alpha \times P_{F(0.9t)} \times (0.38t + 0.66) \quad \text{Eq. 2.22}$$

$$P_{CS\text{-}EQ} = \beta \times P_{F(0.9t)} \times (0.25t + 0.78) \quad \text{Eq. 2.23}$$

$$P_{CD\text{-}EQ} = \beta \times P_{F(0.9t)} \times (0.16t + 0.87) \quad \text{Eq. 2.24}$$

where $P_{F(0.9t)}$ is the shear connector resistance of the favourable stud with a profiled sheeting thickness of 0.9 mm, $t$ is the profiled sheeting thickness (mm), $\alpha$ and $\beta$ are factors to be taken from Table 2.4.

Table 2.4 Factors of $\alpha$ and $\beta$

| Concrete grade (MPa) | Factor $\alpha$ | | Factor $\beta$ | |
|---|---|---|---|---|
| | Single stud | Double studs | Single stud | Double studs |
| C12 | 0.85 | 0.94 | 0.99 | 0.98 |
| C20 | 0.81 | 0.87 | 0.94 | 0.96 |
| C30 | 0.76 | 0.79 | 0.90 | 0.90 |
| C40 | 0.73 | 0.77 | 0.86 | 0.88 |

Despite the applicability of these equations were confirmed against previous relevant tests, these equations, however, cannot be applied to predict the shear capacity of stud placed in a 146 mm deep decking for example. It is simply because these equations require the shear connector resistance in a favourable position to be known first. A fact that placing headed studs in a favourable or unfavourable position in a 146 mm deep decking is not an option due to the rib geometry narrowness of such steel decking.

Recently, an experimental and numerical work related to the primary composite beams was done by Chen et al. (2016). The study presented the behaviour of headed stud embedded in composite slabs with parallel steel sheeting at elevated temperatures. Eight push specimens were experimentally prepared and tested under different temperature levels ranged from 20 to 600ºC. Headed studs of 19 × 100 mm were welded through 76 mm deep decking as one single stud per connection. The elevated temperatures were concentrated at 5 and 10 mm from stud's base. For both locations, test results revealed almost 50% decrease in the shear stud capacity when the temperature was raised from 20 to 600ºC. At ambient temperature, the failure mode was combined of the stud shearing and concrete failure, while at high temperatures, the failure mode was only stud shearing.

A three-dimensional finite element model was developed in the same study using ABAQUS/Explicit package to simulate the thermal-mechanical behaviour of the headed stud. The FE model was verified against the experiments and found that the load-slip curves compared well with the experiments at different temperature levels. A parametric study was

then conducted to validate the accuracy of the design guidance in Eurocode 4 (EN1994-1-1 2005) at elevated temperatures. It was observed that the EC4 gave conservative estimations of about 10% of the FE results when the studs were heated between 300 to 600$^{o}$C. A new design equation was proposed to determine the decrease of stud connectors with increasing temperatures. It should be mentioned that the same study procedure was previously demonstrated by Chen et al. (2015) to study the behaviour of headed stud in composite slabs with perpendicular steel sheeting at elevated temperatures.

A successful 3-D FE model was developed by Katwal et al. (2018) to capture load-slip curves and different types of failure modes in composite beams. The "dynamic implicit" approach in ABAQUS was used for the analysis and the concrete material was defined by the concrete damage plasticity model (CDP). The reliability of the FE model was verified against 22 full-scale composite beams taken from 9 different studies. The nature of specimens varied from single-span beam under positive or negative moment to two-span continuous beam. The FE results showed that the load-deformation curves including the post-peak behaviour was better captured using the surface-to-surface interaction between studs and concrete than using embedded interaction or connector elements approach to simulate studs. Although this research contributed to a better understanding of the behaviour of composite beams by numerical analysis, the study limited the depth of steel decks to 80 mm at most.

## 2.5 Summary and research gaps

This chapter has presented many studies on the steel-concrete composite beams mainly with profiled steel decking. Much considerations were given to the position and number of headed stud connectors within ribs, size of stud connectors, the orientation of composite steel decks, rib deck geometries, and position and amount of slab reinforcement. To date, all composite beams that were tested with profiled steel decking had a maximum rib height ($h_p$) of 80 mm. The rib deck ratio ($b_o/h_p$) higher than 1.5 has received wide attention. As a result, all the existing design equations to determine the shear stud capacity with profiled slabs were derived based on the common steel deck shapes used in practice (60-80 mm deep deck). However, the recent production of a profiled steel decking with a very deep dimension of 146 mm and narrow geometry ($b_o/h_p$) of 0.67 exposes several questions that need to be answered.

In case of composite beams with perpendicular steel decking. Some research gaps and questions can be drawn below:

1. No research has been made to investigate the effect of steel decks in excess of 80 mm deep on the shear connector resistance, ductility and failure mode of composite beams. Doing so will certainly add fresh information to the literature.

2. With very deep and narrow deck geometry, it is unknown how the behaviour of headed stud will be different than those embedded in conventional steel decks in terms of load-slip behaviour and failure mode.

3. It is uncertain whether the available design equations with their current forms can accurately predict the shear stud capacity embedded in very deep and narrow steel deck.

4. No attempt was made to examine the alternative distribution of headed studs along ribs (i.e. presence in one rib and absence in the next rib). It is useful to address this with profiled steel decks like 100 and 146 mm deep.

5. The change in the total depth of concrete slab and embedding double steel reinforcement within the slab depth need further clarification.

6. Placing steel bars at different locations in the concrete embedded within ribs has received no attention. It is also useful to examine such parameter with very deep profiled decking.

As per composite beams with parallel steel decking. Some research gaps and questions can be addressed below:

1. Lack of research is on the behaviour of composite beams with narrow ribbed decks. All previous studies involved wide ribbed decks ($b_o/h_p \geq 1.5$). The literature needs to be enriched with rib geometries below 1.5.

2. Because the existing design equations were derived from the geometries of wide and mid-deep steel decks, it is unclear that those formulae can be reliable to predict the shear stud capacity with narrow and very deep steel decks.

3. Based on previous studies, the increase in the rib deck ratio is said to increase the shear connector resistance. Given the rib ratio of 146 mm deep deck is 0.67, the shear stud capacity would be theoretically low. However, the author is not convinced about this concept, feeling a necessity to examine the correlation between narrow and wide ribbed decks regarding the shear stud capacity.

4. The concrete part surrounds the headed studs is subjected to a pure shear force during the push tests. This suggests that the area of concrete particularly where the studs are placed could be a function of the shear connector resistance. The lack of research on this aspect requires further investigation to clarify that.

5. The parametric study should be extended to cover the sheeting thickness up to 2.0 mm and the influence of large diameter of headed stud of 22 mm.

The following chapters will bridge the above-mentioned research gaps and add a new insight into the understanding of the behaviour of composite beams with profiled steel decking.

# Chapter 3 Development of Finite Element Models for Push-off Tests

# Chapter 3

# Development of Finite Element Models for Push-off Tests

## 3.1 Introduction

This chapter aims to develop a suitable three-dimensional finite element model using ABAQUS. Push-off tests with trapezoidal profiled sheeting oriented perpendicular and parallel to the steel beam are modelled to simulate the behaviour of headed shear studs in composite beams. Through the numerical modelling, some techniques are investigated namely mass scaling factor, mesh size of elements and loading rate to achieve the best compromise between accuracy and computational efficiency. The results are then validated against experiments based on the shear connector resistance, load-slip behaviour, and modes of failure. Eventually, the most efficient techniques that give accurate results will be adopted for further investigations in the next chapters.

## 3.2 ABAQUS Finite Element Analysis

This work uses ABAQUS to simulate push tests with trapezoidal profiled sheeting and study the behaviour of composite beams. In case of structural parts, both ABAQUS/Standard and ABAQUS/Explicit can be used with linear and non-linear finite element applications. ABAQUS can simulate structures with complicated contact interaction like composite beams. Several researchers such as Nguyen and Kim (2009), Mirza and Uy (2010) and Wang (2011) used ABAQUS package to investigate the behaviour of push test with or without profiled sheeting. ABAQUS was found very effective at predicting the mechanism of load-slip capacity and mode of failure in push tests.

ABAQUS/Explicit is seen to be more effective than ABAQUS/Standard in analysing complicated contact interaction between a profiled sheeting and concrete in composite beams. ABAQUS/Explicit is suitable for nonlinear applications, complicated contact interaction and damage patterns. With large models, the finite element analysis consumes much time and computer memory due to the equilibrium iteration. Also, the material damage and failure cause convergence problems which often happen with the static method such as

the RIKS. Thus, the actual load capacity and failure could not be simulated. However, the dynamic explicit analysis method does not encounter iteration or convergence issues during the analysis. This is because the explicit time integration method does not solve the complex inverse stiffness matrix directly, but instead, it solves for the simpler mass matrix then updates the stiffness matrix at the end of each time increment and carries it to the next. Concrete is defined as a brittle material and expected to fail suddenly with a significant drop in the load capacity; this approach can be obtained using ABAQUS/Explicit. As a push test requires a quasi-static solution, it is essential to apply slow load which reduces the inertia effects to the lowest possible.

Qureshi (2010) found that ABAQUS/Explicit was significantly more applicable than ABAQUS/Standard in simulating push tests with profiled sheeting. Both Standard and Explicit methods were used, but the Explicit method was more effective at catching the load-slip capacity and failure modes of numerical push tests. Similarly, the Explicit method was used by Chen et al. (2015), and Chen et al. (2016) to study the performance of composite beams with perpendicular and parallel profiled sheeting at elevated temperatures. Accordingly, the current research will use the Explicit method to model and investigate the performance of composite beams with very deep profiled sheeting.

## 3.3 General description of validated push-off tests with perpendicular sheeting

The numerical models were verified against previous tests conducted by Smith and Couchman (2010) and Rambo-Roddenberry (2002). The dimensions of the push-off tests are summarised in Table 1. The study initially modelled the push-off tests carried out by Smith and Couchman (2010). The test set up had two concrete slabs connected to an I-steel beam with dimensions of 203 × 102 × 30 kg/m. The general arrangement of the push test is shown in Figure 3.1. The specimens were subjected to a vertical hydraulic jack on the top surface of the steel beam, an additional load as much as 12 % of the total vertical load was also applied to the exposed concrete surfaces. Note that the research by Rambo-Roddenberry (2002) was conducted without the additional normal load. The current research considered two different push-off tests set up to ascertain the ability of the FE model to simulate the behaviour of composite beam under different conditions.

The width of the concrete slab was 750 mm, and the total depth varied from 140 mm to 225 mm. The concrete slab was reinforced with one layer of A193 mesh fabric (7 mm in diameter) having 200 mm centre to centre spacing. A stud dimension of 19 × 100 mm was used and placed in a favourable position due to the existence of stiffeners in the bottom centre of profiled sheeting. The profiled sheeting had a total net depth of 60 mm, average trough width of 150 mm, and sheeting thickness of 0.9 mm. The parametric study involved the slab depth change, number of headed studs per trough, transverse spacing between stud pairs, and the wire-mesh position. In some specimens, the wire-mesh was rested on top of the sheeting, while in other specimens it was placed 25 mm below the top surface of the concrete slab.

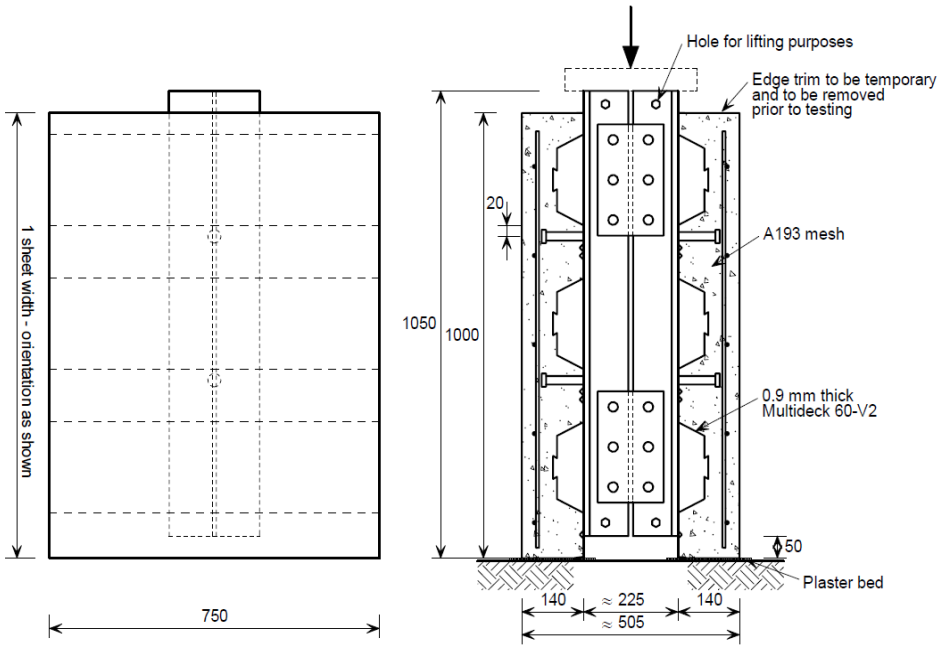


Figure 3.1 Push-off test arrangement (Smith and Couchman 2010)

Table 3.1 Push-off test sets and dimensions of validated studies

| Series | Concrete strength $f_c$ (MPa) | Profiled sheeting (mm) | | | Headed stud (mm) | | | | Slab dimension (mm) | | | Tested by |
|---|---|---|---|---|---|---|---|---|---|---|---|---|
| | | $t_s$ | $b_o$ | $h_p$ | $d$ | $h_{sc}$ | $n_r$ | Position | $L$ | $W$ | D | |
| D20 | 24.2 | 0.9 | 152.4 | 76.2 | 9.5 | 127 | 1 | F | 914.4 | 914.4 | 152.4 | Rambo-Roddenberry (2002) |
| D21 | 24.2 | 0.9 | 152.4 | 76.2 | 22 | 127 | 1 | F | 914.4 | 914.4 | 152.4 | |
| D22 | 24.2 | 0.9 | 152.4 | 76.2 | 9.5 | 127 | 1 | U | 914.4 | 914.4 | 152.4 | |
| D23 | 24.2 | 0.9 | 152.4 | 76.2 | 22 | 127 | 1 | U | 914.4 | 914.4 | 152.4 | |
| D24 | 24.2 | 1.5 | 76.2 | 114.3 | 19 | 152.4 | 1 | C | 914.4 | 914.4 | 171.5 | |
| D25 | 24.2 | 1.5 | 88.9 | 152.4 | 19 | 197 | 1 | C | 914.4 | 914.4 | 222.3 | |
| A1U | 18.92 | 0.9 | 155 | 60 | 19 | 100 | 1 | F | 1000 | 750 | 140 | Smith and Couchman (2010) |
| A1D | 19.04 | 0.9 | 155 | 60 | 19 | 100 | 1 | F | 1000 | 750 | 140 | |
| B1U | 19.05 | 0.9 | 155 | 60 | 19 | 100 | 1 | F | 1000 | 750 | 225 | |
| A2DX | 19.32 | 0.9 | 155 | 60 | 19 | 100 | 2 | F | 1000 | 750 | 140 | |
| A2UY | 19.32 | 0.9 | 155 | 60 | 19 | 100 | 2 | F | 1000 | 750 | 140 | |
| A2DY | 21.07 | 0.9 | 155 | 60 | 19 | 100 | 2 | F | 1000 | 750 | 140 | |
| A2DZ | 19.32 | 0.9 | 155 | 60 | 19 | 100 | 2 | F | 1000 | 750 | 140 | |
| B2U | 18.92 | 0.9 | 155 | 60 | 19 | 100 | 2 | F | 1000 | 750 | 225 | |
| A3D | 18.92 | 0.9 | 155 | 60 | 19 | 100 | 3 | F | 1000 | 750 | 140 | |

## 3.4 Finite Element Modelling of push tests with perpendicular sheeting

Ideally, the total load in push test transfers equally to all headed studs that embedded inside the concrete slab. Thus, the strength of a headed stud is measured by dividing the total load by the number of headed studs. Accordingly, only one concrete slab geometry was modelled due to the symmetry alongside the centre line of steel beam web. This technique is appropriate to reduce the computational time. The finite element model consisted of steel beam, headed shear studs, profiled steel sheeting, concrete slab, and wire-mesh reinforcement. All parts are assembled to produce the push model as shown in Figure 3.2. The reason for modelling multiple troughs rather than one or two troughs is to achieve the closest behaviour of composite beams.

ABAQUS/Explicit provides linear geometric order for stress/displacement analysis. It also provides quadratic beam and modified tetrahedron and triangle elements, yet they are beyond the scope of this study. Hence, all finite elements are meshed using the linear geometric order. During the analysis, numerical methods are used by ABAQUS to integrate various quantities over the volume of each element; the material response is calculated at each integration point in most elements using Gaussian quadrature technique. Full or reduced integration can be used for elements; the latter approach is significantly effective in reducing shear locking in solid elements and computational time of the analysis. Shear locking occurs when the deformation in finite element analysis bends, and there are not enough elements across the geometry to capture the distortion. Thus, the stiffness of the structure is remarkably overestimated (ABAQUS Documentation, 2014).

For steel beam, headed shear stud and concrete parts, three-dimensional continuum eight-node reduced integration elements were used to model those parts and referred to as (C3D8R). Also, a three-dimensional six-node wedge element was used in some places where elements were triangular prism and referred to as (C3D6R). A four-node doubly curved shell element with reduced integration (S4R) was used for the profiled steel sheeting part, using this approach allows the stress and strains to be calculated separately at each integration point through the shell thickness and enables the non-linear material behaviour to occur. Finally, a two-node three-dimensional truss element (T3D2) was used to model the wire-mesh reinforcement.

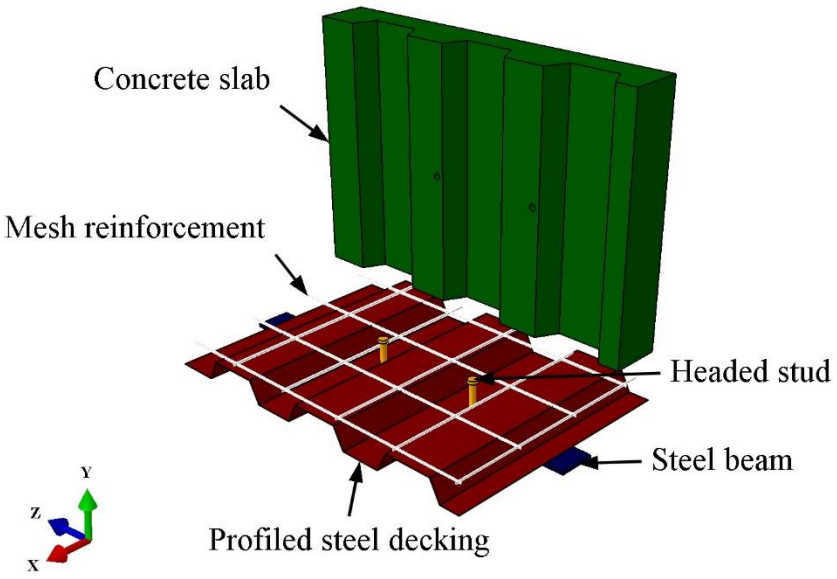


(a) Push test assembly with uplifted concrete slab

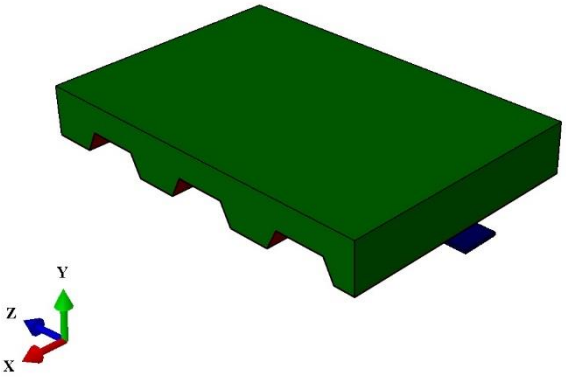


Figure 3.2 Finite element push test arrangement for Smith and Couchman (2010)

## 3.5 Material modelling for steel parts

The behaviour of a steel material is considered linear elastic until the yielding point $f_y$. Afterwards, the behaviour tends to be non-linear plastic. In the finite element modelling, the headed shear stud part was modelled together with the steel beam. However, the properties of materials were different. Because the steel beam has no effect on the behaviour of headed studs during the push test, so the steel beam part was treated as elastic material, this approach was successfully used in Qureshi and lam (2012). The Young's modulus of elasticity of the

steel beam was taken as 210 GPa, while 200 GPa was assumed for the headed studs, profiled sheeting and wire-mesh reinforcement.

The headed studs and profiled sheeting were considered fully plastic. The yield stress for headed studs and profiled sheeting were taken as 475.6 MPa and 350 MPa respectively the same as in Smith and Couchman (2010). The properties for wire-mesh reinforcement is not mentioned in the validated research, so the nominal yield stress is taken as 627 MPa (Hicks and Smith, 2014). Finally, the density of all steel parts was taken as 7800 kg/m$^3$.

## 3.6 Material modelling for Concrete

The concrete material in a push-off test has a significant effect on the general behaviour of the test. The compressive strength of concrete is assumed as one of the main functions of failure in composite beams. Modelling a concrete material using the finite element method is very important to simulate the real failure mechanism and obtain accurate results. Concrete is defined as a brittle material in which inelastic behaviour is considered. Several techniques are provided in ABAQUS library to model concrete such as Concrete Smeared Cracking, Brittle Cracking, Drucker-Prager Hardening and Concrete Damage Plasticity.

The current research uses the Concrete Damage Plasticity to define the concrete material, which is briefly discussed in the next section. The reason this method was selected is because its capability of capturing the inelastic behaviour of concrete in both compression and tension, and representing the softening behaviour in compression and tension. While other methods such as Brittle Cracking and Concrete Smeared Cracking are tensile related models, meaning that it is not possible to capture the behaviour of concrete under compression. Moreover, these methods are more sensitive to the analysis when compared to the Concrete Damage Plasticity which can cause convergence problems.

### 3.6.1 Concrete Damage plasticity (CDP)

The Concrete Damage Plasticity model is suitable to model the behaviour of concrete under any load condition whether it is static or dynamic, or even both combined. The inelastic behaviour of concrete was modelled based on the isotropic damage plasticity, isotropic tensile and compressive plasticity. Concrete Damage Plasticity takes into account the degradation of the elastic stiffness which is caused by the plastic straining in compression

and tension. Two main failure mechanisms define this model namely tensile cracking and compressive crushing. Softening stress-strain response represents the post-failure under compression. While tension stiffening represents the strain softening of the concrete cracks (ABAQUS Documentation 2014).

#### 3.6.1.1 Plasticity parameters

Non-linear volume change is observed in concrete during hardening; this trend is indicated as dilation. Previous studies showed that inelastic volume change happens at the beginning of yielding, while volume dilation occurs between 75 to 90% of ultimate stress ($f_{ck}$). A potential plastic function can represent the dilation while the yield surface is used for the flow rule (Kmiecik and Kaminski 2011). Table 3.2 shows the parameters for Concrete Damage Plasticity model; the values were taken as default from ABAQUS Documentation (2014), except the dilation angle was assumed 36°.

Table 3.2 Parameters for Concrete Damage Plasticity model

| $\Psi$ | ε | $f_{b0} / f_{c0}$ | $K$ | $\mu$ |
|---|---|---|---|---|
| 36° | 0.1 | 1.16 | 0.667 | 0 |

where

$\Psi$ = The dilation angle in the $p$-$q$ plane at high confining pressure. Where $p$ is the hydrostatic pressure stress, and $q$ is the Mises equivalent effective stress.

ε = The flow potential eccentricity which is calculated as a ratio of tensile strength to compressive strength.

$f_{b0} / f_{c0} = \sigma_{b0} / \sigma_{c0}$ is a ratio of the strength in the biaxial state to the strength of the uniaxial state.

$K$ = The ratio of the second stress invariant on the tensile meridian, $q$(TM), to that on the compressive meridian, $q$(CM), at initial yield for any given value of the pressure invariant $p$ such that the maximum principal stress is negative, $\sigma_{max} < 0$. It must satisfy the condition $0.5 < K_c \leq 1$.

$\mu$ = The viscosity parameter, it is used for the visco-plastic regularisation of the concrete constitutive equations in Abaqus/Standard analyses. This parameter is ignored in Abaqus/Explicit.

### 3.6.1.2 Compressive behaviour

The general non-linear behaviour of concrete stress-strain relationship is illustrated in Figure 3.3. To define the values of compressive stress responses to inelastic strain in CDP input, Equation 3.1 was used for that purpose which is suggested by BS EN 1992-1-1.

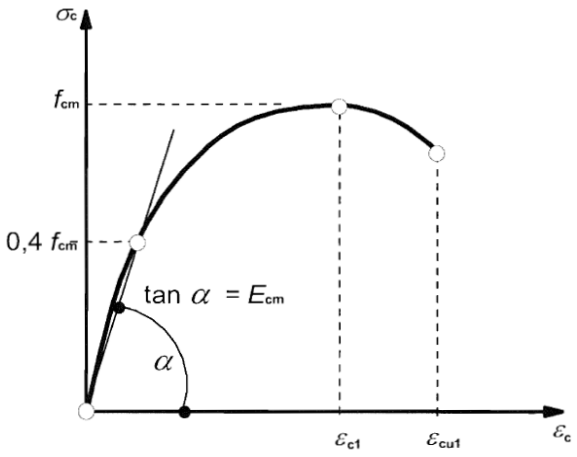


Figure 3.3 Stress-strain relationship of concrete material (BS EN 1992-1-1)

$$\sigma_c = f_{cm}\frac{k\eta - \eta^2}{1+(k-2)\eta} \qquad \text{Eq. 3.1}$$

where

$\sigma_c$ = Compressive stress in concrete

$f_{cm}$ = Mean compressive strength of concrete ($f_{ck}$ + 8) (MPa)

$\eta = \varepsilon_c / \varepsilon_{c1}$

$\varepsilon_c$ = Compressive strain in concrete

$\varepsilon_{c1}$ = Compressive strain in concrete at the peak stress $f_c$, ($0.7 f_{cm}^{0.31} \leq 0.0028$)

$$K = \frac{1.05 Ecm \times |\varepsilon_c|}{f_{cm}}$$

In Figure 3.3, $\varepsilon_{cu1}$ is the ultimate nominal strain which equals 0.0035 when the characteristic compressive strength $f_{ck}$ of concrete varies from 12 to 50 MPa. If the characteristic compressive strength is larger than 50 MPa, the ultimate nominal strain is calculated by Equation 3.2 according to BS EN 1992-1-1. For Smith and Couchman (2010) push tests, the characteristic compressive strength $f_{ck}$ and mean compressive strength $f_{cm}$ are 12 and 20 MPa respectively. Therefore, the stress-strain curve of concrete can be seen in Figure 3.4.

$$\varepsilon_{cu1} = 2.8 + 27\,[(98 - f_{cm}) / 100]^4 \qquad \text{Eq. 3.2}$$

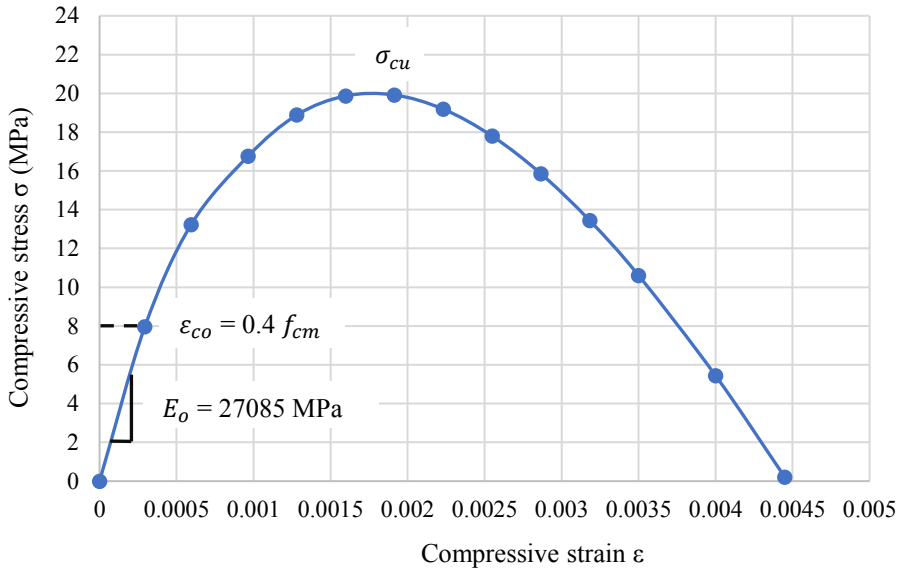


Figure 3.4 Stress-strain curve of concrete

Under compressive loading, concrete material responds linearly up to the initial yield stress $\sigma_{co}$ as shown in Figure 3.5. After that, the material acts nonlinearly until the ultimate compressive stress $\sigma_{cu}$ which is characterised by stress hardening, the plastic response continues subsequently to the end with strain softening where the post-failure behaviour of concrete is identified. The elastic stiffness of the concrete reduces when the load is increased at any point on the strain softening of the stress-strain curve, this stage is represented by compressive damage variables $d_c$.

Compressive damage variables in concrete are calculated using Equation 3.3 as given in the ABAQUS Documentation (2014). The obtained values should be neither negative nor decreasing as the stresses increase because it will lead to errors before the finite element analysis starts. The zero values indicate that the concrete material is undamaged, while 1 indicates full damage. In ABAQUS, the damaged compressive values are entered versus the compressive inelastic stain (crushing stain) $\varepsilon_c^{\sim in}$ that is calculated from Equation 3.4 in the ABAQUS Documentation (2014).

$$d_c = 1 - (\sigma_c / f_{cm}) \qquad \text{Eq. 3.3}$$

$$\varepsilon_c^{\sim in} = \varepsilon_c^{\sim pl} + \frac{d_c}{1-d_c} \cdot \frac{\sigma_c}{E_0} \qquad \text{Eq. 3.4}$$

$E_o$ considers the elastic stiffness of undamaged concrete, $\sigma_c$ is the yield stress, and $\varepsilon_c^{\sim pl}$ is the compressive plastic strain.

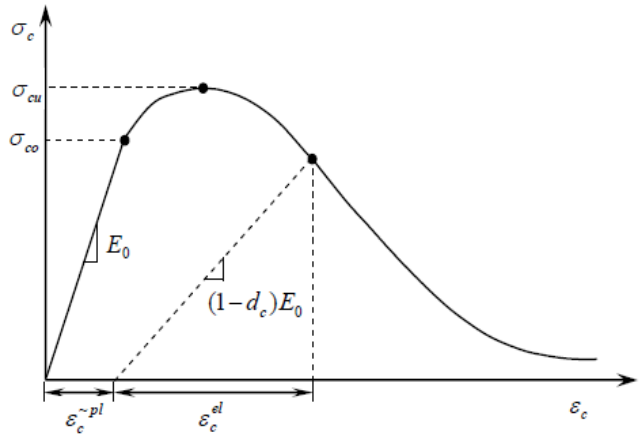


Figure 3.5 Uniaxial loading response of concrete in compression (ABAQUS Documentation 2014)

### 3.6.1.3 Tensile behaviour

There are two ways to define the tensile behaviour of concrete in ABAQUS namely stress-strain relationship in tension or the brittle behaviour which is demonstrated by fracture energy cracking. The post-failure stress-strain approach is used to simulate concrete material with steel reinforcement, while the fracture energy cracking method is used for concrete with little or no reinforcement as in push tests. Fracture energy $G_f$ is defined as the energy needed to

form a unit area of crack (Hillerborg et al. 1976). The fracture energy to any concrete grade is represented by the stress-crack opening curve, particularly the area under the unloading part (ABAQUS Documentation 2014).

The softening behaviour of concrete in tension can be calculated using the linear function as shown in Figure 3.6(a) from The ABAQUS Documentation (2014). The linear function is reliable in giving accurate results, yet the response of the material is likely to be stiff. Hillerborg (1985) proposed a bilinear function as presented in Figure 3.6(b) to evaluate the softening behaviour of concrete, the bilinear function tends to be more precise than the linear function. However, Qureshi (2010) successfully used an exponential function as shown in Figure 3.6(c) which was derived by Cornelissen et al. (1986). The latter approach was found to be the most suitable way to represent the softening behaviour of concrete. Therefore, this research uses the exponential function for all push test models.

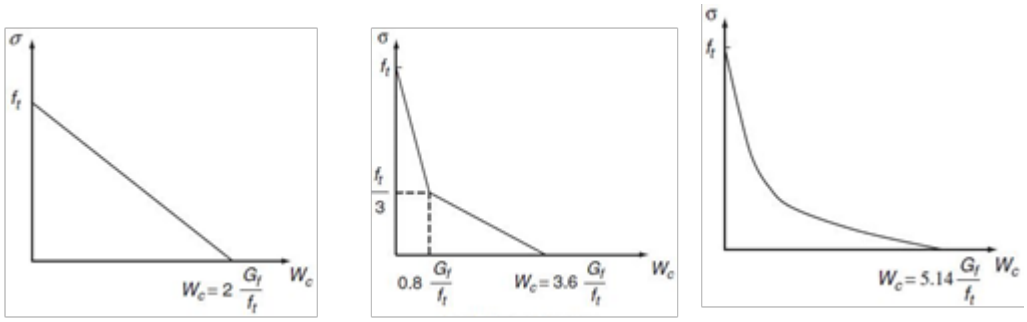


(a) Linear function (b) Bilinear function (c) Exponential function

Figure 3.6 Linear (ABAQUS manual), Bilinear (Hillerborg, 1985) and Exponential (Cornelissen et al. 1986) functions for softening behaviour of concrete in tension

The tensile stress $\sigma_t$ versus crack opening displacement is calculated from Equation 3.5. For those push tests which have the characteristic compressive strength of 12 MPa, the tensile stress versus cracking displacement curve is shown in Figure 3.7.

$$\sigma_t = f_t \left( f(w) - \frac{w}{w_c} f(w_c) \right) \quad \text{Eq. 3.5}$$

$$f(\mathrm{w}) = \left[ 1 + \left( \frac{c_1 w}{w_c} \right)^3 \right] \exp\left( -\frac{c_2 w}{w_c} \right) \quad \text{Eq. 3.6}$$

where

$w$ = the crack opening displacement

$w_c$ = the ultimate crack opening displacement and can be calculated from equation ($w_c = 5.14\ G_f / f_t$)

$c_1$ and $c_2$ = material constants which are taken as 3.0 and 6.93 respectively for normal density concrete

The fracture energy was measured from equation $G_f = G_{fo}\ (f_{cm} / f_{cmo})^{0.7}$ as suggested by MC 10 CEB-FIP design code. $f_{cmo}$ equals 10 represents the base value of mean compressive cylinder strength. $G_{fo}$ is obtained from Table 3.3, and it is the base value of the fracture energy and depends on the maximum aggregate size. Finally, the tensile damage variable was measured from the formula ($d_t = 1 - \sigma_t / f_t$), the tensile damage values against cracking displacement for the characteristic compressive strength of 12 MPa is shown in Figure 3.8.

Table 3.3 Base values of fracture energy $G_{fo}$ (MC 10 CEB-FIP, 2010)

| $d_{max}$ (mm) | $G_{fo}$ (Nmm/mm$^2$) |
|---|---|
| 8 | 0.025 |
| 16 | 0.030 |
| 32 | 0.058 |

where $d_{max}$ is the maximum aggregate size in mm.

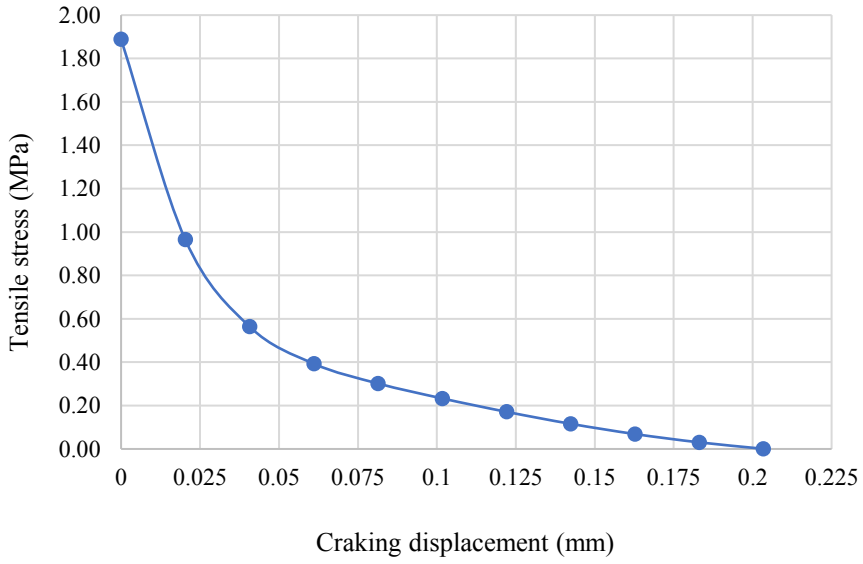


Figure 3.7 Tensile stress versus cracking displacement curve

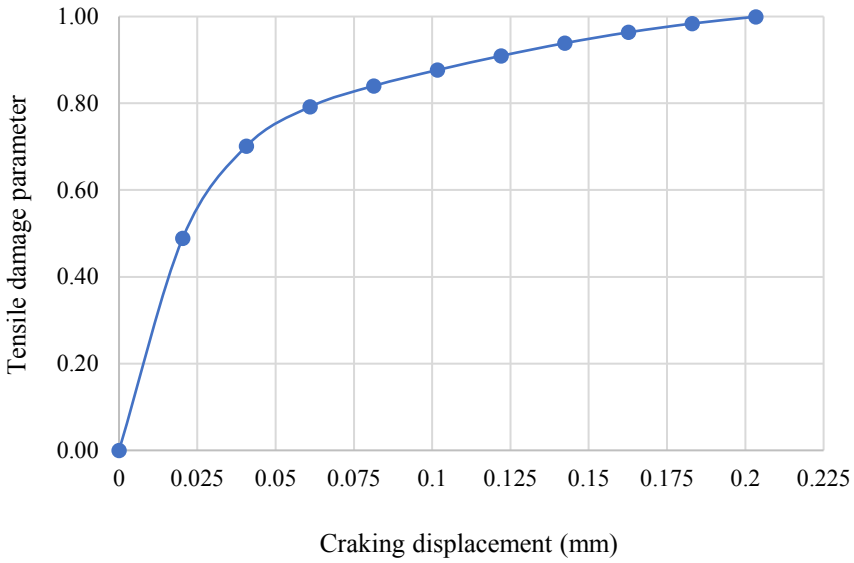


Figure 3.8 Tensile damage variables versus cracking displacement curve

## 3.7 Contact interactions and constraints

A surface to surface contact pair algorithm was used to define stud-concrete and deck-concrete contact surfaces. The tangential and normal behaviour were used to define the interaction properties between surfaces. The normal behaviour was defined by the default option "Hard" contact pressure-overclosure relationship. This option ensures minimum penetration of a slave surface into a master surface. The tangential behaviour was defined via the frictional penalty formulation with a coefficient of friction of 0.5 as recommended by EC4. The stud-concrete contact was defined by treating the stud as a master and concrete as a slave surface. In deck-concrete contact, concrete surface was taken as master due to its higher stiffness and steel deck as a slave. The beam-deck contact was specified by general contact algorithm with the frictionless formulation.

In experiments, headed shear studs are welded to the flange surface of steel beam through the profiled sheeting. Hence, the constraint mechanism between headed studs and steel beam in the finite element model was already fixed as both materials were modelled as one part. This means headed stud splits from the steel beam when the physical material of headed stud fails. By using the tie constraint method, the nodes of profiled sheeting around the headed stud circumference were tied to the nodes of the headed shank at the base. The wire-mesh reinforcement was embedded in the concrete slab using the embedded constraint method.

## 3.8 Boundary conditions

In push-off tests done by Smith and Couchman (2010), two concrete slabs were connected by a steel beam and placed vertically to the ground. A vertical load was applied on the upper surface of the steel beam, alongside an additional load (normal load) which was subjected horizontally to the exposed concrete surfaces. In finite element analysis, only one side of the concrete slab was modelled. Therefore all nodes of the lower surface of steel beam as indicated in Figure 3.9 was restricted from moving in the Y direction and rotation in the X and Z direction due to symmetry. The surface of the profiled sheeting and concrete slab which was layered on the ground was presented by surface 2 and restrained from moving in the Z direction as shown in Figure 3.9.

The vertical load (shear load) which was applied on the top surface of the steel beam is represented by Surface 3 in the finite element model as shown in Figure 3.9. The normal load was applied on the concrete surface in the finite element model and indicated as Surface 4 in Figure 3.9. The amount of normal load was taken as 12% of the total vertical load similar to experiments. In the finite element analysis, the normal load had been applied before the vertical load, the same as in the experiment.

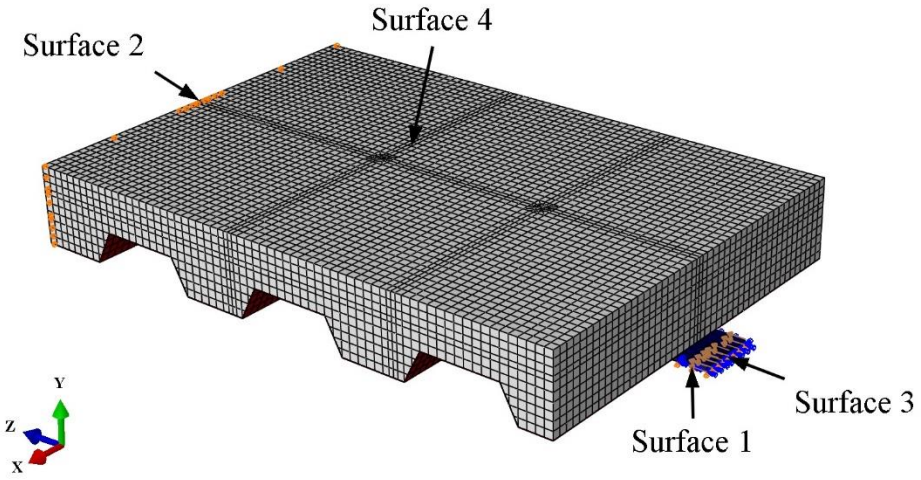


Figure 3.9 Boundary conditions in finite element models of Smith and Couchman (2010)

## 3.9 Convergence study

It is important to select the most effective techniques in finite element analysis that simulates the real behaviour of structure to avoid obtaining wrong results. The mesh element size, mass scaling factor and loading rate are likely to affect the accuracy of results. Initially, the first three specimens conducted by Smith and Couchman 2010 (i.e. A1U, A1D and B1U) were modelled and investigated based on the three different approaches. The achieved results were then validated against the experiments regarding shear connector resistance. The most efficient technique that shows good agreement with the experiment will be selected and used for further finite element models in this thesis.

### 3.9.1 Mass scaling factor

The mass scaling factor is often used in ABAQUS/Explicit to control the load increment and make the overall dynamic behaviour of the model negligible. The quasi-static solution in dynamic explicit is ensured by applying the load very slowly. There are two ways to achieve that solution, either specifying the mass scaling factor or increasing the time increment. The mass scaling factor is introduced in this research, and three amounts of mass scaling were checked namely 10, 100 and 1000. The ratio of kinetic energy to internal energy (ALLKE/ALLIE) of the model should always be less than 10% to ensure the stability during analysis and obtain the quasi-static solution. The initial mesh size element and loading rate were taken as 15 × 15 mm and 0.25 mm/sec respectively. The relationship between the kinetic energy and internal energy versus slip capacity for 10, 100 and 1000 mass scaling are presented in Figure 3.10. The results were taken from the sample A1U; the 10 % limit is referred as 0.1 in all curves.

Results exhibited that using the mass scaling factor of 1000 led to exceed the 10% limit, so this approach is neglected. Although 100 mass scaling resulted in 3%, it may not be safe for the remaining study as the ratio might exceeds the 10% limit under different conditions. Using mass scaling factor of 10 is then considered the most appropriate way to ensure the quasi-static solution as the ratio is minimal which can be reliable to use under any condition. Hence, mass scaling factor of 10 will be applied to all finite element push models in this study.

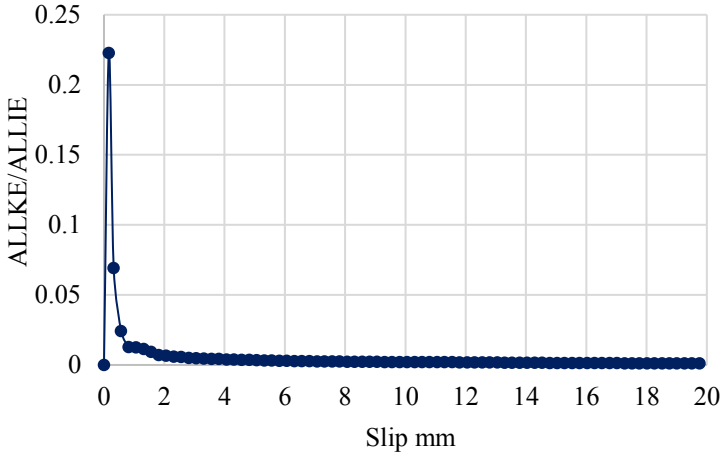


(a) Mass scaling factor of 1000

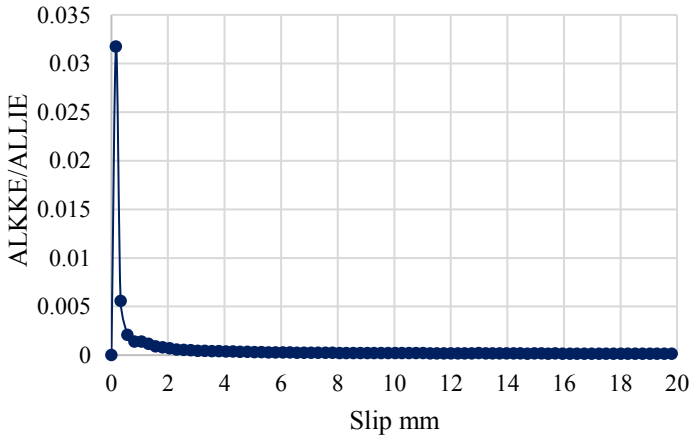


(b) Mass scaling factor of 100

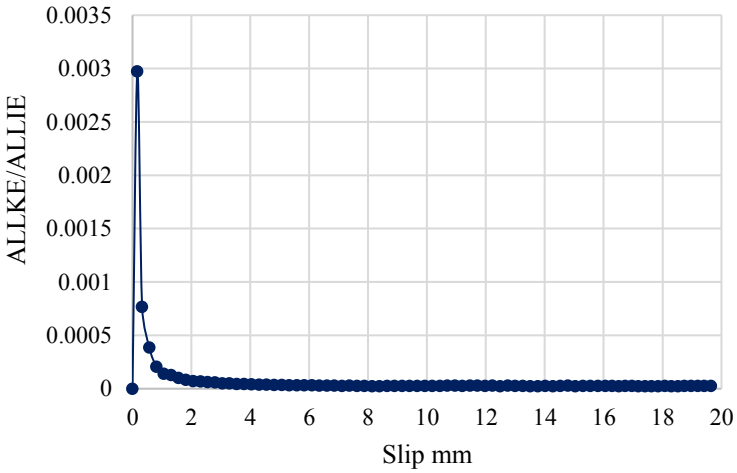


(c) Mass scaling factor of 10

Figure 3.10 The ratio of kinetic energy over internal energy versus slip capacity

### 3.9.2 Mesh element size

Three types of element size were explored, namely a fine mesh of 10 × 10 mm, a medium-mesh of 15 × 15 mm and a coarse mesh of 20 × 20 mm as shown in Figure 3.11. The mass scale factor and loading rate were taken as 10 and 0.25 mm/sec respectively. Numerical results were then compared to the experiments based on the accuracy and computational time. Numerical results of the experiments are illustrated in Table 3.4.

Table 3.4 Comparison results between numerical and experiment for different mesh size

| Test ref. | Average $P_{exp.}$ (kN) | Mesh size 10 × 10 | | Mesh size 15 × 15 | | Mesh size 20 × 20 | |
|---|---|---|---|---|---|---|---|
| | | $P_{FE}$ (kN) | $P_{exp.}/P_{FE}$ | $P_{FE}$ (kN) | $P_{exp.}/P_{FE}$ | $P_{FE}$ (kN) | $P_{exp.}/P_{FE}$ |
| A1U | 91.21 | 88.9 | 1.02 | 89.6 | 1.02 | 94.9 | 0.96 |
| A1D | 116.42 | 107.7 | 1.08 | 109.9 | 1.06 | 118.3 | 0.98 |
| B1U | 112.11 | 109 | 1.03 | 111.8 | 1 | 116.3 | 0.96 |

From Table 3.4, it is obvious that the numerical results with the coarse mesh size 20 × 20 overestimated the headed stud capacity in experiments. As for both fine and medium mesh size, all numerical results were in good agreement with experiments, yet the computational time should be considered. The fine mesh size took much longer time than the medium mesh size to finish. Thus it is more effective to use the medium mesh size 15 × 15 in further investigations due to its accuracy and time-saving.

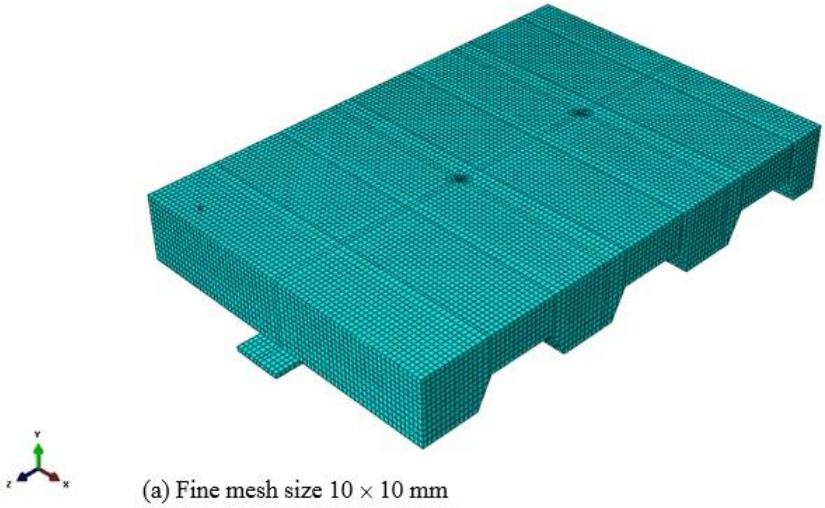

(a) Fine mesh size 10 × 10 mm

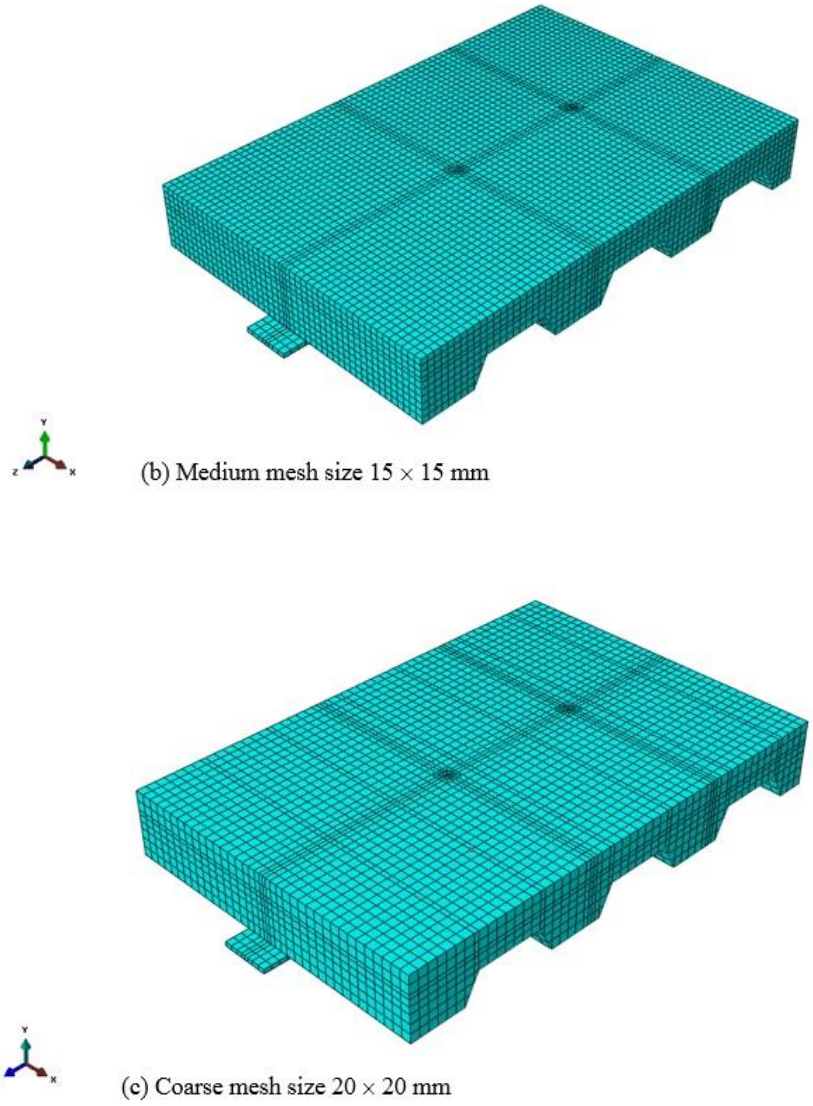


Figure 3.11 Mesh element sizes for A1U

### 3.9.3 Loading rate

In the finite element analysis, the samples were pushed by applying a uniform velocity at the loading surface as shown in Figure 3.9. To ensure the stability of the uniform velocity, a smooth amplitude function was applied as suggested by ABAQUS Documentation (2014) to manage the uniform velocity along the time analysis. The loading rates were 0.1, 0.25, 0.5, and 1 mm/sec. Three push models namely A1U, A1D, and B1U were examined for this purpose; the finite element models were performed using 15 × 15 mesh size with a mass scale factor of 10. The best loading rate was selected based on the accuracy of results and computational time. Numerical results against experiments are presented in Table 3.5.

Table 3.5 Comparison of numerical and experimental results for different loading rates

| Test ref. | Average $P_{exp.}$ (kN) | Loading rate 0.1 mm/sec | | Loading rate 0.25 mm/sec | | Loading rate 0.5 mm/sec | | Loading rate 1 mm/sec | |
|---|---|---|---|---|---|---|---|---|---|
| | | $P_{FE}$ | $P_{exp.}/P_{FE}$ | $P_{FE}$ | $P_{exp.}/P_{FE}$ | $P_{FE}$ | $P_{exp.}/P_{FE}$ | $P_{FE}$ | $P_{exp.}/P_{FE}$ |
| A1U | 91.11 | 90 | 1.01 | 89.6 | 1.02 | 90.4 | 1 | 91.6 | 0.99 |
| A1D | 116.42 | 111.1 | 1.05 | 109.9 | 1.06 | 111.6 | 1.04 | 113 | 1.03 |
| B1U | 112.11 | 111.1 | 1 | 111.8 | 1 | 112 | 1 | 112.5 | 0.99 |

It can be noticed that all loading rate resulted in a good agreement with experiments. However, the ratio of kinetic energy to internal energy versus slip capacity exceeded the 10 % limit in case of the loading rate of 1 mm/sec, so this amount of loading rate was neglected. The rest of loading rates did not lead the ratio of kinetic energy to internal energy versus slip capacity to exceed the 10 % limit, besides all numerical results were conservative. The loading rate of 0.5 mm/sec gave the best results in terms of accuracy and computational efficiency. Hence, a loading rate of 0.5 mm/sec is adopted for this research.

## 3.10 Validation of FE models: perpendicular sheeting

After choosing the best techniques in dealing with the push test models, these were applied to the rest of the experiments from Smith and Coachman (2010) and Rambo-Rodenberry (2002). The shear connector resistance, load-slip behaviour, and failure modes were obtained. The comparison between the FE results and experiments is reported in Table 3.6. The FE results showed a close agreement with experiments, the average ratio of $P_{Test}/P_{FE}$ is 0.97, and the coefficient of variation is 8.86%. In case of Smith and Couchman (2010), the slip at the intersection of a straight line at a characteristic load level and falling branch of the load-slip curve is termed as the characteristic slip capacity. The characteristic shear stud resistance was measured from BS EN 1994-1-1, clause 6.6.3.1, whereas the nominal stud strength is not divided by the partial factor (recommended as 1.25). The characteristic values in the finite element models were determined in the same way as in the experiments. Slip capacities of the push tests conducted by Rambo-Roddenberry (2002) are not provided, therefore slip capacities obtained from the numerical analysis are not considered for verification.

Numerical load versus slip curves are compared with selected experiments in Figures 3.12-14. In case of the validated specimens from Rambo-Roddenberry (2002), the failure mode was concrete cone and stud shearing for the series D20-21, rib punching and stud shearing for the series D22-23, and rib shearing or (rib cracking) for the series D24-25 which incorporate profiled sheeting greater than 100 mm deep (see Figure 3.15). A very similar failure pattern was observed in the numerical models.

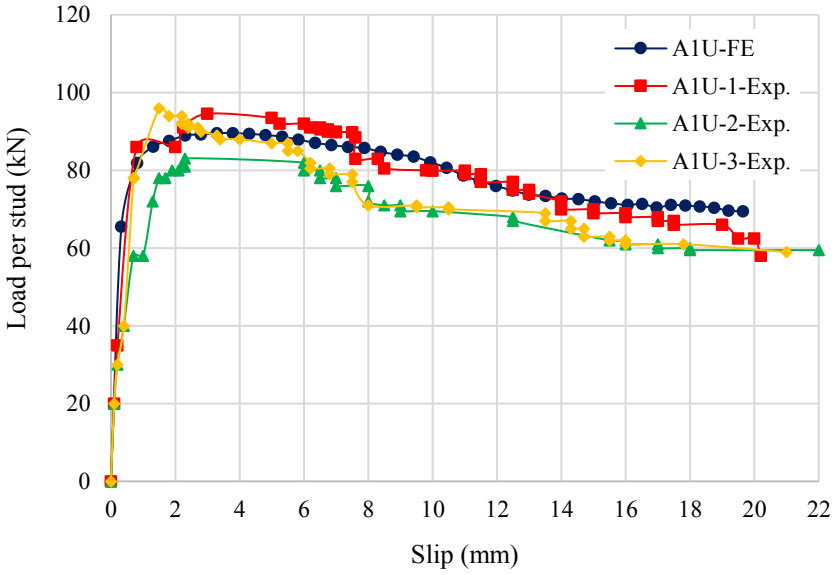


Figure 3.12 Experimental and numerical load-slip behaviour comparison for push test A1U

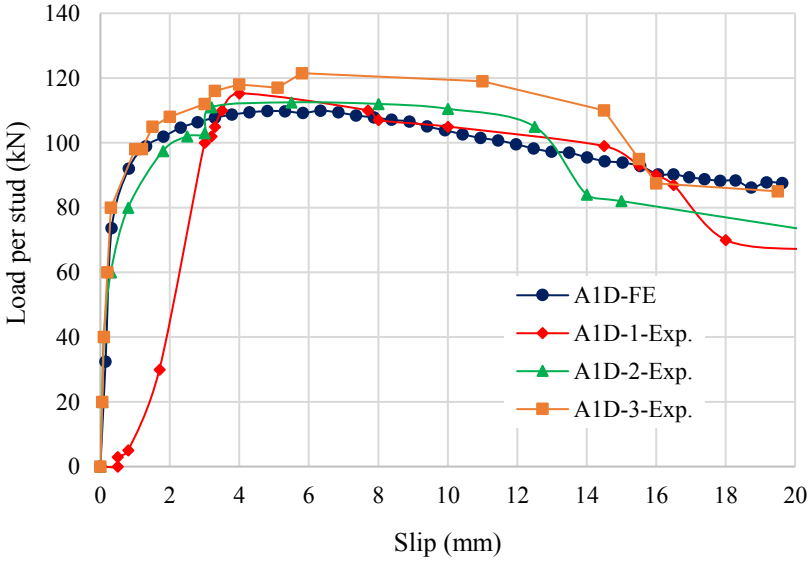


Figure 3.13 Experimental and numerical load-slip behaviour comparison for push test A1D

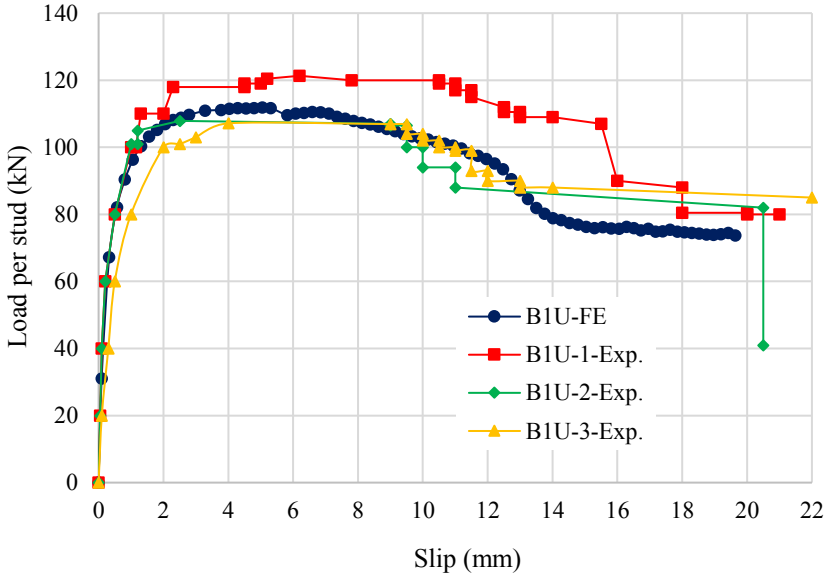


Figure 3.14 Experimental and numerical load-slip behaviour comparison for push test B1U

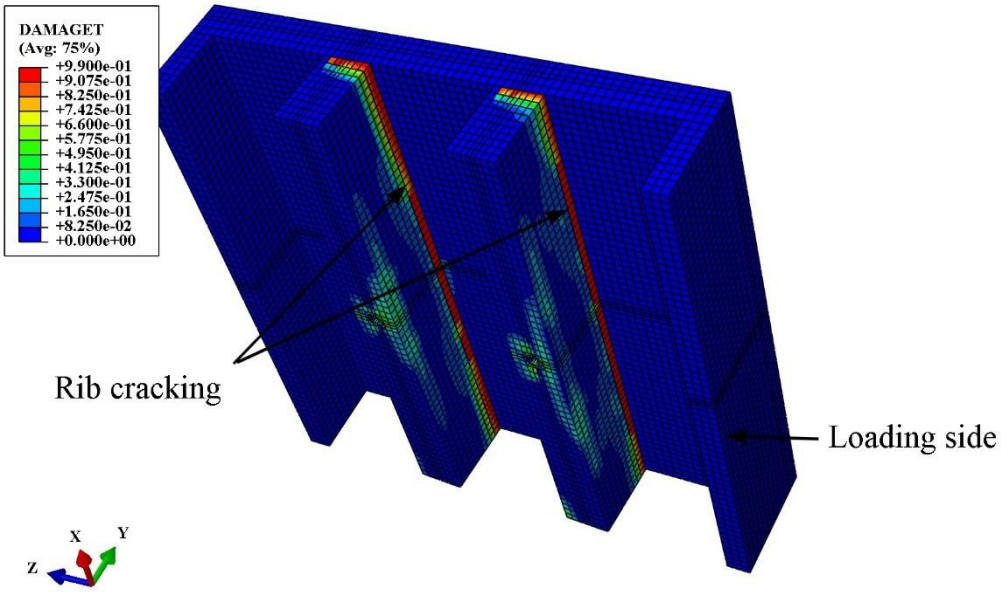


Figure 3.15 Rib shearing (rib cracking) of series D25 from Rambo-Roddenberry (2002)

Regarding the tests from Smith and Couchman (2010), it was clear that the numerical characteristic slips lied in an acceptable range with experiments, even though the characteristic slip in experiments resulted in a diverse range. All tests typically failed by concrete cones around headed studs and formation of a horizontal crack along the surface of the concrete slab. Likewise, all push models ended with the same mode of failure as in the experiment as shown in Figure 3.16. The concrete began to crush around the shank of headed

studs forming wedge shapes and then rode over the profiled sheeting. The webs of sheeting remarkably bent to the opposite direction of load, and the headed studs bent to the opposite direction of the applied load.

As for push tests with double or three-headed studs, the failure mode was similar except the concrete cones around headed studs were combined as shown in Figure 3.17. In the finite element, the tensile damage variable $d_t$ defines the crack in the concrete slab, the complete tensile failure of material is represented when the value of tensile damage equals one, while the value zero refers to no tensile damage. It can be concluded that ABAQUS/Explicit with the concrete damage plasticity method was capable of capturing the shear connector resistance, load-slip behaviour, and the mode of failure of push tests with perpendicular profiled sheeting.

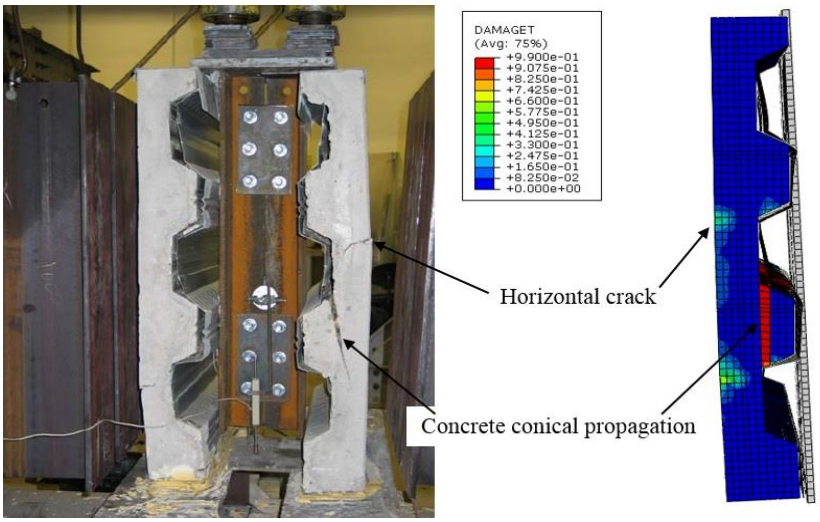


Figure 3.16 Typical failure in experimental and numerical work of Smith and Couchman (2010)

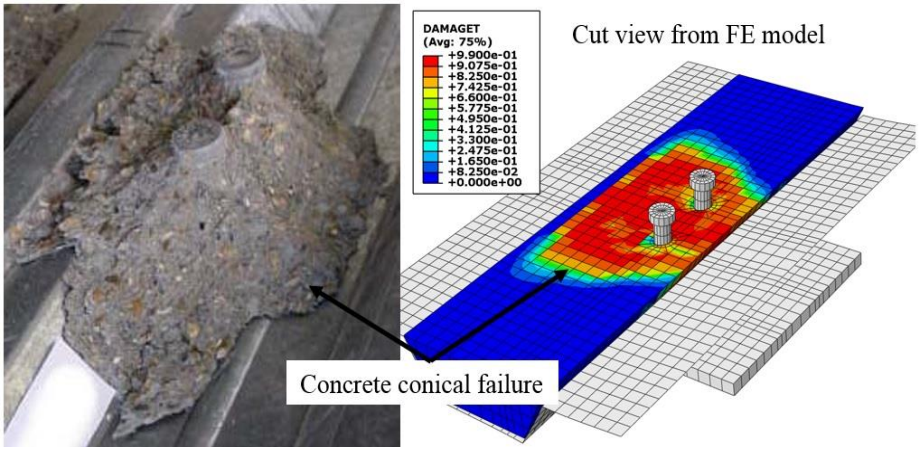


Figure 3.17 Concrete cones failure for double studs in Smith and Couchman (2010)

Table 3.6 Comparison of FE results against experiments

| Test ref. | Load per stud (kN) | | | Average (kN) | $P_{FE}$ (kN) | $P_{Ave.}$ / $P_{FE}$ | Shear stud characteristic resistance $P_{RK}$ (kN) | Slip capacity at characteristic resistance (mm) | | | $\Delta_{FE}$ (mm) | Tested by |
|---|---|---|---|---|---|---|---|---|---|---|---|---|
| | Test 1 | Test 2 | Test 3 | | | | | Test 1 | Test 2 | Test 3 | | |
| A1U | 94.56 | 83.09 | 95.98 | 91.21 | 90.40 | 1.01 | 69.06 | 15.38 | 11.11 | 13.24 | 19.64 | Smith and Couchman (2010) |
| A1D | 115.28 | 112.49 | 121.49 | 116.42 | 111.60 | 1.04 | 91.58 | 16.78 | 13.62 | 19.18 | 15.80 | |
| B1U | 121.32 | 107.87 | 107.14 | 112.11 | 112.00 | 1.00 | 86.62 | 19.33 | 14.23 | 15.49 | 13.24 | |
| A2DX | 57.85 | 62.93 | 66.60 | 62.46 | 63.88 | 0.98 | 47.94 | 15.30 | 9.99 | 15.42 | 16.20 | |
| A2UY | 55.10 | 47.90 | 65.10 | 56.03 | 50.87 | 1.10 | 38.18 | 11.28 | 14.69 | 15.25 | 16.01 | |
| A2DY | 76.15 | 70.88 | 74.04 | 74.02 | 69.90 | 1.06 | 58.93 | 13.34 | 11.41 | 12.81 | 13.60 | |
| A2DZ | 54.40 | 64.90 | 66.50 | 61.93 | 56.88 | 1.09 | 45.23 | 6.15* | 10.30 | 11.45 | 13.77 | |
| B2U | 76.50 | 69.40 | 78.20 | 74.70 | 78.37 | 0.95 | 57.52 | 14.18 | 10.87 | 16.65 | 13.23 | |
| A3D | 52.90 | 47.30 | 39.00 | 46.40 | 47.13 | 0.98 | 31.47 | 20.16 | 17.51 | 11.17 | 19.21 | |
| D20 | 26.82 | 36.03 | 42.26 | 35.04 | 43.46 | 0.81 | - | - | - | - | - | Rambo-Roddenberry (2002) |
| D21 | 58.80 | 53.24 | 69.43 | 60.49 | 63.51 | 0.95 | - | - | - | - | - | |
| D22 | 24.02 | 29.71 | 28.73 | 27.48 | 34.36 | 0.80 | - | - | - | - | - | |
| D23 | 50.22 | 83.98 | 76.86 | 70.35 | 74.62 | 0.94 | - | - | - | - | - | |
| D24 | 38.07 | 33.58 | 32.33 | 34.66 | 36.81 | 0.94 | - | - | - | - | - | |
| D25 | 30.74 | 27.44 | 24.82 | 27.67 | 27.80 | 0.99 | - | - | - | - | - | |
| Mean | | | | | | 0.97 | | | | | | |
| CoV % | | | | | | 8.86 | | | | | | |

* Neglected by the authors to avoid distorting in analysis

## 3.11 Description of push-off tests with parallel sheeting

Push-off tests incorporating profiled sheeting parallel to the steel beam were also modelled using ABAQUS/Explicit. The finite element simulation covered numbers of push-off tests conducted by Jayas and Hosain (1988), and Johnson and Yuan (1998a). The purpose of modelling push-off tests with profiled sheeting oriented parallel to the steel beam is to ascertain the efficiency of the finite element techniques examined previously in this chapter. The validated experiments involved two reinforced concrete slabs attached to the steel beam by headed studs. The specimens were subjected to a vertical hydraulic load on the top surface of the steel beam, and the slip between the slab and steel beams were measured.

For the push-off tests conducted by Jayas and Hosain (1988), the steel beams section was 210 × 205 × 59 kg/m. The total length, width, and depth of concrete slabs were 712, 508, and 102 mm respectively. The general arrangement of the push test is shown in Figure 3.18. The depth of the concrete slab was chosen to provide a 25-mm cover of concrete above the stud head. The profiled sheeting had a total net depth of 38 mm, average trough width of 159.2 mm, and sheeting thickness of 0.9 mm. The corresponding headed studs were 16 × 76 mm in all specimens. The full details of the test set up are given in Table 3.7.

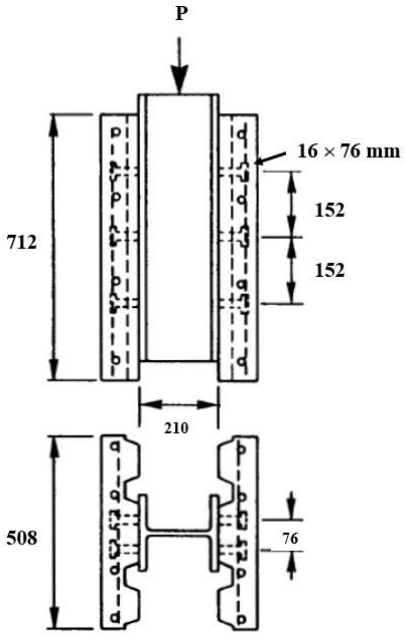


Figure 3.18 Push test arrangement of JDT-3 in Jayas and Hosain (1988)

The test set up in case of Johnson and Yuan (1998a) consisted of two rows of headed stud welded to a 205 × 205 × 52 kg/m steel beam as shown in Figure 3.19. Different types of profiled sheeting were used, the depths of sheeting varied from 46 to 80 mm, the thickness also varied from 0.9 to 1.2 mm. For push tests with profiled sheeting less than 80 mm deep, the corresponding headed studs were 19 × 95 mm, while headed studs of 19 × 195 mm were used for push models with 80 mm deep sheeting. All concrete slabs were 620 mm square, the concrete cover above the head of studs was 25 mm in specimens. The push-off specimens which involved light-weight concrete material were excluded from the simulation as the light-weight concrete is beyond the scope of this research. The full details of the test set up are given in Table 3.7.

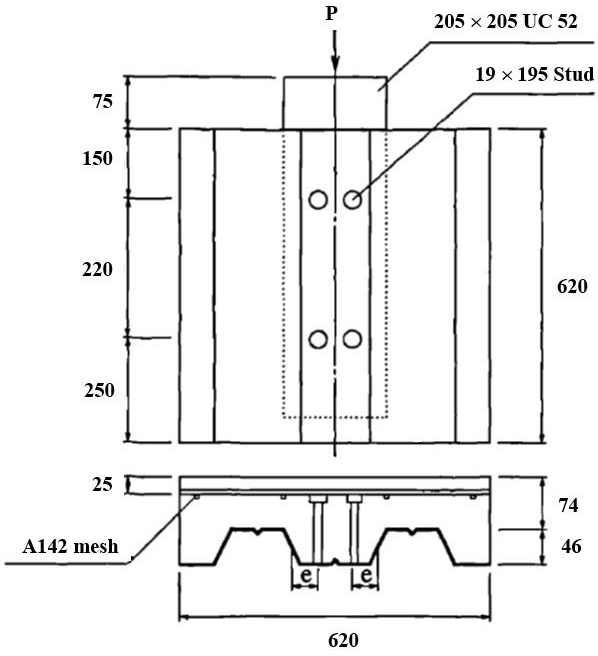


Figure 3.19 Push test arrangement of G15P in Johnson and Yuan (1998a)

## 3.12 Finite Element Modelling of push tests with parallel sheeting

The concrete damage plasticity method (CDP) was used to define the concrete slab geometry in all validated models. Due to symmetry alongside the centre line of steel beam, and to reduce the computational time, only one concrete slab geometry was modelled. All parts were meshed using 15 × 15 mesh element size. The Young's modulus of elasticity of the steel beam was taken as 210 GPa, while 200 GPa was assumed for the rest of the steel parts. For specimens conducted by Jayas and Hosain (1988), the ultimate tensile strength of headed

stud was taken as 470 MPa same as in experiments, while the yield stress of profiled sheeting was assumed 350 MPa since it is not given in experiment. For specimens conducted by Johnson and Yuan (1998a), the yield stress of profiled sheeting was taken as 280 MPa, the ultimate tensile strength for the 95-mm studs was 486 MPa and 472 MPa for the 125-mm studs.

The contact interactions and constraints were similar as in push-off models with perpendicular profiled sheeting. The boundary conditions and the loading surface of the push-off models are shown in Figure 3.20. All nodes of the lower surface of steel beam were restricted from moving in the Y direction and rotation in the X and Z direction as presented by Surface 1. The surface of profiled decking and concrete slab were restrained from moving in the Z direction as presented by Surface 2. All models were pushed slowly until failure (presented by Surface 3) using a loading rate of 0.5 mm/sec with a mass scaling factor of 10.

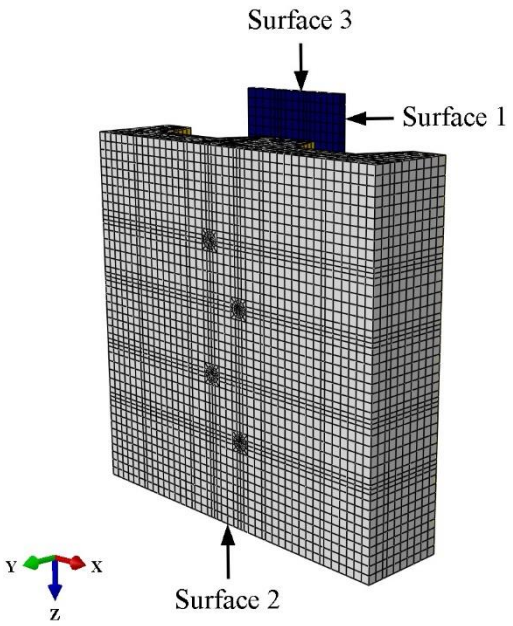


Figure 3.20 Boundary conditions for validated push-off tests with parallel sheeting

### 3.13 Validation of FE models: parallel sheeting

Table 3.7 shows the finite element results compared to the experiments from Jayas and Hosain (1988), and Johnson and Yuan (1998a). The validation was based on the shear connector resistance, load-slip behaviour, and mode of failure. The results showed a close

agreement with experiments, the average ratio of $P_{exp.}/P_{FE}$ was 1.01, corresponding to a coefficient of variation of 5.1%. Numerical load versus slip curves for selected push tests are compared with experiments in Figures 3.21-22. In Jayas and Hosain (1988), the slip capacities were measured at the maximum load per stud. While the slip capacities in case of Johnson and Yuan (1998a) were measured as 80% of the mean maximum load. The slip values in the finite element models were determined in the same way for each relevant experiment. It can be said that the slip capacities obtained from the numerical analysis are reasonable compared to those in experiments, despite the results being slightly diverse in some cases.

The mode of failure in all models was observed. For push tests in Jayas and Hosain (1988), numerical results showed the same mode of failure as in experiments. Stud shearing occurred in JD-1, JD-2, and JD-3, while longitudinal shear failure occurred in JD-4 and JD-5. In Figure 3.21, stud shearing is obvious from the sudden drop in the load-slip curve; the load-bearing capacity had risen again due to the resistance of another stud before it sheared too causing further fall. Regarding Johnson and Yuan (1998a), all experiments failed by splitting (crushing of concrete adjacent to the stud shank), except G10P that it failed by concrete pull-out. In the numerical analysis, a very similar failure pattern was observed in all models. Some failure modes are given in Figures 3.23-24.

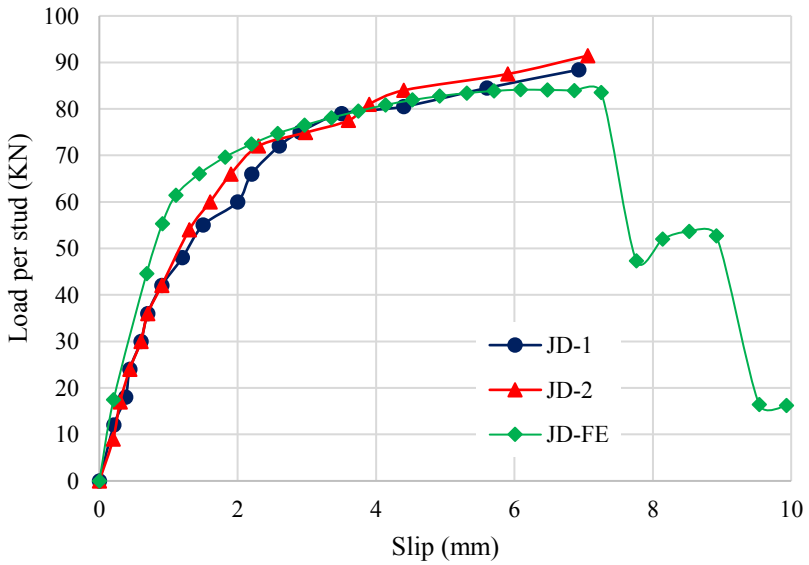


Figure 3.21 Experimental and numerical load-slip curves for JD-1 and JD-2 (Jayas and Hosain 1988)

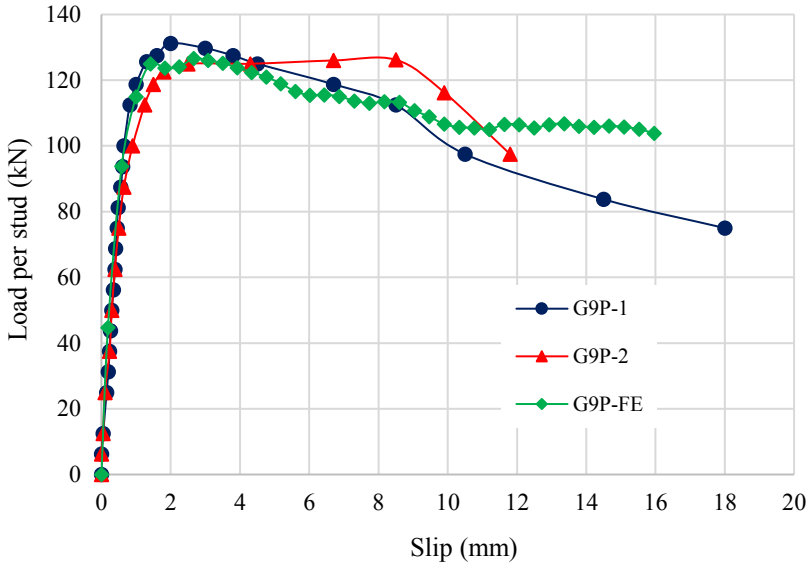


Figure 3.22 Experimental and numerical load-slip curves for G9P (Johnson and Yuan 1998a)

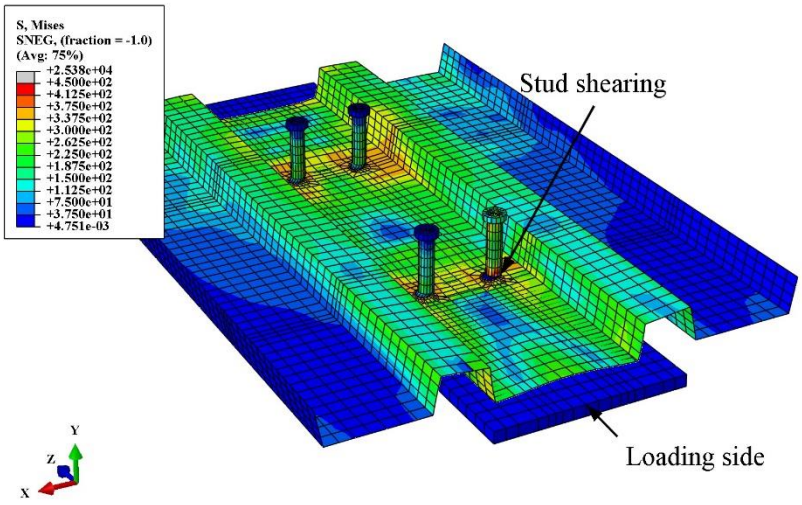


Figure 3.23 Stud shearing failure in Jayas and Hosain (1988)

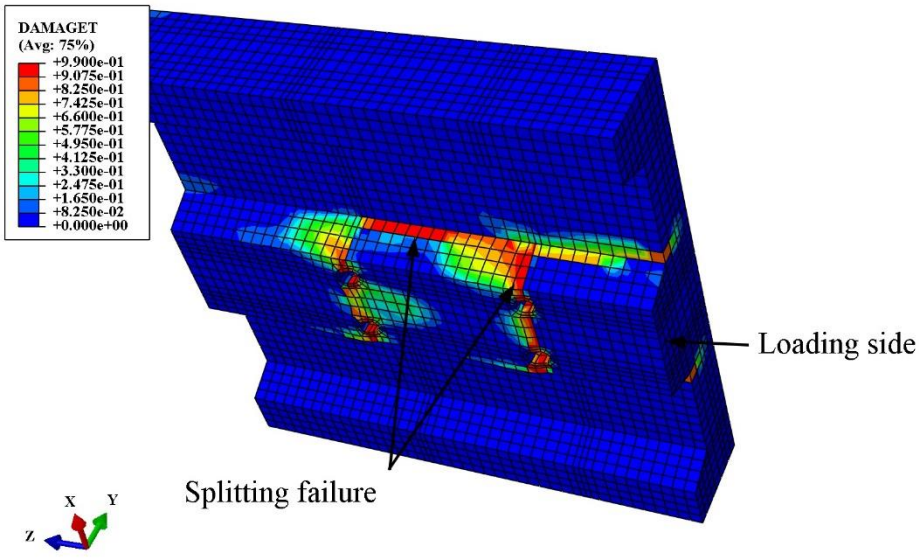


Figure 3.24 Splitting failure in Johnson and Yuan (1998a)

Table 3.7 Comparison of experimental results and finite element analysis for push tests with parallel sheeting

| Test | Concrete strength $f_c$ (MPa) | Profiled sheeting (mm) | | | Headed stud | | | $P_{exp.}$ (kN) | $P_{FE}$ (kN) | $P_{exp.}$ / $P_{FE}$ | Slip capacity in experiment (mm) | Slip capacity in FE (mm) | $\Delta_{exp.}$ / $\Delta_{FE}$ | Tested by |
|---|---|---|---|---|---|---|---|---|---|---|---|---|---|---|
| | | $t_s$ | $b_o$ | $h_p$ | Number per slab | Size $d \times h_{sc}$ mm × mm | Longitudinal spacing (mm) | | | | | | | |
| JD-1 | 29.8 | 0.9 | 159.2 | 38 | 4 | 16 × 76 | 305 | 88.43 | 84.14 | 1.05 | 6.93 | 8.6 | 0.81 | Jayas and Hosain (1988) |
| JD-2 | 29.8 | 0.9 | 159.2 | 38 | 4 | 16 × 76 | 305 | 91.54 | | 1.09 | 7.06 | | 0.82 | |
| JD-3 | 26.4 | 0.9 | 159.2 | 38 | 6 | 16 × 76 | 152 | 78.40 | 72.30 | 1.08 | 6.81 | 7.8 | 0.87 | |
| JD-4 | 26.4 | 0.9 | 159.2 | 38 | 8 | 16 × 76 | 102 | 66.76 | 69.45 | 0.96 | 6.29 | 8.2 | 0.77 | |
| JD-5 | 26.4 | 0.9 | 159.2 | 38 | 8 | 16 × 76 | 102 | 70.37 | | 1.01 | 6.60 | | 0.80 | |
| G9P-1 | 28.6 | 1.2 | 140 | 80 | 4 | 19 × 125 | 250 | 131.1 | 126.6 | 1.04 | 9.6 | 12.5 | 0.77 | Johnson and Yuan (1998a) |
| G9P-2 | 28.6 | 1.2 | 140 | 80 | 4 | 19 × 125 | 250 | 126.2 | | 0.99 | | | | |
| G10P-1 | 25.8 | 0.9 | 113 | 60 | 4 | 19 × 95 | 250 | 70.3 | 75.2 | 0.93 | 3.7 | 5.8 | 0.64 | |
| G10P-2 | 25.8 | 0.9 | 113 | 60 | 4 | 19 × 95 | 250 | 72.1 | | 0.96 | | | | |
| G13P-1 | 25.1 | 0.9 | 113 | 60 | 4 | 19 × 95 | 220 | 92.1 | 96.2 | 0.96 | 14.0 | 12.8 | 1.09 | |
| G13P-2 | 25.1 | 0.9 | 113 | 60 | 4 | 19 × 95 | 220 | 91.8 | | 0.95 | | | | |
| G14P-1 | 23.5 | 1.2 | 140 | 80 | 4 | 19 × 125 | 220 | 112.1 | 106.1 | 1.06 | 12.0 | 15.6 | 0.77 | |
| G14P-2 | 23.5 | 1.2 | 140 | 80 | 4 | 19 × 125 | 220 | 114.2 | | 1.07 | | | | |
| G15P-1 | 30.2 | 1.0 | 132 | 46 | 4 | 19 × 95 | 220 | 101.9 | 95.9 | 1.06 | 5.5 | 7.6 | 0.72 | |
| G15P-2 | 30.2 | 1.0 | 132 | 46 | 4 | 19 × 95 | 220 | 96.3 | | 1.0 | | | | |
| G16P-1 | 33.2 | 1.0 | 160 | 50 | 4 | 19 × 95 | 220 | 108.8 | 110.3 | 0.98 | 8.7 | 8.4 | 1.04 | |
| G16P-2 | 33.2 | 1.0 | 160 | 50 | 4 | 19 × 95 | 220 | 114.5 | | 1.04 | | | | |
| G17P-1 | 22.1 | 1.2 | 173 | 60 | 6 | 19 × 95 | 110 | 87.8 | 80.2 | 1.09 | 5.8 | 5.1 | 1.14 | |
| G17P-2 | 24.1 | 1.2 | 173 | 60 | 6 | 19 × 95 | 110 | 85.7 | 84.5 | 1.01 | 5.8 | 5.4 | 1.07 | |
| Mean | | | | | | | | | | 1.017 | | | | |
| COV (%) | | | | | | | | | | 0.051 | | | | |

## 3.14 Conclusions

A three-dimensional finite element model was developed using ABAQUS/Explicit in this chapter. The numerical analysis involved simulating previous push-off tests with profiled steel decks oriented perpendicular and parallel to the steel beam. The finite element results were validated against experiments concerning shear connector resistance, load-slip behaviour, and mode of failure. In the finite element analysis, Concrete Damage Plasticity (CDP) method was used to define the concrete slab geometry. Numerical techniques such as mass scale factor, mesh element size and loading rate were examined on some preliminary samples in order to obtain the best compromise between accuracy and computational efficiency.

It was observed that a mass scaling factor of 10, a medium mesh element size of 15 × 15 mm and a loading rate of 0.5 mm/sec were the most appropriate techniques to simulate the behaviour of composite beams with profiled steel sheeting. The conclusion was based on the accuracy of results and time-consuming. These techniques were then applied to many secondary and primary push-off tests which involved different sizes of headed stud and ribs and studs' arrangement. The numerical results were found in a very good agreement with experiments. ABAQUS/Explicit was capable of reasonably predicting the shear connector resistance, load-slip behaviour, and mode of failure in both secondary and primary composite beams. Accordingly, the development of a finite element model is confidently suitable to be used in modelling further investigations in this thesis. The next chapters will include modelling enormous push-off tests featuring a broad range of deck geometries from narrow to wide, different deck depths from 50 to 146 mm, and both perpendicular and parallel orientations.

# Chapter 4 Finite element modelling of push-off tests with perpendicular profiled sheeting

# Chapter 4

## Finite element modelling of push-off tests with perpendicular profiled sheeting

### 4.1 Introduction

In this chapter, 3-D finite element models are developed to predict the behaviour of secondary composite beams with steel decks deeper than 80 mm. A total number of 54 push tests are modelled and grouped in order to investigate the shear connector resistance, load-slip behaviour and mode of failure. The target of this part of the study is to observe the influence of narrow ribbed ($b_o/h_p < 1.5$) and very deep decks on the behaviour of the headed stud. Several parametric studies are performed including rib geometries, studs' layout, number of studs per rib, slab reinforcement and slab depth. The findings will bridge the gap of understanding the performance of composite beams with such narrow and very deep decks. All FE results are presented in this chapter, accompanied by illustrative figures of the load-slip curves and failure modes.

### 4.2 Description of push test modelling

All push models were numerically analysed based on a horizontal push test arrangement. Previously, the horizontal push test was performed by Ernst et al. (2010), and Qureshi (2010). The typical horizontal push test is made by casting single concrete slab which is connected to a steel beam by sets of shear connectors with a profiled sheeting lying between them. Then, the specimen is pushed laterally by subjecting the load on a side surface of the concrete slab. In this study, a full-scale model of push test was created including five ribs of deep profiled sheeting positioned perpendicular to the steel beam. The push test model consisted of five parts namely steel beam, headed studs, profiled sheeting, concrete slab and wire-mesh reinforcement. Each part was modelled using its material properties. The parts were created separately except for the steel beam and headed studs which were created together but with different properties. The section of steel beam was chosen to be 254 × 254 × 73 UC.

The test program involved modelling composite beams with two different types of steel decks. One with a deep deck of 100 mm produced by Tata Steel company, and the other with

a deep deck of 146 mm produced by Kingspan company. Although the first deck is produced for non-composite beams, it felt necessary to account it for composite beam action in order to help formulate a generic equation later in this study. The average rib width ($b_o$) was made herein to be 100 mm to achieve a rib deck ratio ($b_o/h_p$) of 1.0. Details of the 100 mm deep deck are shown in Figure 4.1. In case of the 146 mm deep deck, it comes with an average rib width of 97.5 mm, resulting in a rib deck ratio of 0.67. The sheeting thickness ($t_s$) varies from 1.2 to 2.0 mm. Figure 4.2 displays details of 146 mm deep deck.

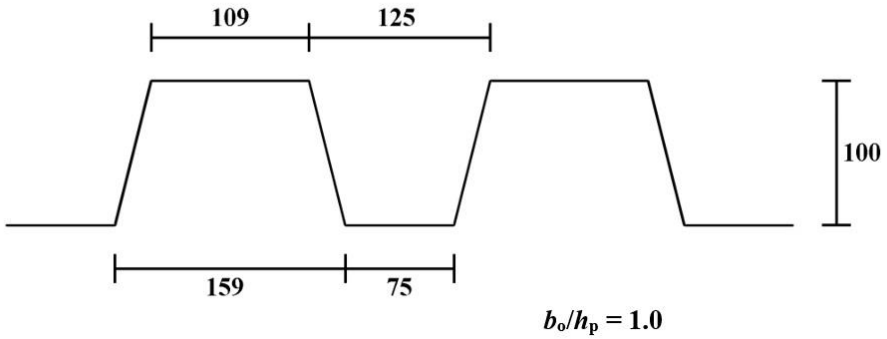


Figure 4.1 Details of the 100 mm deep decking

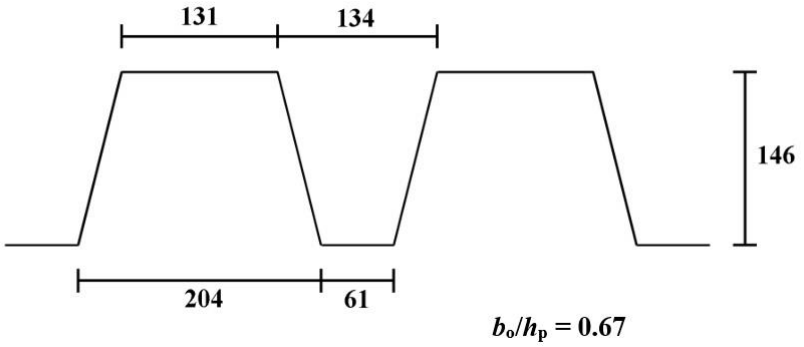


Figure 4.2 Details of the 146 mm deep decking

A headed stud dimension of 19 × 140 mm and 19 × 195 mm were used for the 100 and 146 mm deep decks respectively. The yield stresses of the profiled decking and the headed stud in all tests were assumed to be 350 MPa and 420 MPa respectively. Because of the narrowness at the bottom surface of both decks' ribs, it was not possible to place the headed

studs anywhere but in the centre. Therefore, the headed studs were positioned in the centre of troughs through the profiled decking in all models of this study.

Normal weight concrete of 2400 kg/m$^3$ density was used to define the concrete slab. The width of the concrete slab in all models was 600 mm since it is the minimum width requirement in Eurocode 4. Concrete Damage Plasticity method (CDP) was used to define the concrete slab geometry; this method was thoroughly illustrated in Chapter 3. The concrete slab was reinforced with A193 wire-mesh (7 mm in diameter) having 200 mm centre to centre spacing. The number and position of wire-mesh reinforcement were variants; this will be explained later. All geometries were meshed using 15 × 15 mm mesh element size and then assembled to produce the push test model. The general push test arrangement with the 100 and 146 mm deep deck are shown in Figures 4.3 and 4.4 respectively. The concrete slabs are raised in both Figures to enable the embedded parts inside the concrete to be seen.

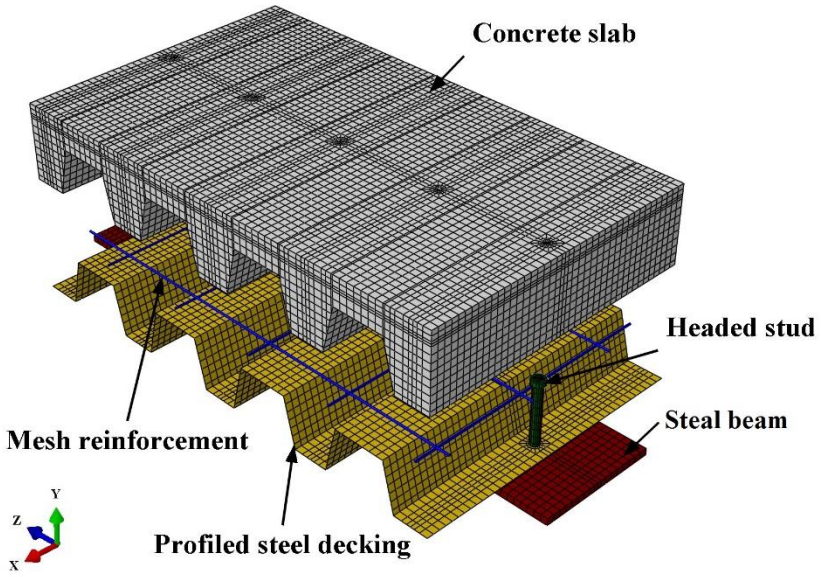


Figure 4.3 General push test arrangement with the 100 mm deep decking

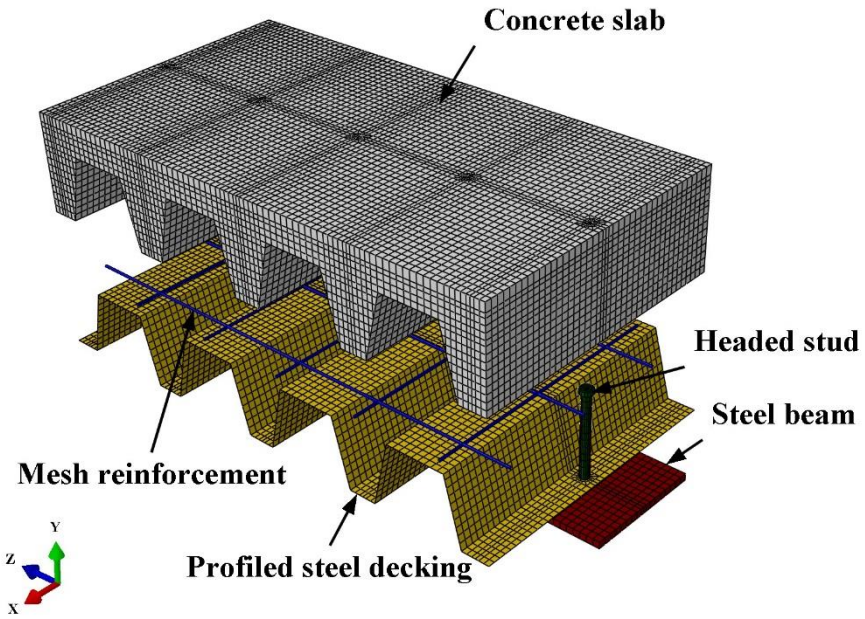


Figure 4.4 General push test arrangement with the 146 mm deep decking

### 4.2.1 Constraints and contact interactions

The procedure to define the relationships between the contacted surfaces in push models with parallel profiled sheeting was similar to numerical tests conducted in Chapter 3, Section 3.7.

### 4.2.2 Boundary conditions and load application

The boundary conditions and load application are shown in Figure 4.5. Basically, the steel beam in an experiment is fully restrained from moving, therefore the lower surface of a steel beam in the finite element modelling was restrained from moving and rotating in all directions, this boundary condition is defined by surface 1. While Surface 2 represents the loading surface on which the horizontal shear loading is subjected.

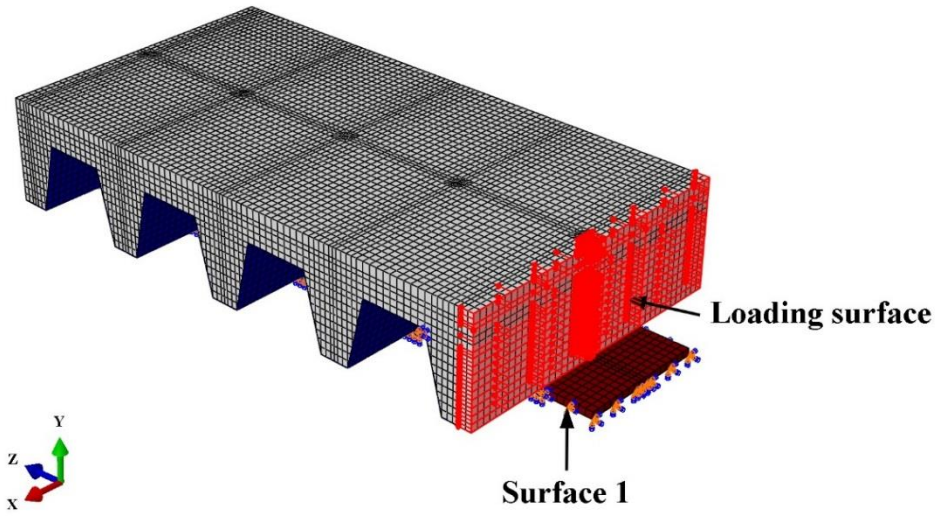


Figure 4.5 Boundary conditions for the push models with perpendicular profiled decking

## 4.3 Parametric Study

The numerical study in this chapter consists of 54 push test models with very deep steel decks. The study was divided into six groups, each group contained one parametric study, the description of push models in each group was fully reported. The parameters were rib geometries, studs' layout, number of studs per, slab reinforcement and slab depth.

### 4.3.1 Group A: effect of rib geometries

Eight push models (T1-8) were performed in this group. Four tests incorporated a 100 mm deep deck with rib deck ratio of 1.0, and four tests contained a 146 mm deep deck with rib deck ratio of 0.67. The wire-mesh reinforcement was placed on the deck surface in all tests. The slab depth was 160 and 215 mm for tests with 100 and 146 mm deep decks respectively. Four different characteristics of compressive strength of concrete ($f_c$) were used namely 12, 20, 30 and 40 MPa. All tests consisted of a sheeting thickness of 1.2 mm and one shear stud connector in each rib. The full details of this group are illustrated in Table 4.1. The tests performed in this group were considered as the control case and are compared to the rest of the models later in this study.

Table 4.1 Details of the push test models in Group A

| Test | $f_c$ (MPa) | Profiled decking | | | Headed stud | |
|---|---|---|---|---|---|---|
| | | $b_o$ (mm) | $h_p$ (mm) | $b_o/h_p$ | $n_r$ | $d \times h_{sc}$ (mm) |
| T1 | 12 | 100 | 100 | 1.0 | 5 | 19 × 140 |
| T2 | 20 | 100 | 100 | 1.0 | 5 | 19 × 140 |
| T3 | 30 | 100 | 100 | 1.0 | 5 | 19 × 140 |
| T4 | 40 | 100 | 100 | 1.0 | 5 | 19 × 140 |
| T5 | 12 | 97.5 | 146 | 0.67 | 5 | 19 × 195 |
| T6 | 20 | 97.5 | 146 | 0.67 | 5 | 19 × 195 |
| T7 | 30 | 97.5 | 146 | 0.67 | 5 | 19 × 195 |
| T8 | 40 | 97.5 | 146 | 0.67 | 5 | 19 × 195 |

The shear connector resistance per stud in group A was determined as reported in Figure 4.6. The numerical results revealed that the shear stud capacity with narrow and very deep decks varied from 48 to 83 kN when the concrete grade was raised from 12 to 40 MPa. Tests with 100 mm deep decks showed a slight increase in the shear stud capacity compared to those obtained from 146 mm deep decks. This could be due to the small difference between both rib geometries which did not contribute towards remarkable shear stud development. Figures 4.7 and 4.8 show the load-slip curves for tests with 100 and 146 mm deep decks respectively.

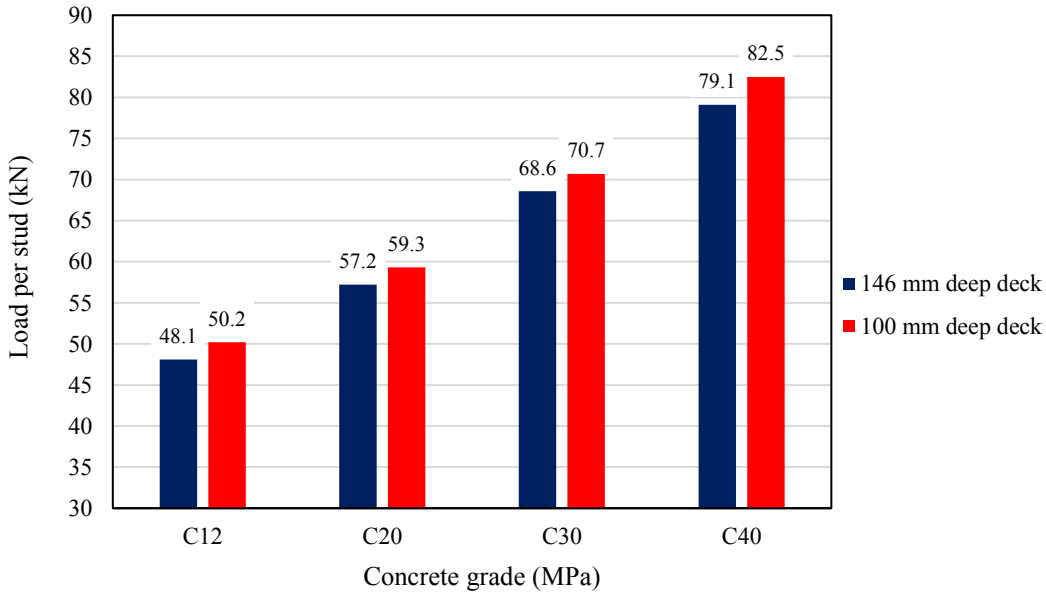


Figure 4.6 Shear connector resistance per stud with very deep decks

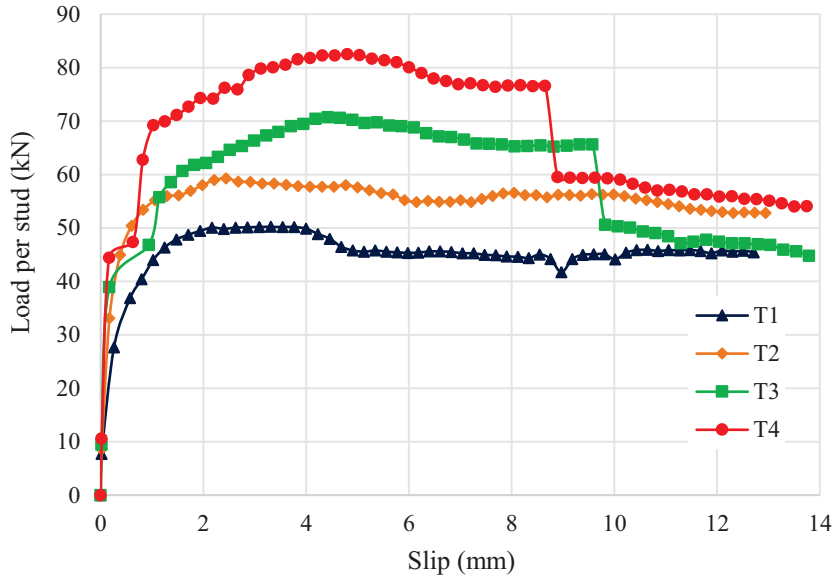


Figure 4.7 Load-slip curves for tests with 100 mm deep decking

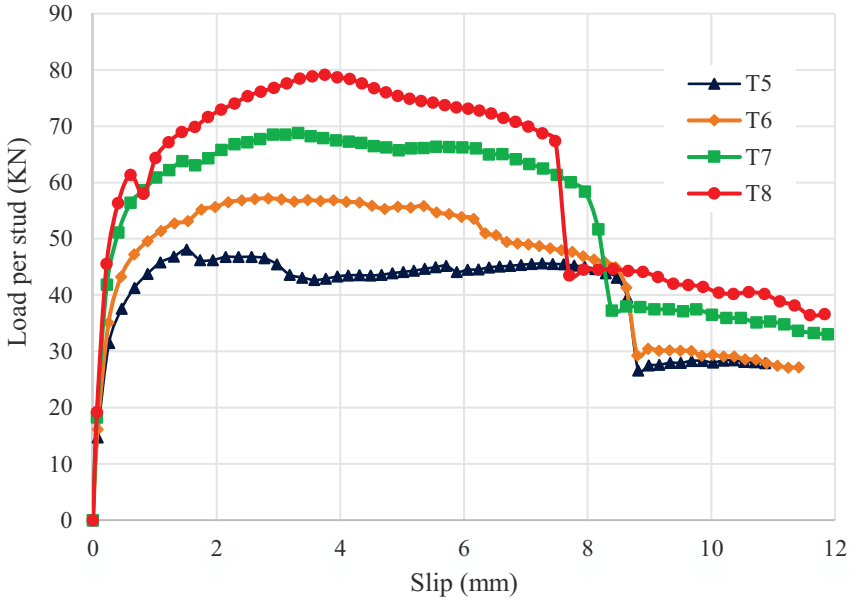


Figure 4.8 Load-slip curves for tests with 146 mm deep decking

The mode of failure in group A was observed. All tests failed by a combination of concrete cones and rib punching failure. The concrete part in the first rib adjacent to the applied load started to crack around the headed stud. As the load continued to increase, the concrete part within the rest of ribs started to crack and propagated upwards forming wedge shapes at the end of the test. Also, the concrete damage developed entirely across the width of the ribs at the mid-height of some troughs, the typical concrete cone configuration is shown in Figure

4.9. The webs of decking began to buckle and yield as soon as the load reached the peak point. Eventually, the steel decking significantly bulged outwards owing to studs pushing the crushed concrete in front; the rib punching at the end of the test is shown in Figure 4.10. Rib punching failure mostly happens with unfavourable headed stud position or narrow troughs as there is not enough concrete volume in front of the stud to resist the shear load (Johnson and Yuan, 1998a).

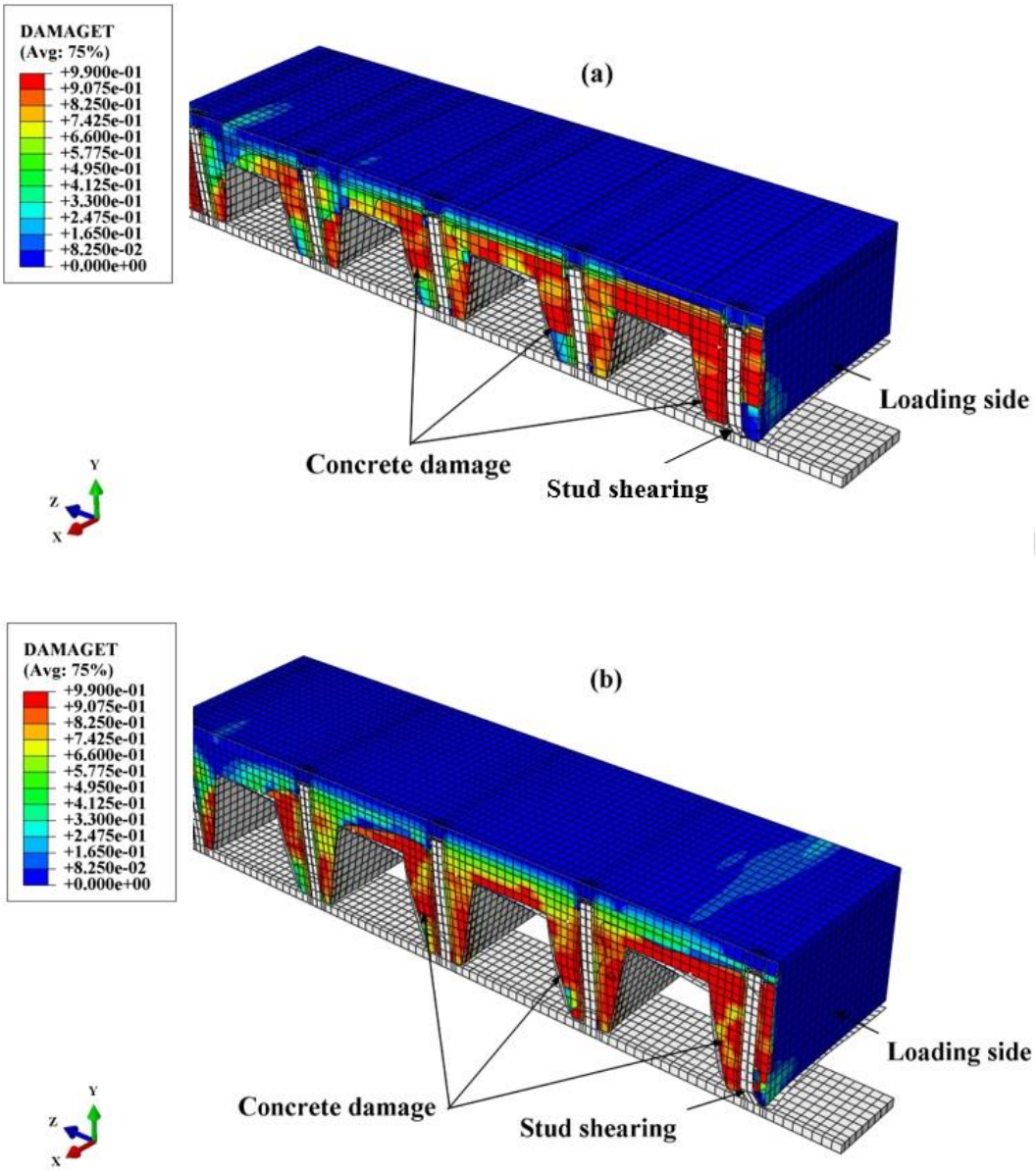


Figure 4.9 Side cut view of concrete failure among push models: (a) 100 mm deep deck (b) 146 mm deep deck

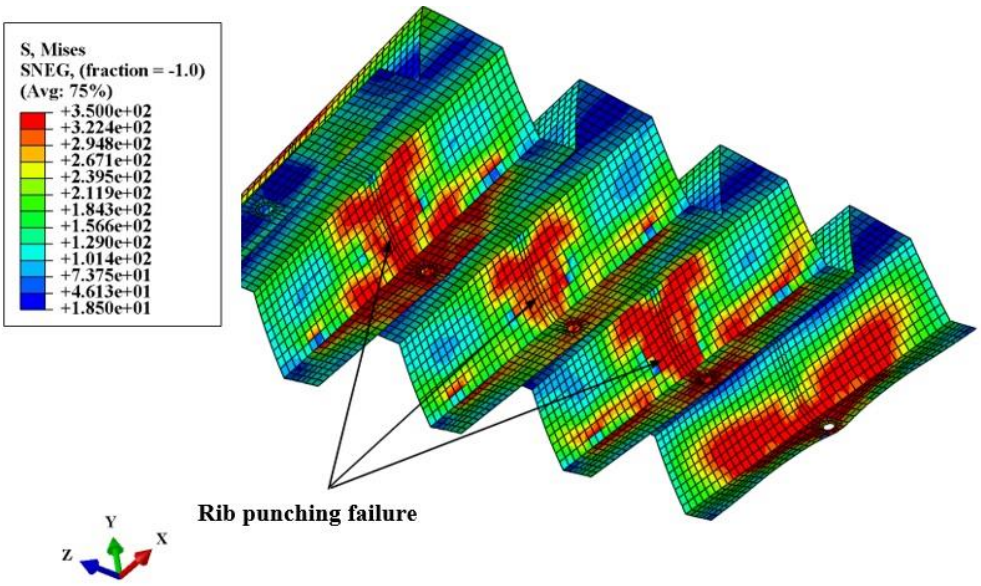


Figure 4.10 Typical rib punching in very deep decking

Regarding the headed stud deformation, the first stud close to the applied load sheared off at the base in most tests at the late stage of the applied load. This trend can be noticed in Figures 4.7 and 4.8 as the load-slip curves suddenly dropped prior to the end of the test. The remaining studs experienced a double curvature deformation or two plastic hinges (Nellinger et al. 2017). This behaviour of shear connector studs is predominant when a rib of the profiled sheeting is narrow, therefore more moment is resisted by the stud which causes the double curvature in the stud. This mode was previously reported by Lawson (1997). The headed studs' deformation of 19 × 195 mm is shown in Figure 4.11.

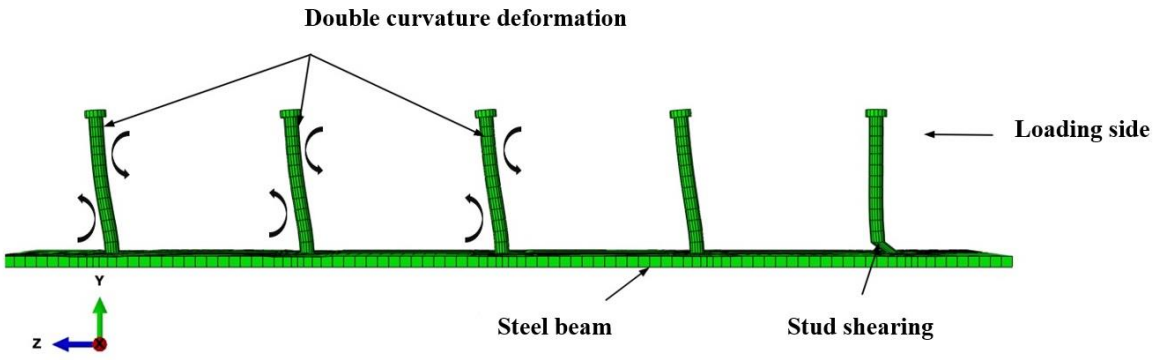


Figure 4.11 General deformation of 19 × 195 mm headed studs

This part has provided the first information on the behaviour of the headed stud with narrow and very deep decks. It was necessary to do so in order to find the correlation between narrow and wide rib geometries regarding the shear connector resistance. Therefore, the shear stud capacities obtained from steel decks deeper than 80 mm are compared to previous studies conducted with the common steel decks. For push tests having 60 mm deep decking, 1.2 mm sheeting thickness, 19 mm diameter stud and central position of studs, the shear capacity per stud varied from 75 to 120 kN when the concrete strength was changed from 12 to 40 MPa (Qureshi et al. 2011b). For the same push tests arrangement, but having 76 mm deep decking, Robinson (1988) found that the shear capacity per stud was 81.6 kN with a concrete strength of 24.9 MPa. In this research, that experimental result was normalised to the concrete grades of C12, C20, C30, and C40 using Equation 4.1. This equation was previously used by Robinson (1988) and Lloyd and Wright (1990).

$$P_{normalised} = [f_c / f_{c(test)}]^{0.5} P_{test} \quad \text{Eq. 4.1}$$

The shear capacity per stud would then vary from 56.6 to 103.4 kN when the concrete strength is changed from 12 to 40 MPa. The comparison of shear stud capacities with different rib geometries are given in Figure 4.12. Apparently, the use of narrow and very deep steel decks has caused a drastic decrease in the shear connector resistance. The shear stud capacity obtained from very deep decks is 65-70% of those obtained from the mid-depth decks. This is attributed to the narrow geometry of very deep decks which provides relatively less concrete volume around studs. Thus, the small rib geometry will naturally cause less shear stud capacity. This raises the concern of how the current design equations are capable of coping with the geometries of modern decks deeper than 80 mm. In fact, all design equations were derived from geometries up to the limit of 80 mm deep deck and rib deck ratio $\geq$ 1.5. Provided that no past research clarified this issue, the next chapter will answer this question and bridge this major knowledge gap.

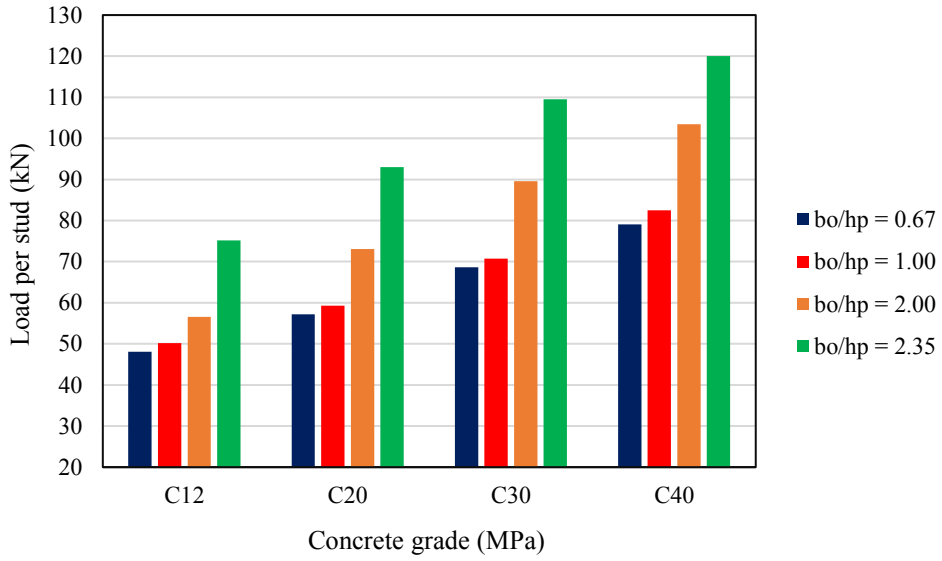


Figure 4.12 Shear connector resistance with different rib geometries

### 4.3.2 Group B: effect of studs' layout

This part aims to examine the extent to which the existence of headed studs in certain troughs can add benefit to the practice. Placing headed stud connectors in every alternative trough has received no attention. If this configuration can enhance the shear connector resistance, then this will certainly bring advantage to the secondary composite beams with narrow and very deep steel decks. In particular, the shear capacity per stud experiences a significant decrease when such decks are used. For this reason, eight push tests (T9-16) were modelled. The headed studs were arranged in a way that there was no stud in the second and fourth ribs as shown in Figure 4.13. This arrangement was labelled as "Layout 1". Another eight tests (T17-24) were modelled and labelled as "Layout 2". However this time, the headed studs were placed in the three middle troughs, hence there was no stud in the first and last ribs as seen in Figure 4.14. It was also interesting to investigate the effect of this layout on the behaviour of the headed stud. For each layout, tests were equally divided between 100 and 146 mm deep decks. Full details of this group are given in Table 4.2.

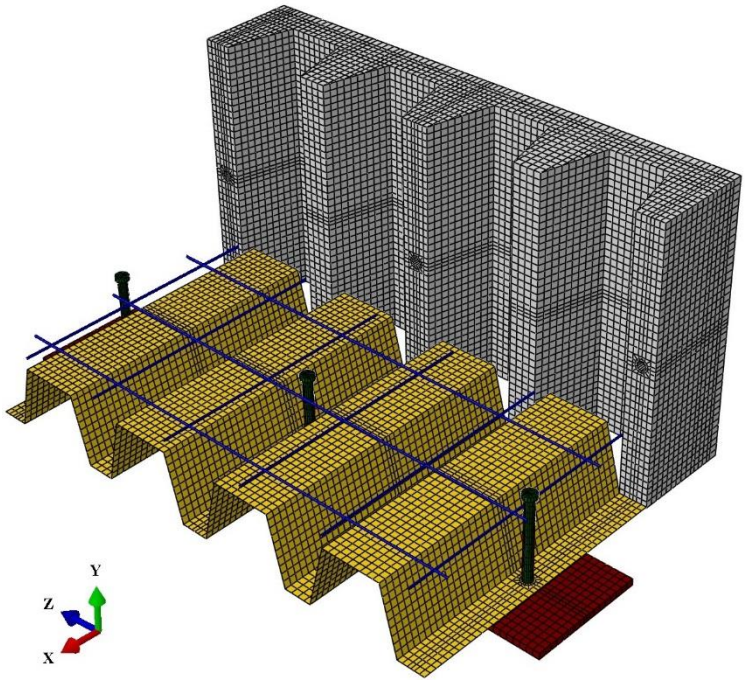


Figure 4.13 Push test with headed studs placed in every alternative trough

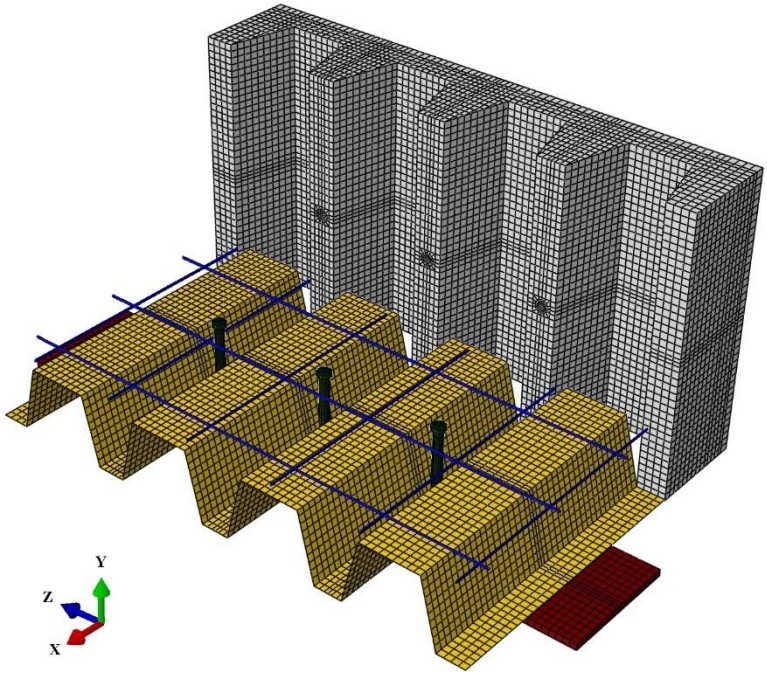


Figure 4.14 Push test with headed studs placed in the three middle troughs

Table 4.2 Details of the push test models in group B

| Layout | Type of deck | C12 | C20 | C30 | C40 |
|---|---|---|---|---|---|
| 1* | 100 mm deep | T9 | T10 | T11 | T12 |
| | 146 mm deep | T13 | T14 | T15 | T16 |
| 2** | 100 mm deep | T17 | T18 | T19 | T20 |
| | 146 mm deep | T21 | T22 | T23 | T24 |

* No stud in the second and fourth ribs
** No stud in the first and last ribs

Figures 4.15 and 4.16 present the shear stud capacities of models with different studs' layout containing 100 and 146 mm deep decks respectively. A significant increase in the shear connector resistance was found in models with studs placed in every alternative rib. The average increase of load per stud was 20% and 22% for models with 100 and 146 mm deep decks respectively as compared to the control case (single studs in every rib). This is due to the extra concrete volume and greater longitudinal spacing between studs. It was also interesting to see that this unique arrangement made the shear stud capacities with very deep decks fairly close to the resistance obtained from tests with 76 mm deep decks (highlighted as green bars in Figures 4.15-16). Contrarily, omitting studs from the first and last rib, and placing studs in the middle three ribs did not add any benefit. It only tends to reduce the shear connector resistance in all cases.

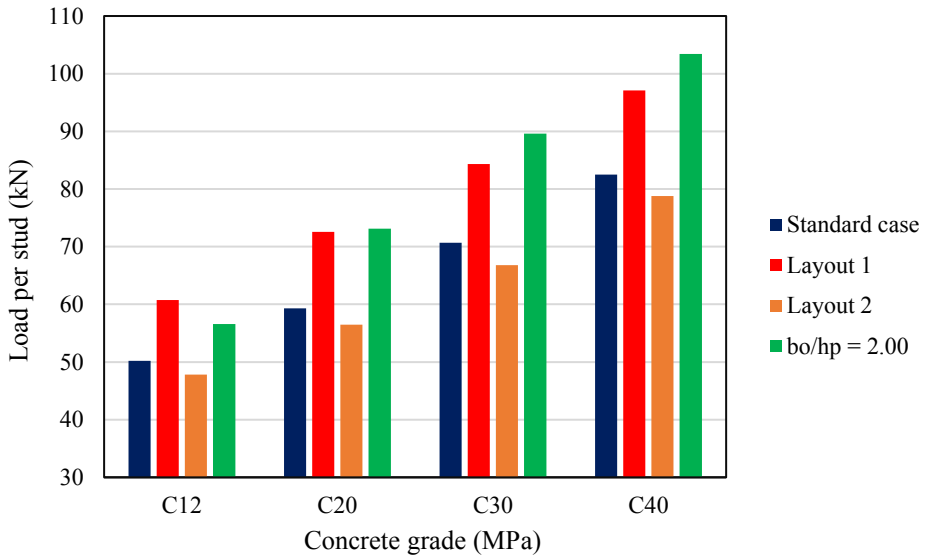


Figure 4.15 Comparison of tests with 100 mm deep deck and different studs' layout against tests with 76 mm deep deck

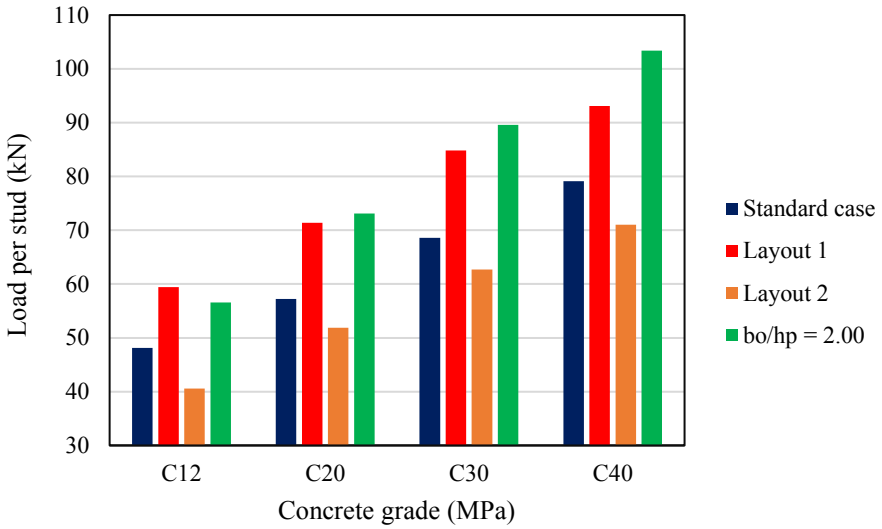


Figure 4.16 Comparison of tests with 146 mm deep deck and different studs' layout against tests with 76 mm deep deck

A combination of concrete cones and rib punching failure was observed in all models regardless of the stud layout. The failure mechanism was similar to those in the control case. However, the concrete part in troughs where there was no stud remained completely intact throughout the test as shown in Figure 4.17. Likewise, the webs of decking did not experience any buckling but only bending in the direction of the applied load (see Figure 4.18). This less tendency of damage could also justify the reason behind the development of shear resistance of stud placed in every alternative trough. The first studs sheared in the layout where there was a stud in the first rib. Aside from that, all studs depicted a double curvature deformation. Overall, the findings suggest that placing studs in every alternative trough of narrow and very deep decks has benefits, including concrete damage control, and most importantly, a 20% increase in the shear connector resistance. This unique layout can be implemented in practice for better performance in composite beams.

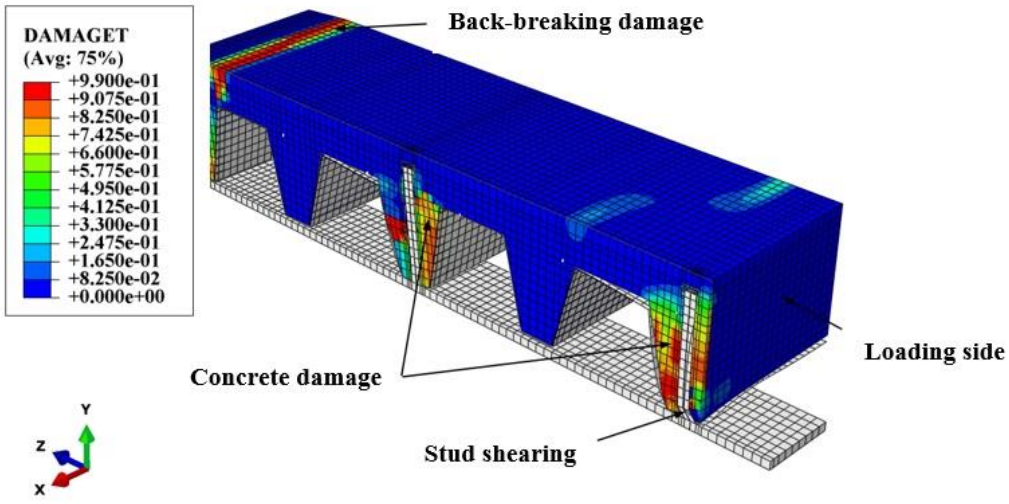


Figure 4.17 Side cut view of concrete damage in models with studs placed in alternative ribs

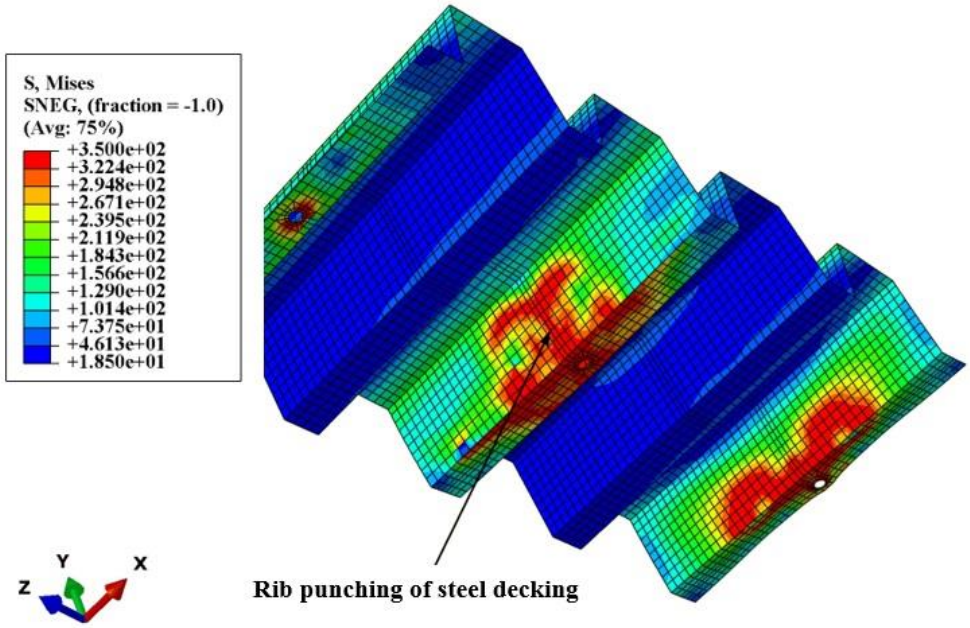


Figure 4.18 Stress contours of the very deep deck with studs placed in alternative ribs

### 4.3.3 Group C: effect of the number of studs per rib

This group involves eight models (T25-32). The push test arrangement resembles the one in group A, except two stud connectors per rib were embedded this time. Hence, each model contains 10 headed studs in total. The centre-to-centre transverse spacing between studs was

chosen to be five times the diameter of the stud (5*d*). It should be noted that the minimum transverse spacing is recommended to be (4*d*) by Eurocode 4. Although the influence of stud pairs was studied before, it was necessary to account for this parameter among tests with decks deeper than 80 mm. This is to help evaluate the accuracy of the current design equations in predicting the shear connector resistance when double studs are embedded in very deep decks. Moreover, it could help formulate new generic equations for more accurate and realistic predictions if needed. This part shall be discussed in detail in the next chapter.

Figures 4.19 and 4.20 illustrate the comparison between shear stud capacities of single and double studs for tests with 100 mm and 146 mm deep decks respectively. The FE results exhibited a significant reduction in the shear connector resistance when stud pairs were used. The average decrease of load per stud was 22% and 25% for models with 100 and 146 mm deep decks respectively as compared to their companions with single studs. This is due to the shortage of deformation capacity as the embedded concrete volume in ribs around studs is relatively less than the concrete volume in ribs with one stud. All tests ended by concrete cones failure without experiencing rib punching. Placing stud pairs at the same line restrained the concrete from moving laterally; this led to less pressure on the webs coming from the concrete, and thus rib punching did not happen. The mode of failure in very deep decks appeared to be influenced by the number of studs per rib.

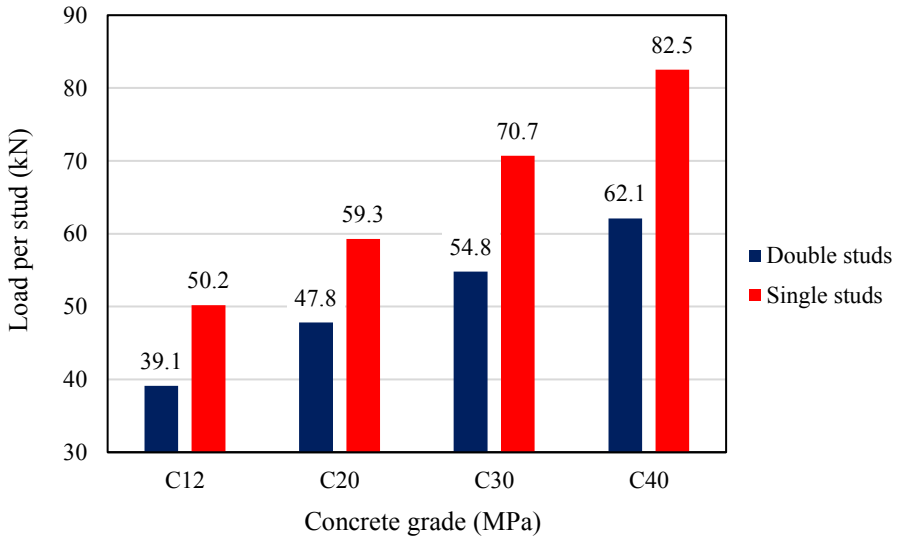


Figure 4.19 Comparison of shear stud capacities between single and double studs in models with 100 mm deep deck

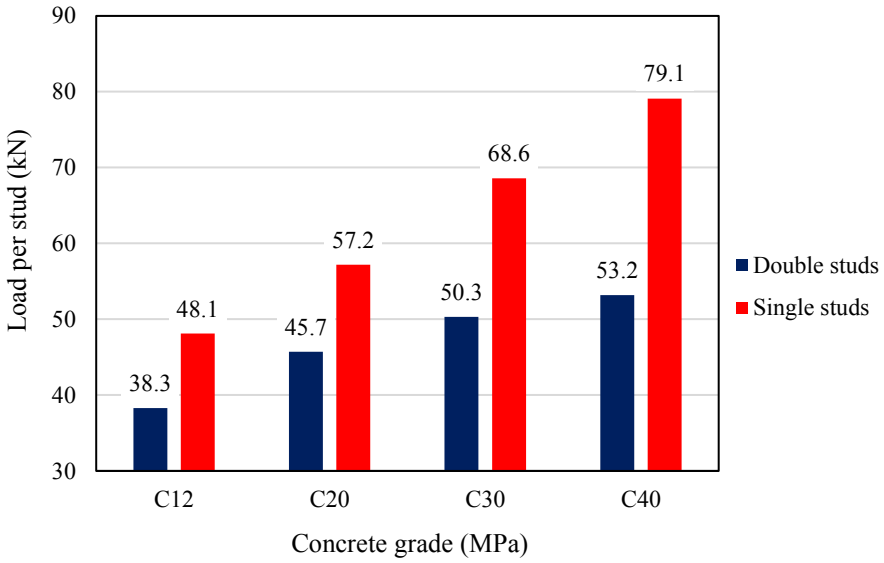


Figure 4.20 Comparison of shear stud capacities between single and double studs in models with 146 mm deep deck

### 4.3.4 Group D: effect of double mesh reinforcement

This group is meant to investigate the effect of double mesh reinforcement on the behaviour of the headed stud in very deep decks. Past research mainly focused on single wire-mesh placing at different levels within the concrete part above the steel deck. However, placing two separate wire-meshes, one on the steel deck and the other at a distance from the top concrete surface is limited. Studying this parameter is useful to investigate whether the concrete part above the steel deck affects the shear connector resistance and failure mode in very deep decks. Eight models (T33-40) were considered for this group. The test arrangement was similar to group A, except where the concrete slab was reinforced by two wire-meshes. The first was rested on the steel deck, and the second was located 20 mm below the top surface of concrete (see Figure 4.21).

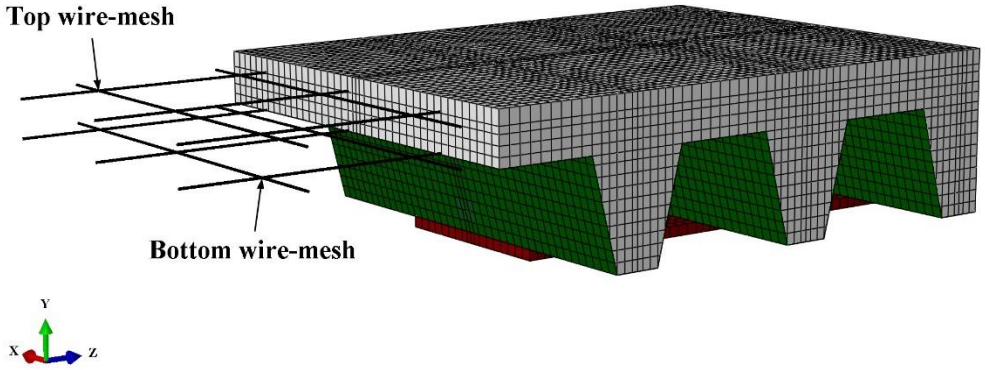


Figure 4.21 Models with very deep deck reinforced by double wire-mesh

The FE results showed that the double wire-mesh arrangement had a negligible effect on the shear connector resistance and load-slip behaviour. Figure 4.22 shows the load-slip curves obtained from single and double wire-mesh arrangements for tests with 146 mm deep decks. The failure mode was also unaffected by this type of slab reinforcement. Except that the back-breaking damage did not happen in the last rib. This is because the top wire-mesh allowed more tensile shear stresses to transfer through the steel reinforcement instead of the concrete and consequently inhibited that concrete damage. Nevertheless, the shear connector resistance is not a function of this failure, as the damage occurred at the late stage of the test when the headed stud had already realised its highest shear capacity.

Ideally, the main purpose of mesh reinforcement is to control temperature and shrinkage cracking in concrete. In normal cases, the general pattern of concrete failure initiates near the head of the stud and propagates diagonally downwards to the corner of the profiled decking (i.e. where the web and the upper flange meet) (Patrick, 2000). However, in models with very deep decks, the concrete embedded in ribs started to crack around the headed studs' shank and then propagated upwards, which means that the concrete did not fail along the assumed concrete failure plane. This can be the reason why the influence of mesh position on the behaviour of headed stud did not come into play. In conclusion, the behaviour of the headed stud in very deep decks seems to be influenced by the concrete volume within ribs. This concept is emphasised in the next section.

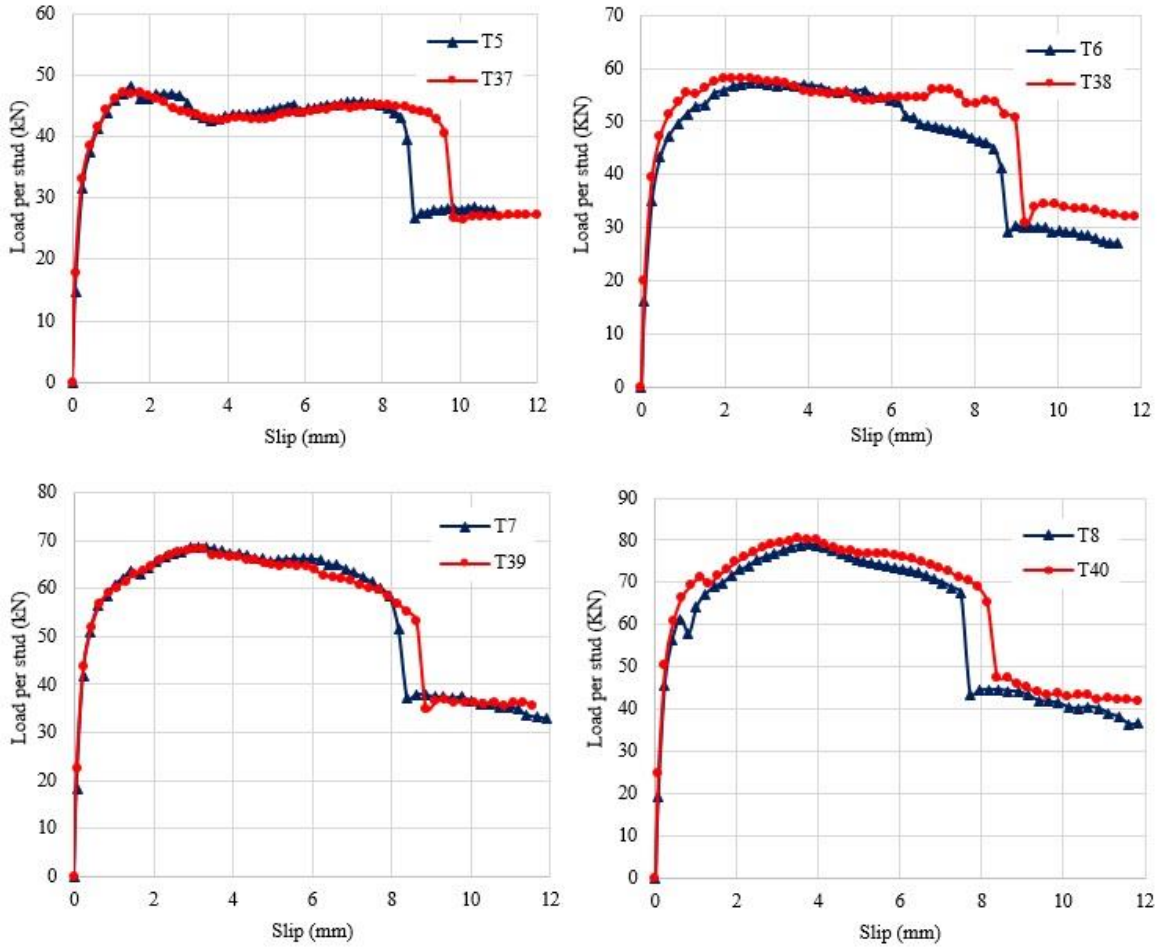


Figure 4.22 Comparison between single and double mesh reinforcement in models with 146 mm deep deck

### 4.3.5 Group E: effect of slab depth

The change in the slab depth is said to affect the behaviour of a headed stud connector. Around 30% increase was achieved in the shear connector resistance when the slab depth was increased from 140 to 225 mm. This behaviour was found in an experiment done by Smith and Couchman (2010) among push tests with only 60 mm deep deck. The authors recommended further study to ratify this behaviour. For this reason, the change in the slab depth is considered herein to see if such parameter has a possible effect on the shear connector resistance with very deep decks. According to Kingspan company (2011), the slab depth of 146 mm deck can be increased to 305 mm. Therefore, three different depths were selected to be investigated including 245, 275, and 305 mm. The concrete grade was only 20

and 40 MPa. The total number of models are six (T41-46). Details of this group are reported in Table 4.3.

Table 4.3 Details of the push test models in Group F

| Test | Concrete grade (MPa) | Profiled decking | | | Headed stud | | Slab depth (mm) |
|---|---|---|---|---|---|---|---|
| | | $b_o$ (mm) | $h_p$ (mm) | $b_o/h_p$ | $n_r$ | $d \times h_{sc}$ (mm) | |
| T41 | 20 | 97.5 | 146 | 0.67 | 5 | 19 × 195 | 245 |
| T42 | 20 | 97.5 | 146 | 0.67 | 5 | 19 × 195 | 275 |
| T43 | 20 | 97.5 | 146 | 0.67 | 5 | 19 × 195 | 305 |
| T44 | 40 | 97.5 | 146 | 0.67 | 5 | 19 × 195 | 245 |
| T45 | 40 | 97.5 | 146 | 0.67 | 5 | 19 × 195 | 275 |
| T46 | 40 | 97.5 | 146 | 0.67 | 5 | 19 × 195 | 305 |

Test results suggested that the slab depth variation had a negligible effect on the shear connector resistance and load-slip behaviour. Figures 4.23 and 4.24 present various slab depths associated with the load-slip curves. The shear stud capacity gained only 5% increment when the slab depth increased from 215 to 245 mm, but no further increase was remarked beyond 245 mm deep. The findings oppose the significant development seen before among push tests with mid-depth decks. From the observation, the failure mechanism of models with very deep decks concentrates in the lower section of the concrete slab (i.e. the concrete volume within ribs). Thus, any extra concrete above the head of the stud connector would not be beneficial. This is another evidence that the shear stud resistance is highly governed by the concrete embedded around the stud rather than the concrete volume above the stud's head.

All models in group F failed by a combination of concrete cone and rib punching, except for T46 which failed due to rib punching and stud shearing. In case of T46, concrete cones did not fully develop as shown in Figure 4.25. Another observation on the tensile concrete damage was made by cutting models across their middle lengths as seen in Figure 4.26. Clearly, all models experienced complete concrete damage except T46. This is due to higher strength concrete (C40) together with the high depth of slab (305 mm), which shifted failure to weaker and less stiff components, such as steel decking. For this reason, the steel sheeting experienced more local buckling than any other model. Similar to group A, the last three studs experienced double curvature deformation. In conclusion, the findings of this group

helped to emphasise that the concrete damage within ribs control the behaviour of headed stud in very deep decks. The next section discusses a unique slab reinforcement to overcome the challenge of the concrete damage in very deep decks.

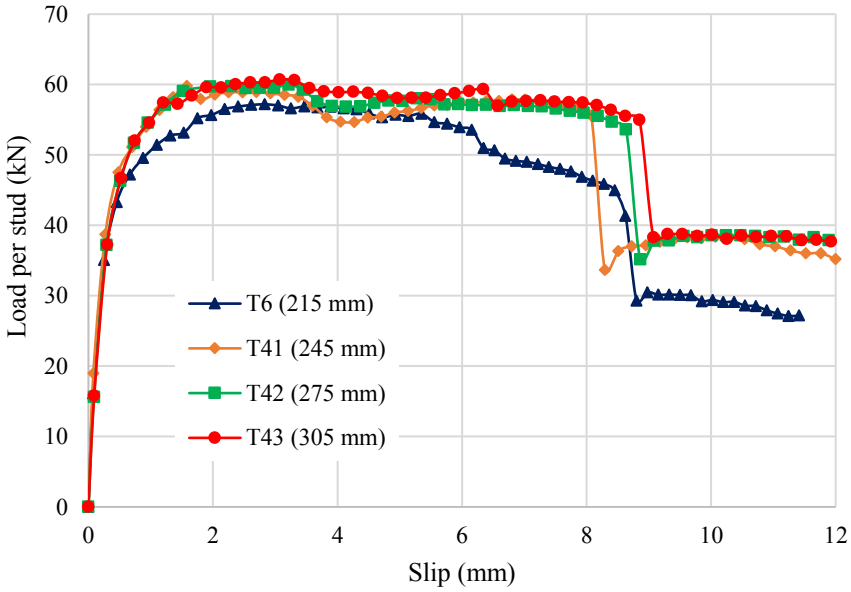


Figure 4.23 Load-slip curves of models with different slab depths and C20 concrete grade

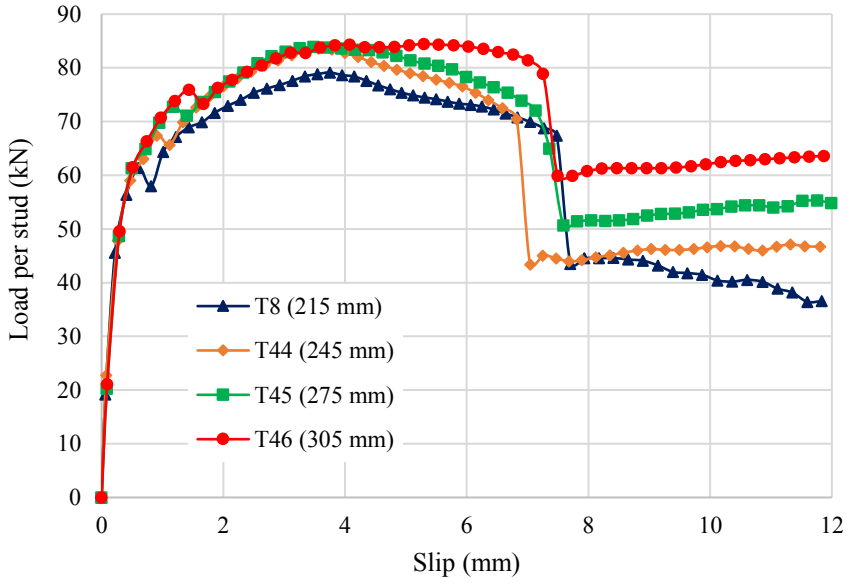


Figure 4.24 Load-slip curves of models with different slab depths and C40 concrete grade

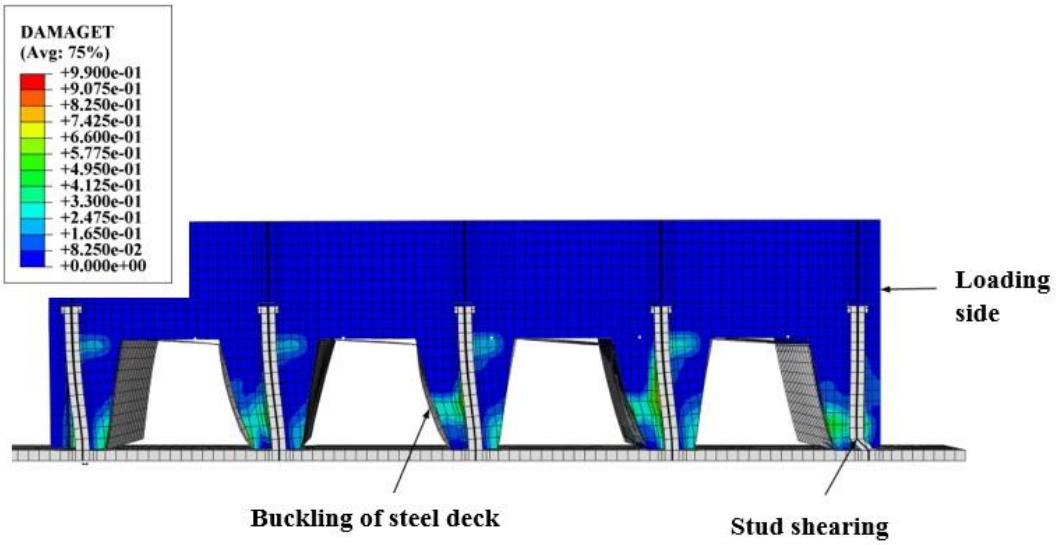


Figure 4.25 Side cut view of T46 at the end of the numerical analysis

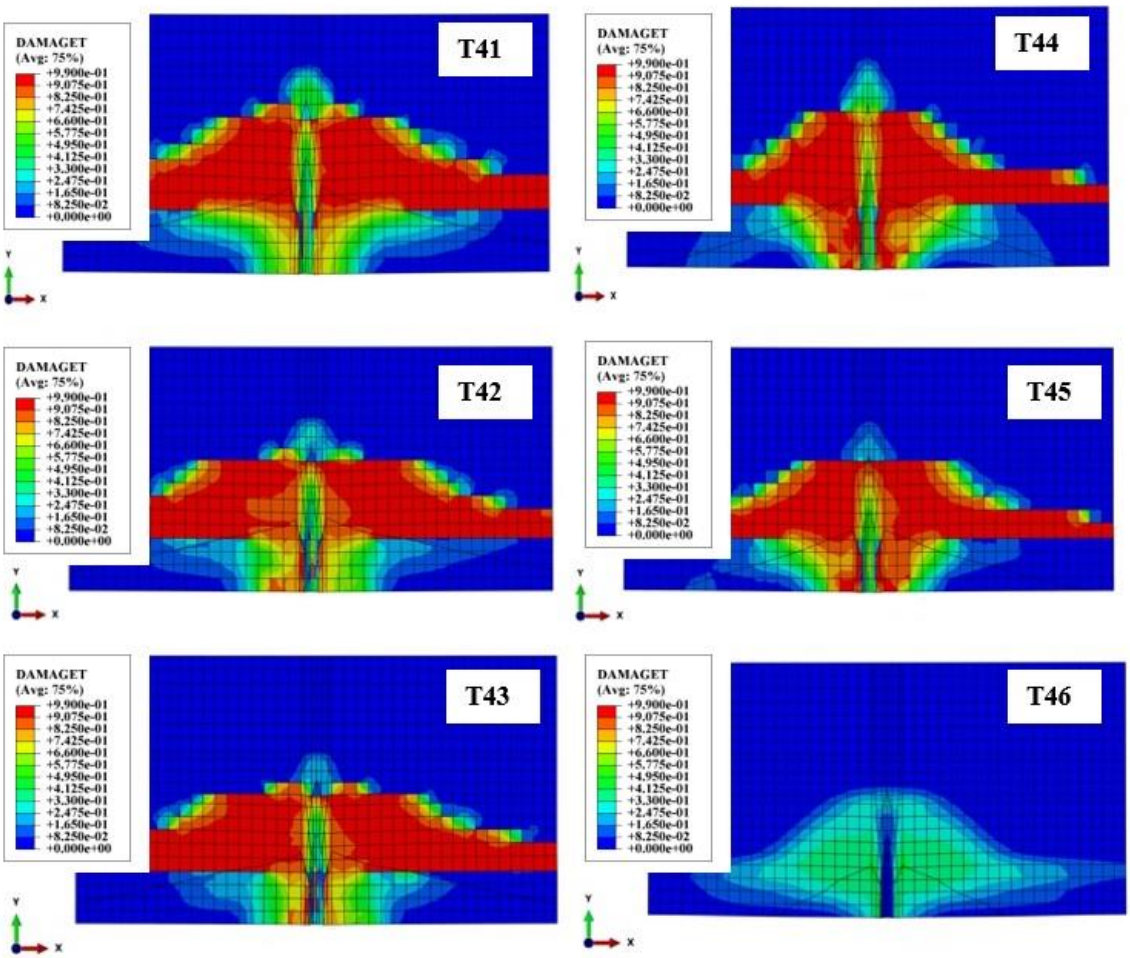


Figure 4.26 Concrete cones formation of models in group E

### 4.3.6 Group F: special case of slab reinforcement

It is now clear that the concrete volume within ribs is the critical zone where the behaviour of the headed stud is controlled. From the initial observations on models with very deep decks, the tensile concrete damage generates within the ribs and mainly propagates through the concrete part surrounding the stud connectors. This behaviour was attributed to the narrow geometry of composite decks deeper than 80 mm that offers little concrete volume to resist the shear load. The brittle failure of concrete will be a natural consequence causing less shear connector resistance. If the tendency of the concrete damage was suppressed, it would allow more load-bearing capacity to achieve. Because the traditional slab reinforcement was unfeasible, a new slab reinforcement technique was proposed.

The wire-mesh reinforcement was assembled based on the path of concrete damage. This means that vertical and horizontal steel bars were considered. For the inner three ribs, the wire-mesh bars were positioned at the back and front to the stud connectors, while the outer ribs only contained one wire-mesh bars layout. A193 wire-mesh (7 mm in diameter) was used and assembled with the traditional slab reinforcement above the steel deck as one part. Afterwards, it was embedded inside the concrete slab using the embedded constraint method. This unique technique of slab reinforcement can be easily implemented in practice. The model of such wire-mesh bars is illustrated in Figure 4.27. This group contains eight models (T47-54), the test arrangement was similar to group A.

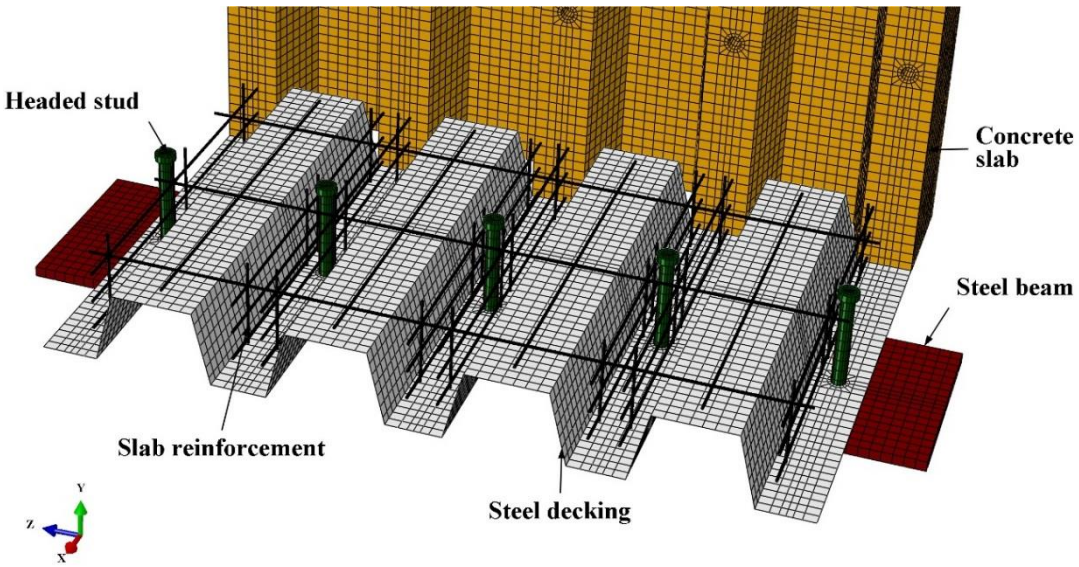


Figure 4.27 Push test with very deep deck reinforced by unique wire-mesh bars

The use of the unique wire-mesh bars appeared to be a successful means in developing the behaviour of headed stud placed in very deep decks. This technique led for the stud connector to gain an average of 26% and 23% more shear resistance for models with 100 and 146 m deep decks respectively. Also, the load bearing capacity was significantly improved resulting in more ductile response as compared to those obtained from the control case. Figures 4.28 and 4.29 present a comparison between the load-slip curves obtained from this group and those from the control case. This development was because the proposed new technique of slab reinforcement was capable of suppressing the concrete damage within the ribs. As a result, the stud connector gained more shear resistance and ductility. The failure propagation is shown in Figure 4.30. The failure mode in all cases was stud shearing and rib punching failure. Overall, this part of the study brings a new approach in strengthening the profiled slab with very deep decks to which both strength and ductility of headed stud develop.

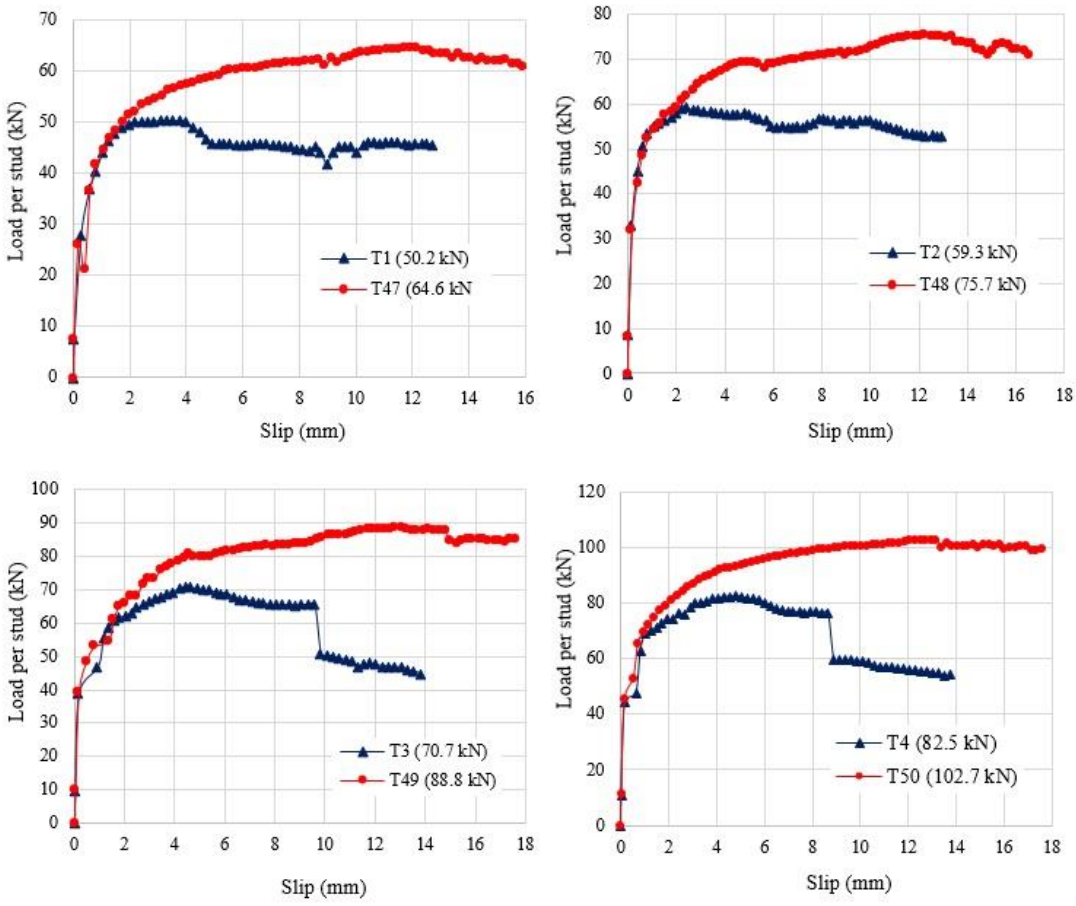


Figure 4.28 Comparison between load-slip curves obtained from group A and F for tests with 100 mm deep decks

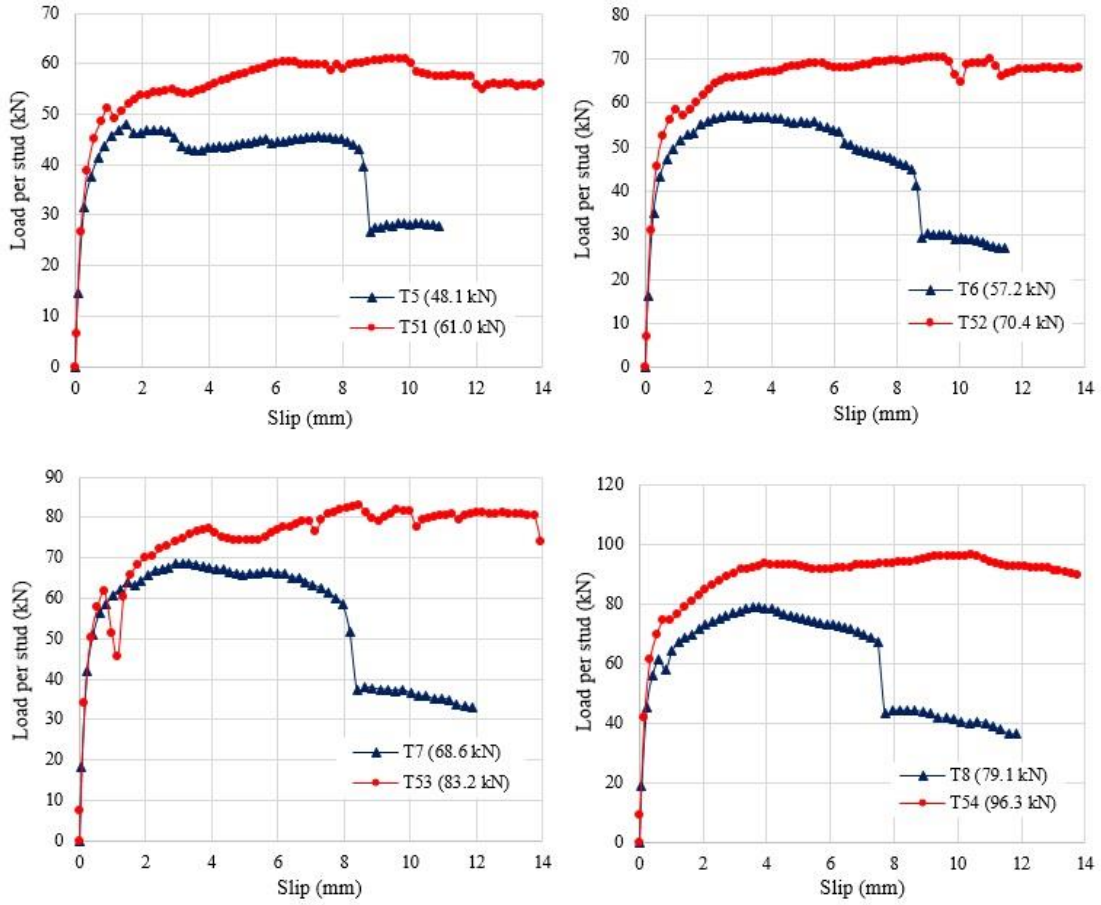


Figure 4.29 Comparison between load-slip curves obtained from group A and F for tests with 146 mm deep decks

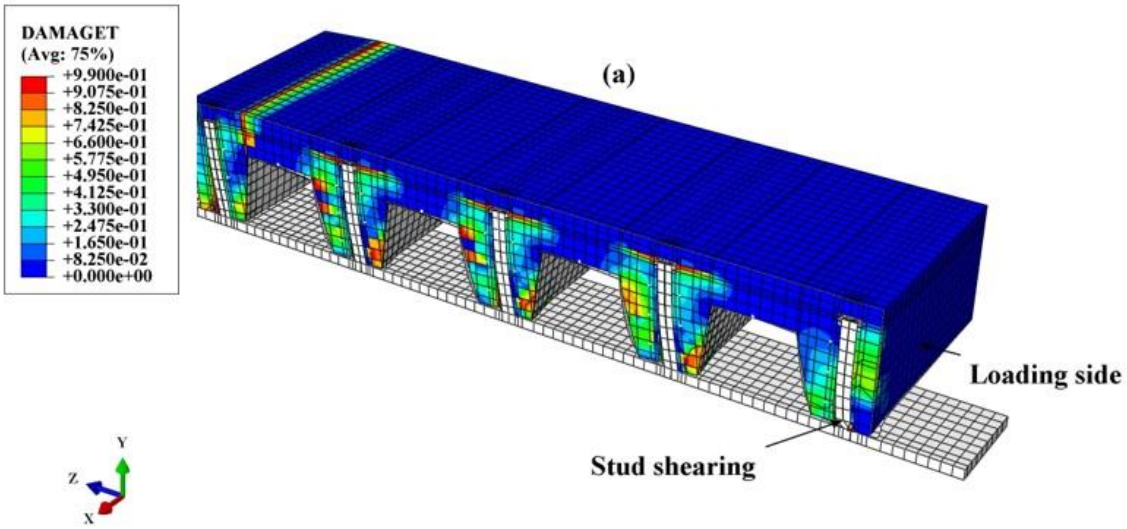

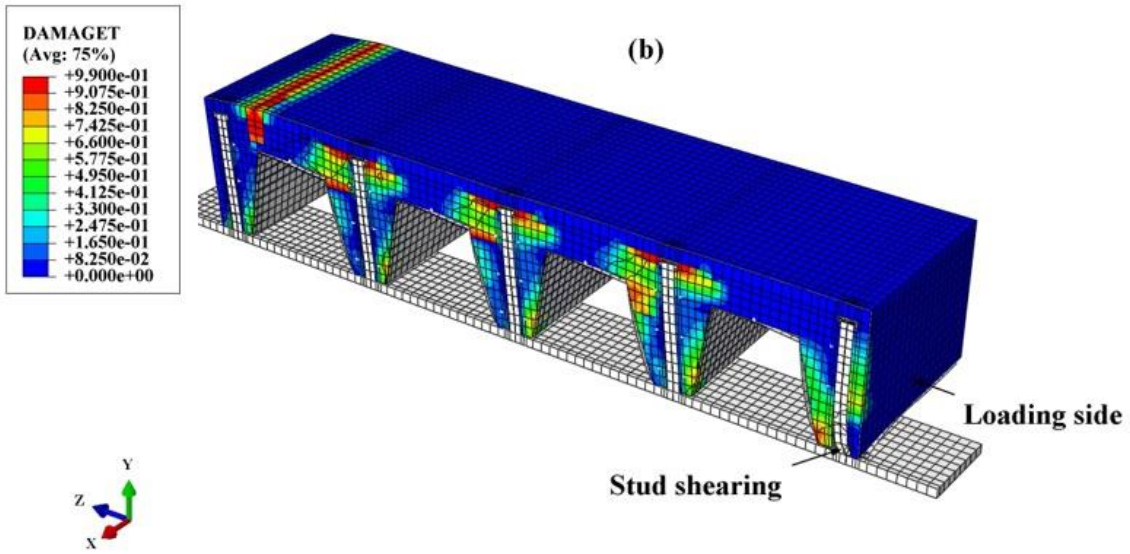


Figure 4.30 Failure at the end for models reinforced by special wire-mesh bars: (a) 100 mm deep deck (b) 146 mm deep deck

Table 4.4 FE results of models with perpendicular steel decks of 100 and 146 mm deep

| Group | Test | Concrete grade (MPa) | Steel decking | | | Headed stud | | Slab depth (mm) | Load per stud (kN) | Parameter |
|---|---|---|---|---|---|---|---|---|---|---|
| | | | $b_o$ (mm) | $h_p$ (mm) | $b_o/h_p$ | $n_r$ | $d \times h_{sc}$ (mm) | | | |
| A | T1 | 12 | 100 | 100 | 1.00 | 5 | 19 × 140 | 160 | 50.2 | Rib geometries |
| | T2 | 20 | 100 | 100 | 1.00 | 5 | 19 × 140 | 160 | 59.3 | |
| | T3 | 30 | 100 | 100 | 1.00 | 5 | 19 × 140 | 160 | 70.7 | |
| | T4 | 40 | 100 | 100 | 1.00 | 5 | 19 × 140 | 160 | 82.5 | |
| | T5 | 12 | 97.5 | 146 | 0.67 | 5 | 19 × 195 | 215 | 48.1 | |
| | T6 | 20 | 97.5 | 146 | 0.67 | 5 | 19 × 195 | 215 | 57.2 | |
| | T7 | 30 | 97.5 | 146 | 0.67 | 5 | 19 × 195 | 215 | 68.6 | |
| | T8 | 40 | 97.5 | 146 | 0.67 | 5 | 19 × 195 | 215 | 79.1 | |
| B | T9 | 12 | 100 | 100 | 1.00 | 3 | 19 × 140 | 160 | 60.7 | Studs placed in alternative rib |
| | T10 | 20 | 100 | 100 | 1.00 | 3 | 19 × 140 | 160 | 72.6 | |
| | T11 | 30 | 100 | 100 | 1.00 | 3 | 19 × 140 | 160 | 84.3 | |
| | T12 | 40 | 100 | 100 | 1.00 | 3 | 19 × 140 | 160 | 97.1 | |
| | T13 | 12 | 97.5 | 146 | 0.67 | 3 | 19 × 195 | 215 | 59.4 | |
| | T14 | 20 | 97.5 | 146 | 0.67 | 3 | 19 × 195 | 215 | 71.4 | |
| | T15 | 30 | 97.5 | 146 | 0.67 | 3 | 19 × 195 | 215 | 84.8 | |
| | T16 | 40 | 97.5 | 146 | 0.67 | 3 | 19 × 195 | 215 | 93.1 | |
| | T17 | 12 | 100 | 100 | 1.00 | 3 | 19 × 140 | 160 | 47.8 | Studs placed in the three middle ribs |
| | T18 | 20 | 100 | 100 | 1.00 | 3 | 19 × 140 | 160 | 56.5 | |
| | T19 | 30 | 100 | 100 | 1.00 | 3 | 19 × 140 | 160 | 66.8 | |
| | T20 | 40 | 100 | 100 | 1.00 | 3 | 19 × 140 | 160 | 78.8 | |
| | T21 | 12 | 97.5 | 146 | 0.67 | 3 | 19 × 195 | 215 | 40.6 | |
| | T22 | 20 | 97.5 | 146 | 0.67 | 3 | 19 × 195 | 215 | 51.9 | |
| | T23 | 30 | 97.5 | 146 | 0.67 | 3 | 19 × 195 | 215 | 62.7 | |
| | T24 | 40 | 97.5 | 146 | 0.67 | 3 | 19 × 195 | 215 | 71.0 | |
| C | T25 | 12 | 100 | 100 | 1.00 | 10 | 19 × 140 | 160 | 39.1 | Stud pairs |
| | T26 | 20 | 100 | 100 | 1.00 | 10 | 19 × 140 | 160 | 47.8 | |

| | | | | | | | | | | |
|---|---|---|---|---|---|---|---|---|---|---|
| | T27 | 30 | 100 | 100 | 1.00 | 10 | 19 × 140 | 160 | 54.8 | |
| | T28 | 40 | 100 | 100 | 1.00 | 10 | 19 × 140 | 160 | 62.1 | |
| | T29 | 12 | 97.5 | 146 | 0.67 | 10 | 19 × 195 | 215 | 38.3 | |
| | T30 | 20 | 97.5 | 146 | 0.67 | 10 | 19 × 195 | 215 | 45.7 | |
| | T31 | 30 | 97.5 | 146 | 0.67 | 10 | 19 × 195 | 215 | 50.3 | |
| | T32 | 40 | 97.5 | 146 | 0.67 | 10 | 19 × 195 | 215 | 53.2 | |
| D | T33 | 12 | 100 | 100 | 1.00 | 5 | 19 × 140 | 160 | 51.4 | Double wire-mesh reinforcement |
| | T34 | 20 | 100 | 100 | 1.00 | 5 | 19 × 140 | 160 | 60.8 | |
| | T35 | 30 | 100 | 100 | 1.00 | 5 | 19 × 140 | 160 | 72.3 | |
| | T36 | 40 | 100 | 100 | 1.00 | 5 | 19 × 140 | 160 | 84.6 | |
| | T37 | 12 | 97.5 | 146 | 0.67 | 5 | 19 × 195 | 215 | 47.2 | |
| | T38 | 20 | 97.5 | 146 | 0.67 | 5 | 19 × 195 | 215 | 58.2 | |
| | T39 | 30 | 97.5 | 146 | 0.67 | 5 | 19 × 195 | 215 | 68.3 | |
| | T40 | 40 | 97.5 | 146 | 0.67 | 5 | 19 × 195 | 215 | 80.4 | |
| E | T41 | 20 | 97.5 | 146 | 0.67 | 5 | 19 × 195 | 245 | 59.8 | Slab depth |
| | T42 | 20 | 97.5 | 146 | 0.67 | 5 | 19 × 195 | 275 | 60.0 | |
| | T43 | 20 | 97.5 | 146 | 0.67 | 5 | 19 × 195 | 305 | 60.7 | |
| | T44 | 40 | 97.5 | 146 | 0.67 | 5 | 19 × 195 | 245 | 83.6 | |
| | T45 | 40 | 97.5 | 146 | 0.67 | 5 | 19 × 195 | 275 | 83.9 | |
| | T46 | 40 | 97.5 | 146 | 0.67 | 5 | 19 × 195 | 305 | 84.5 | |
| F | T47 | 12 | 100 | 100 | 1.00 | 5 | 19 × 140 | 160 | 64.6 | Special wire-mesh bars |
| | T48 | 20 | 100 | 100 | 1.00 | 5 | 19 × 140 | 160 | 75.7 | |
| | T49 | 30 | 100 | 100 | 1.00 | 5 | 19 × 140 | 160 | 88.8 | |
| | T50 | 40 | 100 | 100 | 1.00 | 5 | 19 × 140 | 160 | 102.7 | |
| | T51 | 12 | 97.5 | 146 | 0.67 | 5 | 19 × 195 | 215 | 61.0 | |
| | T52 | 20 | 97.5 | 146 | 0.67 | 5 | 19 × 195 | 215 | 70.4 | |
| | T53 | 30 | 97.5 | 146 | 0.67 | 5 | 19 × 195 | 215 | 83.2 | |
| | T54 | 40 | 97.5 | 146 | 0.67 | 5 | 19 × 195 | 215 | 96.3 | |

## 4.4 Conclusions

This chapter addressed the behaviour of headed stud connector in secondary composite beams with steel decks deeper than 80 mm. The literature has been enriched with new investigations considering two different types of steel decks including 100 and 146 mm deep decks. The FE modelling involved 54 push tests to conduct a parametric study. This was made of rib geometries, studs' layout, number of studs per rib, slab reinforcement and slab depth. These parameters were linked to the shear connector resistance, load-slip behaviour and failure mode. Test results revealed that the shear stud capacity with narrow ($b_o/h_p < 1.5$) and very deep decks was almost 65% of that obtained from the traditional steel decks (60-80 mm deep). The narrow geometry of very deep decks which offers relatively less concrete volume was the main reason behind that drastic difference.

Attempts were made aiming at developing the strength and ductility of headed stud placed in very deep decks. Reinforcing the concrete slab above the steel deck or adding extra concrete volume above the stud's head were ineffective at meeting that goal. The behaviour of headed stud appeared to be mainly affected by the concrete volume embedded within ribs. New techniques were proposed in this study to the push test arrangements including placing studs in every alternative rib and reinforcing the concrete embedded within ribs by special wire-mesh bars layout. The first technique led for the shear stud capacity to increase by an average of 20%. The use of the special wire-mesh bars was successful in suppressing the concrete damage. This resulted in an average of 24% increase in the shear stud capacity besides achieving higher ductility than the control case. These techniques would enhance the behaviour of the headed stud if they were implemented in practice.

Knowing that the narrow and very deep decks make drastic changes in the shear connector resistance, the applicability of the current design equations is under question. It is uncertain if those equations can provide accurate shear stud strength predictions if such steel decks are used. The next chapter will discuss this part in detail.

# Chapter 5 Comparison of push-off models results with perpendicular profiled sheeting against existing strength prediction methods

# Chapter 5

# Comparison of push-off models results with perpendicular profiled sheeting against existing strength prediction methods

## 5.1 General

In this chapter, the FE results obtained from the push-off models with 100 and 146 mm deep decks oriented perpendicular to the steel beam are compared to some standard provisions and other theoretical methods that have been previously proposed. This part of the study aims to discover whether any of the existing strength prediction methods accurately predict the shear stud capacity placed in steel decks deeper than 80 mm. As it is found later that there is a necessity to introduce a modern formula to deal with different types of open trapezoidal profiled sheeting, an extensive finite element push models will be carried out considering various parameters that influence the shear connector resistance in a profiled sheeting. Eventually, a multi-linear regression analysis done on the observed results will yield new inclusive equations, which provide a prediction of shear connector resistance considering different rib geometries, stud's layout and other parameters.

## 5.2 Comparison of FE results against design codes and developed theoretical equations

In fact, there is no specific formula in the literature to predict the shear capacity of the headed stud in a profiled decking greater than 80 mm deep. The existing proposed equations in the design codes and elsewhere were developed based on the dimensions of common profiled sheeting (i.e. 60 and 80 mm deep). With the deep and narrow ribs of the modern composite decks, the author feels that the applicability of the currently proposed equations is questionable. It is not certain whether the current equations cope with the geometry effect of decks deeper than 80 mm. Thus, it was decided to see how well these equations meet the obtained results from the parametric study.

The shear resistance of studs obtained from the parametric study in Chapter Four is compared with the nominal design strengths of headed stud connectors predicted by the European Code (EC4), American specification ANSI/AISC 360-2016, and some analytical methods

proposed by Johnson and Yuan (1998b), Konrad (2011), and Nellinger et al. (2018). The FE results are taken from the control case including those with single studs (T1-8) and stud pairs (T25-32).

## 5.3 Eurocode 4 provisions

The nominal strength of headed shear stud connector is taken as the lesser value obtained from Equations 5.1 and 5.2 and multiplied by a reduction factor using Equation 5.3.

$$P_{EC4} = 0.29\ \alpha\ d^2 \sqrt{f_c\ E_{cm}} \qquad \text{Eq. 5.1}$$

$$P_{EC4} = 0.8\ f_u \frac{\pi d^2}{4} \qquad \text{Eq. 5.2}$$

$$k_t = \frac{0.7}{\sqrt{Nr}} \frac{b_o}{h_p} \left[\frac{h_{sc}}{h_p} - 1\right] \qquad \text{Eq. 5.3}$$

where $\alpha = 0.2\ (h_{sc}/d + 1)$ for $(3 \leq h_{sc}/d \leq 4)$ and $\alpha = 1.0$ for $(h_{sc}/d > 4)$, $h_{sc}$ and $d$ are the height and diameter of the stud respectively, $E_{cm}$ is the mean value of Young's modulus of concrete taken from the European Code (EC2), $f_u$ is the ultimate tensile strength of headed stud (not greater than 450 MPa), $b_o$ is the average width of trough, $N_r$ is the number of stud per rib, and $h_p$ are the of rib deck. The factor $k_t$ should not be taken greater than the appropriate value $k_{tmax}$ given in Table 5.1.

Table 5.1 Upper limits $k_{tmax}$ for the reduction factor $k_t$ according to EC4

| Number of stud connectors per rib | Thickness of sheeting (mm) | Stud not exceeding 20 mm in diameter and welded through profiled sheeting | Profiled sheeting with holes and studs 19 mm or 22 mm in diameter |
|---|---|---|---|
| 1 | ≤ 1.0 | 0.85 | 0.75 |
| | > 1.0 | 1.0 | 0.75 |
| 2 | ≤ 1.0 | 0.70 | 0.60 |
| | > 1.0 | 0.80 | 0.60 |

The relationship between the load per stud obtained from the FE analysis and the EC4 predicted strengths is shown in Figure 5.1 and Table 5.4. Apparently, the EC4 equations greatly underestimated shear stud capacities with very deep decks. Some prediction were 4

and 5 times lower than the FE results. The average ratio of $P_{FE}/P_{EC4}$ is 3.99 with the coefficient of variation of 27.5%. It is obvious that the equations in EC4 are not applicable in predicting the shear connector resistance in very deep profiled decks. Applying the dimensions of a 100 and 146 mm deep deck with their relevant stud heights in Equation 5.3 resulted in very low reduction factor $k_t$ ranging from 0.11 to 0.28. For the trapezoidal profiled decking, equal to or less than 80 mm deep, the ratios of average rib width to the rib height ($b_o/h_p$) are greater than 1.5 in most cases. However, in narrow and deep decks, the rib deck ratio ($b_o/h_p$) ≤ 1.0. This is the reason Equation 5.3 resulted in low reduction factor values which in turn gave very low predicted strengths. It is recommended that Equation 5.3 should be calibrated again particularly the terms ($b_o/h_p$) and ($h_{sc}/h_p$) to account for the geometries of composite decks deeper than 80 mm.

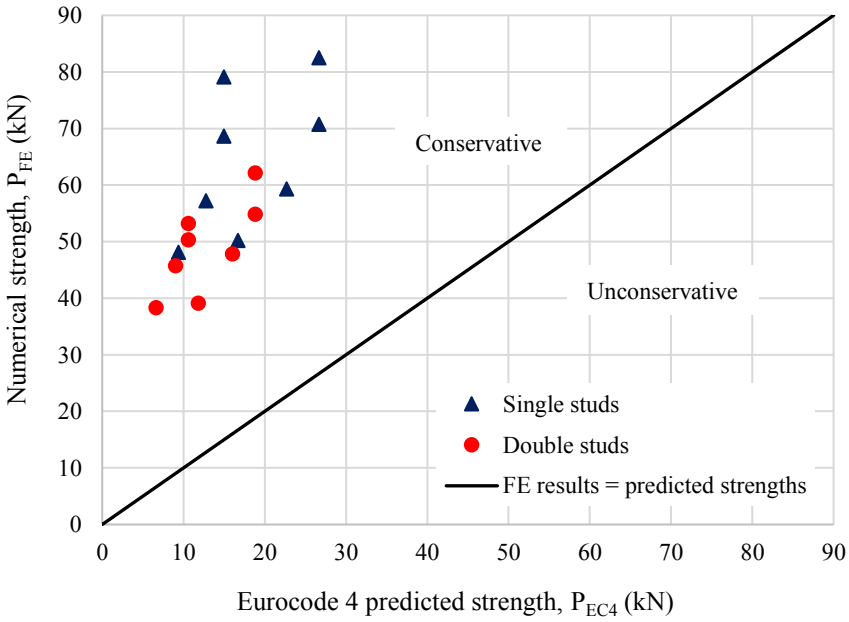


Figure 5.1 FE strengths versus EC4 predicted strengths

## 5.4 ANSI/AISC 306-2016 provisions

The nominal strength of one headed stud connector embedded in a solid concrete slab is determined by using Equation 5.4.

$$P_{AISC} = 0.5\, A_s \sqrt{f_c E_c} \leq R_g\, R_p\, A_s f_u \qquad \text{Eq. 5.4}$$

where $A_s$ is the cross-sectional area of the steel headed stud, $E_c$ modulus of elasticity of concrete ($0.043\ w_c^{1.5}\sqrt{f_c}$), $w_c$ is the density of concrete (kg/m$^3$), $f_u$ is the specified minimum tensile strength of headed stud and $R_g$ and $R_p$ are factors given in Table 5.2.

Table 5.2 Values of $R_g$ and $R_p$ according to ANSI/AISC 306-2016 provisions

| Condition | $R_g$ | $R_p$ |
|---|---|---|
| Decking oriented perpendicular to the steel beam<br>Number of headed studs per rib | | |
| 1 | 1.0 | 0.6* |
| 2 | 0.85 | 0.6* |
| 3 or more | 0.7 | 0.6* |

The FE results are compared to the ANSI/AISC predicted strengths in Figure 5.2 and Table 5.4. It was found that ANSI/AISC equations gave unsafe predictions in general. The average ratio of $P_{FE}/P_{AISC}$ is 0.79, the corresponding coefficient of variation is 16.96%. It was noticed that the controlling equation was the steel failure ($R_g\ R_p\ A_s\ f_u$) when the strength of concrete was higher than 20 MPa. The predicted strengths of the headed stud in case of single and double studs remained constant when the concrete strength was greater than 20 MPa. This suggests that the use of equations in the American specifications would result in unreliable values as they are not capable of dealing with different variables such as the concrete strength and number of studs per rib. Moreover, the American code comes with the drawback that the geometries of steel decks are not considered.

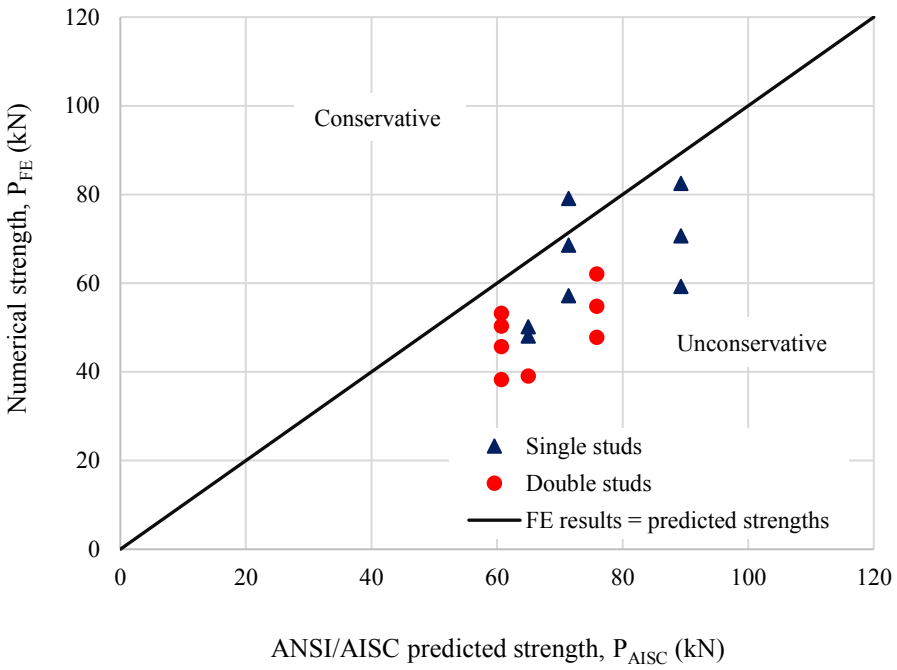


Figure 5.2 FE strengths versus ANSI/AISC predicted strengths

## 5.5 Comparison with analytical methods according to Johnson and Yuan (1998b)

Based on a theoretical analysis carried out by Johnson and Yuan (1998b), the researchers proposed several equations to predict the shear stud capacity in composite beams with transverse sheeting. Those equations were developed based on five modes of failure including shank shearing (SS), rib punching (RP), rib punching with shank shearing (RPSS), rib punching with concrete pull-out (RPCP), and concrete pull-out (CPT). In this research, two analytical approaches were selected, namely the developed equations from RPCP, and the developed equation from CPT. The RP equations were neglected because they do not consider the number of studs per rib, and they are only relevant to tests with unfavourable stud position, where studs can only be placed in the central position in very deep decks.

### 5.5.1 Combined concrete pull-out and rib punching failure (RPCP)

For combined rib punching and concrete pull-out failure of studs in slabs with two studs placed in series or diagonally in a rib, the stud placed on the favourable side is assumed to fail by concrete pull-out, whilst the stud placed on the unfavourable side is assumed to fail

by rib punching. Eventually, the shear resistance of each stud $P_{RPCP}$ is assumed to be the mean value of $P_{RP}$ and $P_{CP}$ as given in Equation 5.5.

$$P_{RPCP} = (P_{RP} + P_{CP}) / 2 \quad \text{Eq. 5.5}$$

For the rib punching failure mode, the equations are as follow:

$$P_{RP} = k_{rp} P_{EC4} \quad \text{Eq. 5.6}$$

$$k_{rp} = [\eta_{rp} + \lambda_{rp} (1 + \lambda_{rp}^2 - \eta_{rp}^2)^{0.5}] / (1 + \lambda_{rp}^2) \leq 1.0 \quad \text{Eq. 5.7}$$

$$\eta_{rp} = [(e + h_{sc} - h_p) t_s f_{yp}] / P_{EC4} \quad \text{Eq. 5.8}$$

$$\lambda_{rp} = e T_y / 2 h_p P_{EC4} \quad \text{Eq. 5.9}$$

$$T_y \cong 0.8 A_s f_u \quad \text{Eq. 5.10}$$

where $P_{EC4}$ is the shear strength of stud in a solid slab calculated from Equations 5.1 and 5.2, $\eta_{rp}$ is non-dimensional group for rib punching in RPCP failure mode, $\lambda_{rp}$ is non-dimensional group for rib punching in RPCP failure mode, $e$ is the distance from centre of stud to nearer wall of rib (i.e. 50 and 48.75 mm for 100 and 146 mm deep decks respectively), $t_s$ is the thickness of sheeting and $f_{yp}$ is the yield strength of sheeting.

For the concrete pull-out failure mode, the equations are as follows:

$$P_{CP} = k_{cp} P_{EC4} \quad \text{Eq. 5.11}$$

$$k_{cp} = [\eta_{cp} + \lambda_{cp} (1 + \lambda_{cp}^2 - \eta_{cp}^2)^{0.5}] / (1 + \lambda_{cp}^2) \leq 1.0 \quad \text{Eq. 5.12}$$

$$\eta_{cp} = [0.56 v_{tu} h_{sc}^2 (e + s_t - \tfrac{h_{sc}}{4})] / h_p P_{EC4} \quad \text{if } 0.75h_{sc} \leq (e + st) \quad \text{Eq. 5.13}$$

$$\eta_{cp} = [v_{tu} (e + s_t)^2 (0.75h_{sc} - \tfrac{(e+s_t)}{3})] / h_p P_{EC4} \quad \text{if } 0.75h_{sc} > (e + st) \quad \text{Eq. 5.14}$$

$$\lambda_{cp} = e T_y / h_p P_{EC4} \quad \text{Eq. 5.15}$$

$$T_y \cong 0.8 A_s f_u \quad \text{Eq. 5.16}$$

$$v_{tu} = 0.8 f_{cu}^{0.5} \leq 5 \quad \text{Eq. 5.17}$$

where $\eta_{cp}$ is non-dimensional group for concrete pull-out in RPCP failure mode, $\lambda_{cp}$ is non-dimensional group for concrete pull-out in RPCP failure mode, $h_{sc}$ is the total height of stud, $s_t$ is the spacing between studs, and $v_{tu}$ is the shear strength of concrete. Theoretically, the

equations developed from the RPCP failure mode are not suitable for composite beams with very deep decks, especially the equations for concrete pull-out failure. These formulae were developed based on placing two studs in series or staggered in a trough. In the current research, it is not possible to place two studs in any arrangement but the same line due to the narrowness of rib. Nevertheless, if these equations were meant to be used, then $s_t$ would be zero in case of single studs, and $s_t$ would be assumed as the transverse spacing between studs in case of stud pairs. Thus, Equation 5.14 would be used for single and double studs of 19 × 195 mm, as it justifies the condition of $0.75h_{sc} > (e + st)$. On the other hand, Equation 5.13 would be used for single and double studs of 19 × 140 mm, as it justifies the condition of $0.75h_{sc} \leq (e + st)$.

The predicted strengths of the developed equation based on RPCP failure were compared to the numerical results. The comparison is shown in Figure 5.3 and Table 5.4. The average ratio of $P_{FE}/P_{RPCT}$ is 1.18, and the coefficient of variation is 29.84%. In case of the push models with single studs, the developed equations underestimated the shear resistance of headed stud when the concrete grade was C12 and C20 with a deviation of over 20%. However, the deviation in results became much higher when the concrete grade was C30 and C40. The predicted strengths remained within the range of 47-51 kN and 39-42 for tests with 100 and 146 mm deep decks respectively and did not reveal a significant rise as the concrete strength increased.

In case of the push models with double studs, the predicted strengths considerably overestimated the headed stud strengths obtained from the numerical analysis. It was noticed that the predicted values were even higher than the ones achieved for the single studs which ideally should be lower. The cause of this scatter was that the number of studs per rib is not recognised as a variable in this particular method. In conclusion, the proposed equations from the RPCP failure would give unsteady results for the composite beams with very deep decks. The large discrepancy in results is due to the way in which the equations were developed which was based on the studs' arrangement, and it is different from the studs' layout in the current research.

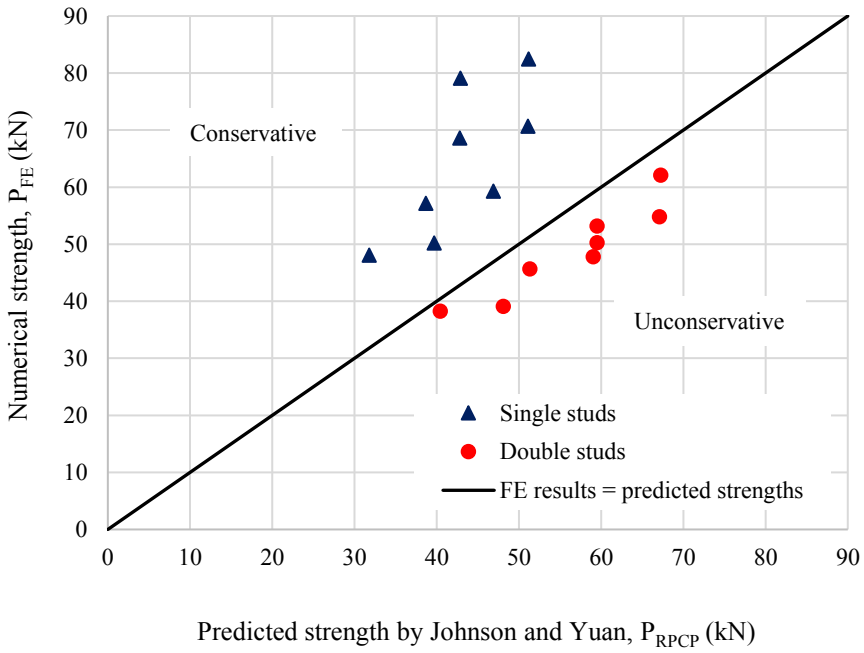


Figure 5.3 FE strengths versus $P_{RPCT}$ predicted strengths

### 5.5.2 Concrete pull-out failure (CPT)

For concrete pull-out failure of studs in slabs with single or double studs per trough, in a central or favourable position, the strength is determined by multiplying the shear strength of stud in a solid slab calculated from Equations 5.1 and 5.2 by the reduction factor $k_{cpt}$ as shown below:

$$P_{CPT} = k_{cpt} P_{EC4} \quad \text{Eq. 5.18}$$

$$k_{cpt} = [\eta_{cpt} + \lambda_{cpt} (1 + \lambda_{cpt}^2 - \eta_{cpt}^2)^{0.5}] / (1 + \lambda_{cpt}^2) \leq 1.0 \quad \text{Eq. 5.19}$$

$$\eta_{cpt} = [0.56 v_{tu} h_{sc}^2 (b_0 - \frac{h_{sc}}{4})] / h_p N_r P_{EC4} \leq 1.0 \quad \text{Eq. 5.20}$$

$$\lambda_{cpt} = e T_y / h_p P_{EC4} \quad \text{Eq. 5.21}$$

$$T_y \cong 0.8 A_s f_u \quad \text{Eq. 5.22}$$

where $k_{cpt}$ is the reduction factor for CPT failure mode, $\eta_{cpt}$ is non-dimensional group for CPT failure mode, $\lambda_{cpt}$ is non-dimensional group for CPT failure mode.

The predicted strengths based on CPT failure are compared with the numerical results as shown in Figure 5.4 and Table 5.4. In general, the average ratio of $P_{FE}/P_{CPT}$ is 1.06 with the coefficient of variation of 11.00%. In terms of the push models with single studs, the developed equations appeared to adequately predict the strength capacity of stud up to the concrete grade of 30 MPa, while the predicted strengths were conservative for the concrete grade of 40 MPa. On the other hand, the predicted strengths were in good agreement with the numerical results from the push models with stud pairs. The maximum scatter in results was 15%.

Although the developed equations from CPT failure did not closely predict the stud capacity in some cases, they seemed more relevant than the ones from RPCP failure to deal with composite beams with very deep decks. In fact, the equations consider the number of studs per trough, and they were developed based on placing studs in a central or favourable position which meets the way the studs are arranged in very deep decks (central position). Furthermore, the scatter in results was not significantly high. Hence, the developed equations from CPT failure could precisely predict the strength of stud if they are calibrated again to cover the geometries of steel decks deeper than 80 mm.

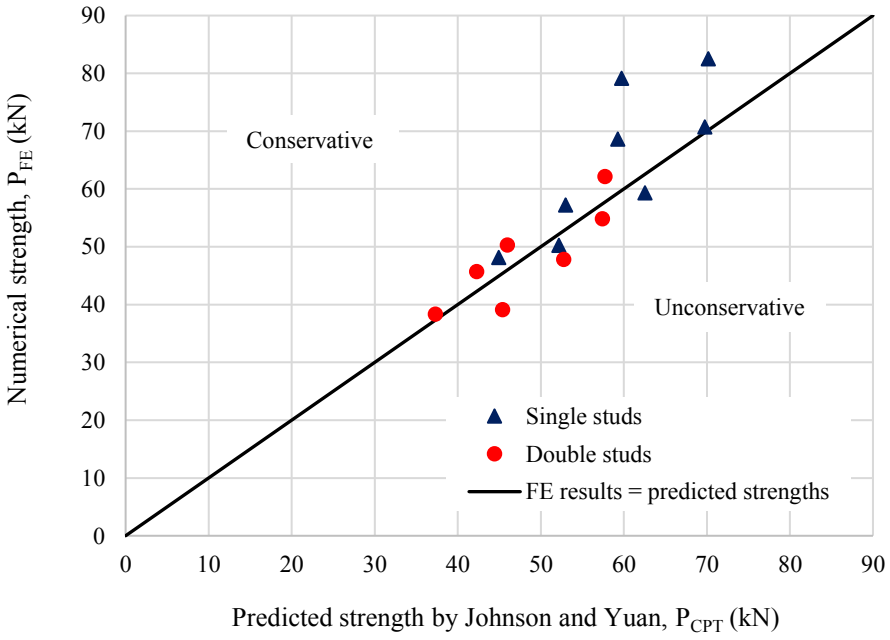


Figure 5.4 FE strengths versus $P_{CPT}$ predicted strengths

## 5.6 Comparison with analytical approach according to Konrad (2011)

New formulae were developed by Konrad (2011) which consider the influence of the welding position of the stud on the shear resistance. The mean shear strength of stud in a profiled decking is the smaller value of Equations 5.23 and 5.24. The reduction factor ($k_t$) in Equation 5.25 is for the mid-position of the stud and the case of $h_{sc}/h_p \leq 1.56$, whilst Equation 5.26 relates to the reduction factor for the mid-position of the stud and the case of $h_{sc}/h_p > 1.56$. For both the 100 and 146 mm deep decks, the rib deck ratio ($b_o/h_p$) is less than 1.56, thus Equation 5.25 is adopted. The author assumed that the geometry of decking does not affect the resistance of stud rupture, and thus the reduction factor is only included in the concrete failure equation.

$$P_{m,s} = 39.85\, A_{Wulst,eff} f_c^{2/3} + 0.59\, f_u\, d^2 \qquad \text{Eq. 5.23}$$

$$P_{m,c} = k_t\,(39.85\, A_{Wulst,eff} f_c^{2/3} + 3.75\, d^2 f_c^{1/3} f_u^{1/2}) \qquad \text{Eq. 5.24}$$

$$k_t = k_n\,[6.79\times10^{-4}\,(b_o/h_p)^2 + 0.17\,(b_o/h_p) + 0.25\,(h_{sc}/h_p)] \quad \leq 1.0 \qquad \text{Eq. 5.25}$$

$$k_t = k_n\,[0.042\,(b_o/h_p) + 0.663] \quad \leq 1.0 \qquad \text{Eq. 5.26}$$

where $A_{Wulst,eff}$ is the effective area of weld collar = 0.5 $h_{Wulst}$ $d_{Wulst}$ (see Table 5.3), $k_n = 1$ for single studs per rib, and $k_n = 0.8$ for stud pairs.

Table 5.3 Effective area of weld collar according to Konrad (2011)

| Diameter of stud (mm) | Height of weld collar ($h_{Wulst}$) (mm) | Diameter of weld collar ($d_{Wulst}$) (mm) | Effective area of weld collar ($A_{Wulst,eff}$) (mm$^2$) |
|---|---|---|---|
| 10 | 2.5 | 13.0 | 16.3 |
| 13 | 3.0 | 17.0 | 25.5 |
| 16 | 4.5 | 21.0 | 47.3 |
| 19 | 6.0 | 23.0 | 63.0 |
| 22 | 6.0 | 29.0 | 87.0 |
| 25 | 7.0 | 40.0 | 140.0 |

Figure 5.5 and Table 5.4 present the comparison between the shear connection resistance from the numerical results and the proposed equations by Konrad (2011). It can be noticed that the proposed equations significantly underestimated the headed stud strengths of all push models, the average ratio of $P_{FE}/P_{Konrad}$ is 1.39, and the corresponding coefficient of variation is 6.41%. This is because of the value before the term $(b_o/h_p)^2$ in Eq. 5.26 being very small

which resulted in a reduction factor ($k_t$) ≤ 0.521. It is then recommended that if the equations proposed by Konrad (2011) were meant to predict the shear connector resistance in very deep decks, Equation 5.25 should be calibrated again in order to give more realistic reduction factor which in turn would result in more accurate strength capacity.

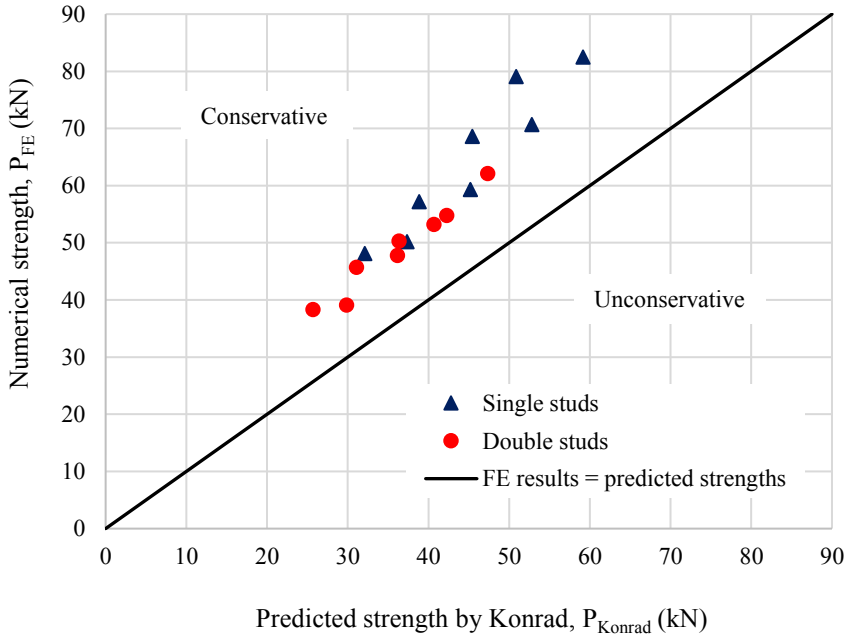


Figure 5.5 FE strengths versus $P_{Konrad}$ predicted strengths

## 5.7 Comparison with the analytical method according to Nellinger et al. (2018)

New equations for the shear resistance of headed stud in transverse profiled sheeting were developed by Nellinger et al. (2018). The mean shear resistance of the headed stud is the smaller value of Equations 5.27 and 5.28. The resultant of a plastic shear-stress distribution in the stud shank is represented by the resistance for steel failure in Equation 5.27. While the resistance of concrete failure in Equation 5.28 is the elastic resistance of the concrete rib in bending and compression plus the plastic bending resistance of the shear stud.

$$P_{Rm} = 1.26 \left(\frac{f_{uk}}{\sqrt{3}}\right) \pi d^2/4 \qquad \text{Eq. 5.27}$$

$$P_{Rm} = 1.23\left[\frac{\left[\alpha_{ct} f_{ctm} + (N_q + N_{sc})/A\right] W + N_{sc} e_1}{h_p\, n_r} + \frac{n_y M_{PL}}{h_s - d/2}\right] \qquad \text{Eq. 5.28}$$

$$N_{sc} = 0.1\, n_r f_{uk}\, \pi d^2/4 \qquad \text{Eq. 5.29}$$

$$A = [2.4h_{sc} + (n_r - 1)\, e_s]\, b_{max} \quad \text{Eq. 5.30}$$

$$W = \frac{1}{6}\,[2.4h_{sc} + (n_r - 1)\, e_s]\, \frac{b_{max}^3}{b_o} \quad \text{Eq. 5.31}$$

$$n_y = 2 \text{ for } h_{sc} \geq h_p + 2d\sqrt{n_r} \quad \text{Eq. 5.32}$$

$$n_y = 1 \text{ for } h_{sc} < h_p + 2d\sqrt{n_r} \quad \text{Eq. 5.33}$$

$$M_{pl} = f_{uk}\, d^3/6 \quad \text{Eq. 5.34}$$

$$h_{sc} = \frac{\beta h_{sc} + [(n_r - 1)(h_p + h_{sc})e_s]/4.8h_{sc}}{1 + [(n_r - 1)e_s/2.4h_{sc}]} \quad \text{Eq. 5.35}$$

where $\alpha_{ct} = 0.85$, $\beta = 0.45$ for trapezoidal decking, and $\beta = 0.41$ for re-entrant decking, $f_{uk}$ is characteristic tensile strength of stud material, $f_{ctm}$ is tensile strength of concrete, $N_q$ is transverse compression force per deck rib, $e_1$ is eccentricity of stud to centreline of rib, $e_s$ is transverse spacing between studs, and $b_{max}$ is the largest width of rib.

Figure 5.6 and Table 5.4 show the relationship between the shear connection resistance obtained from the numerical results and the proposed equations by Nellinger et al. (2018). It is obvious that the proposed equations underestimated the headed stud strengths of all cases, significantly among tests with stud pairs. Some of the predicted values were even lower than those obtained from Konrad's method (2011). The average ratio of $P_{FE}/P_{Nellinger}$ is 1.47 with the coefficient of variation of 21.73%. The resistance of concrete failure in Equation 5.28 considers the inclusion of transverse compression force (normal load) and the eccentricity of the stud to centreline of the rib. This means that both terms ($N_q$ and $e_1$) would be zero if headed studs are placed in a central position, and there is no additional load applied to the concrete slab surfaces. This is the reason the predicted strengths were very low. Thus, the developed equations by Nellinger et al. (2018) are more suitable for predicting the shear resistance of headed stud in composite beams with off-centre studs and presence of a normal load.

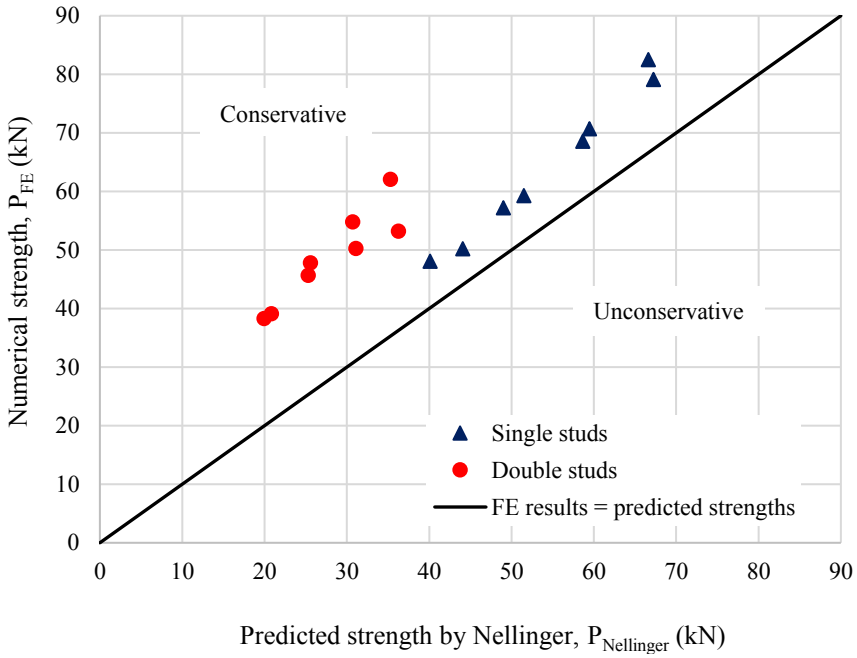


Figure 5.6 FE strengths versus $P_{Nellinger}$ predicted strengths

Table 5.4 FE results against existing strength prediction methods – push models with perpendicular profiled sheeting

| Test | $f_c$ (MPa) | Steel decking | | Headed stud | | $P_{FE}$ | $P_{EC4}$ | $P_{AISC}$ | $P_{RPCP}$ | $P_{CPT}$ | $P_{Konrad}$ | $P_{Nellinger}$ | $P_{FE}$ / $P_{EC4}$ | $P_{FE}$ / $P_{AISC}$ | $P_{FE}$ / $P_{RPCP}$ | $P_{FE}$ / $P_{CPT}$ | $P_{FE}$ / $P_{Konrad}$ | $P_{FE}$ / $P_{Nellinger}$ |
|---|---|---|---|---|---|---|---|---|---|---|---|---|---|---|---|---|---|---|
| | | $h_p$ | $b_o/h_p$ | $n_r$ | $d \times h_{sc}$ | | | | | | | | | | | | | |
| T1 | 12 | 100 | 1.00 | 5 | 19 × 140 | 50.2 | 16.7 | 65.0 | 39.7 | 52.2 | 37.4 | 44.1 | 3.00 | 0.77 | 1.26 | 0.96 | 1.34 | 1.14 |
| T2 | 20 | 100 | 1.00 | 5 | 19 × 140 | 59.3 | 22.7 | 89.3 | 46.9 | 62.6 | 45.2 | 51.5 | 2.61 | 0.66 | 1.26 | 0.95 | 1.31 | 1.15 |
| T3 | 30 | 100 | 1.00 | 5 | 19 × 140 | 70.7 | 26.7 | 89.3 | 51.1 | 69.8 | 52.8 | 59.5 | 2.65 | 0.79 | 1.38 | 1.01 | 1.34 | 1.19 |
| T4 | 40 | 100 | 1.00 | 5 | 19 × 140 | 82.5 | 26.7 | 89.3 | 51.2 | 70.2 | 59.2 | 66.6 | 3.09 | 0.92 | 1.61 | 1.18 | 1.39 | 1.24 |
| T5 | 12 | 146 | 0.67 | 5 | 19 × 195 | 48.1 | 9.4 | 65.0 | 31.8 | 44.9 | 32.1 | 40.1 | 5.12 | 0.74 | 1.51 | 1.07 | 1.50 | 1.20 |
| T6 | 20 | 146 | 0.67 | 5 | 19 × 195 | 57.2 | 12.8 | 71.4 | 38.7 | 53.0 | 38.9 | 49.0 | 4.48 | 0.80 | 1.48 | 1.08 | 1.47 | 1.17 |
| T7 | 30 | 146 | 0.67 | 5 | 19 × 195 | 68.6 | 15.0 | 71.4 | 42.8 | 59.3 | 45.4 | 58.6 | 4.58 | 0.96 | 1.60 | 1.16 | 1.51 | 1.17 |
| T8 | 40 | 146 | 0.67 | 5 | 19 × 195 | 79.1 | 15.0 | 71.4 | 42.9 | 59.7 | 50.9 | 67.2 | 5.28 | 1.11 | 1.84 | 1.32 | 1.55 | 1.18 |
| T25 | 12 | 100 | 1.00 | 10 | 19 × 140 | 39.1 | 11.8 | 65.0 | 48.1 | 45.4 | 29.9 | 20.8 | 3.31 | 0.60 | 0.81 | 0.86 | 1.31 | 1.88 |
| T26 | 20 | 100 | 1.00 | 10 | 19 × 140 | 47.8 | 16.0 | 75.9 | 59.0 | 52.7 | 36.2 | 25.6 | 2.98 | 0.63 | 0.81 | 0.91 | 1.32 | 1.87 |
| T27 | 30 | 100 | 1.00 | 10 | 19 × 140 | 54.8 | 18.9 | 75.9 | 67.1 | 57.4 | 42.3 | 30.7 | 2.91 | 0.72 | 0.82 | 0.95 | 1.30 | 1.79 |
| T28 | 40 | 100 | 1.00 | 10 | 19 × 140 | 62.1 | 18.9 | 75.9 | 67.2 | 57.7 | 47.3 | 35.3 | 3.29 | 0.82 | 0.92 | 1.08 | 1.31 | 1.76 |
| T29 | 12 | 146 | 0.67 | 10 | 19 × 195 | 38.3 | 6.6 | 60.7 | 40.4 | 37.3 | 25.7 | 19.9 | 5.77 | 0.63 | 0.95 | 1.03 | 1.49 | 1.92 |
| T30 | 20 | 146 | 0.67 | 10 | 19 × 195 | 45.7 | 9.0 | 60.7 | 51.3 | 42.3 | 31.1 | 25.3 | 5.07 | 0.75 | 0.89 | 1.08 | 1.47 | 1.81 |
| T31 | 30 | 146 | 0.67 | 10 | 19 × 195 | 50.3 | 10.6 | 60.7 | 59.5 | 46.0 | 36.3 | 31.1 | 4.75 | 0.83 | 0.85 | 1.09 | 1.38 | 1.62 |
| T32 | 40 | 146 | 0.67 | 10 | 19 × 195 | 53.2 | 10.6 | 60.7 | 59.5 | 46.3 | 40.7 | 36.3 | 5.02 | 0.88 | 0.89 | 1.15 | 1.31 | 1.47 |
| Mean | | | | | | | | | | | | | 3.99 | 0.79 | 1.18 | 1.06 | 1.39 | 1.47 |
| CoV (%) | | | | | | | | | | | | | 27.48 | 16.96 | 29.84 | 11.00 | 6.41 | 21.73 |

## 5.8 Summary

The comparison showed that the European code provisions are not applicable in the evaluation of the stud capacity in deep profiled decking. The main equations do not consider the position of studs within the trough if they are placed off the centre (favourable or unfavourable position). Also, the relevant reduction factor equation appeared to be ineffective when the rib of steel decking is narrow. Hence, there is a definite need to calibrate the rules in EC4 to account for the depth and narrowness geometry of steel decking greater than 80 mm deep. On the other hand, the American specification ANSI/AISC 360-2016 was unconservative in most cases. The rules gave inaccurate results for specimens having concrete strength more than 20 MPa, and specimens with two studs per rib. Also, the rules do not take into account some factors such as the rib of profiled sheeting and stud' layout.

Among equations developed in previous studies, the equations from the concrete pull-out failure (CPT) by Johnson and Yuan (1998b) were the most accurate to predict the stud capacities obtained from the parametric study in most cases. However, the method comes with some drawbacks including its complexity, the discrepancy in some results, and the most important concern is that the failure mode must be predicted first before the method is used, which makes it theoretically appropriate to tests with only concrete pull-out failure. This leads to raising some questions about how to guarantee a particular failure mode in the first place, and what if the targeted failure mode would be different. Therefore, the application of this method is not an ideal solution. On the other hand, the developed equations by Konrad (2011) underestimated the shear resistance of stud in very deep decks. Likewise, the method of Nellinger et al. (2018) was not suitable to estimate the capacity of shear connection with studs placed in the central position of the rib and where the normal load was absent. This gap of study necessitates introducing new equations that first consider steel decks deeper than 80 mm, and second, deal with variant geometries of decks and stud's position.

## 5.9 Parametric study

A comprehensive parametric study was carried out to investigate the shear connector resistance per stud when an open trapezoidal profiled sheeting is used in composite beams. Full-scale finite element model of the push tests with slab width of 600 mm was adopted.

The push test arrangement is similar to those suggested by Hicks (2007), except that the push models were pushed horizontally herein (see Figure 5.7). Accordingly, headed studs are only involved in two main ribs of the profiled sheeting. This particular push test arrangement can significantly save the computational time instead of creating several ribs which in turn makes the modelling process exhaustive. The parametric study covered the geometry effect of profiled sheeting as the depth changes from 50 to 146 mm, the diameter of the stud, number of studs per rib, studs' layout, and concrete strength. This extensive parametric study will contribute to formulating new generalised equations in order to predict the shear stud capacity placed in perpendicular steel decks.

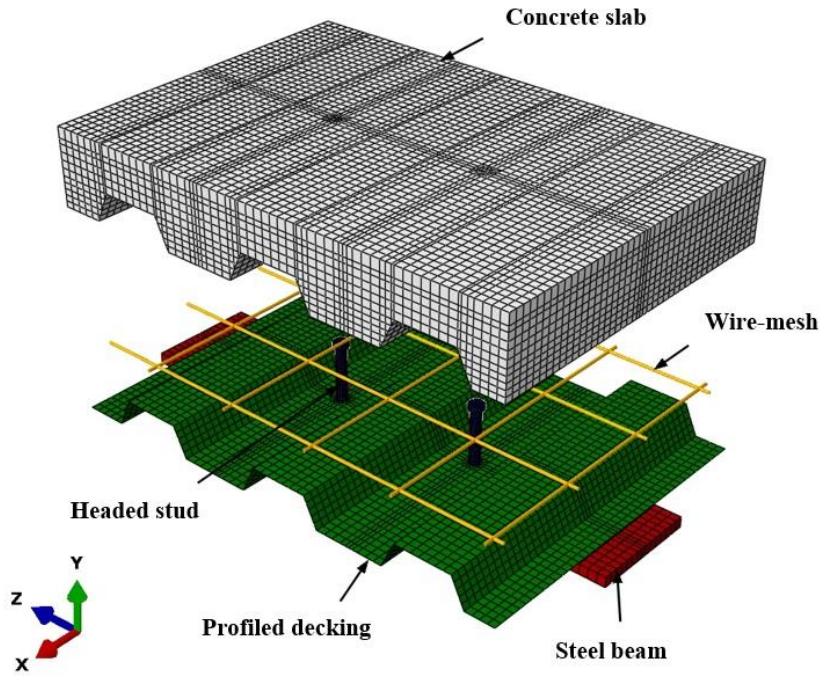


Figure 5.7 Finite element push model used for parametric study

Six different types of profiled sheeting were considered in the parametric study, the ratio of average rib width to the rib height ($b_o/h_p$) varied from 0.67 to 3.2, the cross-sectional details of these metal decks are shown in Figure 5.8. This study is the first to account for narrow geometries ($b_o/h_p \leq 1.5$) and very deep decks greater than 80 mm and bridge it with the commonly used steel decks. It was decided to neglect such profiled sheeting with rib height less than 50 mm, as those types are not being widely used in the industry nowadays. The change in the diameter of stud varied from 19 to 22 mm. Single and double studs were used and placed in central, favourable, and unfavourable positions, and they were arranged side

by side in case of stud pairs. Qureshi (2010) found that the effect of transverse spacing between studs came to play when studs were placed in a distance of 5*d* and upwards. Hence, all stud pairs were located 5*d* centre to centre from each other in this part of the study. It was not possible to place the shear studs in any position but central in case of profiled sheeting of 100 mm and 146 mm deep, as these come with narrow rib geometry. Finally, four concrete grades were used, namely, C12, C20, C30, and C40.

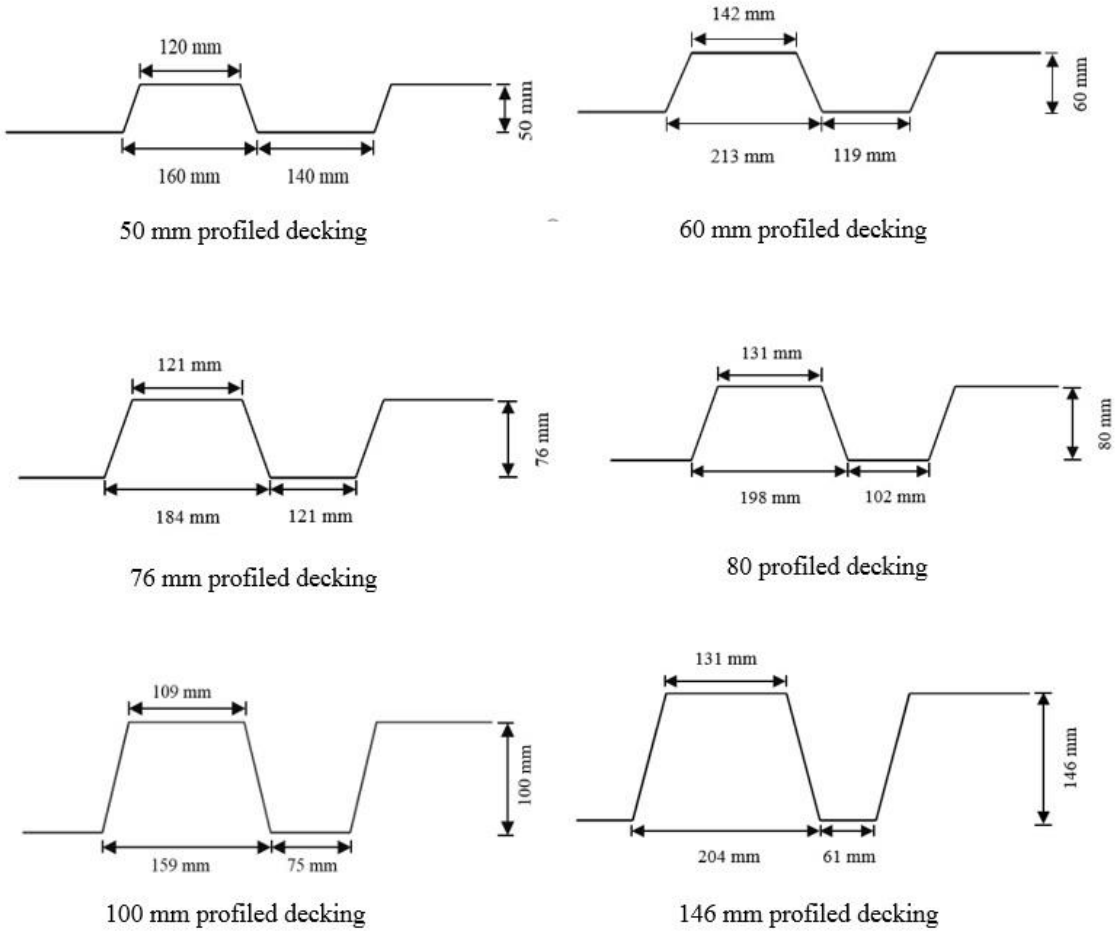


Figure 5.8 Details of the profiled decks used

The sheeting thickness was kept constant at 1.2 mm in all push models, and the slab depth was made in each numerical test to provide at least 20 mm cover from the stud's head. The concrete slab was reinforced with A193 wire-mesh (7 mm in diameter) having 200 mm centre-to-centre spacing, and it was placed on the surface of profiled sheeting in all tests. The procedure of boundary conditions, constraints, load application, contact surfaces, and finite element mesh size were the same as what was introduced in Chapter Four. After the analysis,

the shear connector resistance in each push model was obtained. The FE results are given in Table 5.5, the total number of push models conducted was 224.

Table 5.5 Finite element results of push models

| Group | Concrete grade | Profiled sheeting | | | Stud details (mm) $d \times h_{sc}$ | Single stud | | | Double stud | | | Notes |
|---|---|---|---|---|---|---|---|---|---|---|---|---|
| | | $b_o$ (mm) | $h_p$ (mm) | $b_o/h_p$ | | C | F | U | C | F | U | |
| A | C12 | 160 | 50 | 3.2 | 19 × 95 | 62.1 | 67.1 | 61.7 | 46.2 | 49.9 | 45.9 | Push models with 50 mm deep profiled sheeting |
| | C20 | 160 | 50 | 3.2 | 19 × 95 | 80.3 | 87.5 | 77.0 | 58.0 | 62.9 | 55.4 | |
| | C30 | 160 | 50 | 3.2 | 19 × 95 | 99.2 | 108.1 | 90.8 | 66.2 | 70.8 | 60.5 | |
| | C40 | 160 | 50 | 3.2 | 19 × 95 | 115.6 | 126.5 | 101.2 | 75.1 | 84.6 | 70.7 | |
| | C12 | 160 | 50 | 3.2 | 22 × 95 | 77.0 | 80.5 | 74.0 | 61.7 | 66.7 | 61.3 | |
| | C20 | 160 | 50 | 3.2 | 22 × 95 | 99.1 | 105.0 | 92.4 | 72.3 | 78.7 | 69.3 | |
| | C30 | 160 | 50 | 3.2 | 22 × 95 | 117.9 | 129.8 | 109.0 | 85.5 | 93.5 | 78.5 | |
| | C40 | 160 | 50 | 3.2 | 22 × 95 | 130.3 | 151.9 | 121.5 | 98.7 | 109.4 | 88.5 | |
| B | C12 | 154.5 | 60 | 2.58 | 19 × 100 | 59.1 | 63.8 | 58.7 | 43.6 | 45.7 | 42.0 | Push models with 60 mm deep profiled sheeting |
| | C20 | 154.5 | 60 | 2.58 | 19 × 100 | 76.2 | 83.1 | 73.1 | 54.7 | 58.8 | 51.7 | |
| | C30 | 154.5 | 60 | 2.58 | 19 × 100 | 94.4 | 102.9 | 86.4 | 62.3 | 68.6 | 57.6 | |
| | C40 | 154.5 | 60 | 2.58 | 19 × 100 | 111.7 | 122.3 | 97.8 | 72.6 | 83.4 | 66.7 | |
| | C12 | 154.5 | 60 | 2.58 | 22 × 100 | 72.5 | 76.6 | 70.5 | 56.0 | 59.5 | 54.8 | |
| | C20 | 154.5 | 60 | 2.58 | 22 × 100 | 93.1 | 99.7 | 87.7 | 66.6 | 71.6 | 63.0 | |
| | C30 | 154.5 | 60 | 2.58 | 22 × 100 | 111.2 | 123.5 | 103.7 | 79.8 | 88.4 | 74.2 | |
| | C40 | 154.5 | 60 | 2.58 | 22 × 100 | 126.1 | 146.8 | 117.4 | 92.9 | 106.2 | 84.9 | |
| C | C12 | 152.5 | 76 | 2.00 | 19 × 116 | 56.8 | 61.9 | 54.6 | 41.5 | 43.7 | 38.5 | Push models with 76 mm profiled sheeting |
| | C20 | 152.5 | 76 | 2.00 | 19 × 116 | 73.3 | 80.3 | 64.5 | 52.0 | 57.5 | 46.2 | |
| | C30 | 152.5 | 76 | 2.00 | 19 × 116 | 89.7 | 98.2 | 75.4 | 59.2 | 67.6 | 51.9 | |
| | C40 | 152.5 | 76 | 2.00 | 19 × 116 | 103.6 | 113.4 | 82.9 | 67.3 | 81.4 | 59.5 | |
| | C12 | 152.5 | 76 | 2.00 | 22 × 116 | 68.5 | 74.3 | 65.5 | 50.3 | 53.5 | 47.2 | |
| | C20 | 152.5 | 76 | 2.00 | 22 × 116 | 88.5 | 96.3 | 77.4 | 60.8 | 68.5 | 55.1 | |
| | C30 | 152.5 | 76 | 2.00 | 22 × 116 | 105.7 | 117.9 | 90.5 | 74.0 | 85.4 | 65.6 | |

Table 5.5 (continued)

| | | | | | | | | | | | | |
|---|---|---|---|---|---|---|---|---|---|---|---|---|
| | C40 | 152.5 | 76 | 2.00 | 22 × 116 | 117.0 | 136.1 | 99.5 | 87.2 | 101.2 | 74.0 | |
| D | C12 | 135.5 | 80 | 1.69 | 19 × 125 | 54.2 | 59.1 | 49.4 | 39.3 | 43.6 | 36.2 | Push models with 80 mm deep profiled sheeting |
| | C20 | 135.5 | 80 | 1.69 | 19 × 125 | 69.2 | 75.4 | 54.8 | 48.4 | 54.7 | 41.8 | |
| | C30 | 135.5 | 80 | 1.69 | 19 × 125 | 84.6 | 95.2 | 64.1 | 55.8 | 62.5 | 48.1 | |
| | C40 | 135.5 | 80 | 1.69 | 19 × 125 | 98.8 | 110.7 | 75.5 | 64.2 | 78.3 | 57.4 | |
| | C12 | 135.5 | 80 | 1.69 | 22 × 125 | 65.4 | 70.9 | 55.7 | 47.4 | 49.4 | 40.8 | |
| | C20 | 135.5 | 80 | 1.69 | 22 × 125 | 83.6 | 92.5 | 65.8 | 58.0 | 63.4 | 46.1 | |
| | C30 | 135.5 | 80 | 1.69 | 22 × 125 | 99.6 | 114.7 | 76.9 | 71.2 | 80.3 | 53.8 | |
| | C40 | 135.5 | 80 | 1.69 | 22 × 125 | 111.6 | 129.2 | 90.6 | 84.4 | 97.1 | 68.1 | |
| E | C12 | 100 | 100 | 1.00 | 19 × 140 | 50.2 | N/A | N/A | 39.1 | N/A | N/A | Push models with 100 mm deep profiled sheeting |
| | C20 | 100 | 100 | 1.00 | 19 × 140 | 59.3 | N/A | N/A | 47.8 | N/A | N/A | |
| | C30 | 100 | 100 | 1.00 | 19 × 140 | 70.7 | N/A | N/A | 54.8 | N/A | N/A | |
| | C40 | 100 | 100 | 1.00 | 19 × 140 | 82.5 | N/A | N/A | 62.1 | N/A | N/A | |
| | C12 | 100 | 100 | 1.00 | 22 × 140 | 60.1 | N/A | N/A | 45.7 | N/A | N/A | |
| | C20 | 100 | 100 | 1.00 | 22 × 140 | 71.2 | N/A | N/A | 55.6 | N/A | N/A | |
| | C30 | 100 | 100 | 1.00 | 22 × 140 | 82.9 | N/A | N/A | 62.6 | N/A | N/A | |
| | C40 | 100 | 100 | 1.00 | 22 × 140 | 92.9 | N/A | N/A | 72.4 | N/A | N/A | |
| F | C12 | 134 | 146 | 0.67 | 19 × 195 | 48.1 | N/A | N/A | 38.3 | N/A | N/A | Push models with 146 mm deep profiled sheeting |
| | C20 | 134 | 146 | 0.67 | 19 × 195 | 57.2 | N/A | N/A | 45.7 | N/A | N/A | |
| | C30 | 134 | 146 | 0.67 | 19 × 195 | 68.6 | N/A | N/A | 50.3 | N/A | N/A | |
| | C40 | 134 | 146 | 0.67 | 19 × 195 | 79.1 | N/A | N/A | 53.2 | N/A | N/A | |
| | C12 | 134 | 146 | 0.67 | 22 × 195 | 58.0 | N/A | N/A | 45.7 | N/A | N/A | |
| | C20 | 134 | 146 | 0.67 | 22 × 195 | 69.1 | N/A | N/A | 53.8 | N/A | N/A | |
| | C30 | 134 | 146 | 0.67 | 22 × 195 | 80.8 | N/A | N/A | 57.1 | N/A | N/A | |
| | C40 | 134 | 146 | 0.67 | 22 × 195 | 90.8 | N/A | N/A | 63.2 | N/A | N/A | |

## 5.10 Strength prediction equations for shear stud connectors placed in perpendicular profiled sheeting

The author believes that besides good predictions the equations provide, they should be easy to use, flexible, and grasp as many parameters as possible. Based on that, multi-linear regression method was utilised to analyse the FE results obtained from the parametric study. It was decided to introduce relevant equations for each stud position (i.e. central, favourable, and unfavourable) to ensure better predictions and avoid a wide discrepancy in results. For each case of stud position, four independent variables were included in the multiple regression analysis. These are the concrete strength ($f_c$), the cross-section area of the stud ($A_s$), the ratio of average rib width to the rib height ($b_o/h_p$), and the ratio of stud height to rib height ($h_{sc}/h_p$). In addition, the number of studs per rib was represented as a factor in the equations. The reliability of the equations yielded from the regression analysis was evaluated against various previous experiments incorporating different parameters, such as rib geometry ratio, number of studs per rib, etc.

The equations developed from this study were also evaluated with some existing methods, including the Eurocode 4, ANSI/AISC 360-2016, Johnson and Yuan's analytical method (1998b), and Konrad's analytical method (2011). This was meant to investigate whether the equations developed from the regression analysis work as effectively as the other existing rules or even better. At this stage, the formulae introduced by Nellinger et al. (2018) were excluded as the method requires a normal load application. For this reason, any push test series conducted with normal load was not considered in the comparison, like push tests performed by Lyons et al. (1996), and Rambo-Roddenberry (2002). Because it is not logical to validate results achieved from equations which were developed from push tests without normal load against results obtained from push tests with normal load. The use of normal load has been found to greatly enhance the shear connector resistance by roughly 40% or 25% as reported by Qureshi (2010), and Hick and Smith (2014) respectively.

### 5.10.1 Central stud position

The least square regression analysis was conducted by an add-in program called "Solver" which is available in Microsoft Excel. This program adjusts the variable cells to achieve a

maximum or minimum residual sum of squares (SSE). The SSE measures the total deviation between the actual and predicted values. In this case, the Solver was used to find the optimal variable cells that result in the minimum residual sum of squares. A low SSE indicates a close fit of the predicted value to the actual ones. This process was repeated in all formulae developed in this research.

The FE results obtained from 48 tests with the central position of single studs were used for the regression analysis. With careful examination, the variables of concrete strength ($f_c$), cross-sectional area of the stud ($A_s$) and the ratio of stud height to rib height ($h_{sc}/h_p$) deem to have a linear correlation with the shear connector resistance. This linear relationship can be expressed in Equation 5.36, where x stands for a variable, A and B are constant and intercept respectively. However, the rib deck ratio ($b_o/h_p$) draws a non-linear correlation with the shear connector resistance as shown in Figure 5.9. Therefore, Equation 5.37 was assumed to demonstrate such a relationship.

$$P = A\,x + B \qquad \text{Eq. 5.36}$$

$$P = A\,(b_o/h_p)^2 + B\,(b_o/h_p) + C \qquad \text{Eq. 5.37}$$

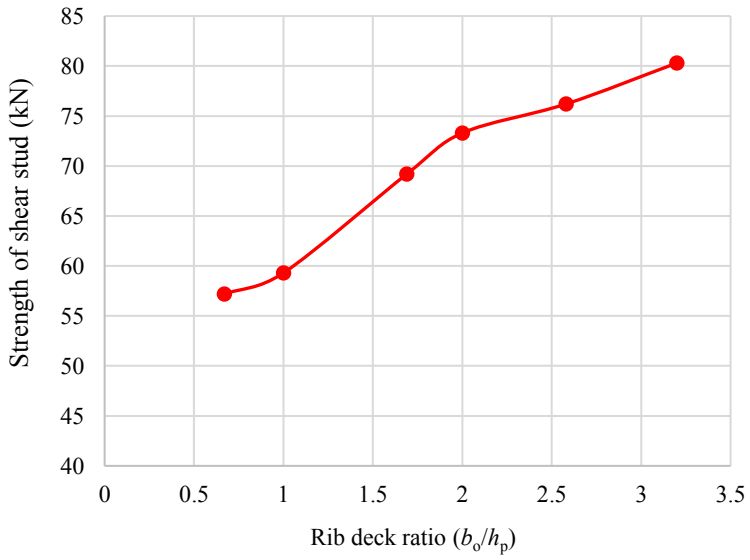


Figure 5.9 Relationship between rib deck ratio and shear strength of studs for the concrete grade of C20

By substituting each independent variable in their relevant equations, and adding all of them together, Equation 5.38 was obtained.

$$P_C = A\, f_{ck} + B\, A_s + C\, (h_{sc}/h_p) + D\, (b_o/h_p)^2 + E\, (b_o/h_p) + F \qquad \text{Eq. 5.38}$$

Using the add-in solver analysis to determine A, B, C, D, E, and F, the least square regression analysis yielded Equation 5.39. This is the final form of the equation for predicting the shear capacity of central studs placed in transverse steel decks. The regression analysis gave a coefficient of correlation ($R^2$) of 0.964; the predicted strengths were then compared to the observed values to see how close the correlation is. The mean of the observed strengths to the predicted results and the coefficient of variation were 1.02 and 4.74% respectively, whilst the scatter in results lied within $\pm$7%. The parametric study showed that the average ratio of shear connector resistance of double studs to the ones with single studs was 0.72. Hence, the relationship between the use of single and double studs in Equation 5.39 can be represented as the square root of the number of studs per rib. Figure 5.10 shows the relationship between the predicted and the observed strengths associated with the best linear fit method. Details of the predicted strengths using the regression analysis are given in Appendix A (Table A.1).

$$P_C = [1.472\, f_{ck} + 0.140\, A_s + 24.978\, h_{sc}/h_p - 3.670\, b_o/h_p^2 + 16.412\, b_o/h_p - 57.577] \,/\sqrt{N_r} \qquad \text{Eq. 5.39}$$

where:

$P_C$ = shear capacity per stud placed in a central position of transverse steel decking

$f_{ck}$ = characteristic cylinder strength of concrete (MPa)

$A_s$ = cross-sectional area of shear studs ($mm^2$)

$b_o$ = mean width of rib (mm)

$h_{sc}$ = stud height (mm)

$h_p$ = rib height (mm)

$N_r$ = number of stud per rib

Note that the rib geometry ratio ($b_o/h_p$) varies between 0.67 to 3.2, the height of rib should not be less than 50 mm, or more than 146 mm. The characteristic cylinder strength of concrete varies from 12 to 40 MPa.

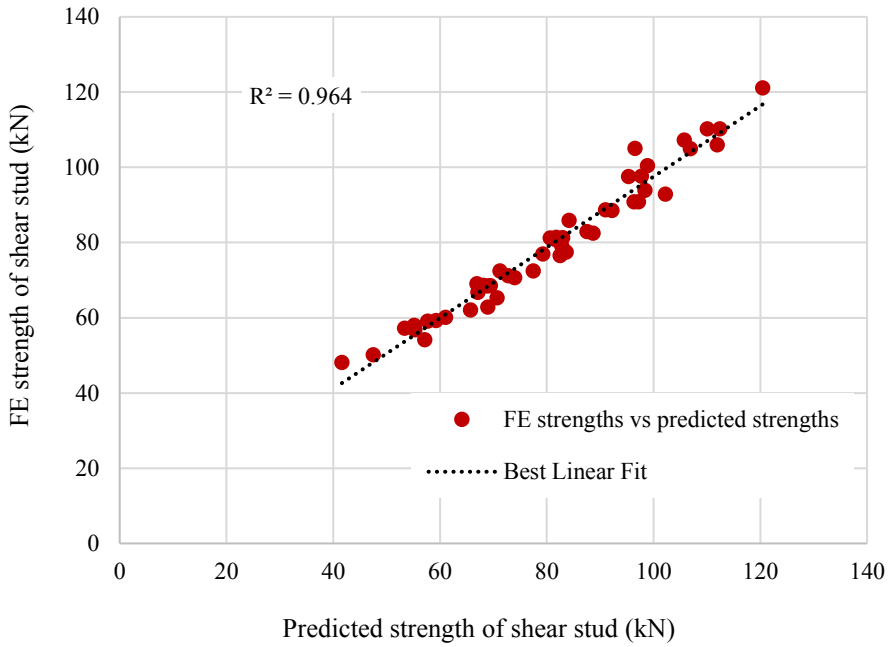


Figure 5.10 FE versus predicted strengths for single studs placed in a central position

The applicability of Equation 5.39 was validated against some previous experiments as illustrated in Table 5.6. All push tests in this comparison incorporated trapezoidal profiled steel decking and shear studs placed in a central position of the rib. The validation also involved predicted strengths achieved from the Eurocode 4, American specifications ANSI/AISC 360-2016, concrete pull-out failure method (CPT) developed by Johnson and Yuan (1998b), and Konrad's analytical method (2011). As for Konrad's method, Equations 5.23 and 5.24 were used, and the lesser value was multiplied by the relevant reduction factor among Equations 5.25 and 5.26.

As shown in Table 5.6, the best shear stud strength predictions and the least coefficient of variation were achieved through the use of Equation 5.39. With the mean and coefficient of variation of the predicted results of 0.98 and 5.4% respectively, it can be said that the equation developed in this research based on the multi-linear regression analysis is effective and reliable. Figure 5.11 shows the comparison between the predicted strengths obtained from Equation 5.39 and the observed strengths achieved from the experiments. The deviation in results remained within ±10%.

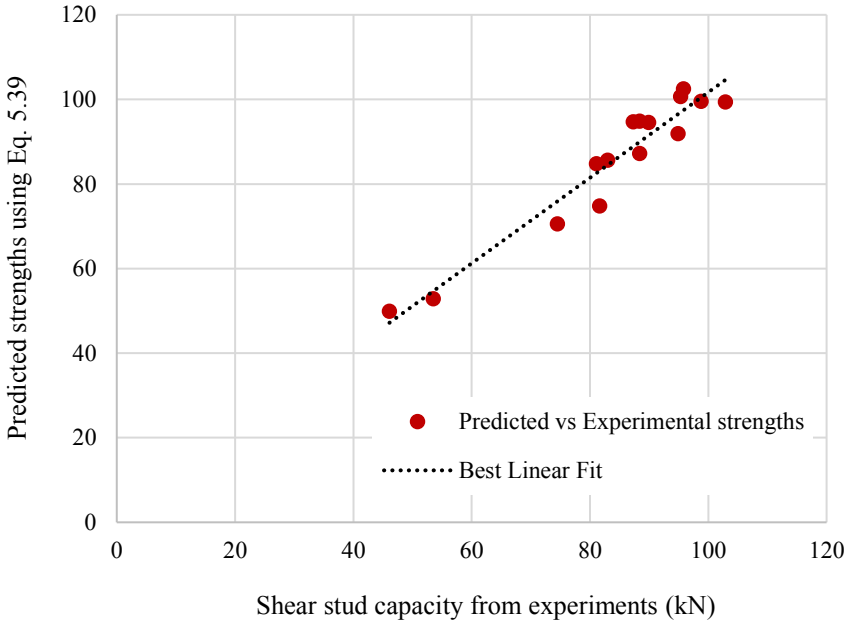


Figure 5.11 Comparison between predicted strengths using Eq. 5.39 and experimental results

On the other hand, the mean and coefficient of variation of the predicted strengths from both Eurocode 4 and American Specifications indicated that the discrepancy in results is relatively high and the correlation is not as close to 1.0 as desired. This is attributed to the fact that the formulae in both existing rules are not flexible in most cases. The predicted strengths were seen to be governed by the stud failure equation when the concrete strength is high, and the effect of double studs is not well considered, particularly in the ANSI/AISC 360-2016, which in turn led for the predicted values to be highly overestimated. This promotes the idea that the existing rules in the EC4 and ANSI/AISC should be recalibrated for better predictions and more flexibility regarding rib geometry effects, and number of studs per rib.

The comparison revealed that the adequacy of the equations proposed by Johnson and Yuan (1998b) to predict the shear strength of central studs is not reliable. Despite the good agreement noticed for the shear strength predictions among tests with single studs, the correlations for the double studs' strength predictions were poor and insufficient. As a result, the mean of experiments over predicted results was relatively far from 1.0, and the coefficient of variation appeared to be high. This indicates that the equations proposed by Johnson and Yuan (1998b) are not able to accurately evaluate the shear stud capacity when two studs are placed in one rib.

It was noticed that the equations proposed by Konrad (2011) are as effective as the equations developed in this research. However, Konrad's equations are only limited for wide ribbed decks, which make them inconvenient for narrow ribbed and very deep decks as seen previously in this chapter. This leads to conclude that the equation developed in this research is the most effective and practical approach to predict the shear strength of central studs, due to being the first equation to address the effect of depth and narrowness of profiled sheeting, coping with various rib geometries and providing better strength predictions as compared to the other methods. Also, the equation is flexible and easy to use.

Table 5.6 Comparison of shear connector resistance from experiments and developed equations for push-off tests with central studs

| Ref. | Test | Concrete strength $f_{ck}$ (MPa) | Profiled sheeting details | | | Stud details | | Average experimental load per stud $P_{Test}$ (kN) | $P_C$ (kN) | $P_{EC4}$ (kN) | $P_{AISC}$ (kN) | $P_{CPT}$ (kN) | $P_{Konrad}$ (kN) | $P_{Test}/P_C$ | $P_{Test}/P_{EC4}$ | $P_{Test}/P_{AISC}$ | $P_{Test}/P_{CPT}$ | $P_{Test}/P_{Konrad}$ |
|---|---|---|---|---|---|---|---|---|---|---|---|---|---|---|---|---|---|---|
| | | | $b_o$ (mm) | $h_p$ (mm) | $b_o/h_p$ | $d \times h_s$ (mm) | $N_r$ | | | | | | | | | | | |
| Yuan (1996) | G2C | 21.8 | 162 | 55 | 2.95 | 19 × 125 | 1 | 88.4 | 87.2 | 85.4 | 95.7 | 81.1 | 72.5 | 1.01 | 1.04 | 0.92 | 1.09 | 1.22 |
| Lloyd and Wright (1990) | S1 | 35.8 | 150 | 50 | 3.00 | 19 × 100 | 1 | 95.3 | 100.7 | 102.1 | 95.7 | 100.6 | 88.1 | 0.95 | 0.93 | 1.00 | 0.95 | 1.08 |
| | S2 | 28.2 | 150 | 50 | 3.00 | 19 × 100 | 1 | 81.1 | 84.8 | 100.0 | 95.7 | 99.6 | 80.3 | 0.96 | 0.81 | 0.85 | 0.81 | 1.01 |
| | S3 | 31.6 | 150 | 50 | 3.00 | 19 × 100 | 1 | 89.9 | 94.6 | 102.1 | 95.7 | 100.1 | 83.9 | 0.95 | 0.88 | 0.94 | 0.90 | 1.07 |
| | S4 | 37.0 | 150 | 50 | 3.00 | 19 × 100 | 1 | 95.8 | 102.5 | 102.1 | 95.7 | 100.7 | 89.2 | 0.93 | 0.94 | 1.00 | 0.95 | 1.07 |
| | S5 | 34.9 | 150 | 50 | 3.00 | 19 × 100 | 1 | 102.9 | 99.4 | 102.1 | 95.7 | 100.5 | 87.2 | 1.04 | 1.01 | 1.08 | 1.02 | 1.18 |
| | S6 | 35.0 | 150 | 50 | 3.00 | 19 × 100 | 1 | 98.8 | 99.6 | 102.1 | 95.7 | 100.5 | 87.3 | 0.99 | 0.97 | 1.03 | 0.98 | 1.13 |
| | S7 | 29.8 | 150 | 50 | 3.00 | 19 × 100 | 1 | 94.9 | 91.9 | 102.1 | 95.7 | 99.8 | 82.0 | 1.03 | 0.93 | 0.99 | 0.95 | 1.16 |
| | S8 | 31.7 | 150 | 50 | 3.00 | 19 × 100 | 1 | 87.3 | 94.7 | 102.1 | 95.7 | 100.1 | 84.0 | 0.92 | 0.86 | 0.91 | 0.87 | 1.04 |
| | S9 | 31.8 | 150 | 50 | 3.00 | 19 × 100 | 1 | 88.4 | 94.8 | 102.1 | 95.7 | 100.1 | 84.1 | 0.93 | 0.87 | 0.92 | 0.88 | 1.05 |
| Robinson (1988) | RI | 24.8 | 102.0 | 51 | 2.00 | 19 × 91 | 1 | 83.0 | 85.6 | 92.4 | 95.7 | 79.8 | 72.3 | 0.97 | 0.90 | 0.87 | 1.04 | 1.15 |
| | QI | 24.8 | 152.5 | 76 | 2.00 | 19 × 116 | 1 | 81.6 | 74.8 | 68.3 | 95.7 | 86.5 | 70.2 | 1.09 | 1.19 | 0.85 | 0.94 | 1.16 |
| | QII | 24.8 | 152.5 | 76 | 2.00 | 19 × 116 | 2 | 53.5 | 52.9 | 48.3 | 81.3 | 76.8 | 56.2 | 1.01 | 1.11 | 0.66 | 0.70 | 0.95 |
| Jayas and Hosain (1988) | JDT-7 | 19.5 | 152.5 | 76 | 2.00 | 19 × 127 | 2 | 46.1 | 49.9 | 53.5 | 81.3 | 72.1 | 52.8 | 0.92 | 0.86 | 0.57 | 0.64 | 0.87 |
| | JDT-8 | 19.5 | 152.5 | 76 | 2.00 | 19 × 127 | 1 | 74.5 | 70.6 | 75.0 | 93.5 | 83.2 | 66.0 | 1.06 | 0.99 | 0.80 | 0.90 | 1.13 |
| Mean | | | | | | | | | | | | | | 0.98 | 0.95 | 0.89 | 0.91 | 1.09 |
| Coefficient of Variation % | | | | | | | | | | | | | | 5.4% | 10.8% | 15.4% | 13.3% | 8.5% |

### 5.10.2 Favourable stud position

The FE results obtained from the parametric study of 32 tests with favourable single studs were utilised through a multiple linear regression analysis. In this case, the rib deck ratio ($b_o/h_p$) ranged from 1.69 to 3.2. As seen in Figure 5.9, the relationship between the rib deck ratio and the shear connector resistance is more linear. Therefore, there was no need to address the non-linear assumption. By substituting each independent variable in Equation 5.36, and adding all of them together, Equation 5.40 was initially obtained.

$$P_F = A\, f_{ck} + B\, A_s + C\, (h_{sc}/h_p) + D\, (b_o/h_p) + E \qquad \text{Eq. 5.40}$$

Using the built-in solver, the least square regression analysis determined the values of A, B, C, D and E, and yielded Equation 5.41. This equation was achieved with a coefficient of correlation ($R^2$) of 0.973, the predicted strengths from Equation 5.41 were then compared to the observed values. The mean of predicted strengths to the observed results and the coefficient of variation are 1.00 and 4.9% respectively, and most of the discrepancy in results vary between $\pm$10%. Figure 5.12 shows the relationship between the predicted strengths and the observed values represented by the best linear fit method. Finally, the parametric study revealed that the average ratio of shear connector resistance of double studs to the ones with single studs was 0.71. Thus, the relationship between the use of single and double studs in Equation 5.41 is represented as the square root of the number of studs per rib. Details of the predicted strengths using the regression analysis are given in Appendix A (Table A.2).

$$P_F = [(2.273\, f_{ck} + 0.201\, A_s + 11.250\, h_{sc}/h_p - 5.007\, b_o/h_p) - 24.7] / \sqrt{N_r} \qquad \text{Eq. 5.41}$$

where:

$P_F$ = the shear capacity per stud placed in a favourable position of transverse steel decking (kN)

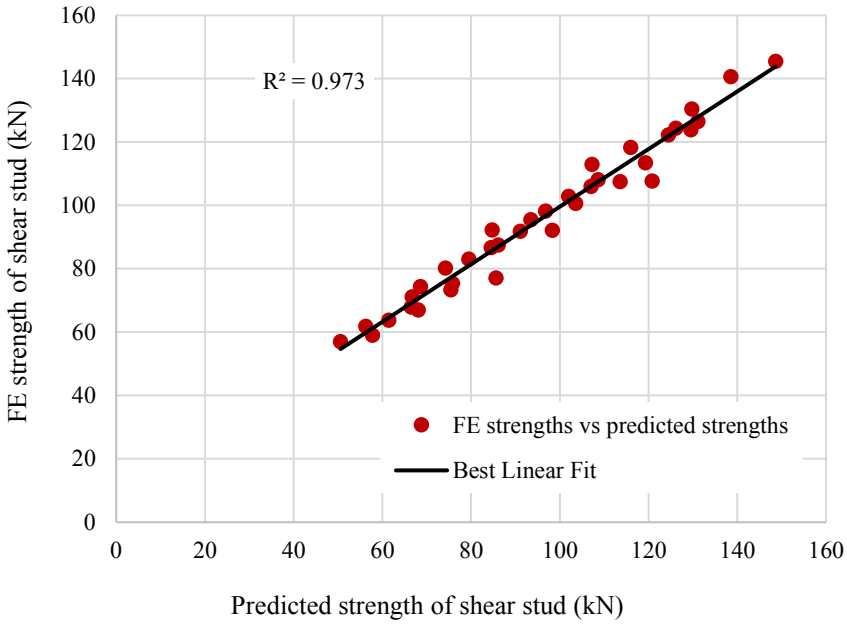


Figure 5.12 FE versus predicted strengths for single studs placed in a favourable position

The applicability of Equation 5.41 was verified through some previous experiments as shown in Table 5.7 and Figure 5.13. All push tests in this comparison have favourable studs placed in the trapezoidal profiled sheeting. The same prediction strength methods used with the central position of studs is involved here, except with Konrad's method (2011), whereas the lesser values achieved from Equations 5.23 or 5.24 should be multiplied by a reduction factor obtained from Equation 5.42 or Equation 5.43 for favourable studs.

$$k_t = k_n \left[0.030 \left(b_o/h_p\right)^2 + 0.145 \left(b_o/h_p\right) + 0.240 \left(h_{sc}/h_p\right)\right] \quad \leq 1.0 \quad \text{if } h_{sc}/h_p \leq 1.56 \qquad \text{Eq. 5.42}$$

$$k_t = k_n \left[0.084 \left(b_o/h_p\right) + 0.663\right] \quad \leq 1.0 \quad \text{if } h_{sc}/h_p > 1.56 \qquad \text{Eq. 5.43}$$

Considering the mean of experimental over predicted strengths and the coefficient of variation from Table 5.7, it can be said that the equation introduced in this research to predict the shear strength of favourable studs provided the most desirable results. The predicted strengths achieved from Equation 5.41 showed much better correlations than the EC4 and ANSI/AISC, reducing the coefficient of variation to 10.8% after being around 20.0% in both standard provisions. The deficiency of both standard provisions is because the fact that the favourable studs pattern is not recognised, in addition to reasons regarding the effects of rib geometries and the number of studs per rib which were previously explained, all these factors eventually led to having a wide scatter in results.

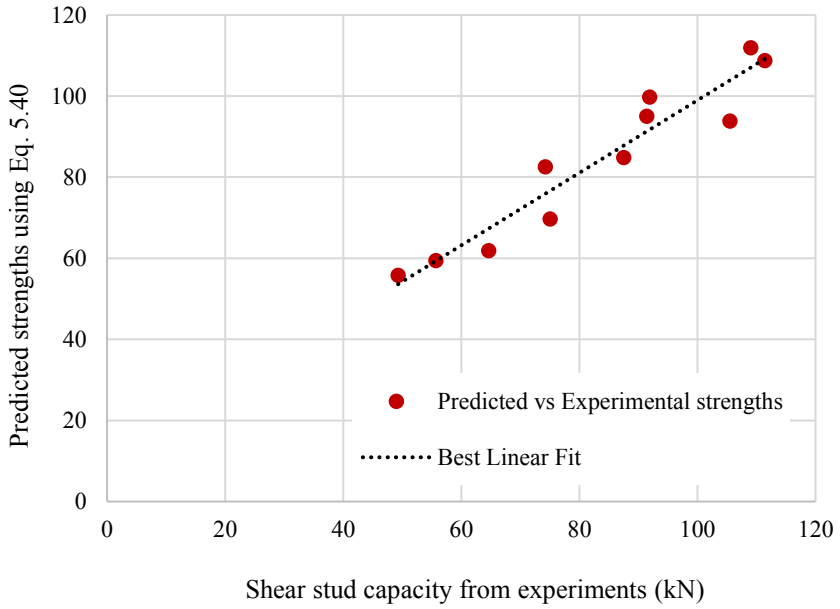


Figure 5.13 Comparison between predicted strengths using Eq. 5.41 and experimental results

As for the other analytical methods, Equation 5.41 also appeared to be more effective than the equations proposed by Johnson and Yuan (1998b) and Konrad (2011) by giving the least coefficient of variation. This is attributed to the flexibility of Equation 5.40 in addressing various rib geometries which are not widely covered elsewhere. Overall, the new equation proposed in this research is better than any methods in predicting the shear strength of favourable studs and offering flexibility and ease of use.

Table 5.7 Comparison of shear connector resistance from experiments and developed equations for push-off tests with favourable studs

| Ref. | Test | Concrete strength $f_{ck}$ (MPa) | profiled sheeting details | | | Stud details | | Average experimental load per stud $P_{Test}$ (kN) | $P_F$ (kN) | $P_{EC4}$ (kN) | $P_{AISC}$ (kN) | $P_{CPT}$ (kN) | $P_{Konrad}$ (kN) | $P_{Test}/P_F$ | $P_{Test}/P_{EC4}$ | $P_{Test}/P_{AISC}$ | $P_{Test}/P_{CPT}$ | $P_{Test}/P_{Konrad}$ |
|---|---|---|---|---|---|---|---|---|---|---|---|---|---|---|---|---|---|---|
| | | | $b_o$ (mm) | $h_p$ (mm) | $b_o/h_p$ | $d \times h_s$ (mm) | $N_r$ | | | | | | | | | | | |
| Qureshi (2010) | PTS | 21.3 | 154.5 | 60 | 2.58 | 19 × 100 | 1 | 74.2 | 86.6 | 84.2 | 95.7 | 76.8 | 80.3 | 0.86 | 0.88 | 0.78 | 0.97 | 0.92 |
| | PTD | 21.0 | 154.5 | 60 | 2.58 | 19 × 100 | 2 | 49.3 | 55.8 | 70.9 | 81.3 | 65.5 | 63.9 | 0.88 | 0.70 | 0.61 | 0.75 | 0.77 |
| Hick (2007) | H1 | 20.4 | 150 | 60 | 2.50 | 19 × 100 | 1 | 87.5 | 84.9 | 82.0 | 95.7 | 74.2 | 78.5 | 1.03 | 1.07 | 0.91 | 1.18 | 1.11 |
| | H2 | 20.4 | 150 | 60 | 2.50 | 19 × 100 | 2 | 55.7 | 59.4 | 67.7 | 81.3 | 63.7 | 62.8 | 0.94 | 0.82 | 0.68 | 0.87 | 0.89 |
| Yuan (1996) | G1F | 28.0 | 140 | 80 | 1.75 | 19 × 125 | 1 | 91.9 | 104.7 | 99.6 | 95.7 | 81.0 | 73.1 | 0.88 | 0.92 | 0.96 | 1.13 | 1.26 |
| Lloyd and Wright (1990) | A1 | 30.8 | 160 | 50 | 3.2 | 19 × 100 | 1 | 111.4 | 108.8 | 102.1 | 95.7 | 98.0 | 98.1 | 1.02 | 1.09 | 1.16 | 1.14 | 1.14 |
| | A2 | 32.2 | 160 | 50 | 3.2 | 19 × 100 | 1 | 106.0 | 112.0 | 102.1 | 95.7 | 98.4 | 99.8 | 0.95 | 1.04 | 1.11 | 1.08 | 1.06 |
| Mottram and Johnson (1990) | R30-1-F | 26.0 | 170 | 60 | 2.83 | 19 × 95 | 1 | 113.4 | 95.0 | 95.1 | 95.7 | 86.4 | 88.8 | 1.19 | 1.19 | 1.19 | 1.31 | 1.28 |
| | R30-2 | 28 | 170 | 60 | 2.83 | 19 × 95 | 2 | 75.0 | 69.7 | 99.6 | 81.3 | 75.9 | 73.1 | 1.08 | 0.75 | 0.92 | 0.99 | 1.03 |
| Robinson (1988) | TI | 24.8 | 181.5 | 76 | 2.38 | 19 × 116 | 1 | 105.5 | 93.9 | 81.3 | 95.7 | 86.0 | 85.6 | 1.12 | 1.30 | 1.10 | 1.23 | 1.23 |
| | TII | 22.4 | 181.5 | 76 | 2.38 | 19 × 116 | 2 | 64.6 | 61.9 | 54.0 | 81.3 | 65.5 | 65.8 | 1.04 | 1.20 | 0.79 | 0.99 | 0.98 |
| Mean | | | | | | | | | | | | | | 1.00 | 1.00 | 0.93 | 1.06 | 1.06 |
| Coefficient of Variation | | | | | | | | | | | | | | 10.8% | 19.6% | 21.3% | 15.4% | 15.3% |

### 5.10.3 Unfavourable stud position

The same procedure applied to the favourable position was used herein. The process involved analysing the FE results taken from 32 tests with unfavourable single studs. The four variables were associated with the linear assumption of the shear connector resistance. As a result, the least square regression analysis using the add-in solver introduced Equation 5.44 to calculate the shear strength of unfavourable studs. The coefficient of correlation ($R^2$) obtained from the regression analysis was 0.973. A relationship between the load per stud obtained from the parametric study and those predicted by Equation 5.44 is presented in Figure 5.14. The mean of predicted strengths to the observed results and the coefficient of variation are 1.00 and 3.8% respectively. Details of the predicted strengths using the regression analysis are given in Appendix A (Table A.3). The parametric study indicated that the average ratio of shear connector resistance of stud pairs to the ones with single studs was 0.73. Hence, the relationship between the use of single and double studs in Equation 5.44 is associated with the square root of the number of studs per rib.

$$P_U = [(1.339\, f_{ck} + 0.149\, A_s + 8.179\, b_o/h_p + 27.571\, h_{sc}/h_p) - 70.027] / \sqrt{N_r} \qquad \text{Eq. 5.44}$$

where:

$P_U$ = the shear capacity per stud placed in an unfavourable position of transverse profiled sheeting (kN)

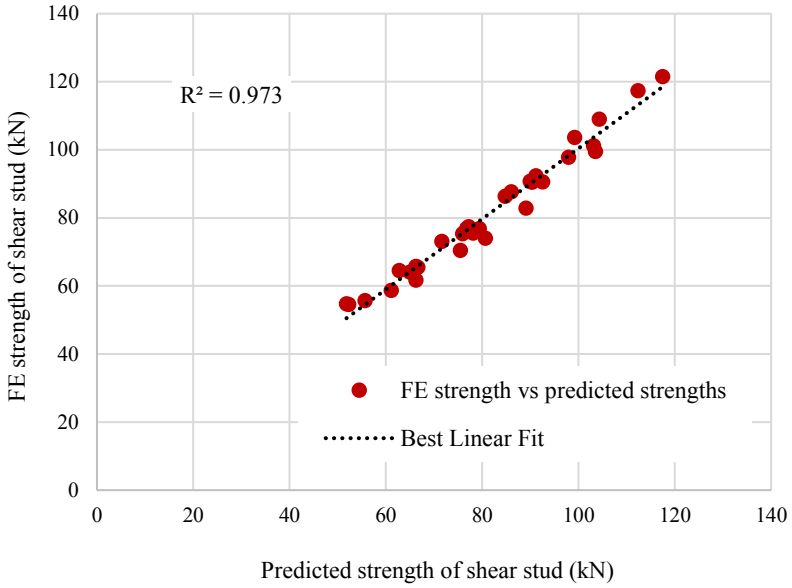


Figure 5.14 FE versus predicted strengths for single studs placed in an unfavourable position

In experimental studies conducted by Mottram and Johnson (1990), and Johnson and Yuan (1998a), some tests were examined with a staggered arrangement of shear studs (i.e. one favourable and one unfavourable). Those tests were accompanied with other tests having the same properties, but with single unfavourable studs. It is interesting to find how the shear connector resistance of unfavourable single stud and staggered arrangement are related. This could lead to link the load per stud of these two aspects and formulate an equation that would predict the shear strength of stud when a rib metal deck involves stud pairs placed in a staggered way. Accordingly, the results of the experiments were analysed in this study (see Table 5.8), by normalising them to the concrete grades C12, C20, C30, and C40 using Equation 5.45. Later, the mean of shear strength of staggered to the unfavourable single stud was found to be 0.92. If this mean value is assumed to be a factor and inserted to Equation 5.44, then the load per stud of staggered arrangement is likely to be predicted. Thus, Equation 4.46 was introduced for this purpose. The objective now is to evaluate the reliability of Equations 4.44 and 4.46 and compare their effectiveness with the other strength prediction methods.

$$P_{normalised} = [f_c / f_{c(test)}]^{0.5} P_{test} \qquad \text{Eq. 4.45}$$

$$P_{ST} = [(1.232 f_{ck} + 0.138 A_s + 7.525 b_o/h_p + 25.365 h_{sc}/h_p) - 64.425] \qquad \text{Eq. 5.46}$$

where:

$P_{ST}$ = the shear capacity per stud placed in a staggered layout transverse profiled sheeting (kN)

Table 5.8 Relationship between single unfavourable stud and staggered layout

| Ref. | Test | Concrete strength $f_{ck}$ (MPa) | Stud position | Average load per stud (kN) | Unfavourable position | | Staggered layout | | $P_S/P_U$ |
|---|---|---|---|---|---|---|---|---|---|
| | | | | | Concrete grade (MPa) | $P_{Normalised}$ | Concrete grade (MPa) | $P_{Normalised}$ | |
| Mottram and Johnson (1990) | R30-1-U | 25.3 | 1U | 73.2 | 12 | 50.4 | 12 | 49.1 | 0.97 |
| | | | | | 20 | 65.1 | 20 | 63.4 | 0.97 |
| | R30-2-S | 24.7 | S | 70.5 | 30 | 79.7 | 30 | 77.7 | 0.97 |
| | | | | | 40 | 92.0 | 40 | 89.7 | 0.97 |
| | R30-1-UD | 27.7 | 1U | 89.3 | 12 | 58.8 | 12 | 55.4 | 0.94 |
| | | | | | 20 | 75.8 | 20 | 71.5 | 0.94 |
| | R30-2-SD | 24.7 | S | 79.5 | 30 | 92.9 | 30 | 87.6 | 0.94 |
| | | | | | 40 | 107.3 | 40 | 101.1 | 0.94 |
| Johnson and Yuan (1998a) | G5U | 28.0 | 1U | 69.2 | 12 | 45.3 | 12 | 41.4 | 0.91 |
| | | | | | 20 | 58.5 | 20 | 53.5 | 0.91 |
| | G8D | 25.8 | S | 60.8 | 30 | 71.6 | 30 | 65.5 | 0.91 |
| | | | | | 40 | 82.7 | 40 | 75.7 | 0.91 |
| | G6U | 21.8 | 1U | 52.6 | 12 | 39.0 | 12 | 34.5 | 0.88 |
| | | | | | 20 | 50.4 | 20 | 44.6 | 0.88 |
| | G7D | 25.8 | S | 50.7 | 30 | 61.7 | 30 | 54.6 | 0.88 |
| | | | | | 40 | 71.2 | 40 | 63.1 | 0.88 |
| Mean | | | | | | | | | 0.92 |
| Coefficient of variation | | | | | | | | | 3.8% |

The shear strength of unfavourable stud according to Konrad (2011) is calculated as the lesser values obtained from Equations 5.24 or 5.25, then multiplied by a reduction factor taken from Equation 5.47 or 5.48. Since no such formula developed by Konrad (2011) concerning staggered layout, it was decided to apply the equations relevant to unfavourable stud to predict the load per stud of tests with the staggered layout. This approach will provide an indication of how workable the unfavourable stud equations are when two studs per rib are placed in a staggered way.

$$k_t = k_n\,[0.036\,(b_o/h_p)^2 + 0.004\,(b_o/h_p) + 0.305\,(h_{sc}/h_p) - 0.095] \le 0.8 \text{ if } h_{sc}/h_p \le 1.56 \quad \text{Eq. 5.47}$$

$$k_t = k_n\,[0.317\,(b_o/h_p) + 0.06] \quad \le 0.8 \quad \text{if } h_{sc}/h_p > 1.56 \quad \text{Eq. 5.48}$$

According to Johnson and Yuan (1998b), the shear strength of stud placed in the unfavourable position is measured by Equation 5.49. While for staggered layout, Equation 5.5 was used for this purpose.

$$P_{RP} = k_{rp}\, P_{EC4} \qquad \text{Eq. 5.49}$$

$$k_{rp} = [\eta_{rp} + \lambda_{rp}\,(1 + \lambda_{rp}^2 - \eta_{rp}^2)^{0.5}] \,/\, (1 + \lambda_{rp}^2) \leq 1.0 \qquad \text{Eq. 5.50}$$

$$\eta_{rp} = [1.8\,(e + h_{sc} - h_p)\, t_s f_{yp}] \,/\, P_{EC4} \qquad \text{Eq. 5.51}$$

$$\lambda_{rp} = e\, T_y \,/\, 2\, h_p\, P_{EC4} \qquad \text{Eq. 5.52}$$

$$T_y \cong 0.8\, A_s f_u \qquad \text{Eq. 5.53}$$

As seen in Table 5.9, both European and American design codes reveal the highest scatter and most insufficient correlations as compared to the other strength prediction methods. The coefficient of variation in both codes is higher than 20%. Both design codes do not consider the influence of the stud's layout on the shear connector resistance. Due to the wide scatter found from the equations proposed by Johnson and Yuan (1998b) in most cases, this method is believed not to be safe enough. The first reason is that Equation 5.49 does not consider the number of stud per rib. As a result, the equation will provide unreliable values in case of tests with stud pairs. The second reason is that the method, in general, is mainly associated with the predicted strengths of EC4. This means that if inaccurate results or big scatter are obtained from EC4, this for sure will badly reflect on the accuracy of results taken from any equation proposed by Johnson and Yuan (1998b).

On the other hand, both methods proposed by Konrad (2011) as well as this research showed the least discrepancies in results, indicating to be the most workable equations among the others, yet the equations proposed in this research showed more effectiveness than Konrad's method as noted by the coefficient of variation. Figure 5.15 displays the predicted results obtained from Equation 5.44 and 5.46 against the experiments. Even though the equations for unfavourable studs developed by Konrad (2011) are not theoretically appropriate for staggered studs, they were seen to give fair predictions for load per stud in a staggered layout. However, it may not work under all conditions or parameters in the future. This leaves Eq. 5.43 to be the only relevant equation so far to deal with the staggered layout. Nevertheless,

further investigation needs to be done on tests with staggered studs to ascertain the reliability of Eq. 5.43 due to the paucity of research on the staggered arrangement.

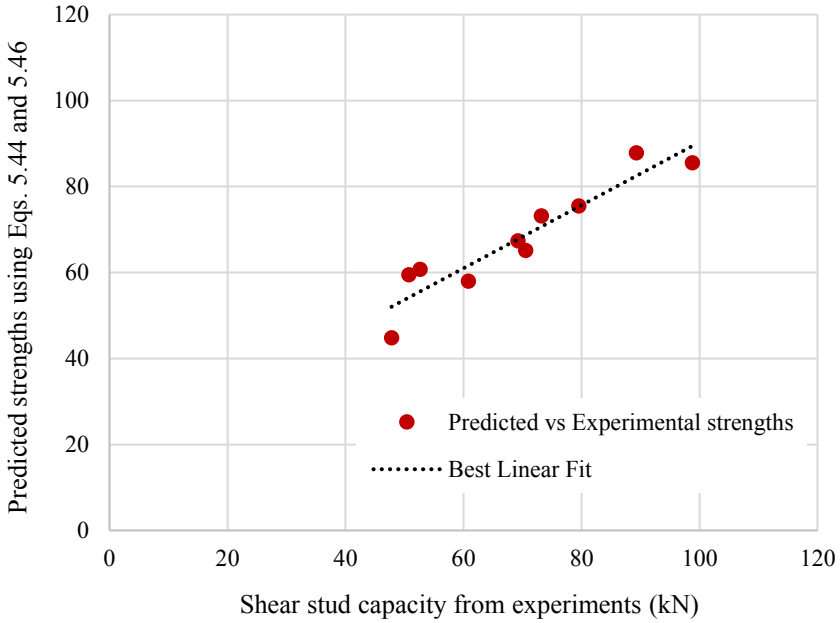


Figure 5.15 Comparison between predicted strengths using Eqs. 5.44 and 5.46 and experimental results

Table 5.9 Comparison of shear connector resistance from experiments and developed equations for push-off tests with unfavourable and staggered studs

| Ref. | Test | Concrete strength $f_{ck}$ (MPa) | profiled sheeting details | | | Stud details | | Average experimental load per stud $P_{Test}$ (kN) | $P_U$ or $P_{ST}$ (kN) | $P_{EC4}$ (kN) | $P_{AISC}$ (kN) | $P_{J\&Y}$ (kN) | $P_{Konrad}$ (kN) | $P_{Test}/P_U$ or $P_{Test}/P_{ST}$ | $P_{Test}/P_{EC4}$ | $P_{Test}/P_{AISC}$ | $P_{Test}/P_{J\&Y}$ | $P_{Test}/P_{Konrad}$ |
|---|---|---|---|---|---|---|---|---|---|---|---|---|---|---|---|---|---|---|
| | | | $b_o$ (mm) | $h_p$ (mm) | $b_o/h_p$ | $d \times h_s$ (mm) | Position | | | | | | | | | | | |
| Yuan (1996) | G5U | 28 | 140 | 80 | 1.75 | 19 × 125 | 1U | 69.2 | 67.4× | 99.6 | 95.6 | 67.5* | 62.4 | 1.03 | 0.69 | 0.72 | 0.98 | 1.11 |
| | G8D | 25.8 | 140 | 80 | 1.75 | 19 × 125 | S | 60.8 | 58.0×× | 94.7 | 81.3 | 66.9** | 48.3 | 1.05 | 0.64 | 0.75 | 1.10 | 1.26 |
| | G6U | 21.8 | 113 | 60 | 1.88 | 19 × 95 | 1U | 52.6 | 60.7× | 85.4 | 95.6 | 50.4* | 60.6 | 0.87 | 0.62 | 0.55 | 0.96 | 0.87 |
| | G7D | 25.8 | 113 | 60 | 1.88 | 19 × 95 | S | 50.7 | 59.5×× | 94.7 | 81.3 | 59.8** | 51.7 | 0.85 | 0.54 | 0.62 | 1.18 | 0.98 |
| Mottram and Johnson (1990) | R30-1-U | 25.3 | 170 | 60 | 2.83 | 19 × 95 | 1U | 73.2 | 73.2× | 93.5 | 95.6 | 71.8* | 78.1 | 1.00 | 0.78 | 0.77 | 0.98 | 0.94 |
| | R30-1-UD | 27.7 | 170 | 60 | 2.83 | 19 × 120 | S | 89.3 | 87.9× | 98.9 | 95.6 | 82.5* | 80.8 | 1.02 | 0.90 | 0.93 | 0.92 | 1.10 |
| | R30-2-S | 24.7 | 170 | 60 | 2.83 | 19 × 95 | 1U | 70.5 | 65.1×× | 92.2 | 81.3 | 77.1** | 74.1 | 1.08 | 0.76 | 0.87 | 1.09 | 0.95 |
| | R30-2-SD | 24.7 | 170 | 60 | 2.83 | 19 × 120 | S | 79.5 | 75.5×× | 92.2 | 81.3 | 77.1** | 77.4 | 1.05 | 0.86 | 0.98 | 0.97 | 1.03 |
| Lloyd and Wright (1990) | A3 | 30.8 | 160 | 50 | 3.20 | 19 × 100 | U | 98.8 | 85.5× | 102 | 81.3 | 79.8* | 84.2 | 1.16 | 0.96 | 1.21 | 0.81 | 1.17 |
| Robinson (1988) | TVIII | 22.4 | 181 | 76 | 2.38 | 19 × 116 | 2U | 47.8 | 44.9× | 86.8 | 81.3 | 58.2* | 43.6 | 1.07 | 0.55 | 0.59 | 1.22 | 1.10 |
| Mean | | | | | | | | | | | | | | 1.02 | 0.73 | 0.80 | 1.02 | 1.05 |
| Coefficient of Variation | | | | | | | | | | | | | | 9.1% | 20.2% | 25.4% | 12.3% | 11.3% |

× Use of Eq. 5.44
×× Use of Eq. 5.46
* Use of Eq. 5.49
** Use of Eq. 5.5

## 5.11 Conclusions

This chapter initially aimed at observing the effectiveness of some design codes and analytical methods at predicting the shear capacity of the stud in narrow and very deep transverse steel decks. The applicability of these selected methods was felt questionable among tests with steel decks deeper than 80 mm. Therefore, the shear stud capacities obtained from tests with 100 and 146 mm deep decks were compared to the predicted strengths achieved from the existing design equations. The comparison indicated that all design equations did not account for narrow ribbed ($b_o/h_p \leq 1.5$) and very deep decks. Large deviations of up to 50% were found between the observed and predicted strengths in most cases. This brought a strong rationale to introduce new inclusive equations for better predictions.

The numerical results obtained from 240 push-off tests were used to yield new formulae using the least square regression analysis method. The new developed equations accounted for each studs' layout (Central, Favourable, Unfavourable and Staggered). For central stud position, the relevant equation covered for the first time a wide range of ribbed geometries including narrow and very deep decks. This part has bridged an important knowledge gap by adding new information about steel decks deeper than 80 mm. The applicability of the developed equations was checked against many previous experiments. The comparison showed that the new equations were not only as effective as previous design equations but were also proven to be more valid. The accuracy in results remained within ±10%. Besides the accuracy, the new equations are easy to use. This will help the designers to apply these equations in practice directly without pre-conditions.

# Chapter 6 Finite element modelling of push-off tests with parallel profiled decking

# Chapter 6

## Finite element modelling of push-off tests with parallel profiled decking

### 6.1 Introduction

This chapter examines the behaviour of composite beams incorporating parallel steel decking. The FE modelling included a set of various types of steel decks aiming at addressing the correlation between narrow and wide ribbed composite decks, and bridging the gap between the geometries of common profiled sheeting (i.e. 60 and 80 mm deep) and very deep decking up to 146 mm. A parametric study was carried out including rib deck ratios, stud geometries, the effective cross-sectional area of concrete, longitudinal stud spacing, the diameter of the headed stud and sheeting thickness. The effects of these parameters were linked to the shear connector resistance, ductility, and failure mode of headed shear studs in composite beams. The results and discussion of the FE modelling are detailed in this chapter, accompanied by illustrative figures of the load-slip curves and failure modes.

### 6.2 Description of push-off tests modelling

#### 6.2.1 General

The push-off test consists of a steel beam, headed studs, steel decking, concrete slab, and wire-mesh reinforcement (see Figure 6.1). At first, a 146 mm deep decking was used, this modern type of steel decking comes with an average rib width to rib height ($b_o/h_p$) of 0.67. Since this part of the research intends to investigate the influence of different geometries of steel decking, the 146 mm deep decking was modified with some improvisations. That included inverting and/or cutting the steel decking at different levels of its depth to provide the desired rib deck ratios. The details of all steel decks investigated are shown in Figure 6.2. Four rows of studs were applied in all models. The corresponding diameter of the stud was mostly 19 mm, except for some specimens examined with a diameter of stud of 22 mm for a parametric study purpose. The parametric study on the deck geometry resulted in three different depths. Thus, the overall height of stud for 60, 76 and 146 mm deep deck was 100, 125 and 195 mm respectively.

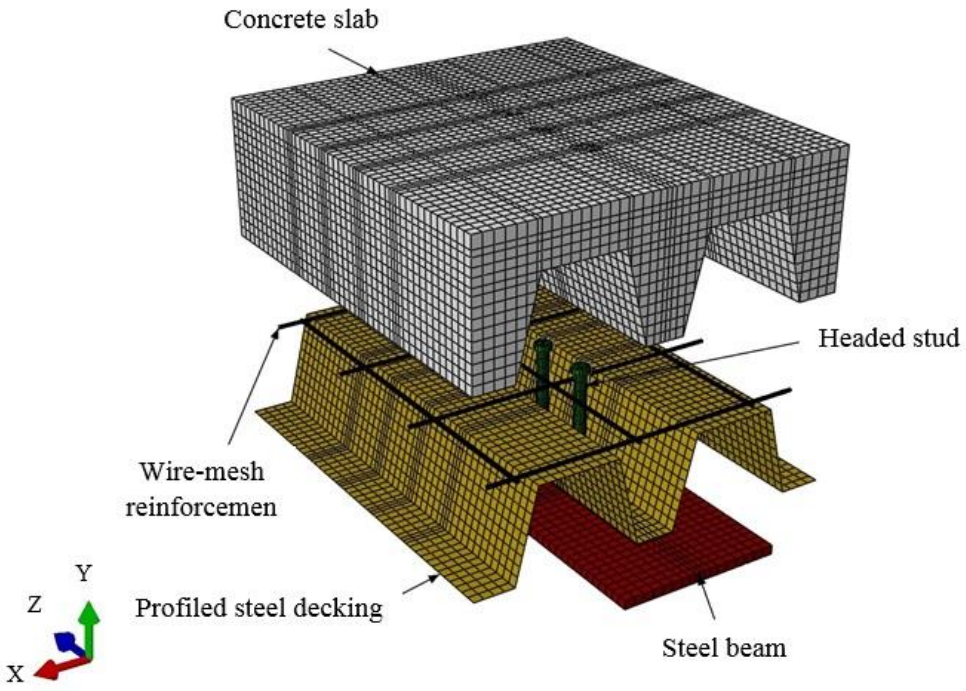


Figure 6.1 Push-off test parts

Normal weight concrete was used to identify the concrete slab geometry in all specimens. Concrete Damage Plasticity method (CDP) was used to specify the concrete material. The length and width of the concrete slabs were varied with the longitudinal stud spacing and the rib geometry size. Note that the distance from the centre of both first and last headed stud to the concrete edge parallel to the applied load was kept constant at 150 mm. The other intention of this chapter is to highlight the effect of a cross-sectional area of the concrete slab. Figure 6.2 addresses the effective cross-sectional area of concrete (highlighted as dark grey) for each type of steel decking investigated. This effective zone is measured as the embedded area of concrete within a rib decking, plus the area of concrete above it. The concrete slab in all tests was reinforced with A193 mesh-wire (7 mm in diameter) having 200 mm centre to centre spacing and was placed on the steel decking surface. All geometries were meshed using 15 × 15 mm mesh element size and assembled to produce the push-off test model as shown in Figure 6.3.

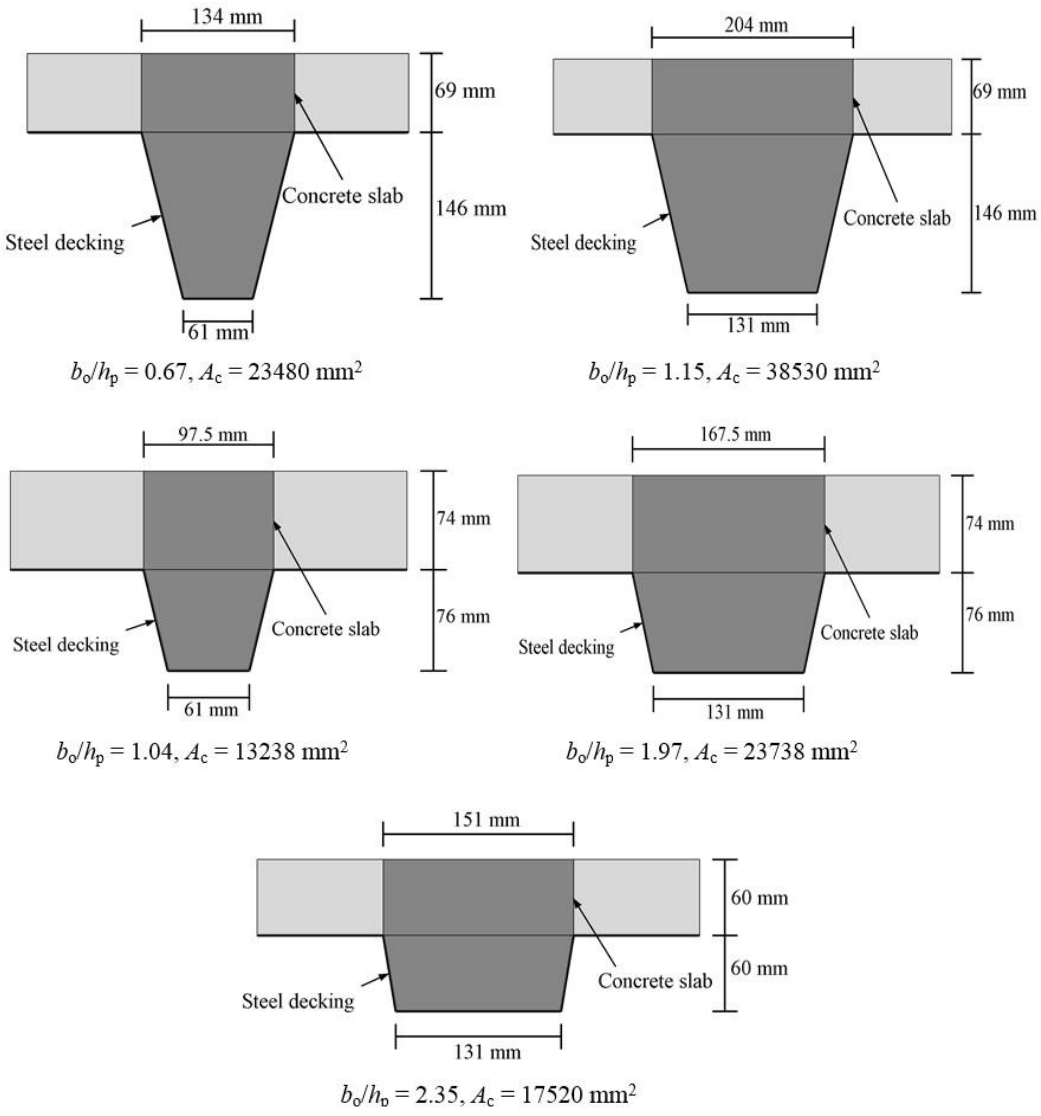


Figure 6.2 Details of steel decking with their effective cross-sectional area of concrete ($A_c$)

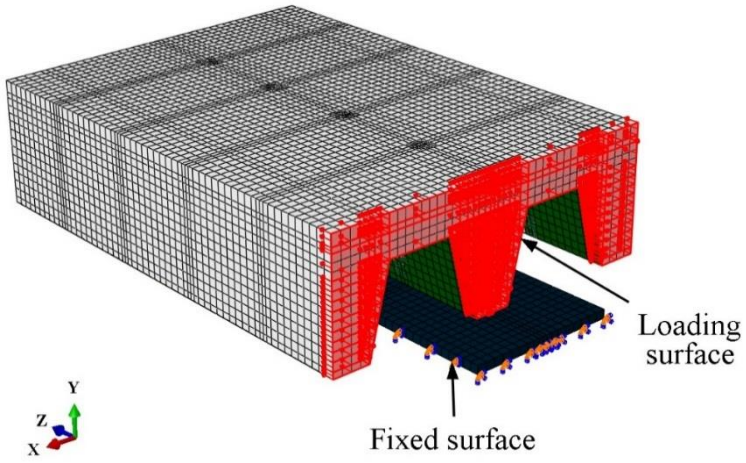


Figure 6.3 Assembly of push-off models with parallel steel decking

### 6.2.2 Constraints and contact interactions

The procedure to define the relationships between the contacted surfaces in push models with parallel profiled sheeting was similar to numerical tests conducted in Chapter 3, Section 3.7.

### 6.2.3 Boundary conditions and load application

The boundary conditions and load application were similar in all push models. As indicated in Figure 6.3, the base of the steel beam was restrained from moving and rotating in all directions. During the analysis, all finite element models were pushed horizontally and slowly from one side until failure using a loading rate of 0.5 mm/sec and mass scaling factor of 10. The average slip capacity was measured at the concrete surface opposite to the applied load.

## 6.3 Test program

A total number of 136 push-off tests were modelled and divided into four phases as described below. Moreover, the full details of the test program are presented in Table 6.1.

### 6.3.1 Phase I: One stud per row

This phase contains 64 tests which were equally split into four groups (i.e. A, B, C, and D). All tests featured one stud per row and sheeting thickness of 1.2 mm. For each group, four different longitudinal stud spacings were considered: 3d, 4.5d, 6d, and 8d, and for each spacing, the concrete strength varied from 12 to 40 MPa. Although the Eurocode 4 requires the minimum longitudinal spacing between studs to be five times the diameter of the stud (5d), it was felt necessary to consider some longitudinal spacings below the minimum limit suggested by the EC4 for the following reasons. First, to provide an insight in measuring such effect on the load-slip capacity and mode of failure of composite beams. Second, to see how well the longitudinal stud spacing is presented among some existing design equations. And third, if necessary, to develop equations which take into consideration a wide range of longitudinal stud spacings.

Each group was addressed with one specific rib deck ratio: 0.67, 1.04, 1.15, and 1.97, which the corresponding effective cross-sectional area of concrete was 23480, 13238, 38530, and

23738 $mm^2$ respectively. The corresponding diameter of the headed stud was 19 mm in all tests, while the height was 125 and 195 mm for tests with 76 and 146 mm deep decking respectively. The main purpose of this phase is to investigate the effect of rib deck ratios, stud geometry and the effective cross-sectional area of concrete on the behaviour of composite beams.

### 6.3.2 Phase II: Two studs per row

This phase contains three groups (i.e. E, F, and G) resulting in a total number of 48 specimens. The parameters to be studied in this phase are similar to those in Phase I, but this time, the push-off models were featured with two studs per row. For this phase, three different types of steel decks were considered: 60, 76, and 146 mm deep decking, the relating rib deck ratios were 1.15, 1.97, and 2.35 respectively, and the corresponding effective cross-sectional area of concrete was 38530, 23738 and 17520 $mm^2$ respectively. This part did not account for tests with 0.67 rib deck ratio as it was not possible to place two studs in narrow geometry.

The diameter of a headed stud used in all tests was 19 mm, whilst the height was 100, 125 and 195 mm for tests with 60, 76 and 146 mm deep decking respectively. Previous studies suggested that in order for the best performance of two studs per row on one line to be realised, they should be placed at a distance close to 4 times the stud's diameter. Thus, the transverse stud spacing between studs was kept constant at 76 mm (4d). Other than that, the rest aspects are similar to those in phase I.

### 6.3.3 Phase III: Sheeting thickness

This phase highlights the influence of thicker profiled sheeting on the behaviour of composite beams with parallel metal decks. In most cases of push-off tests with parallel sheeting conducted by Yuan (1996), the profiled sheeting experienced a local buckling, particularly in the area around the headed studs. This suggests that the profiled sheeting may have influence on the shear connector resistance, and how the damage patterns propagate if the sheeting thickness is changed. In fact, there is a lack of research investigating the change in the sheeting thickness on the behaviour of composite beams with parallel metal decks. Thus, it is important to examine how this parameter could be influential. Phase III involves testing 16 specimens divided into four groups (i.e. H, I, J, and K). Group H and I each consists of 4 tests featuring one stud per row, 0.67 rib deck ratio, and only longitudinal stud spacing of

4.5d. Group H was associated with 1.5 mm sheeting thickness, while Group I with 2.0 mm. For groups J and K, the layout resembles groups H and I respectively, with the exception that all tests contain two studs per row and 1.15 rib deck ratio.

### 6.3.4 Phase IV: Diameter of stud

The increase in the diameter of the headed stud from 19 to 22 mm is presented in this phase. It is well-known that the cross-sectional area of headed stud plays a major role in the shear connector resistance of composite beams. Therefore, any design equation meant to predict the shear connector resistance in composite beams should not rule out such important effect. As it will be found in the next chapter that there is a necessity to formulate new equations to cope with a wider range of parameters, the cross-sectional area of the headed stud will be one of these terms to be involved in the formulation. Phase IV involves testing 8 specimens divided into two groups (i.e. L and M). Group L consists of 4 tests featuring one stud per row, 0.67 rib deck ratio, and only longitudinal stud spacing of 4.5d. For group M, the layout resembles group L, except that all tests contain two studs per row and 1.15 rib deck ratio.

## 6.4 Failure Mechanism

### 6.4.1 Longitudinal splitting of concrete

This failure mode was predominately associated with push tests with single stud per row. In particular, push tests containing headed studs placed at 3d and 4.5d longitudinal stud spacing. This means that even tests incorporating thicker steel decks, or larger diameter of stud failed by this failure mode. Figure 6.4 presents a typical longitudinal splitting of concrete failure. Specimen B22 had rib deck ratio ($b_o/h_p$) of 1.15, concrete strength of 20 MPa, and the studs were placed at a longitudinal spacing of 4.5d. During the test, a longitudinal crack appeared near the base of studs due to the relatively narrow haunch of concrete in that area which bears little resistance. Shortly after the ultimate load, the longitudinal crack extended up and further propagated as a straight line between studs. Meanwhile, the web of profiled sheeting slightly buckled mainly in the area around the shear studs. As seen in Figure 6.4, the headed studs encountered bending but without shearing off.

It must be mentioned that this failure mode was less likely to happen when the concrete strength reached 40 MPa, despite the headed studs being placed relatively close. This

indicates that the longitudinal splitting of concrete is not only controlled by the longitudinal stud spacing, but also by concrete strength. For tests associated with this failure mode, the brittle failure of concrete was the typical tendency, which in turn, did not allow the headed studs to reach a high ductility. As a result, the ductility hardly exceeded 4 mm. Figure 6.5 represents the typical load-slip curve of the longitudinal splitting of concrete failure taken from some push-off tests.

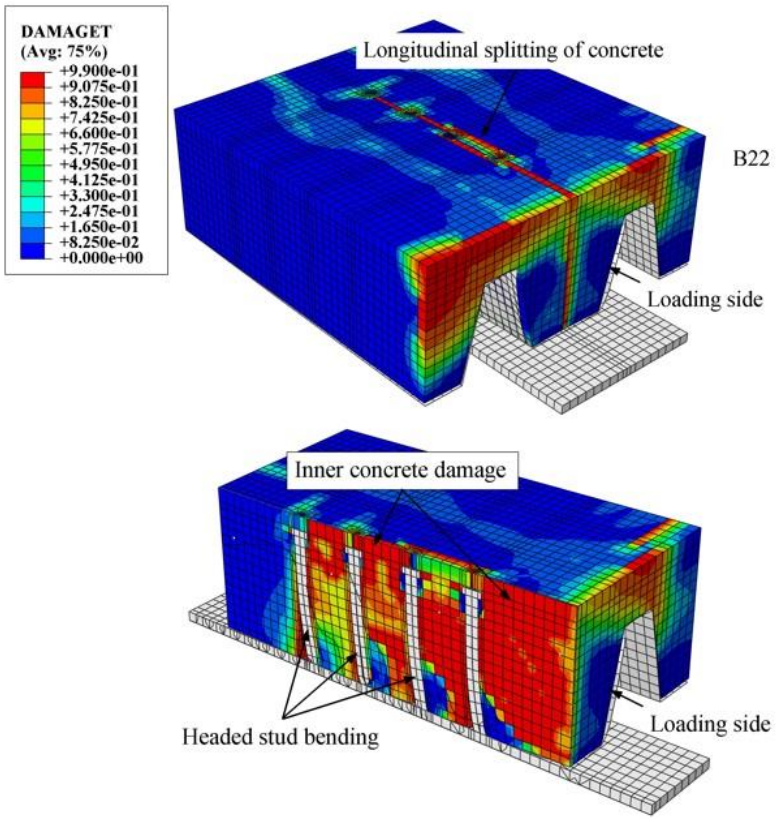


Figure 6.4 Typical longitudinal splitting failure of concrete

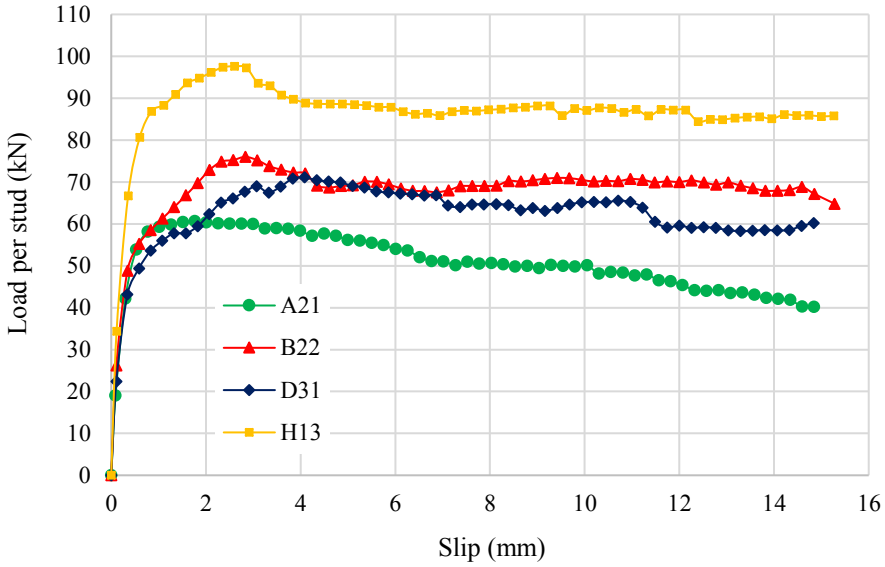


Figure 6.5 Load-slip curves of some tests which failed by longitudinal splitting of concrete

### 6.4.2 Shank shearing of stud

This failure mode was mainly governed by the number of studs per row, longitudinal stud spacing, and concrete strength. For push tests with single stud per row, shank shear failure mostly occurred when studs were placed at 6d or higher, and concrete strength was equal to or more than 30 MPa. However, shank shear failure was even observed in some specimens with the concrete grade of 20 MPa, but only when the longitudinal stud spacing was 8d. On the other hand, shank shear failure did not occur among specimens with double stud per row as often as their companions with single stud per row. It was found that that specimen containing longitudinal stud spacing of 8d and concrete strength of 40 MPa ended with this type of failure. A typical shank shear failure of studs is shown in Figure 6.6. Specimen A44 had rib deck ratio ($b_o/h_p$) of 0.67, concrete strength of 40 MPa, and 8d longitudinal stud spacing.

The cause of this failure is attributed to the physical failure of the headed stud's material (i.e. the ultimate tensile strength of stud is exceeded). Although the concrete part visually remained intact, there were some signs of local damage adjacent to the stud assembly. This was due to some bending of studs before they sheared off. Figure 6.7 shows load-slip curves of some tests associated with the shank shearing of the stud. The sudden drop in the load-slip curve indicates that the headed studs sheared off after they had achieved their maximum

shear resistance. With this failure mode, the headed studs reached the highest ductility compared to any ductility spotted with the other failure modes. The FE results showed that the ductility at the ultimate load per stud could reach 10 mm or higher. The reason behind that is because the sufficient longitudinal spacing provided between stud along with high concrete strength being undamaged during the test, and that led for the ductility of the headed stud to be realised.

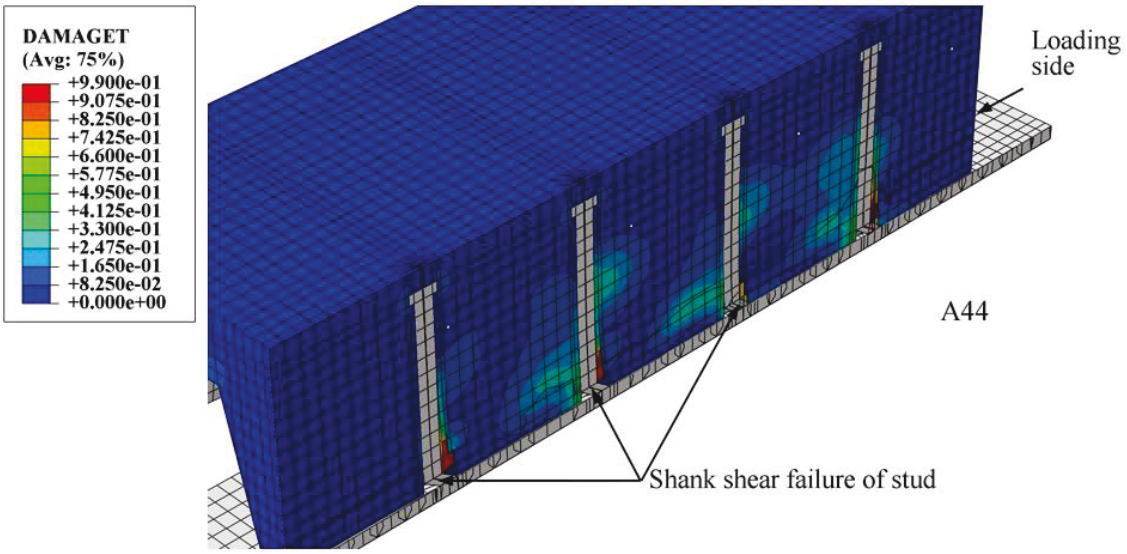


Figure 6.6 Cut-view of the typical shank shear stud failure

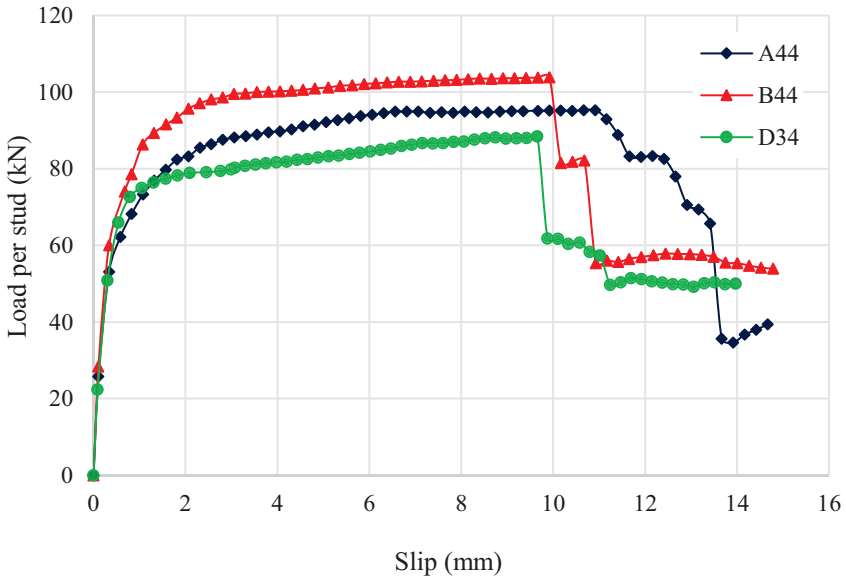


Figure 6.7 Load-slip curves of some tests failed by shank shearing of stud

### 6.4.3 Concrete shear plane failure

Push tests with double studs per row were more likely to end with concrete shear plane failure. This failure mode was only aligned with tests featuring narrow ribbed metal deck ($b_o/h_p < 1.5$), and it occurred in all tests labelled as group E. The failure originated at a close level to the headed studs acting as a horizontal plane and further propagated as the load increased. The web of steel decking experienced some buckling but not as prominent as those seen with single stud per row. This type of failure was reported by Jayas and Hosain (1988) and said to resemble a concrete pull-out failure with respect to specimens incorporating perpendicular ribbed steel decking. Figure 6.8 presents a typical concrete shear plane failure. Specimen E23 involved 146 mm deep decking with 1.15 rib deck ratio ($b_o/h_p$), concrete strength of 20 MPa, and the studs were placed at a longitudinal spacing of 6d. It was also apparent that headed studs experienced bending causing some significant concrete damage in the vicinity of stud connectors.

The load-slip curve associated with this failure mode behaved linearly at the early stage of loading. The complete shear damage of concrete did not happen abruptly but within stages. This allowed some time for headed studs to experience bending before failure, resulting in a significant plateau shape in the load-slip curve as shown in Figure 6.9. The prolonged loading resulted in some headed stud ductility around 6 mm. The load-slip curve started to decline when the shear plane of concrete extended further between the headed studs. In all tests featuring this failure mode, the headed studs did not shear off even with high concrete strength and studs being placed relatively away. This suggests that the concrete failure had taken place before the ultimate tensile strength of headed stud was achieved.

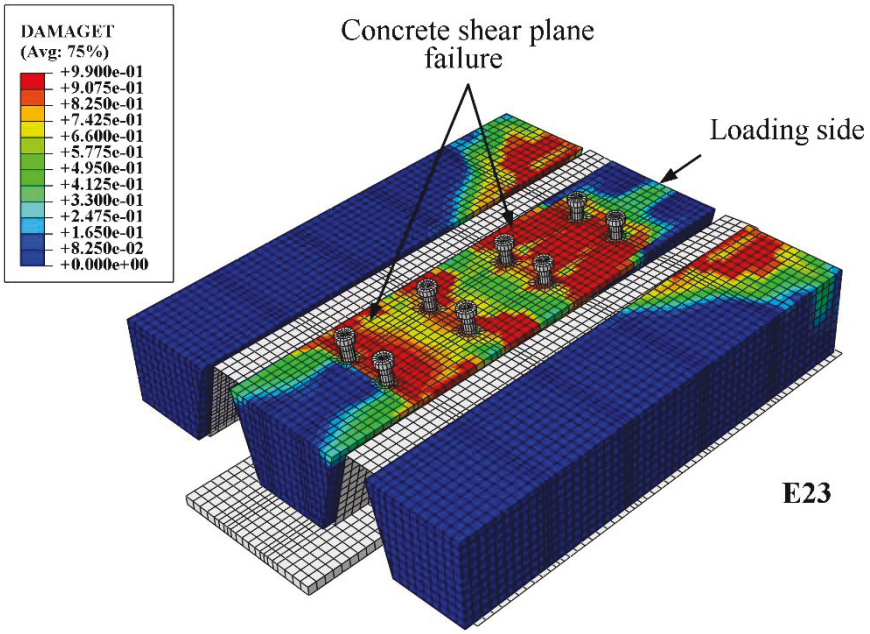


Figure 6.8 Cut-view of the typical concrete shear plane failure

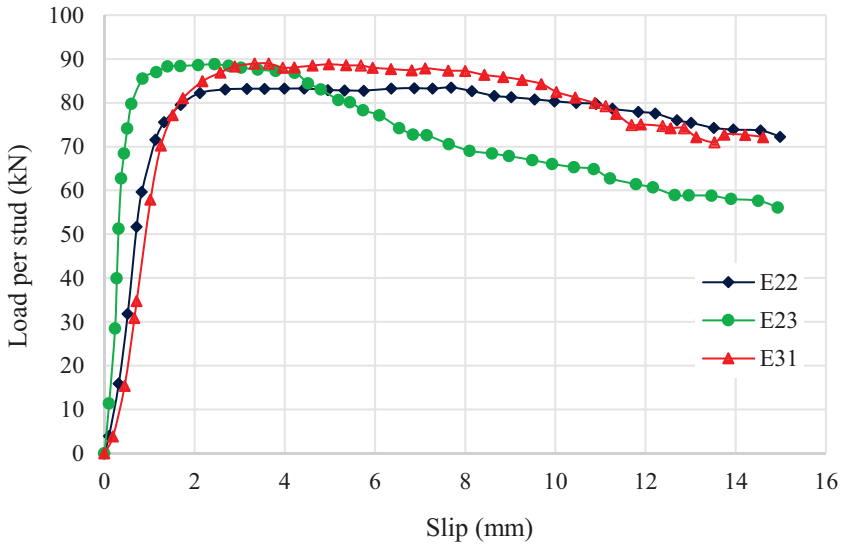


Figure 6.9 Prolongment of load-slip curves associated with tests failed by concrete shear plane

### 6.4.4 Concrete splitting and crushing failure

This mode of failure was generally related with specimens featuring two studs per row and wide ribbed steel deck ($b_o/h_p \geq 1.5$). All tests with wide ribbed steel deck ended with this mode of failure, except one specimen having rib deck ratio of 1.97, concrete strength of 40 MPa, and 8d longitudinal stud spacing, which the failure mode was a combination of the

longitudinal splitting of concrete and shank shear stud. The failure began when a longitudinal crack had originated near the base of studs and proceeded to the top surface of the slab forming a longitudinal line across studs. This was accompanied by crushing of concrete around the stud cluster. There was no sign of shank shear failure among headed studs except significant bending to the applied load direction.

Figure 6.10 illustrates concrete splitting and crushing failure in specimen G34 which had double stud per row arranged at 8d, concrete strength of 30 MPa, and rib deck geometry of 2.35. The concrete crushing is related to the concrete failure in compression. Therefore, Figure 6.10 involves two images; one represents the longitudinal splitting of concrete indicated by the tensile damage variable "DAMAGET", while the second image shows the concrete crushing defined by the compressive damage variable "DAMAGEC".

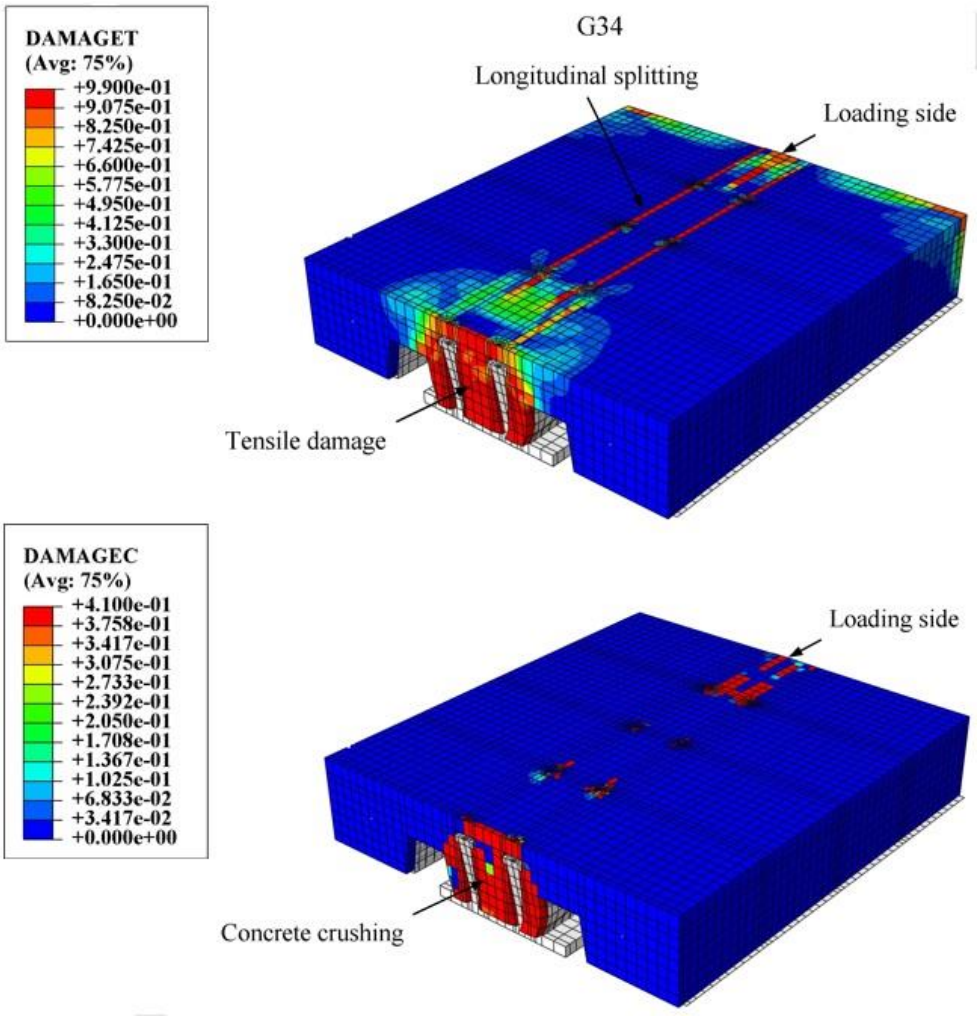


Figure 6.10 Cut-view of the typical concrete splitting and crushing failure

The load-slip curves associated with this failure mode appeared to be quite similar to those related to the shear plane failure. As shown in Figure 6.11, the headed studs had experienced some ductility before the complete damage of concrete occurred. The ductile behaviour of headed stud here is contrary to what was observed earlier that the longitudinal splitting of concrete is likely to result in a brittle failure. To justify this, the failure damage along with the time stage of loading was carefully monitored. It was found that with the tests having double stud per row, the time required to achieve a complete longitudinal splitting is relatively long compared to the tests having single stud per row and ending with the same failure mode. The existence of two studs per row is believed to be the reason for holding off the tendency of damage, and that is likely to explain the prolonged loading associated with further ductility of headed stud before failure.

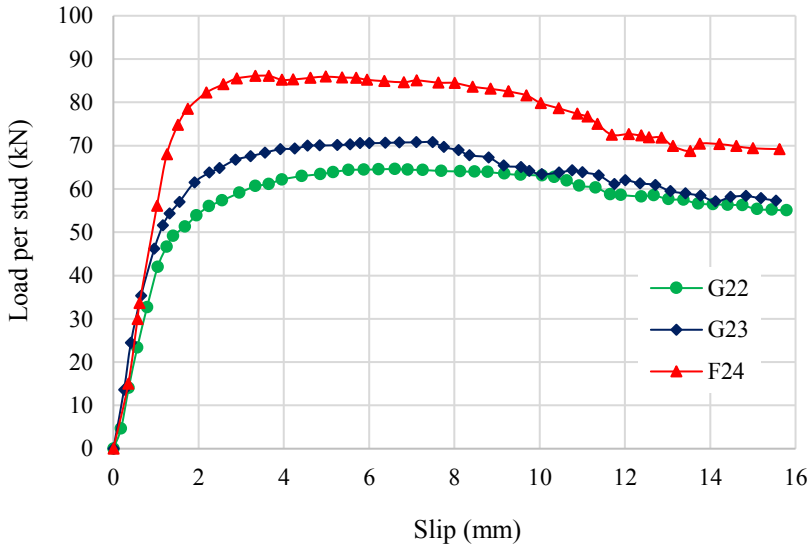


Figure 6.11 Load-slip curves of some tests failed by concrete splitting and crushing failure

### 6.4.5 Combined failure mode

A combination of the longitudinal splitting of concrete and shank shear failure was observed in some push-off tests with single stud per row. Specimens with concrete strength varying from 20 to 30 MPa and studs placed relatively away were more susceptible to generate this type of failure. A similar trend of combined failure was also seen in F44 which had rib deck ratio of 1.97, concrete strength of 40 MPa, and 8d longitudinal stud spacing. In general, concrete-related failure is primarily governed by low strength concrete, studs placed

relatively close, and two studs per row, while stud-related failure is mainly governed by high strength concrete, studs placed relatively far, and single stud per row. Figure 6.12 presents a combined failure in specimen B32 which had one stud per row arranged at 4.5d, concrete strength of 20 MPa, and rib deck geometry of 1.15. Some load-slip curves which were related by a combined failure mode are seen in Figure 6.13.

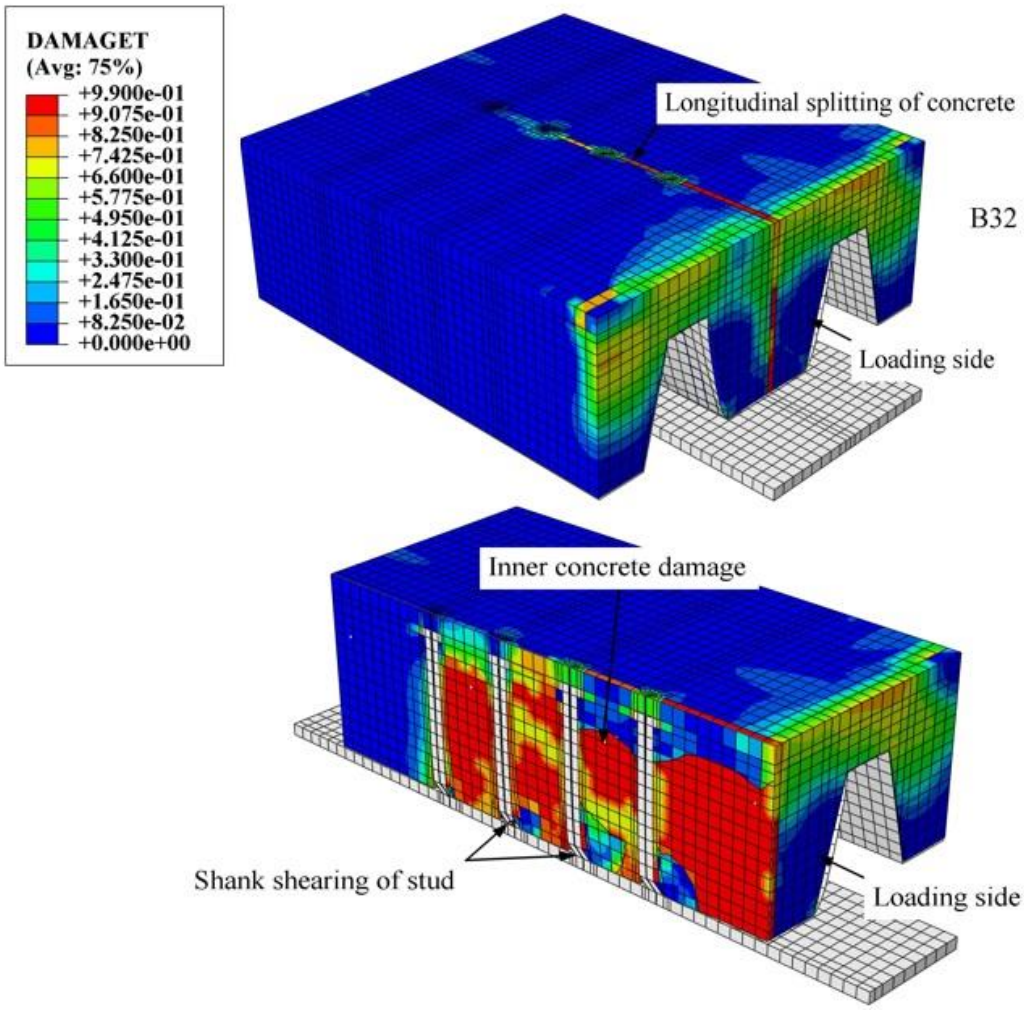


Figure 6.12 A combined failure of longitudinal splitting and shank shearing of stud

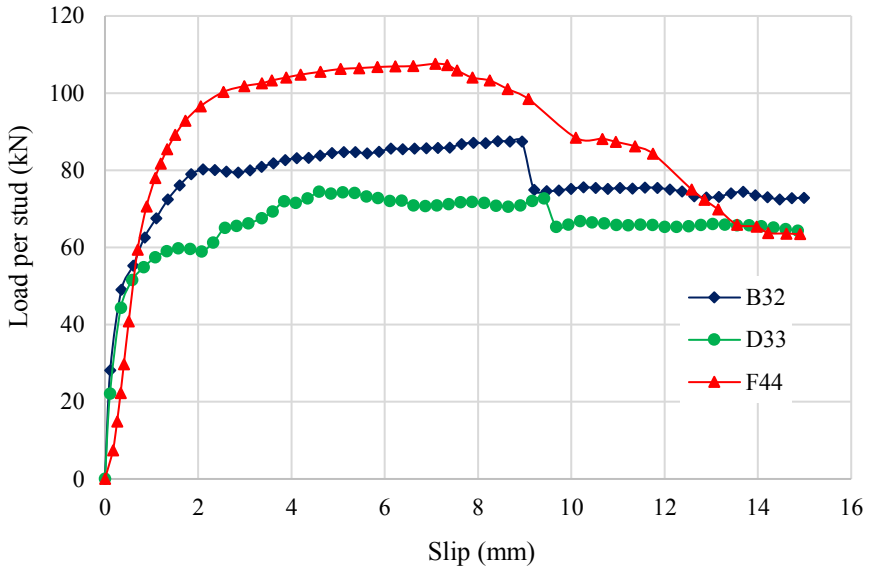


Figure 6.13 Load-slip curves of some tests related to a combined failure mode

## 6.5 Parametric study

The load per stud capacity for each test is given in Table 6.1.

### 6.5.1 Effect of rib deck ratio ($b_o/h_p$)

For push tests with studs in a single row (i.e. Phase I), four different rib deck ratios were investigated, namely, 0.67, 1.04, 1.15, and 1.97. The relative deck height was 146, 76, 146, and 76 mm respectively. Figure 6.14 displays the corresponding stud capacity for each type of steel decking. In this figure, the results were obtained from specimens with C20, and each line represents a longitudinal stud spacing (i.e. 3d, 4.5d, 6d, and 8d). At first, the headed stud capacity significantly declined when the rib deck ratio was changed from 0.67 to 1.04. The percentage of decrease was 17, 11, 12, and 10 for spacings of 3d, 4.5d, 6d, and 8d respectively. However, the stud capacity was considerably enhanced between rib deck ratios of 1.04 and 1.15 despite the different size between the two geometries being marginal. The percentage of increase was 33, 25, 19, and 16 for spacings of 3d, 4.5d, 6d, and 8d respectively.

Interestingly, the load capacity declined again as the rib deck ratio was increased to 1.97. This trend was similarly observed in the remaining tests for each concrete strength. The findings obtained from this part of the study oppose the concept that the rib deck ratio

demonstrates a direct relationship with the shear connector resistance. In other words, increasing the rib deck ratio is likely to increase the stud strength.

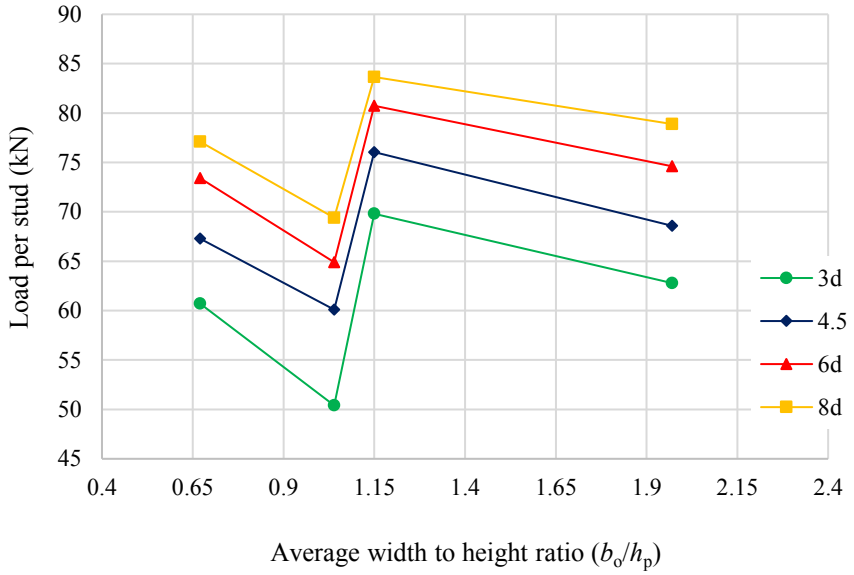


Figure 6.14 Effect of rib deck ratios for tests with one stud per row

This interesting finding was also observed among push-off tests with studs in two rows (i.e. Phase II). In Figure 6.15, three different rib deck ratios were examined: 1.15, 1.97, and 2.35, whereas the corresponding deck height was 146, 76, and 60 mm respectively. The results were also taken from specimens with C20, and each line represents a longitudinal stud spacing. Clearly, the shear stud capacity experienced a significant decrease as the rib deck ratio increased. The percentage of decrease between rib deck ratios of 1.15 and 1.97 was 10, 10, 9, and 7 for spacings of 3d, 4.5d, 6d, and 8d respectively. A further decline in the load capacity was observed as the rib deck ratio approached 2.35.

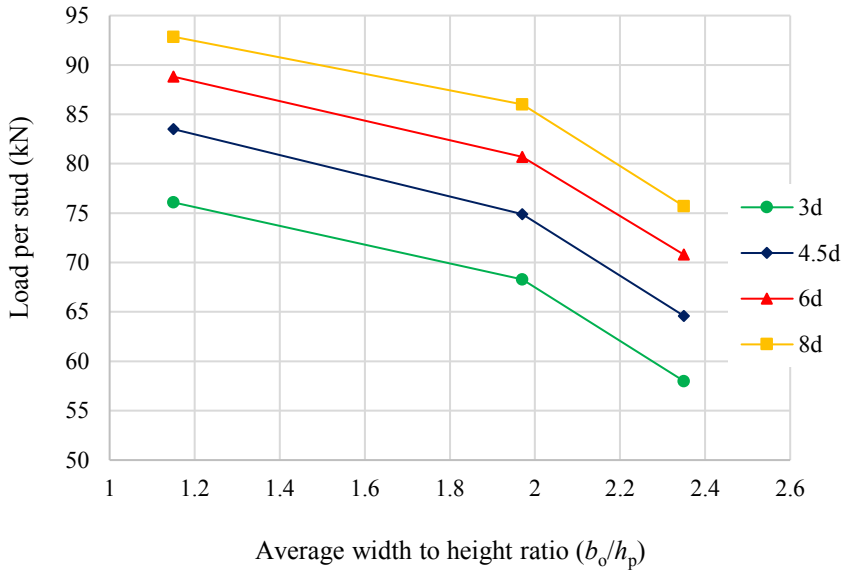


Figure 6.15 Effect of rib deck ratios for tests with two studs per row

At this stage, the effect of the rib deck ratio was only realised when the depth of the decks was constant. In Figure 6.14, the shear connector resistance increased when the rib deck ratio was changed from 0.67 to 1.15 for tests with 146 mm deep deck. A similar trend was found among tests with 76 mm deep deck. However, this research aims to find a common base that links different types of ribbed decks. Therefore, the trend of the shear stud capacity cannot be justified through the rib deck ratio if different types of decks are used. In fact, the correlation between narrow and wide ribbed steel decks regarding the shear connector resistance was never addressed in the past. This research is the first to bring the attention to such aspect, whereas the results suggest that a bigger amount of rib deck ratio is not necessarily to develop the shear connector resistance and vice versa. This correlation could be explained by either the effect of stud geometry or the cross-sectional area of the concrete. Next sections shall bear the answer.

According to experimental research done by Gnanasambandam (1995), the shear stud capacity increased when the rib deck ratio was increased. There were three wide rib deck ratios considered: 1.58, 2.33, and 3.32, but all of them had a constant deck height of 76 mm and stud height of 125 mm. It was suggested that the development of stud capacity was mainly associated with a bigger ratio of the rib. However, if the effective cross-sectional area of concrete was meant to be addressed and measured, then this would result in 19110, 28550, and 38060 $mm^2$ respectively. Therefore, the author of this research would rather attribute

that shear connector resistance development to the cross-sectional area than the influence of rib deck ratio (this is further explained later). In conclusion, a bigger rib deck ratio does not necessarily increase the load capacity, only if the deck height is constant. Otherwise, this concept is unlikely to be applicable considering different deck heights.

The effect of rib deck geometry on the failure mode was inconsistent. For push-off tests with single stud per row, the change in the rib deck geometry from narrow to wide did not seem influential on the way the tests failed. Instead, the failure mode was more governed by the concrete strength and longitudinal stud spacing as discussed before. On the other hand, the rib deck geometry became a function of the failure mode when two studs per row were used. For tests with narrow ribbed deck ($b_o/h_p < 1.5$), the concrete shear plane dictated the failure mode. However, the failure mode shifted to the concrete splitting and crushing failure when the wide ribbed deck was used ($b_o/h_p \geq 1.5$). Because two studs per row were used in this case, the configuration of steel decks including the flute width, edge distance, and rib size would play a major role in generating the failure mode. On the whole, the failure mode is more sensitive to change if two studs per row are used rather than one stud per row.

### 6.5.2 Effect of stud geometry ($h_{sc}/d$)

The stud geometry is defined as the ratio of the stud height to the diameter of the stud ($h_{sc}/d$). For tests with single studs per row, two different stud geometries were considered including 6.6 and 10.3. As for tests with double studs per row, the stud geometries considered were 5.3, 6.6 and 10.3. As known, the higher stud geometry is likely to increase the shear stud capacity. This is clear from the results obtained from tests with two studs per row as the shear stud capacity increased with the increase of the stud geometry (see Figure 6.16). The results were taken from specimens with C20 and longitudinal stud spacing of 6$d$. A similar trend was observed in the remaining tests for each concrete grade and longitudinal spacing. It was initially felt that the stud geometry could be the answer to relate the narrow decks with wide decks in terms of the shear connector resistance.

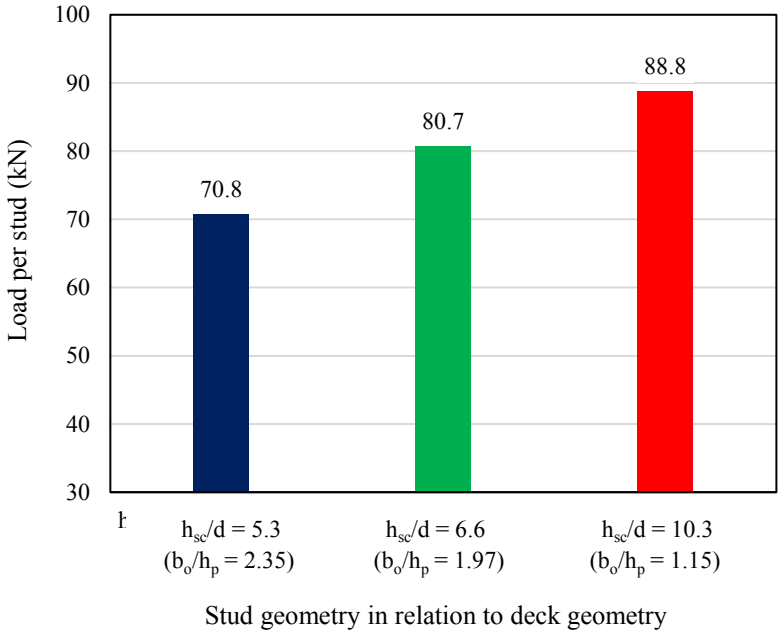


Figure 6.16 Effect of stud geometry in tests with two studs per row

However, when it comes to tests with one stud per row, Figure 6.17 does not confirm this concept. In general, some set of tests with stud geometry of 6.6 revealed close and/or higher shear stud capacities than some set of tests with stud geometry of 10.3. This leads to deduce that the correlation between narrow and wide ribbed decks cannot always be represented by the stud geometry. The only way to realise the effect of stud geometry is when the steel deck is of one type. But the freedom of change in the stud height, for example, is limited by some design rules. In the EC4, the minimum embedment depth of stud in the concrete above the sheeting rib should not be less than 2*d,* and the overall height of the stud should not be greater than ($h_p$ + 75). This means that it is not possible to examine the effect of change in the stud height from 125 to 195 mm placed in 76 mm deep deck.

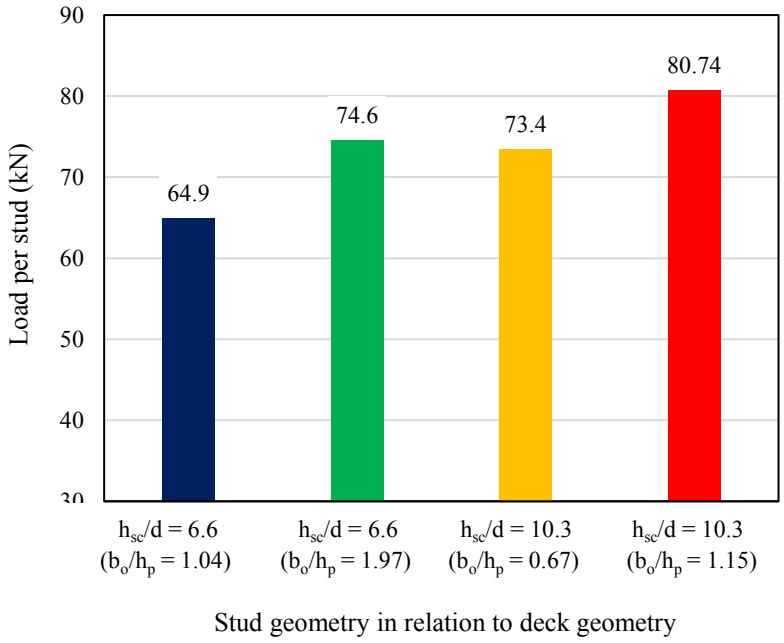


Figure 6.17 Effect of stud geometry in tests with one stud per row

### 6.5.3 Effect of the cross-sectional area of concrete ($A_c$)

As mentioned earlier, the cross-sectional area is meant by measuring the effective net area of concrete where the headed studs are positioned. This involves the embedded area of concrete within a ribbed deck, plus the area of concrete above it. Some cross-sectional areas depending on different types of steel decking were investigated. With respect to specimens featuring studs in a single row, the effective cross-sectional area of rib deck ratios of 0.67, 1.04, 1.15, and 1.97 was 23480, 13238, 38530, and 23738 mm$^2$ respectively. To ensure the consistency, the results were again obtained from specimens with C20 as shown in Figure 6.18, but this time, the stud capacity is linked with the effective cross-sectional area of each steel deck. It is apparent that the highest shear connector resistance was achieved from specimens containing the biggest cross-sectional area. While the smallest cross-sectional area gave the lowest shear connector resistance. It is also interesting to find that specimens which share quite an equal cross-sectional area introduced close shear connector resistance values despite the big difference in their rib deck ratios.

Another illustration of the effect of the cross-sectional area of concrete is aligned with specimens featuring studs in two rows. For this configuration, three different effective cross-sectional areas were used: 17520, 23738, and 38530 mm$^2$ corresponding to rib deck ratios of

2.35, 1.97, and 1.15 respectively. The results obtained from specimens with C20 are shown in Figure 6.19. The total percentage increase in the load capacity due to the change in cross-sectional area from 17520 to 38530 $mm^2$ was 31, 29, 25, and 22 for longitudinal stud spacing of 3d, 4.5d, 6d, and 8d respectively. Certainly, the shear connector resistance development cannot be attributed to the rib deck ratio as it was previously believed. The best logical justification to that increase in this research is because of the large cross-sectional area of concrete subjected to the applied load, which in turn, led the load capacity of the stud to increase. On the whole, the effective cross-sectional area of concrete is deemed to be a primary function of the headed stud strength of composite beams incorporating parallel ribbed deck. In addition, it seems to be more relevant to describe the correlation between narrow and wide ribbed decks than the rib deck geometry.

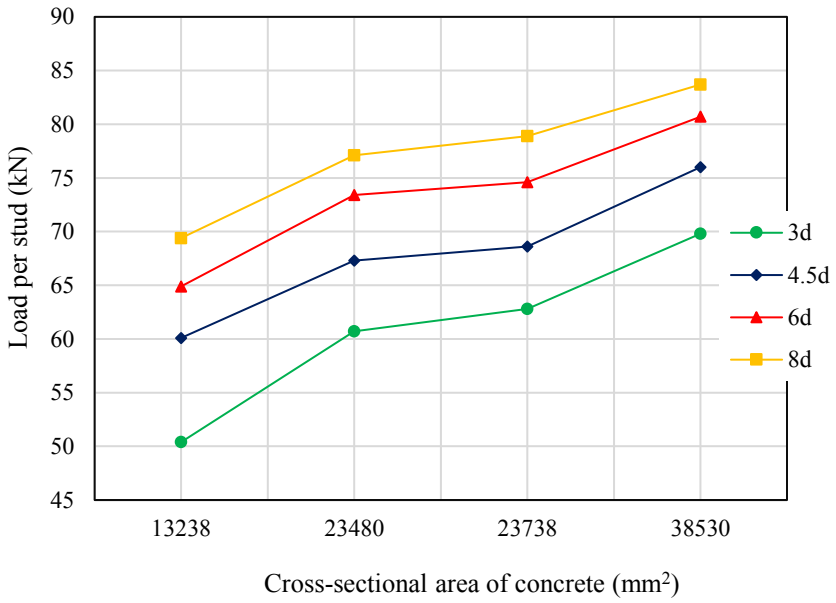


Figure 6.18 Effect of the effective cross-sectional area of concrete for tests with one stud per row

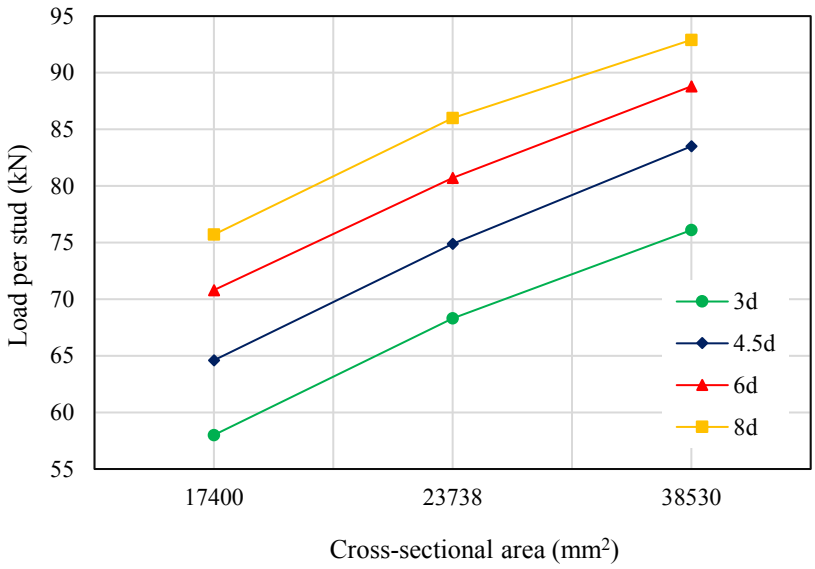


Figure 6.19 Effect of the effective cross-sectional area of concrete for tests with two studs per row

### 6.5.4 Effect of number of headed studs per row

Two arrangements of headed studs were investigated: one stud per row, and two studs per row placed at a transverse spacing of 76 mm (4d). The comparison can be seen between group B featuring one stud per row and group E featuring two studs per row. The common aspects of those groups were the use of 146 mm deep decking with 1.15 rib deck ratio. Another comparison can be found between group D containing one stud per row and group F containing two studs per row. Those groups were modelled with 76 mm deep decking and 1.97 rib deck ratio. Figure 6.20 provides a comparison between groups B and E, while Figure 6.21 involves a comparison between groups D and F. The results given in these figures are obtained from specimens with C20 covering all longitudinal stud spacings (i.e. 3d, 4.5d, 6d, and 8d).

It was found that the specimens with two studs per row carried more load capacity than specimens with one stud per row although the difference was not very high in general. For all longitudinal stud spacings considered, the advantage of double stud per row on single ones varied from 7 to 10% for all longitudinal stud spacings considered. The good performance of two rows configuration over the single is perhaps attributed to the ability of two studs to resist more shear forces, and each stud achieves high load capacity in turn. Past studies found that the performance of headed studs placed in a staggered arrangement was

better than those with a single row of studs (Gnanasambandam 1995, and Yuan 1996). However, the literature lacks any base findings of the impact of two rows configuration compared with a single row of studs. Further studies are therefore needed to verify this concept.

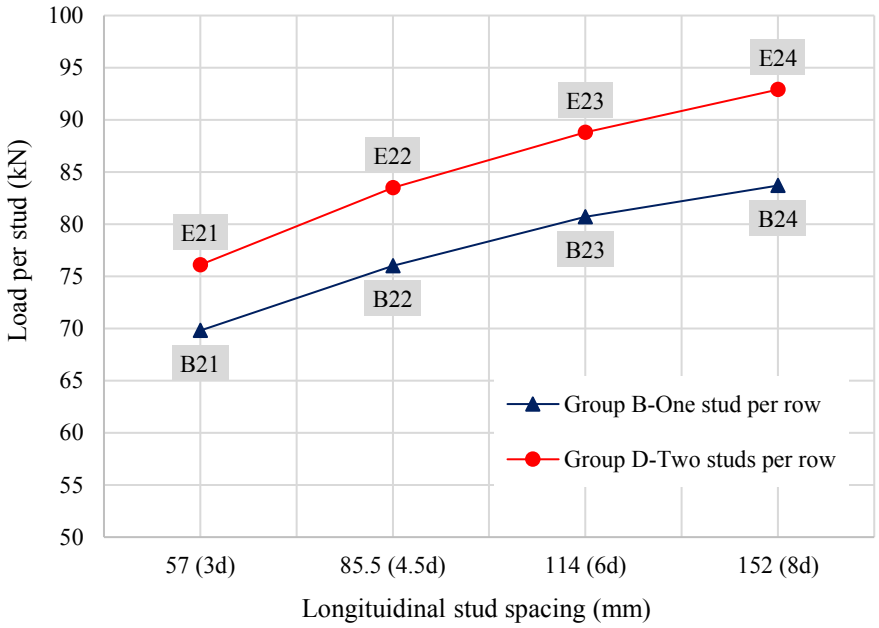


Figure 6.20 Comparison between the single and double arrangement of studs with narrow ribbed deck

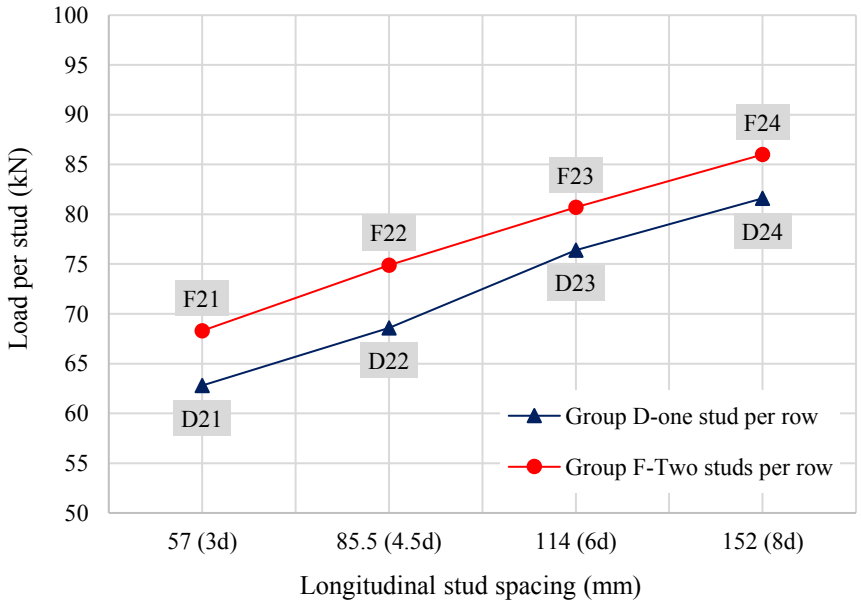


Figure 6.21 Comparison between the single and double arrangement of studs with wide ribbed deck

There are some distinctive characteristics observed between the single and two rows configuration regarding the failure mechanism. First, the concrete shear plane failure was only associated with two rows of studs' configuration. Second, although the longitudinal splitting failure was noticed in both configurations of studs, this failure mode was highly influenced by the longitudinal stud spacings for single stud per row, while it was common among all longitudinal stud spacings for double stud per row. Third, having two rows configuration had allowed the headed studs to experience more ductility before the failure occurred, especially with studs being placed relatively close.

### 6.5.5 Effect of longitudinal stud spacing

Although the longitudinal stud spacing has been previously covered, it is essential to emphasise and provide insight into such effect. Considering a wide range of longitudinal stud spacing will help develop equations if necessary. Taking push-off tests in Group B as an example, the shear connector resistance in relation to the change in the longitudinal stud spacing is shown in Figure 6.22. Those tests had single stud per row, 146 mm deep decking, and 1.15 rib deck ratio. For each stud spacing, four different values of concrete strength were used, varying from 12 to 40 MPa. Considering different values of concrete strength gave further information of how close they are linked with the longitudinal stud spacing. In general, the FE results revealed considerable development in the stud capacity when the longitudinal stud spacing was increased from 3d up to 6d, while the insignificant increase in the stud capacity was observed from 6d to 8d. The FE results obtained from the remaining groups revealed the same concept.

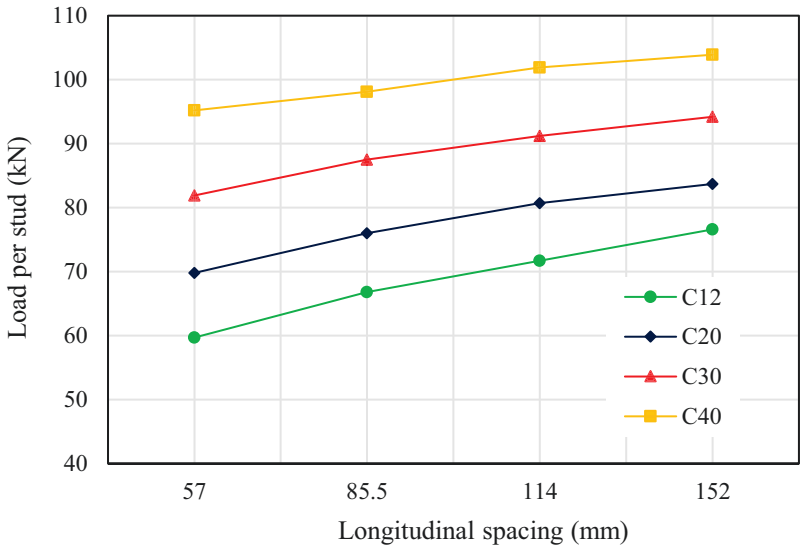


Figure 6.22 Load per stud associated with the longitudinal stud spacing in Group B

Referring to Figure 6.22, for specimens with the concrete strength of 12 MPa, the percentage of increase in the stud capacity from 3d to 4.5d, 4.5d to 6d, and 6d to 8d was approximately 12.0, 7.3, and 6.8 respectively. This suggests that headed studs placed beyond 6d are unlikely to achieve further considerable development in the shear connector resistance. However, when the concrete strength is mostly greater than 30 MPa. The increase in stud capacity was hardly significant even when the longitudinal stud spacing was varied from 3d up to 6d. As seen in Figure 6.22, the curve associated with C40 appears to be fairly plateau. For this group, specimens with C12 exhibited a 28% total increase in the load per stud between spacings of 3d and 8d comparing to only 9% for specimens with C40. This trend was similarly discovered in the rest of the groups regardless of the rib deck geometry and the studs' arrangement. In conclusion, placing headed studs relatively away will cause the load per stud capacity to increase. However, it is strictly dependent upon the concrete strength.

### 6.5.6 Effect of thickness of steel decking

The influence of sheeting thickness was investigated on 16 tests divided into two parts based on the studs' arrangement (Phase III). For the one stud per row layout, the tests had 146 mm deep decking, 0.67 rib deck ratio, and longitudinal stud spacing of 4.5d. The thickness of steel decking was increased beyond 1.2 mm. For this purpose, eight specimens were modelled, four with a thickness of 1.5 mm, and the rest with 2.0 mm. The numerical results revealed a significant increase in the shear connector resistance when the sheeting thickness

was raised. The load per stud in relation to the steel deck thickness is presented in Figure 6.23. Taking specimens with C20 as an example, the load per stud increased by 17% between thicknesses of 1.2 and 1.5 mm. Further increase by 27% was spotted between thicknesses of 1.2 and 2.0 mm. The same trend was observed in all concrete grades considered.

The effect of sheeting thickness on the tests with two studs per row was also fostering. The load per stud in relation to the steel deck thickness is presented in Figure 6.24. Taking specimens with C30 as an example, the load per stud increased by 15% between thicknesses of 1.2 and 1.5 mm. Further increase by 25% was observed between thicknesses of 1.2 and 2.0 mm. It can be concluded that the sheeting thickness plays a major role regarding the shear connector resistance in composite beams featuring parallel steel deck. Normally, when the thickness of steel decking is increased, the metal steel deck will be stiffer. Therefore, the capability of restraining the shear forces that transfer through the concrete embedded within the rib is high. Eventually, the stiffer steel decking will act as a promoting factor, and that culminates in the development of shear connector resistance. This finding necessitates that the sheeting thickness factor should not be ignored when new equations are developed to predict the load per stud capacity in composite beams incorporating parallel ribbed deck.

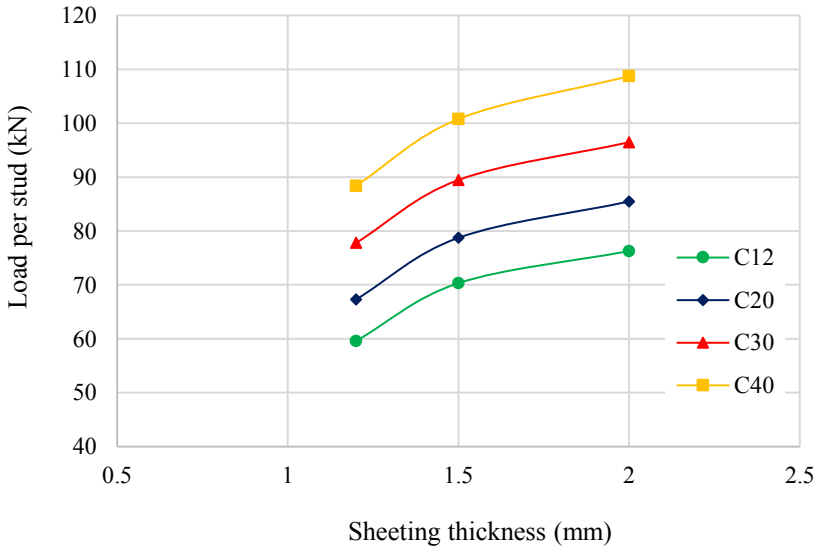


Figure 6.23 Effect of the sheeting thickness on the load per stud for tests with single stud per row

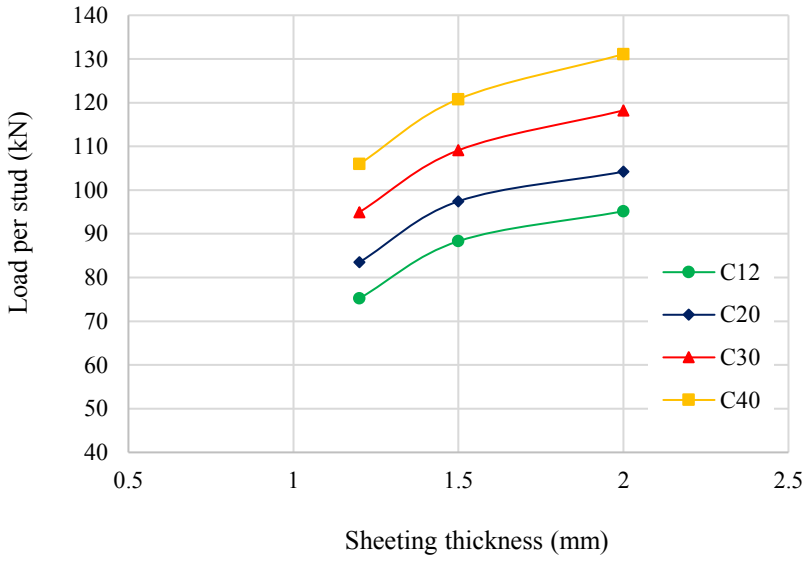


Figure 6.24 Effect of the sheeting thickness on the load per stud for tests with double stud per row

Table 6.1 FE results of push-off tests with parallel steel decks

| Phase | Test | $f_c$ (MPa) | $A_c$ (mm$^2$) | Steel decking details | | | | Headed stud details | | | Failure load (kN) | Failure mode |
|---|---|---|---|---|---|---|---|---|---|---|---|---|
| | | | | $b_o$ (mm) | $h_p$ (mm) | $b_o/h_p$ | $t_s$ (mm) | $d \times h_{sc}$ | $l_s$ (mm) | $S_t$ (mm) | | |
| I | A11 | 12 | 23481 | 97.5 | 146 | 0.67 | 1.2 | 19 × 195 | 57 | 0 | 51.9 | LS |
| | A12 | 12 | 23481 | 97.5 | 146 | 0.67 | 1.2 | 19 × 195 | 85.5 | 0 | 59.6 | LS |
| | A13 | 12 | 23481 | 97.5 | 146 | 0.67 | 1.2 | 19 × 195 | 114 | 0 | 66.4 | LS |
| | A14 | 12 | 23481 | 97.5 | 146 | 0.67 | 1.2 | 19 × 195 | 152 | 0 | 72.3 | LS |
| | A21 | 20 | 23481 | 97.5 | 146 | 0.67 | 1.2 | 19 × 195 | 57 | 0 | 60.7 | LS |
| | A22 | 20 | 23481 | 97.5 | 146 | 0.67 | 1.2 | 19 × 195 | 85.5 | 0 | 67.3 | LS |
| | A23 | 20 | 23481 | 97.5 | 146 | 0.67 | 1.2 | 19 × 195 | 114 | 0 | 73.4 | LS |
| | A24 | 20 | 23481 | 97.5 | 146 | 0.67 | 1.2 | 19 × 195 | 152 | 0 | 77.1 | LS SS |
| | A31 | 30 | 23481 | 97.5 | 146 | 0.67 | 1.2 | 19 × 195 | 57 | 0 | 71.5 | LS |
| | A32 | 30 | 23481 | 97.5 | 146 | 0.67 | 1.2 | 19 × 195 | 85.5 | 0 | 77.8 | SS |
| | A33 | 30 | 23481 | 97.5 | 146 | 0.67 | 1.2 | 19 × 195 | 114 | 0 | 82.9 | SS |
| | A34 | 30 | 23481 | 97.5 | 146 | 0.67 | 1.2 | 19 × 195 | 152 | 0 | 87.2 | SS |
| | A41 | 40 | 23481 | 97.5 | 146 | 0.67 | 1.2 | 19 × 195 | 57 | 0 | 83.6 | LS |
| | A42 | 40 | 23481 | 97.5 | 146 | 0.67 | 1.2 | 19 × 195 | 85.5 | 0 | 88.4 | SS |
| | A43 | 40 | 23481 | 97.5 | 146 | 0.67 | 1.2 | 19 × 195 | 114 | 0 | 92.6 | SS |
| | A44 | 40 | 23481 | 97.5 | 146 | 0.67 | 1.2 | 19 × 195 | 152 | 0 | 95.3 | SS |
| | B11 | 12 | 38531 | 167.5 | 146 | 1.15 | 1.2 | 19 × 195 | 57 | 0 | 59.7 | LS |
| | B12 | 12 | 38531 | 167.5 | 146 | 1.15 | 1.2 | 19 × 195 | 85.5 | 0 | 66.8 | LS |
| | B13 | 12 | 38531 | 167.5 | 146 | 1.15 | 1.2 | 19 × 195 | 114 | 0 | 71.7 | LS |
| | B14 | 12 | 38531 | 167.5 | 146 | 1.15 | 1.2 | 19 × 195 | 152 | 0 | 76.6 | LS |
| | B21 | 20 | 38531 | 167.5 | 146 | 1.15 | 1.2 | 19 × 195 | 57 | 0 | 69.8 | LS |
| | B22 | 20 | 38531 | 167.5 | 146 | 1.15 | 1.2 | 19 × 195 | 85.5 | 0 | 76.0 | LS |
| | B23 | 20 | 38531 | 167.5 | 146 | 1.15 | 1.2 | 19 × 195 | 114 | 0 | 80.7 | LS SS |
| | B24 | 20 | 38531 | 167.5 | 146 | 1.15 | 1.2 | 19 × 195 | 152 | 0 | 83.7 | LS SS |
| | B31 | 30 | 38531 | 167.5 | 146 | 1.15 | 1.2 | 19 × 195 | 57 | 0 | 81.9 | LS |
| | B32 | 30 | 38531 | 167.5 | 146 | 1.15 | 1.2 | 19 × 195 | 85.5 | 0 | 87.5 | LS SS |
| | B33 | 30 | 38531 | 167.5 | 146 | 1.15 | 1.2 | 19 × 195 | 114 | 0 | 91.2 | SS |

| | | | | | | | | | | | |
|---|---|---|---|---|---|---|---|---|---|---|---|
| | B34 | 30 | 38531 | 167.5 | 146 | 1.15 | 1.2 | 19 × 195 | 152 | 0 | 94.2 | SS |
| | B41 | 40 | 38531 | 167.5 | 146 | 1.15 | 1.2 | 19 × 195 | 57 | 0 | 95.2 | LS SS |
| | B42 | 40 | 38531 | 167.5 | 146 | 1.15 | 1.2 | 19 × 195 | 85.5 | 0 | 98.1 | SS |
| | B43 | 40 | 38531 | 167.5 | 146 | 1.15 | 1.2 | 19 × 195 | 114 | 0 | 101.9 | SS |
| | B44 | 40 | 38531 | 167.5 | 146 | 1.15 | 1.2 | 19 × 195 | 152 | 0 | 103.9 | SS |
| | C12 | 12 | 23738 | 150 | 76 | 1.97 | 1.2 | 19 × 125 | 57 | 0 | 53.2 | LS |
| | C12 | 12 | 23738 | 150 | 76 | 1.97 | 1.2 | 19 × 125 | 85.5 | 0 | 60.8 | LS |
| | C13 | 12 | 23738 | 150 | 76 | 1.97 | 1.2 | 19 × 125 | 114 | 0 | 65.2 | LS |
| | C14 | 12 | 23738 | 150 | 76 | 1.97 | 1.2 | 19 × 125 | 152 | 0 | 70.6 | LS |
| | C21 | 20 | 23738 | 150 | 76 | 1.97 | 1.2 | 19 × 125 | 57 | 0 | 62.8 | LS |
| | C22 | 20 | 23738 | 150 | 76 | 1.97 | 1.2 | 19 × 125 | 85.5 | 0 | 68.6 | LS |
| | C23 | 20 | 23738 | 150 | 76 | 1.97 | 1.2 | 19 × 125 | 114 | 0 | 74.6 | LS |
| | C24 | 20 | 23738 | 150 | 76 | 1.97 | 1.2 | 19 × 125 | 152 | 0 | 78.9 | LS |
| | C31 | 30 | 23738 | 150 | 76 | 1.97 | 1.2 | 19 × 125 | 57 | 0 | 71.1 | LS |
| | C32 | 30 | 23738 | 150 | 76 | 1.97 | 1.2 | 19 × 125 | 85.5 | 0 | 79.2 | SS |
| | C33 | 30 | 23738 | 150 | 76 | 1.97 | 1.2 | 19 × 125 | 114 | 0 | 83.9 | SS |
| | C34 | 30 | 23738 | 150 | 76 | 1.97 | 1.2 | 19 × 125 | 152 | 0 | 88.4 | SS |
| | C41 | 40 | 23738 | 150 | 76 | 1.97 | 1.2 | 19 × 125 | 57 | 0 | 84.7 | LS SS |
| | C42 | 40 | 23738 | 150 | 76 | 1.97 | 1.2 | 19 × 125 | 85.5 | 0 | 89.9 | SS |
| | C43 | 40 | 23738 | 150 | 76 | 1.97 | 1.2 | 19 × 125 | 114 | 0 | 94.6 | SS |
| | C44 | 40 | 23738 | 150 | 76 | 1.97 | 1.2 | 19 × 125 | 152 | 0 | 97.0 | SS |
| | D12 | 12 | 13238 | 79.3 | 76 | 1.04 | 1.2 | 19 × 125 | 57 | 0 | 44.9 | LS |
| | D12 | 12 | 13238 | 79.3 | 76 | 1.04 | 1.2 | 19 × 125 | 85.5 | 0 | 53.6 | LS |
| | D13 | 12 | 13238 | 79.3 | 76 | 1.04 | 1.2 | 19 × 125 | 114 | 0 | 60.2 | LS |
| | D14 | 12 | 13238 | 79.3 | 76 | 1.04 | 1.2 | 19 × 125 | 152 | 0 | 65.8 | LS |
| | D21 | 20 | 13238 | 79.3 | 76 | 1.04 | 1.2 | 19 × 125 | 57 | 0 | 50.4 | LS |
| | D22 | 20 | 13238 | 79.3 | 76 | 1.04 | 1.2 | 19 × 125 | 85.5 | 0 | 60.1 | LS |
| | D23 | 20 | 13238 | 79.3 | 76 | 1.04 | 1.2 | 19 × 125 | 114 | 0 | 64.9 | LS |
| | D24 | 20 | 13238 | 79.3 | 76 | 1.04 | 1.2 | 19 × 125 | 152 | 0 | 69.4 | LS |
| | D31 | 30 | 13238 | 79.3 | 76 | 1.04 | 1.2 | 19 × 125 | 57 | 0 | 62.5 | LS |
| | D32 | 30 | 13238 | 79.3 | 76 | 1.04 | 1.2 | 19 × 125 | 85.5 | 0 | 70.7 | SS |

| | | | | | | | | | | | | |
|---|---|---|---|---|---|---|---|---|---|---|---|---|
| | D33 | 30 | 13238 | 79.3 | 76 | 1.04 | 1.2 | 19 × 125 | 114 | 0 | 74.4 | LS SS |
| | D34 | 30 | 13238 | 79.3 | 76 | 1.04 | 1.2 | 19 × 125 | 152 | 0 | 79 | SS |
| | D41 | 40 | 13238 | 79.3 | 76 | 1.04 | 1.2 | 19 × 125 | 57 | 0 | 72.8 | LS |
| | D42 | 40 | 13238 | 79.3 | 76 | 1.04 | 1.2 | 19 × 125 | 85.5 | 0 | 79.7 | SS |
| | D43 | 40 | 13238 | 79.3 | 76 | 1.04 | 1.2 | 19 × 125 | 114 | 0 | 84.1 | SS |
| | D44 | 40 | 13238 | 79.3 | 76 | 1.04 | 1.2 | 19 × 125 | 152 | 0 | 89.2 | SS |
| | E11 | 12 | 38531 | 167.5 | 146 | 1.15 | 1.2 | 19 × 195 | 57 | 76 | 67.1 | CSP |
| | E12 | 12 | 38531 | 167.5 | 146 | 1.15 | 1.2 | 19 × 195 | 85.5 | 76 | 75.2 | CSP |
| | E13 | 12 | 38531 | 167.5 | 146 | 1.15 | 1.2 | 19 × 195 | 114 | 76 | 80.4 | CSP |
| | E14 | 12 | 38531 | 167.5 | 146 | 1.15 | 1.2 | 19 × 195 | 152 | 76 | 85.8 | CSP |
| | E21 | 20 | 38531 | 167.5 | 146 | 1.15 | 1.2 | 19 × 195 | 57 | 76 | 76.1 | CSP |
| | E22 | 20 | 38531 | 167.5 | 146 | 1.15 | 1.2 | 19 × 195 | 85.5 | 76 | 83.5 | CSP |
| | E23 | 20 | 38531 | 167.5 | 146 | 1.15 | 1.2 | 19 × 195 | 114 | 76 | 88.8 | CSP |
| | E24 | 20 | 38531 | 167.5 | 146 | 1.15 | 1.2 | 19 × 195 | 152 | 76 | 92.9 | CSP |
| | E31 | 30 | 38531 | 167.5 | 146 | 1.15 | 1.2 | 19 × 195 | 57 | 76 | 88.8 | CSP |
| | E32 | 30 | 38531 | 167.5 | 146 | 1.15 | 1.2 | 19 × 195 | 85.5 | 76 | 95.0 | CSP |
| | E33 | 30 | 38531 | 167.5 | 146 | 1.15 | 1.2 | 19 × 195 | 114 | 76 | 98.9 | CSP |
| | E34 | 30 | 38531 | 167.5 | 146 | 1.15 | 1.2 | 19 × 195 | 152 | 76 | 102.2 | CSP |
| II | E41 | 40 | 38531 | 167.5 | 146 | 1.15 | 1.2 | 19 × 195 | 57 | 76 | 102.8 | CSP |
| | E42 | 40 | 38531 | 167.5 | 146 | 1.15 | 1.2 | 19 × 195 | 85.5 | 76 | 106.0 | CSP |
| | E43 | 40 | 38531 | 167.5 | 146 | 1.15 | 1.2 | 19 × 195 | 114 | 76 | 110.0 | CSP |
| | E44 | 40 | 38531 | 167.5 | 146 | 1.15 | 1.2 | 19 × 195 | 152 | 76 | 112.2 | CSP |
| | F11 | 12 | 23738 | 150 | 76 | 1.97 | 1.2 | 19 × 125 | 57 | 76 | 59.2 | LS CC |
| | F12 | 12 | 23738 | 150 | 76 | 1.97 | 1.2 | 19 × 125 | 85.5 | 76 | 67.5 | LS CC |
| | F13 | 12 | 23738 | 150 | 76 | 1.97 | 1.2 | 19 × 125 | 114 | 76 | 73.1 | LS CC |
| | F14 | 12 | 23738 | 150 | 76 | 1.97 | 1.2 | 19 × 125 | 152 | 76 | 79.6 | LS CC |
| | F21 | 20 | 23738 | 150 | 76 | 1.97 | 1.2 | 19 × 125 | 57 | 76 | 68.3 | LS CC |
| | F22 | 20 | 23738 | 150 | 76 | 1.97 | 1.2 | 19 × 125 | 85.5 | 76 | 74.9 | LS CC |
| | F23 | 20 | 23738 | 150 | 76 | 1.97 | 1.2 | 19 × 125 | 114 | 76 | 80.7 | LS CC |
| | F24 | 20 | 23738 | 150 | 76 | 1.97 | 1.2 | 19 × 125 | 152 | 76 | 86.0 | LS CC |
| | F31 | 30 | 23738 | 150 | 76 | 1.97 | 1.2 | 19 × 125 | 57 | 76 | 79.5 | LS CC |

| | | | | | | | | | | | |
|---|---|---|---|---|---|---|---|---|---|---|---|
| | F32 | 30 | 23738 | 150 | 76 | 1.97 | 1.2 | 19 × 125 | 85.5 | 76 | 85.6 | LS CC |
| | F33 | 30 | 23738 | 150 | 76 | 1.97 | 1.2 | 19 × 125 | 114 | 76 | 90.0 | LS CC |
| | F34 | 30 | 23738 | 150 | 76 | 1.97 | 1.2 | 19 × 125 | 152 | 76 | 93.3 | LS CC |
| | F41 | 40 | 23738 | 150 | 76 | 1.97 | 1.2 | 19 × 125 | 57 | 76 | 91.2 | LS CC |
| | F42 | 40 | 23738 | 150 | 76 | 1.97 | 1.2 | 19 × 125 | 85.5 | 76 | 97.7 | LS CC |
| | F43 | 40 | 23738 | 150 | 76 | 1.97 | 1.2 | 19 × 125 | 114 | 76 | 102.4 | LS CC |
| | F44 | 40 | 23738 | 150 | 76 | 1.97 | 1.2 | 19 × 125 | 152 | 76 | 107.6 | LS SS |
| | G11 | 12 | 17520 | 141 | 60 | 2.35 | 1.2 | 19 × 100 | 57 | 76 | 49.7 | LS CC |
| | G12 | 12 | 17520 | 141 | 60 | 2.35 | 1.2 | 19 × 100 | 85.5 | 76 | 56.5 | LS CC |
| | G13 | 12 | 17520 | 141 | 60 | 2.35 | 1.2 | 19 × 100 | 114 | 76 | 64.2 | LS CC |
| | G14 | 12 | 17520 | 141 | 60 | 2.35 | 1.2 | 19 × 100 | 152 | 76 | 68.7 | LS CC |
| | G21 | 20 | 17520 | 141 | 60 | 2.35 | 1.2 | 19 × 100 | 57 | 76 | 58.0 | LS CC |
| | G22 | 20 | 17520 | 141 | 60 | 2.35 | 1.2 | 19 × 100 | 85.5 | 76 | 64.6 | LS CC |
| | G23 | 20 | 17520 | 141 | 60 | 2.35 | 1.2 | 19 × 100 | 114 | 76 | 70.8 | LS CC |
| | G24 | 20 | 17520 | 141 | 60 | 2.35 | 1.2 | 19 × 100 | 152 | 76 | 75.7 | LS CC |
| | G31 | 30 | 17520 | 141 | 60 | 2.35 | 1.2 | 19 × 100 | 57 | 76 | 67.7 | LS CC |
| | G32 | 30 | 17520 | 141 | 60 | 2.35 | 1.2 | 19 × 100 | 85.5 | 76 | 74.8 | LS CC |
| | G33 | 30 | 17520 | 141 | 60 | 2.35 | 1.2 | 19 × 100 | 114 | 76 | 81.6 | LS CC |
| | G34 | 30 | 17520 | 141 | 60 | 2.35 | 1.2 | 19 × 100 | 152 | 76 | 87.4 | LS CC |
| | G41 | 40 | 17520 | 141 | 60 | 2.35 | 1.2 | 19 × 100 | 57 | 76 | 80.0 | LS CC |
| | G42 | 40 | 17520 | 141 | 60 | 2.35 | 1.2 | 19 × 100 | 85.5 | 76 | 87.1 | LS CC |
| | G43 | 40 | 17520 | 141 | 60 | 2.35 | 1.2 | 19 × 100 | 114 | 76 | 93.1 | LS CC |
| | G44 | 40 | 17520 | 141 | 60 | 2.35 | 1.2 | 19 × 100 | 152 | 76 | 97.7 | LS CC |
| III | H11 | 12 | 23481 | 97.5 | 146 | 0.67 | 1.5 | 19 × 195 | 85.5 | 0 | 70.3 | LS |
| | H12 | 20 | 23481 | 97.5 | 146 | 0.67 | 1.5 | 19 × 195 | 85.5 | 0 | 78.7 | LS |
| | H13 | 30 | 23481 | 97.5 | 146 | 0.67 | 1.5 | 19 × 195 | 85.5 | 0 | 89.5 | LS |
| | H14 | 40 | 23481 | 97.5 | 146 | 0.67 | 1.5 | 19 × 195 | 85.5 | 0 | 100.8 | LS |
| | I11 | 12 | 23481 | 97.5 | 146 | 0.67 | 2.0 | 19 × 195 | 85.5 | 0 | 76.3 | LS |
| | I12 | 20 | 23481 | 97.5 | 146 | 0.67 | 2.0 | 19 × 195 | 85.5 | 0 | 85.5 | LS |
| | I13 | 30 | 23481 | 97.5 | 146 | 0.67 | 2.0 | 19 × 195 | 85.5 | 0 | 96.5 | LS |
| | I14 | 40 | 23481 | 97.5 | 146 | 0.67 | 2.0 | 19 × 195 | 85.5 | 0 | 108.7 | LS |

| | | | | | | | | | | | | |
|---|---|---|---|---|---|---|---|---|---|---|---|---|
| | J11 | 12 | 38531 | 167.5 | 146 | 1.15 | 1.5 | 19 × 195 | 85.5 | 76 | 88.3 | CSP |
| | J12 | 20 | 38531 | 167.5 | 146 | 1.15 | 1.5 | 19 × 195 | 85.5 | 76 | 97.4 | CSP |
| | J13 | 30 | 38531 | 167.5 | 146 | 1.15 | 1.5 | 19 × 195 | 85.5 | 76 | 109.1 | CSP |
| | J14 | 40 | 38531 | 167.5 | 146 | 1.15 | 1.5 | 19 × 195 | 85.5 | 76 | 120.8 | CSP |
| | K11 | 12 | 38531 | 167.5 | 146 | 1.15 | 2.0 | 19 × 195 | 85.5 | 76 | 95.2 | CSP |
| | K12 | 20 | 38531 | 167.5 | 146 | 1.15 | 2.0 | 19 × 195 | 85.5 | 76 | 104.2 | CSP |
| | K13 | 30 | 38531 | 167.5 | 146 | 1.15 | 2.0 | 19 × 195 | 85.5 | 76 | 118.2 | CSP |
| | K14 | 40 | 38531 | 167.5 | 146 | 1.15 | 2.0 | 19 × 195 | 85.5 | 76 | 131.1 | CSP |
| IV | L11 | 12 | 23481 | 97.5 | 146 | 0.67 | 1.2 | 22 × 195 | 100 | 0 | 74.5 | LS |
| | L12 | 20 | 23481 | 97.5 | 146 | 0.67 | 1.2 | 22 × 195 | 100 | 0 | 84.8 | LS |
| | L13 | 30 | 23481 | 97.5 | 146 | 0.67 | 1.2 | 22 × 195 | 100 | 0 | 96.1 | LS |
| | L14 | 40 | 23481 | 97.5 | 146 | 0.67 | 1.2 | 22 × 195 | 100 | 0 | 110.2 | LS |
| | M11 | 12 | 38531 | 167.5 | 146 | 1.15 | 1.2 | 22 × 195 | 100 | 88 | 91.7 | CSP |
| | M12 | 20 | 38531 | 167.5 | 146 | 1.15 | 1.2 | 22 × 195 | 100 | 88 | 101.5 | CSP |
| | M13 | 30 | 38531 | 167.5 | 146 | 1.15 | 1.2 | 22 × 195 | 100 | 88 | 114.8 | CSP |
| | M14 | 40 | 38531 | 167.5 | 146 | 1.15 | 1.2 | 22 × 195 | 100 | 88 | 127.0 | CSP |

LS: longitudinal splitting of concrete
SS: shank shearing of stud
CSP: concrete shear plane
LS CC: longitudinal splitting and concrete crushing

## 6.6 Conclusions

This chapter presented FE results of 136 push-off tests with parallel ribbed decks. The main purpose was to address for the first time the behaviour of composite beams with very deep and narrow decks and provide an accurate correlation between narrow and wide decks regarding the shear connector resistance. The parametric study was made of rib deck ratios, stud geometries, the effective cross-sectional area of concrete, longitudinal stud spacing, and sheeting thickness. Test results showed that both the rib deck ratio and stud geometry did not demonstrate a direct relationship with the shear connector resistance as it was believed in the past. As a result, these two parameters cannot represent the accurate correlation between narrow and wide ribbed decks regarding the shear connector resistance.

The unique discrepancies found with the rib deck ratio was then attributed to the effective cross-sectional area of concrete. Tests with a large effective cross-sectional area of concrete showed more shear connector resistance than those with a small effective zone, despite the latter having bigger rib deck ratio. This aspect is likely to be justifiable to replace the concept of rib deck ratio for being a function of shear connector resistance. With these findings, the applicability of the current design equations is under question because the rib deck ratio is addressed as a direct relationship with the shear stud capacity. This issue is answered in the next chapter.

A remarkable increase was spotted in the shear stud capacity when thicker steel decking and larger diameter of headed stud were used. This finding necessitates that both factors should not be disregarded if new equations are formulated. Test results also showed that the advantage of double stud per row on single ones varied from 7 to 10% for all longitudinal stud spacings considered. However, this case needs further studies to verify this behaviour.

The longitudinal splitting of concrete and shank shear stud failure were mostly associated with specimens featuring single stud per row irrespective of the size of the ribbed deck. While arranging two studs per row resulted in either concrete shear plane or longitudinal splitting and crushing concrete failure.

# Chapter 7 Validation of the existing headed stud strength prediction equations for the composite beams with parallel steel decking

# Chapter 7

# Validation of the existing headed stud strength prediction equations for the composite beams with parallel steel decking

## 7.1 Introduction

In this chapter, the FE results obtained from chapter six are validated against the accuracy of some design codes, and other theoretical methods that have been previously proposed. This concern was raised in the previous chapter when the findings revealed that it was not possible to draw a steady correlation between narrow and wide ribbed decks through their rib deck ratios. This has led to putting the reliability of the relevant equations into question since the rib deck ratio is addressed as a direct relationship with the load capacity.

To answer this question, the shear resistance of studs obtained from 136 tests are compared to the nominal design strengths of headed stud predicted by the Eurocode 4, American specifications ANSI/AISC 360-2016, and some previous equations proposed by Gnanasambandam (1995), Johnson and Yuan (1998b), and Wu (1998). This part of the research will provide the first information on how good the ribbed steel decks with greater depth than 80 mm and/or narrow geometry ($b_o/h_p < 1.5$) are considered in the existing design equations. If found necessary, this research is willing to bridge this knowledge gap by introducing a new set of equations which are more useful and effective than the current design equations. The significance of the new equations is that they are up-to-date in which a wide range of geometries is covered along with other important factors. As a result, the shear strength of headed stud in composite beams with parallel steel decks would be predicted more effectively.

## 7.2 Eurocode 4 provisions

The nominal strength of headed shear stud connector placed in a parallel steel sheeting is calculated as the lesser value obtained from Equations 7.1 and 7.2, and multiplied by a reduction factor using Equation 7.3 as shown below:

$$P_{EC4} = 0.29\ \alpha\ d^2 \sqrt{f_c\ E_{cm}} \qquad \text{Eq. 7.1}$$

$$P_{EC4} = 0.8 f_u \frac{\pi d^2}{4} \quad \text{Eq. 7.2}$$

$$k_t = 0.6 \frac{b_o}{h_p} [\frac{h_{sc}}{h_p} - 1] \quad \text{Eq. 7.3}$$

where $\alpha = 0.2$ (h/d + 1) for ($3 \leq h/d \leq 4$) and $\alpha = 1.0$ for ($h/d > 4$), h and d are the height and diameter of the stud respectively, and $E_{cm}$ is the mean value of Young's modulus of concrete taken from the European Code (EC2), $f_u$ is the ultimate tensile strength of headed stud (not greater than 450 MPa), $b_o$ is the average width of trough, $h_{sc}$ and $h_p$ are the total height of stud and rib respectively.

Figure 7.1 shows the relationship between the load per stud obtained from the parametric study and the EC4 predicted strengths. It can be seen that the equations specified in the EC4 greatly underestimated the nominal strengths in most cases. The mean ratio of $P_{FE}/P_{EC4}$ is 3.55, with the corresponding standard deviation and coefficient of variation of 2.33 and 65.73% respectively. The scatter in results was mainly associated with tests incorporating narrow rib geometry ($b_o/h_p < 1.5$) and/or steel decks in excess of 80 mm deep. The reason behind this deficiency lies in the reduction factor attained from Equation 7.3 as it gives very low values when the geometry of narrow ribbed decks is applied. It is obvious that the rib deck size is made to act with the shear connector resistance as a direct relationship. This means that the lower rib deck ratio provided, the less shear connector resistance achieved and vice versa. Since this concept was proven wrong in the previous chapter, it is advisable to modify Equation 7.3 and introduce a better correlation between narrow and wide ribbed steel decks.

The drawbacks in the EC4 provisions are not only limited to the flawed representation of the rib deck geometry, but also to the inability in recognising the longitudinal stud spacing, headed studs' arrangement and sheeting thickness. As a result, the predicted strengths remained unchanged. With this issue, and given the fact that in practice, the headed studs are expected to be arranged as single or double and positioned with different spacing, the shear connector resistance will not be accurately estimated for the design purposes. Overall, the current provisions in the EC4 must be calibrated to cope with different parameters so as to provide more reliable and accurate results. Table 7.2 includes the comparison between the load per stud obtained from the FE analysis and the EC4 predicted strengths.

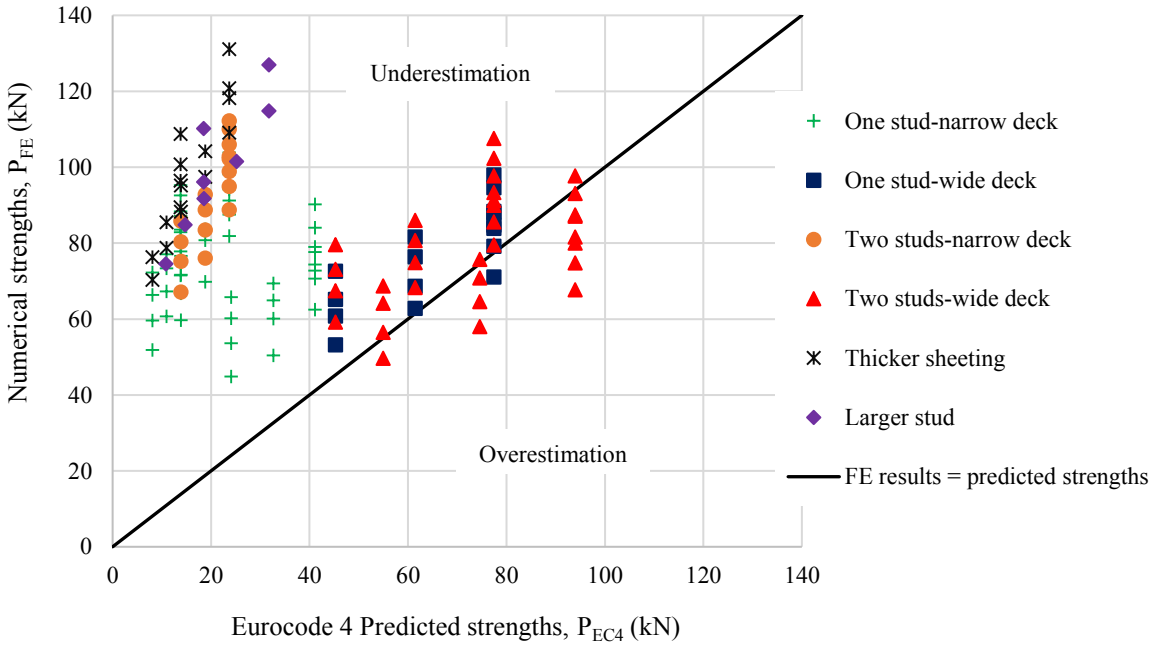


Figure 7.1 FE load per stud capacities versus EC4 predicted strengths

## 7.3 ANSI/AISC 306-2016 provisions

The nominal strength of one headed shear stud connector embedded in a solid concrete slab is determined by using Equation 7.4. In case of a test with steel decking oriented parallel to the steel beam, $R_g$ and $R_p$ are factors given in Table 7.1.

$$P_{AISC} = 0.5\, A_s \sqrt{f_c E_c} \leq R_g\, R_p\, A_s f_u \qquad \text{Eq. 7.4}$$

where $A_s$ is the cross-sectional area of the headed stud, $E_c$ modulus of elasticity of concrete ($0.043\, w_c^{1.5} \sqrt{f_c}$), $w_c$ is the density of concrete (kg/m$^3$), $f_u$ is the specified minimum tensile strength of headed stud.

Table 7.1 Values of $R_g$ and $R_p$ according to ANSI/AISC 306-2016 provisions

| Condition | $R_g$ | $R_p$ |
|---|---|---|
| Decking oriented parallel to the steel beam | | |
| $b_o/h_p \geq 1.5$ | 1.0 | 0.75 |
| $b_o/h_p < 1.5$ | 0.85 | 0.75 |

Figure 7.2 represents the relationship between the load per stud obtained from the parametric study and the ANSI/AISC predicted strengths. The results revealed that the mean ratio of $P_{FE}/P_{AISC}$ is 1.01 with the standard deviation and the coefficient of variation of 0.19 and 19.2% respectively. The situation in the American provisions is not any better than the EC4 standards. This is due to the fact that the controlled equation was the steel failure ($R_g$ $R_p$ $A_s$ $f_u$) when the strength of concrete was higher than 20 MPa. Therefore, the predicted strengths remained unchanged when the concrete strength was 20 MPa and upwards. More importantly, the design equation is very simple in that the effects of the longitudinal stud spacing, rib geometry size, headed studs' arrangement and sheeting thickness are not even recognised. Table 7.2 contains the comparison between the load per stud obtained from the FE analysis and the ANSI/AISC predicted strengths.

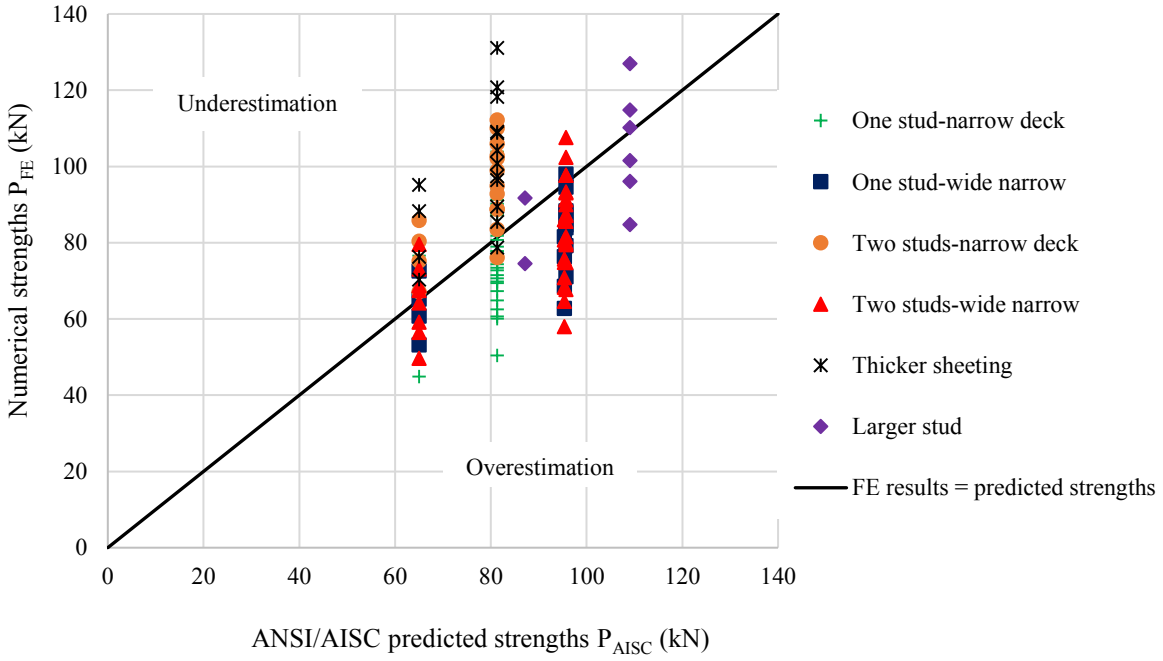


Figure 7.2 FE load per stud capacities versus ANSI/AISC predicted strengths

## 7.4 Comparison with the design equation proposed by Gnanasambandam (1995)

The behaviour of headed studs in push-out specimens with wide parallel steel decks was a part of an experimental investigation conducted by Gnanasambandam (1995). A total number of 40 push-out specimens was performed with wide parallel steel decks varied from 1.58 up to 4.97. The parametric study involved the effects of wide rib geometry size ($b_o/h_p$),

longitudinal and transverse stud spacings, and headed studs' arrangement. The load per stud capacities obtained from the experiment were then utilised to formulate a new design equation with the help of the least square regression analysis. The analysis resulted in the formulation of Equation 7.5 to predict the shear capacity of stud arranged in two rows with a transverse spacing of 4d:

$$P_G = (11\ s_l\ d - 0.82\ s_l^2)\ \sqrt{f_c} + 0.36\ (b_o/h_p)\ d\ h_{sc}\ \sqrt{f_c} \qquad \text{Eq. 7.5}$$

where $s_l$ is the longitudinal stud spacing ($3d \geq s_l \leq 8d$)

A comparison between the load per stud capacities obtained from the parametric study and those predicted by Equation 7.5 are presented in Figure 7.3 and Table 7.2. It is obvious that the predicted strengths were generally on the conservative side with noticeable deviation from the FE results. The mean ratios of $P_{FE}/P_G$ are 1.27, with the corresponding standard deviation and coefficient of variation of 0.21 and 16.34% respectively. The scatter introduced by Equation 7.5 is believed to be from the non-consideration of the narrow rib geometries when the design equation was developed. This has resulted in inaccurate shear capacities of the stud. The variable of $(b_o/h_p)$ in Equation 7.5 was yielded based on what was believed that the rib deck ratio would act as a direct relationship with the shear capacity of the stud. However, the availability of steel composite decks with different sizes requires to introduce equations that provide a better correlation between the size of steel decking and the shear capacity of the stud.

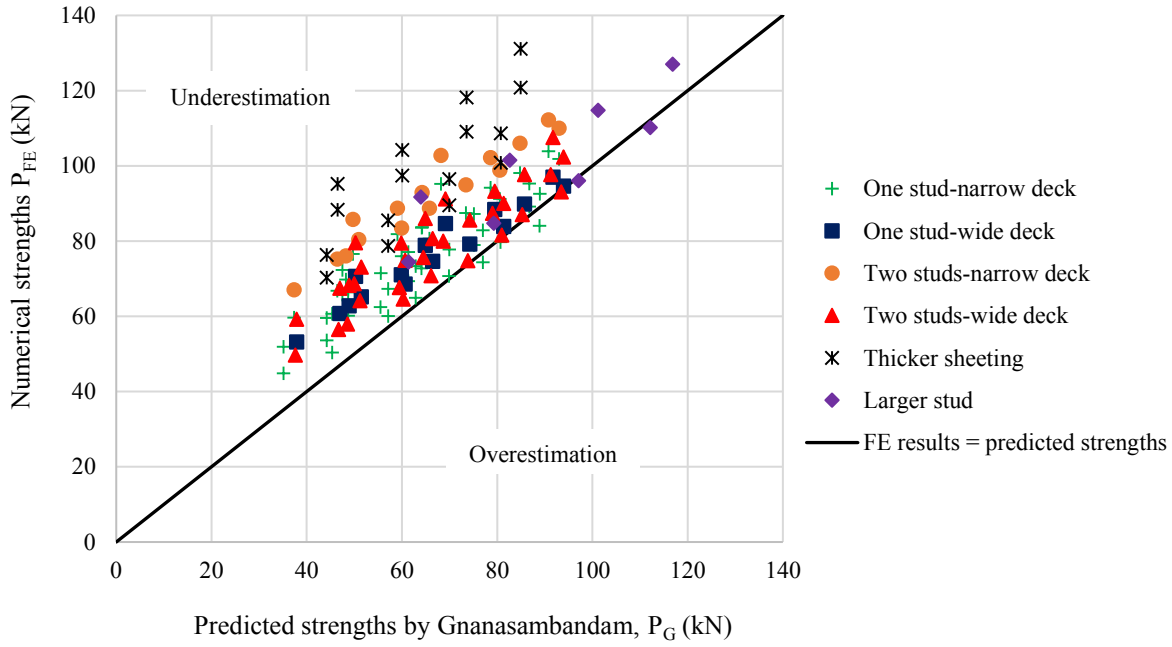


Figure 7.3 FE load per stud capacities versus predicted strengths by Gnanasambandam (1995)

## 7.5 Comparison with the analytical methods according to Johnson and Yuan (1998b)

The behaviour of a headed stud connector placed in a parallel profiled decking was investigated by Johnson and Yuan (1998b). The push-off tests covered various parameters such as the geometry of ribs and the headed studs' layout. Two different failure modes were observed among the specimens including splitting and pulling out failure. With respect to each failure mode, theoretical models were developed yielding a series of equations to predict the headed stud resistance in composite beams incorporating parallel profiled decking. In normal circumstances, it is not realistic for the equations proposed by Johnson and Yuan (1998b) to be used straightaway unless the failure mode achieved matches the one that each equation was developed from. But for the interest of study, those equations will be validated to see if by any chance they are applicable.

To calculate the headed stud shear capacity for the tests which failed by splitting, Equation 7.6 is used. Splitting failure was the result of the gradually dispersed shear force deep into the concrete.

$$P_{sp} = \frac{2.4\,\pi\,e^3 h_{es}\sqrt{f_c}}{(2e-d)^2} + \frac{2.4\,\pi\,d\,h_c^3\sqrt{f_c}}{(2h_c-h_{es})^2} \quad \text{Eq. 7.6}$$

$$h_{es} = \frac{h+h_p}{2} \quad \text{if } \frac{2e}{h_p} \le 1.5 \quad \text{Eq. 7.7}$$

$$h_{es} = h_p + (2.4 - \frac{2e}{h_p})\frac{h-h_p}{1.8} \quad \text{if } \frac{2e}{h_p} > 1.5 \quad \text{Eq. 7.8}$$

While for those tests which ended with pulling out failure, the headed stud shear capacity is measured from Equation 7.9. This failure mode occurred with the close arrangement of the stud connectors where the concrete had a small surface to resist the pulling action. The result was a pulling out of the stud carrying away a cone-shaped portion of concrete.

$$P_r = \frac{2.4\,\pi\,e^3 h_{ep}\sqrt{f_c}}{(2e-d)^2} + 0.56\,A_c\sqrt{f_c} \quad \text{Eq. 7.9}$$

$$h_{ep} = 2\,h_c\,(1 - \sqrt{\frac{1.07 d h_c \pi}{A_c}}) \quad \text{Eq. 7.10}$$

$$A_c = 2A_1 + b_o\frac{h_p}{\sin\theta 1} \quad \text{if } A_1 \le A_2 \quad \text{Eq. 7.11}$$

$$2A_2 + b_o\frac{h_p}{\sin\theta 2} \quad \text{if } A_1 > A_2 \quad \text{Eq. 7.12}$$

When the headed studs are placed symmetrically, $A_1$ and $A_2$ are determined by:

$$A_1 = (s_t + 2e_u)\frac{h-h_p}{\sin\theta 1} \quad \text{Eq. 7.13}$$

$$A_2 = s_v\frac{h-h_p}{2\sin\theta 1} + (s_t + e_u)\frac{h-h_p}{\sin\theta 2} \quad \text{Eq. 7.14}$$

$$\tan\theta_1 = \frac{h-h_p}{e_u} \quad \text{Eq. 7.15}$$

$$\tan\theta_2 = \frac{h-h_p}{s_v/_2} \quad \text{Eq. 7.16}$$

where $e$ is the distance from centre of stud to mid-height of rib, $d$ is the diameter of stud, $h_{es}$ is the effective depth of the bearing area for splitting failure, $h_c$ is the total depth of the concrete slab, $h$ and $h_p$ are the total height of headed stud and rib respectively, $A_c$ is the area of concrete cone surface, $h_{ep}$ is the effective depth of the bearing area for pulling out failure, $s_t$ is the transverse spacing between studs, $s_v$ is the longitudinal stud spacing, and $e_u$ is the

distance from the centre of a stud to the nearer top flange edge of the trough of profiled decking.

Figures 7.4 and 7.5 illustrate the relationship between the load per stud obtained from the parametric study and the predicted strengths based on the splitting and pulling out failure respectively. It is clear that the predicted strengths achieved from both theoretical methods are way too overestimated. The mean ratios of $P_{FE}/P_{sp}$ and $P_{FE}/P_r$ are 0.51 and 0.38 respectively, with the corresponding standard deviation and coefficients of variation of 0.17, 33% and 0.11 and 28.3% respectively. The drawbacks of both theoretical methods lie in three main reasons. First, the geometry including the rib, headed stud, and concrete slab seem to govern the equations. The problem is that those parameters are not limited to some ranges, this in turn, would allow achieving very high predicted strengths if the geometry size was increased (e.g. $h$ = 195 mm, and $h_c$ = 215 mm).

The second reason comes from the fact that at the time when those equations were developed; steel composite decks deeper than 80 mm were not available then. Therefore, it is unlikely for the developed equations to cope with a geometry of very deep decks like the 146 mm deep. Third, the rib geometry ratios considered in Yuan' study were limited to the wide range ($b_o/h_p > 1.5$), and therefore, the load per stud with narrow ribbed decks were inaccurately predicted. Needless to say, the failure mode must match the one by which the relevant equation was developed before the method can be used. This is not practical to rely on because there is no guarantee to achieve the same failure mode under different circumstances. The comparison between the load per stud obtained from the FE analysis and the predicted strengths by Johnson and Yuan (1998b) is given in Table 7.2.

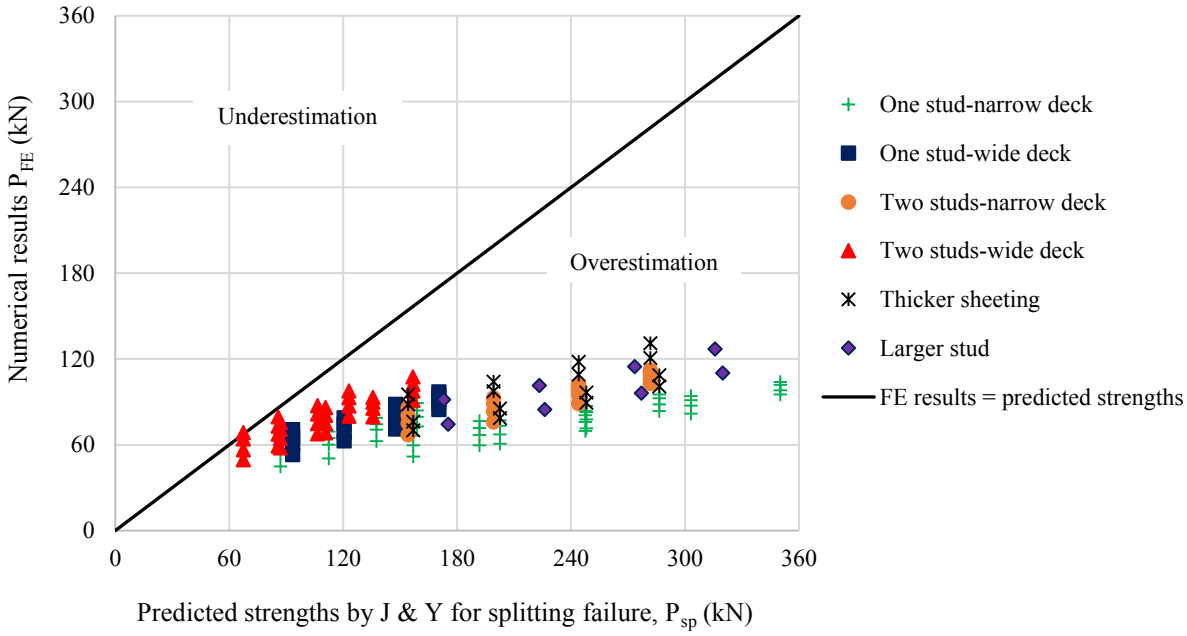


Figure 7.4 FE load per stud capacities versus the predicted strengths based on the splitting failure

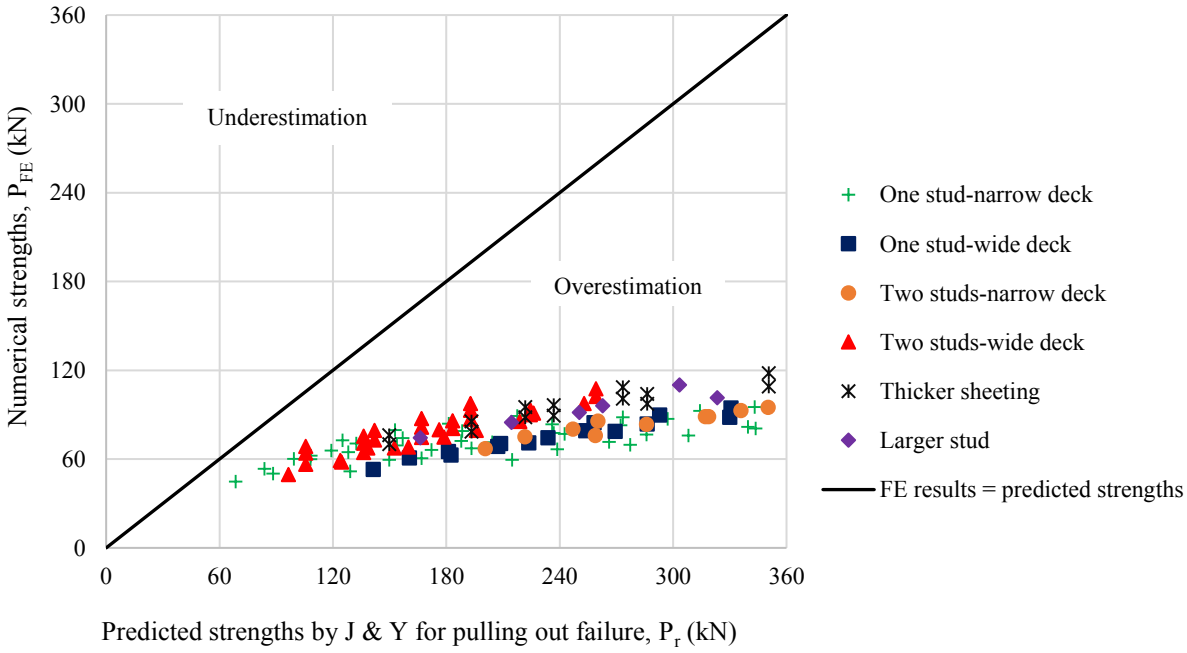


Figure 7.5 FE load per stud capacities versus the predicted strengths based on the pulling out failure

## 7.6 Comparison with the design equation proposed by Wu (1998)

An experimental investigation was carried out by Wu in 1998 on the behaviour of headed studs in push-out specimens with wide parallel steel decks. Forty-four push-out specimens out of 60 were performed with wide steel decks which varied from 1.58 up to 3.32; the deck height was only 76 mm. The parametric study mainly involved the effects of rib geometry size ($b_o/h_p$), longitudinal and transverse stud spacings. Based on the test results, a new design equation was derived using the least square regression analysis. After a series of simplifying steps on the preliminary equation, Equation 7.17 was the final simplified form and was recommended for the design purposes to predict the shear capacity of studs. It should be noted, that the test program only featured specimens with two studs per row arranged at different transverse stud spacings. However, the effect of transverse stud spacing was found insignificant on the load capacity. Thus, the variable of the transverse stud spacing was neglected in the final equation.

$$P_w = [0.264\ (s_l/d) + 0.821\ (b_o/h_p) + 3.12]\ d\ h_{sc}\ \sqrt{f_c} \qquad \text{Eq. 7.17}$$

$$3 \leq s_l/d \leq 8$$

The load per stud capacities obtained from the parametric study and those predicted by Equation 7.17 were compared. It appears from Figure 7.6 that Equation 7.17 gives a good prediction that is generally on the conservative side, yet some estimations were found to be on the unsafe side with big deviation from the FE results. The mean ratios of $P_{FE}/P_w$ are 1.00, with the corresponding standard deviation and coefficient of variation of 0.17 and 17.05% respectively. The overestimation in results was mainly associated with tests having one stud per row and narrow ribbed decks ($b_o/h_p < 1.5$). This was somewhat expected since the design equation was formulated based on results with only wide ribbed decks, besides the single stud configuration was beyond the scope of the research. This suggests that the configuration of headed studs should not be ruled out, and most importantly, the effect of narrow ribbed decks should be established.

The estimation of results regarding tests with two studs per row was mostly on the conservative side, except some scatter spotted on the unsafe side regarding some tests with high concrete grades and large diameter of the stud. It seems that Equation 7.17 is effective at predicting the shear capacity of studs arranged in two rows. However, the variable of $b_o/h_p$

is unlikely to be the best term to represent the correlation between the narrow and wide ribbed steel decks. There was still a noticeable deviation between the predicted and observed values. If Equation 7.17 was modified again and the term ($b_o/h_p$) was to be replaced by the shear area (i.e. effective cross-sectional area of concrete) for example, then the estimations would be relatively more precise.

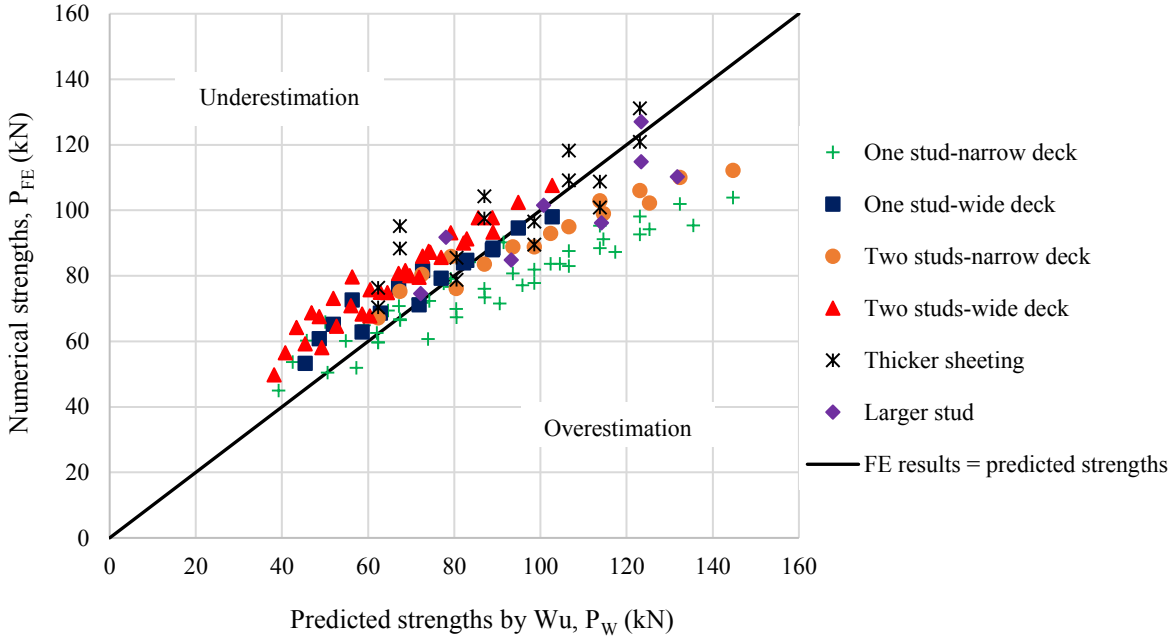


Figure 7.6 FE load per stud capacities versus predicted strengths by Wu (1998)

Table 7.2 Comparison of shear stud capacities obtained from FE analysis and the current shear strength design equations

| Phase | Test | $P_{FE}$ | $P_{EC4}$ | $P_{AISC}$ | $P_G$ | $P_s$ | $P_r$ | $P_W$ | $P_{FE}/P_{EC4}$ | $P_{FE}/P_{AISC}$ | $P_{FE}/P_G$ | $P_{FE}/P_s$ | $P_{FE}/P_r$ | $P_{FE}/P_W$ |
|---|---|---|---|---|---|---|---|---|---|---|---|---|---|---|
| I | A11 | 51.9 | 8.1 | 65.0 | 35.1 | 156.9 | 129.2 | 57.3 | 6.45 | 0.80 | 1.48 | 0.33 | 0.40 | 1.10 |
| | A12 | 59.6 | 8.1 | 65.0 | 44.2 | 156.9 | 149.7 | 62.4 | 7.40 | 0.92 | 1.35 | 0.38 | 0.40 | 1.05 |
| | A13 | 66.4 | 8.1 | 65.0 | 48.7 | 156.9 | 172.1 | 67.4 | 8.25 | 1.02 | 1.36 | 0.42 | 0.39 | 1.02 |
| | A14 | 72.3 | 8.1 | 65.0 | 47.5 | 156.9 | 187.9 | 74.2 | 8.98 | 1.11 | 1.52 | 0.46 | 0.38 | 1.03 |
| | A21 | 60.7 | 10.9 | 81.4 | 45.4 | 202.5 | 166.8 | 73.9 | 5.55 | 0.75 | 1.34 | 0.30 | 0.36 | 1.22 |
| | A22 | 67.3 | 10.9 | 81.4 | 57.1 | 202.5 | 193.3 | 80.5 | 6.16 | 0.83 | 1.18 | 0.33 | 0.35 | 1.20 |
| | A23 | 73.4 | 10.9 | 81.4 | 62.9 | 202.5 | 222.2 | 87.1 | 6.71 | 0.90 | 1.17 | 0.36 | 0.33 | 1.19 |
| | A24 | 77.1 | 10.9 | 81.4 | 61.3 | 202.5 | 242.6 | 95.8 | 7.05 | 0.95 | 1.26 | 0.38 | 0.32 | 1.24 |
| | A31 | 71.5 | 13.8 | 81.4 | 55.6 | 248.1 | 204.3 | 90.5 | 5.19 | 0.88 | 1.29 | 0.29 | 0.35 | 1.27 |
| | A32 | 77.8 | 13.8 | 81.4 | 69.9 | 248.1 | 236.8 | 98.6 | 5.65 | 0.96 | 1.11 | 0.31 | 0.33 | 1.27 |
| | A33 | 82.9 | 13.8 | 81.4 | 77.0 | 248.1 | 272.2 | 106.6 | 6.02 | 1.02 | 1.08 | 0.33 | 0.30 | 1.29 |
| | A34 | 87.2 | 13.8 | 81.4 | 75.1 | 248.1 | 297.2 | 117.3 | 6.33 | 1.07 | 1.16 | 0.35 | 0.29 | 1.35 |
| | A41 | 83.6 | 13.8 | 81.4 | 64.2 | 286.4 | 235.9 | 104.6 | 6.07 | 1.03 | 1.30 | 0.29 | 0.35 | 1.25 |
| | A42 | 88.4 | 13.8 | 81.4 | 80.8 | 286.4 | 273.4 | 113.8 | 6.42 | 1.09 | 1.09 | 0.31 | 0.32 | 1.29 |
| | A43 | 92.6 | 13.8 | 81.4 | 88.9 | 286.4 | 314.3 | 123.1 | 6.72 | 1.14 | 1.04 | 0.32 | 0.29 | 1.33 |
| | A44 | 95.3 | 13.8 | 81.4 | 86.8 | 286.4 | 343.1 | 135.5 | 6.92 | 1.17 | 1.10 | 0.33 | 0.28 | 1.42 |
| | B11 | 59.7 | 13.8 | 65.0 | 37.4 | 191.8 | 214.8 | 62.3 | 4.32 | 0.92 | 1.60 | 0.31 | 0.28 | 1.04 |
| | B12 | 66.8 | 13.8 | 65.0 | 46.5 | 191.8 | 238.7 | 67.4 | 4.83 | 1.03 | 1.44 | 0.35 | 0.28 | 1.01 |
| | B13 | 71.7 | 13.8 | 65.0 | 50.9 | 191.8 | 266.2 | 72.5 | 5.19 | 1.10 | 1.41 | 0.37 | 0.27 | 1.01 |
| | B14 | 76.6 | 13.8 | 65.0 | 49.7 | 191.8 | 286.0 | 79.3 | 5.54 | 1.18 | 1.54 | 0.40 | 0.27 | 1.03 |
| | B21 | 69.8 | 18.8 | 81.4 | 48.2 | 247.6 | 277.3 | 80.5 | 3.72 | 0.86 | 1.45 | 0.28 | 0.25 | 1.15 |
| | B22 | 76.0 | 18.8 | 81.4 | 60.0 | 247.6 | 308.2 | 87.0 | 4.05 | 0.93 | 1.27 | 0.31 | 0.25 | 1.14 |
| | B23 | 80.7 | 18.8 | 81.4 | 65.8 | 247.6 | 343.6 | 93.6 | 4.30 | 0.99 | 1.23 | 0.33 | 0.23 | 1.16 |
| | B24 | 83.7 | 18.8 | 81.4 | 64.2 | 247.6 | 369.3 | 102.3 | 4.46 | 1.03 | 1.30 | 0.34 | 0.23 | 1.22 |
| | B31 | 81.9 | 23.6 | 81.4 | 59.1 | 303.2 | 339.6 | 98.5 | 3.46 | 1.01 | 1.39 | 0.27 | 0.24 | 1.20 |
| | B32 | 87.5 | 23.6 | 81.4 | 73.4 | 303.2 | 377.4 | 106.6 | 3.70 | 1.08 | 1.19 | 0.29 | 0.23 | 1.22 |
| | B33 | 91.2 | 23.6 | 81.4 | 80.5 | 303.2 | 420.9 | 114.6 | 3.86 | 1.12 | 1.13 | 0.30 | 0.22 | 1.26 |

Table 7.2 (continued)

| | Test | $P_{FE}$ | $P_{EC4}$ | $P_{AISC}$ | $P_G$ | $P_s$ | $P_r$ | $P_W$ | $P_{FE}/P_{EC4}$ | $P_{FE}/P_{AISC}$ | $P_{FE}/P_G$ | $P_{FE}/P_s$ | $P_{FE}/P_r$ | $P_{FE}/P_W$ |
|---|---|---|---|---|---|---|---|---|---|---|---|---|---|---|
| | B34 | 94.2 | 23.6 | 81.4 | 78.6 | 303.2 | 452.3 | 125.3 | 3.98 | 1.16 | 1.20 | 0.31 | 0.21 | 1.33 |
| | B41 | 95.2 | 23.6 | 81.4 | 68.2 | 350.1 | 392.1 | 113.8 | 4.03 | 1.17 | 1.40 | 0.27 | 0.24 | 1.20 |
| | B42 | 98.1 | 23.6 | 81.4 | 84.8 | 350.1 | 435.8 | 123.1 | 4.15 | 1.21 | 1.16 | 0.28 | 0.23 | 1.25 |
| | B43 | 101.9 | 23.6 | 81.4 | 93.0 | 350.1 | 486.0 | 132.4 | 4.31 | 1.25 | 1.10 | 0.29 | 0.21 | 1.30 |
| | B44 | 103.9 | 23.6 | 81.4 | 90.8 | 350.1 | 522.2 | 144.7 | 4.39 | 1.28 | 1.14 | 0.30 | 0.20 | 1.39 |
| | C12 | 53.2 | 24.0 | 65.0 | 37.9 | 93.3 | 141.4 | 39.2 | 1.87 | 0.69 | 1.40 | 0.57 | 0.38 | 0.87 |
| | C12 | 60.8 | 24.0 | 65.0 | 47.0 | 93.3 | 160.5 | 42.5 | 2.23 | 0.82 | 1.29 | 0.65 | 0.38 | 0.79 |
| | C13 | 65.2 | 24.0 | 65.0 | 51.5 | 93.3 | 181.1 | 45.7 | 2.51 | 0.93 | 1.27 | 0.70 | 0.36 | 0.76 |
| | C14 | 70.6 | 24.0 | 65.0 | 50.3 | 93.3 | 208.7 | 50.1 | 2.74 | 1.01 | 1.40 | 0.76 | 0.34 | 0.76 |
| | C21 | 62.8 | 32.6 | 81.4 | 48.9 | 120.5 | 182.6 | 50.6 | 1.55 | 0.62 | 1.28 | 0.52 | 0.34 | 1.00 |
| | C22 | 68.6 | 32.6 | 81.4 | 60.6 | 120.5 | 207.1 | 54.8 | 1.84 | 0.74 | 1.13 | 0.57 | 0.33 | 0.91 |
| | C23 | 74.6 | 32.6 | 81.4 | 66.4 | 120.5 | 233.7 | 59.0 | 1.99 | 0.80 | 1.12 | 0.62 | 0.32 | 0.91 |
| | C24 | 78.9 | 32.6 | 81.4 | 64.9 | 120.5 | 269.4 | 64.6 | 2.13 | 0.85 | 1.22 | 0.65 | 0.29 | 0.93 |
| | C31 | 71.1 | 41.1 | 81.4 | 59.9 | 147.6 | 223.6 | 62.0 | 1.52 | 0.77 | 1.19 | 0.48 | 0.32 | 0.99 |
| | C32 | 79.2 | 41.1 | 81.4 | 74.3 | 147.6 | 253.7 | 67.1 | 1.72 | 0.87 | 1.07 | 0.54 | 0.31 | 0.95 |
| | C33 | 83.9 | 41.1 | 81.4 | 81.4 | 147.6 | 286.3 | 72.3 | 1.81 | 0.91 | 1.03 | 0.57 | 0.29 | 0.97 |
| | C34 | 88.4 | 41.1 | 81.4 | 79.5 | 147.6 | 329.9 | 79.2 | 1.92 | 0.97 | 1.11 | 0.60 | 0.27 | 1.00 |
| | C41 | 84.7 | 41.1 | 81.4 | 69.2 | 170.4 | 258.2 | 71.6 | 1.77 | 0.89 | 1.22 | 0.50 | 0.33 | 0.98 |
| | C42 | 89.9 | 41.1 | 81.4 | 85.8 | 170.4 | 292.9 | 77.5 | 1.89 | 0.96 | 1.05 | 0.53 | 0.31 | 1.00 |
| | C43 | 94.6 | 41.1 | 81.4 | 93.9 | 170.4 | 330.6 | 83.5 | 2.05 | 1.03 | 1.01 | 0.56 | 0.29 | 0.99 |
| | C44 | 97.0 | 41.1 | 81.4 | 91.8 | 170.4 | 381.0 | 91.4 | 2.20 | 1.11 | 1.06 | 0.57 | 0.25 | 1.01 |
| | D12 | 44.9 | 45.3 | 65.0 | 35.1 | 87.0 | 68.5 | 45.4 | 1.18 | 0.82 | 1.28 | 0.52 | 0.66 | 0.85 |
| | D12 | 53.6 | 45.3 | 65.0 | 44.2 | 87.0 | 83.8 | 48.7 | 1.34 | 0.94 | 1.21 | 0.62 | 0.64 | 0.80 |
| | D13 | 60.2 | 45.3 | 65.0 | 48.7 | 87.0 | 99.3 | 51.9 | 1.44 | 1.00 | 1.24 | 0.69 | 0.61 | 0.80 |
| | D14 | 65.8 | 45.3 | 65.0 | 47.5 | 87.0 | 119.2 | 56.3 | 1.60 | 1.12 | 1.39 | 0.76 | 0.55 | 0.78 |
| | D21 | 50.4 | 61.5 | 95.3 | 45.3 | 112.4 | 88.4 | 58.6 | 1.02 | 0.66 | 1.11 | 0.45 | 0.57 | 0.93 |
| | D22 | 60.1 | 61.5 | 95.3 | 57.1 | 112.4 | 108.1 | 62.8 | 1.12 | 0.72 | 1.05 | 0.53 | 0.56 | 0.92 |
| | D23 | 64.9 | 61.5 | 95.3 | 62.9 | 112.4 | 128.2 | 67.1 | 1.24 | 0.80 | 1.03 | 0.58 | 0.51 | 0.88 |

Table 7.2 (continued)

| | Test | $P_{FE}$ | $P_{EC4}$ | $P_{AISC}$ | $P_G$ | $P_s$ | $P_r$ | $P_W$ | $P_{FE}/P_{EC4}$ | $P_{FE}/P_{AISC}$ | $P_{FE}/P_G$ | $P_{FE}/P_s$ | $P_{FE}/P_r$ | $P_{FE}/P_W$ |
|---|---|---|---|---|---|---|---|---|---|---|---|---|---|---|
| | D24 | 69.4 | 61.5 | 95.3 | 61.3 | 112.4 | 153.9 | 72.7 | 1.33 | 0.86 | 1.13 | 0.62 | 0.45 | 0.89 |
| | D31 | 62.5 | 77.4 | 95.7 | 55.5 | 137.6 | 108.3 | 71.8 | 0.92 | 0.74 | 1.13 | 0.45 | 0.58 | 1.01 |
| | D32 | 70.7 | 77.4 | 95.7 | 69.9 | 137.6 | 132.4 | 77.0 | 1.02 | 0.83 | 1.01 | 0.51 | 0.53 | 0.97 |
| | D33 | 74.4 | 77.4 | 95.7 | 77.0 | 137.6 | 157.0 | 82.1 | 1.08 | 0.88 | 0.97 | 0.54 | 0.47 | 0.98 |
| | D34 | 79 | 77.4 | 95.7 | 75.1 | 137.6 | 188.5 | 89.0 | 1.14 | 0.92 | 1.05 | 0.57 | 0.42 | 1.01 |
| | D41 | 72.8 | 77.4 | 95.7 | 64.1 | 158.9 | 125.0 | 82.9 | 1.09 | 0.89 | 1.14 | 0.46 | 0.58 | 0.98 |
| | D42 | 79.7 | 77.4 | 95.7 | 80.7 | 158.9 | 152.9 | 88.9 | 1.14 | 0.92 | 0.99 | 0.50 | 0.52 | 1.01 |
| | D43 | 84.1 | 77.4 | 95.7 | 88.9 | 158.9 | 181.3 | 94.8 | 1.22 | 0.99 | 0.95 | 0.53 | 0.46 | 1.00 |
| | D44 | 89.2 | 13.8 | 95.7 | 86.7 | 158.9 | 217.6 | 102.8 | 1.27 | 1.02 | 1.03 | 0.56 | 0.41 | 1.05 |
| **II** | E11 | 67.1 | 13.8 | 65.0 | 37.4 | 154.3 | 200.5 | 62.3 | 4.86 | 1.03 | 1.80 | 0.43 | 0.33 | 0.93 |
| | E12 | 75.2 | 13.8 | 65.0 | 46.5 | 154.3 | 221.5 | 67.4 | 5.44 | 1.16 | 1.62 | 0.49 | 0.34 | 0.90 |
| | E13 | 80.4 | 13.8 | 65.0 | 50.9 | 154.3 | 247.0 | 72.5 | 5.82 | 1.24 | 1.58 | 0.52 | 0.33 | 0.90 |
| | E14 | 85.8 | 18.8 | 65.0 | 49.7 | 154.3 | 260.2 | 79.3 | 6.21 | 1.32 | 1.73 | 0.56 | 0.33 | 0.92 |
| | E21 | 76.1 | 18.8 | 81.4 | 48.2 | 199.2 | 258.9 | 80.5 | 4.05 | 0.94 | 1.58 | 0.38 | 0.29 | 1.06 |
| | E22 | 83.5 | 18.8 | 81.4 | 60.0 | 199.2 | 286.0 | 87.0 | 4.45 | 1.03 | 1.39 | 0.42 | 0.29 | 1.04 |
| | E23 | 88.8 | 18.8 | 81.4 | 65.8 | 199.2 | 318.8 | 93.6 | 4.73 | 1.09 | 1.35 | 0.45 | 0.28 | 1.05 |
| | E24 | 92.9 | 23.6 | 81.4 | 64.2 | 199.2 | 335.9 | 102.3 | 4.95 | 1.14 | 1.45 | 0.47 | 0.28 | 1.10 |
| | E31 | 88.8 | 23.6 | 81.4 | 59.1 | 244.0 | 317.1 | 98.5 | 3.76 | 1.09 | 1.50 | 0.36 | 0.28 | 1.11 |
| | E32 | 95.0 | 23.6 | 81.4 | 73.4 | 244.0 | 350.3 | 106.6 | 4.02 | 1.17 | 1.29 | 0.39 | 0.27 | 1.12 |
| | E33 | 98.9 | 23.6 | 81.4 | 80.5 | 244.0 | 390.5 | 114.6 | 4.19 | 1.22 | 1.23 | 0.41 | 0.25 | 1.16 |
| | E34 | 102.2 | 23.6 | 81.4 | 78.6 | 244.0 | 411.4 | 125.3 | 4.32 | 1.26 | 1.30 | 0.42 | 0.25 | 1.23 |
| | E41 | 102.8 | 23.6 | 81.4 | 68.2 | 281.7 | 366.1 | 113.8 | 4.35 | 1.26 | 1.51 | 0.36 | 0.28 | 1.11 |
| | E42 | 106.0 | 23.6 | 81.4 | 84.8 | 281.7 | 404.5 | 123.1 | 4.48 | 1.30 | 1.25 | 0.38 | 0.26 | 1.16 |
| | E43 | 110.0 | 23.6 | 81.4 | 93.0 | 281.7 | 450.9 | 132.4 | 4.65 | 1.35 | 1.18 | 0.39 | 0.24 | 1.20 |
| | E44 | 112.2 | 45.3 | 81.4 | 90.8 | 281.7 | 475.1 | 144.7 | 4.75 | 1.38 | 1.24 | 0.40 | 0.24 | 1.29 |
| | F11 | 59.2 | 45.3 | 65.0 | 37.9 | 85.9 | 123.9 | 45.4 | 1.31 | 0.91 | 1.56 | 0.69 | 0.48 | 0.77 |
| | F12 | 67.5 | 45.3 | 65.0 | 47.0 | 85.9 | 138.5 | 48.7 | 1.49 | 1.04 | 1.44 | 0.79 | 0.49 | 0.72 |
| | F13 | 73.1 | 45.3 | 65.0 | 51.5 | 85.9 | 142.0 | 51.9 | 1.62 | 1.12 | 1.42 | 0.85 | 0.51 | 0.71 |

Table 7.2 (continued)

| | Test | $P_{FE}$ | $P_{EC4}$ | $P_{AISC}$ | $P_G$ | $P_s$ | $P_r$ | $P_W$ | $P_{FE}/P_{EC4}$ | $P_{FE}/P_{AISC}$ | $P_{FE}/P_G$ | $P_{FE}/P_s$ | $P_{FE}/P_r$ | $P_{FE}/P_W$ |
|---|---|---|---|---|---|---|---|---|---|---|---|---|---|---|
| | F14 | 79.6 | 61.5 | 65.0 | 50.3 | 85.9 | 142.0 | 56.3 | 1.76 | 1.22 | 1.58 | 0.93 | 0.56 | 0.71 |
| | F21 | 68.3 | 61.5 | 95.3 | 48.9 | 110.8 | 159.9 | 58.6 | 1.11 | 0.72 | 1.40 | 0.62 | 0.43 | 0.86 |
| | F22 | 74.9 | 61.5 | 95.3 | 60.6 | 110.8 | 178.8 | 62.8 | 1.22 | 0.79 | 1.24 | 0.68 | 0.42 | 0.84 |
| | F23 | 80.7 | 61.5 | 95.3 | 66.4 | 110.8 | 183.3 | 67.1 | 1.31 | 0.85 | 1.21 | 0.73 | 0.44 | 0.83 |
| | F24 | 86.0 | 77.4 | 95.3 | 64.9 | 110.8 | 183.3 | 72.7 | 1.40 | 0.90 | 1.33 | 0.78 | 0.47 | 0.84 |
| | F31 | 79.5 | 77.4 | 95.7 | 59.9 | 135.7 | 195.8 | 71.8 | 1.03 | 0.83 | 1.33 | 0.59 | 0.41 | 0.90 |
| | F32 | 85.6 | 77.4 | 95.7 | 74.3 | 135.7 | 219.0 | 77.0 | 1.11 | 0.89 | 1.15 | 0.63 | 0.39 | 0.90 |
| | F33 | 90.0 | 77.4 | 95.7 | 81.4 | 135.7 | 224.5 | 82.1 | 1.16 | 0.94 | 1.11 | 0.66 | 0.40 | 0.91 |
| | F34 | 93.3 | 77.4 | 95.7 | 79.5 | 135.7 | 224.5 | 89.0 | 1.21 | 0.97 | 1.17 | 0.69 | 0.42 | 0.95 |
| | F41 | 91.2 | 77.4 | 95.7 | 69.2 | 156.7 | 226.1 | 82.9 | 1.18 | 0.95 | 1.32 | 0.58 | 0.40 | 0.91 |
| | F42 | 97.7 | 77.4 | 95.7 | 85.8 | 156.7 | 252.8 | 88.9 | 1.26 | 1.02 | 1.14 | 0.62 | 0.39 | 0.91 |
| | F43 | 102.4 | 77.4 | 95.7 | 93.9 | 156.7 | 259.2 | 94.8 | 1.32 | 1.07 | 1.09 | 0.65 | 0.40 | 0.93 |
| | F44 | 107.6 | 54.9 | 95.7 | 91.8 | 156.7 | 259.2 | 102.8 | 1.39 | 1.12 | 1.17 | 0.69 | 0.42 | 0.96 |
| | G11 | 49.7 | 54.9 | 65.0 | 37.6 | 67.4 | 96.5 | 38.2 | 0.91 | 0.76 | 1.32 | 0.74 | 0.52 | 0.77 |
| | G12 | 56.5 | 54.9 | 65.0 | 46.7 | 67.4 | 105.6 | 40.8 | 1.03 | 0.87 | 1.21 | 0.84 | 0.54 | 0.72 |
| | G13 | 64.2 | 54.9 | 65.0 | 51.2 | 67.4 | 105.6 | 43.4 | 1.17 | 0.99 | 1.25 | 0.95 | 0.61 | 0.68 |
| | G14 | 68.7 | 74.6 | 65.0 | 50.0 | 67.4 | 105.6 | 46.9 | 1.25 | 1.06 | 1.37 | 1.02 | 0.65 | 0.68 |
| | G21 | 58.0 | 74.6 | 95.3 | 48.6 | 87.0 | 124.6 | 49.3 | 0.78 | 0.61 | 1.19 | 0.67 | 0.47 | 0.85 |
| | G22 | 64.6 | 74.6 | 95.3 | 60.3 | 87.0 | 136.3 | 52.7 | 0.87 | 0.68 | 1.07 | 0.74 | 0.47 | 0.82 |
| | G23 | 70.8 | 74.6 | 95.3 | 66.1 | 87.0 | 136.3 | 56.0 | 0.95 | 0.74 | 1.07 | 0.81 | 0.52 | 0.79 |
| | G24 | 75.7 | 93.9 | 95.3 | 64.5 | 87.0 | 136.3 | 60.5 | 1.02 | 0.79 | 1.17 | 0.87 | 0.56 | 0.80 |
| | G31 | 67.7 | 93.9 | 95.7 | 59.5 | 106.5 | 152.6 | 60.4 | 0.72 | 0.71 | 1.14 | 0.64 | 0.44 | 0.89 |
| | G32 | 74.8 | 93.9 | 95.7 | 73.9 | 106.5 | 166.9 | 64.5 | 0.80 | 0.78 | 1.01 | 0.70 | 0.45 | 0.86 |
| | G33 | 81.6 | 93.9 | 95.7 | 80.9 | 106.5 | 166.9 | 68.6 | 0.87 | 0.85 | 1.01 | 0.77 | 0.49 | 0.84 |
| | G34 | 87.4 | 93.9 | 95.7 | 79.0 | 106.5 | 166.9 | 74.1 | 0.93 | 0.91 | 1.11 | 0.82 | 0.52 | 0.85 |
| | G41 | 80.0 | 93.9 | 95.7 | 68.7 | 123.0 | 176.2 | 69.7 | 0.85 | 0.84 | 1.17 | 0.65 | 0.45 | 0.87 |
| | G42 | 87.1 | 93.9 | 95.7 | 85.3 | 123.0 | 192.7 | 74.5 | 0.93 | 0.91 | 1.02 | 0.71 | 0.45 | 0.85 |
| | G43 | 93.1 | 93.9 | 95.7 | 93.5 | 123.0 | 192.7 | 79.2 | 0.99 | 0.97 | 1.00 | 0.76 | 0.48 | 0.85 |

Table 7.2 (continued)

| | Test | $P_{FE}$ | $P_{EC4}$ | $P_{AISC}$ | $P_G$ | $P_s$ | $P_r$ | $P_W$ | $P_{FE}/P_{EC4}$ | $P_{FE}/P_{AISC}$ | $P_{FE}/P_G$ | $P_{FE}/P_s$ | $P_{FE}/P_r$ | $P_{FE}/P_W$ |
|---|---|---|---|---|---|---|---|---|---|---|---|---|---|---|
| | G44 | 97.7 | 13.8 | 95.7 | 91.3 | 123.0 | 192.7 | 85.6 | 1.04 | 1.02 | 1.07 | 0.79 | 0.51 | 0.88 |
| III | H11 | 70.3 | 8.1 | 65.0 | 44.2 | 156.9 | 149.7 | 62.4 | 8.73 | 1.08 | 1.59 | 0.45 | 0.47 | 0.89 |
| | H12 | 78.7 | 10.9 | 81.4 | 57.1 | 202.5 | 193.3 | 80.5 | 7.20 | 0.97 | 1.38 | 0.39 | 0.41 | 1.02 |
| | H13 | 89.5 | 13.8 | 81.4 | 69.9 | 248.1 | 236.8 | 98.6 | 6.50 | 1.10 | 1.28 | 0.36 | 0.38 | 1.10 |
| | H14 | 100.8 | 13.8 | 81.4 | 80.8 | 286.4 | 273.4 | 113.8 | 7.32 | 1.24 | 1.25 | 0.35 | 0.37 | 1.13 |
| | I11 | 76.3 | 8.1 | 65.0 | 44.2 | 156.9 | 149.7 | 62.4 | 9.47 | 1.17 | 1.72 | 0.49 | 0.51 | 0.82 |
| | I12 | 85.5 | 10.9 | 81.4 | 57.1 | 202.5 | 193.3 | 80.5 | 7.82 | 1.05 | 1.50 | 0.42 | 0.44 | 0.94 |
| | I13 | 96.5 | 13.8 | 81.4 | 69.9 | 248.1 | 236.8 | 98.6 | 7.00 | 1.19 | 1.38 | 0.39 | 0.41 | 1.02 |
| | I14 | 108.7 | 13.8 | 81.4 | 80.8 | 286.4 | 273.4 | 113.8 | 7.89 | 1.34 | 1.35 | 0.38 | 0.40 | 1.05 |
| | J11 | 88.3 | 13.8 | 65.0 | 46.5 | 154.3 | 221.8 | 67.4 | 6.39 | 1.36 | 1.90 | 0.57 | 0.40 | 0.76 |
| | J12 | 97.4 | 18.8 | 81.4 | 60.1 | 199.2 | 286.3 | 87.0 | 5.19 | 1.20 | 1.62 | 0.49 | 0.34 | 0.89 |
| | J13 | 109.1 | 23.6 | 81.4 | 73.6 | 244.0 | 350.7 | 106.6 | 4.62 | 1.34 | 1.48 | 0.45 | 0.31 | 0.98 |
| | J14 | 120.8 | 23.6 | 81.4 | 84.9 | 281.7 | 404.9 | 123.1 | 5.11 | 1.49 | 1.42 | 0.43 | 0.30 | 1.02 |
| | K11 | 95.2 | 13.8 | 65.0 | 46.5 | 154.3 | 221.8 | 67.4 | 6.89 | 1.46 | 2.05 | 0.62 | 0.43 | 0.71 |
| | K12 | 104.2 | 18.8 | 81.4 | 60.1 | 199.2 | 286.3 | 87.0 | 5.55 | 1.28 | 1.73 | 0.52 | 0.36 | 0.84 |
| | K13 | 118.2 | 23.6 | 81.4 | 73.6 | 244.0 | 350.7 | 106.6 | 5.00 | 1.45 | 1.61 | 0.48 | 0.34 | 0.90 |
| | K14 | 131.1 | 23.6 | 81.4 | 84.9 | 281.7 | 404.9 | 123.1 | 5.55 | 1.61 | 1.54 | 0.47 | 0.32 | 0.94 |
| IV | L11 | 74.5 | 10.8 | 87.1 | 61.4 | 175.2 | 166.2 | 72.2 | 6.90 | 0.85 | 1.21 | 0.43 | 0.45 | 0.97 |
| | L12 | 84.8 | 14.7 | 109.1 | 79.3 | 226.2 | 214.5 | 93.2 | 5.78 | 0.78 | 1.07 | 0.37 | 0.40 | 1.10 |
| | L13 | 96.1 | 18.5 | 109.1 | 97.1 | 277.1 | 262.7 | 114.2 | 5.20 | 0.88 | 0.99 | 0.35 | 0.37 | 1.19 |
| | L14 | 110.2 | 18.5 | 109.1 | 112.2 | 319.9 | 303.4 | 131.8 | 5.97 | 1.01 | 0.98 | 0.34 | 0.36 | 1.20 |
| | M11 | 91.7 | 18.5 | 87.1 | 64.0 | 173.0 | 250.4 | 78.1 | 4.95 | 1.05 | 1.43 | 0.53 | 0.37 | 0.85 |
| | M12 | 101.5 | 25.2 | 109.1 | 82.6 | 223.3 | 323.3 | 100.8 | 4.04 | 0.93 | 1.23 | 0.45 | 0.31 | 0.99 |
| | M13 | 114.8 | 31.7 | 109.1 | 101.2 | 273.5 | 395.9 | 123.4 | 3.62 | 1.05 | 1.13 | 0.42 | 0.29 | 1.07 |
| | M14 | 127.0 | 31.7 | 109.1 | 116.8 | 315.9 | 457.2 | 142.5 | 4.01 | 1.16 | 1.09 | 0.40 | 0.28 | 1.12 |
| **Mean** | | | | | | | | | 3.55 | 1.01 | 1.27 | 0.51 | 0.38 | 1.00 |
| **SD** | | | | | | | | | 2.33 | 0.19 | 0.21 | 0.17 | 0.11 | 0.17 |
| **CoV (%)** | | | | | | | | | 65.73 | 19.19 | 16.34 | 32.96 | 28.28 | 17.05 |

## 7.7 Summary

The significance of the work carried out so far in this chapter is that it verified the effectiveness of the current design equations at predicting the shear stud capacity placed in parallel steel decks. The main focus was on the accurate estimation of the shear capacity of the headed stud in very deep and narrow steel decks. Therefore, the shear resistance of studs obtained from 136 tests was evaluated against the nominal strengths taken from the existing design equations.

The findings revealed that the Eurocode 4 provisions greatly under-predicted the shear capacity of studs especially with those having narrow rib geometry ($b_o/h_p < 1.5$) and/or steel decks in excess of 80 mm deep. The problem was in Equation 7.3 as it provided unreasonable reduction factor values causing a deviation from the predicted strengths from the observed values. In addition, the EC4 does not consider the change in the longitudinal stud spacings and studs' arrangement. Altogether, the design equation was unable to result in accurate predictions. Likewise, the use of the American provisions ended with inaccurate predicted strengths. The reason was stemmed from the inflexibility of the design equation and the non-consideration of some variables such as the rib geometry and longitudinal stud spacing. Thus, the predicted strengths were limited to a few ranges of values.

It was found that the correlation between narrow and wide ribbed decks was missing in all the design equations developed in former studies. This was clearly noticed in the design equations developed by Gnanasambandam (1995) and Wu (1998), where a remarkable deviation was seen between the predicted and FE results because those equations were developed based on only wide ribbed decks. As a result, the shear capacity of the stud in such narrow-ribbed decks was miscalculated. The highest scatter in results, however, was observed within the developed formulae by Johnson and Yuan (1998b). Overall, the reliability of the current design equations in predicting the shear capacity of the stud in very deep and/or narrow steel decks is insufficient. To bridge this gap, there is a definite need to introduce an up-to-date set of equations for more accurate results. This work is addressed in the next section.

## 7.8 Headed stud shear capacity in parallel steel decks: Development of new equations

A least square regression analysis method was used to formulate the equations. The numerical results obtained from 136 push-off tests were used for the multi-linear regression analysis. As discussed earlier, the headed stud's arrangement including the single and double configuration makes a difference in the shear capacity of the stud. Therefore, it is more appropriate to formulate two separate equations in order to ensure better predictions and avoid discrepancies in results. The significance of the developed equations is that they will cover a wide range of steel deck geometries including narrow sizes for the first time, and a new rule will be proposed to establish the correlation between the narrow and wide steel decks.

### 7.8.1 Equation development: One stud per row

The initial variables considered forming the equation were the concrete compressive strength, the diameter of the headed stud, longitudinal stud spacing, and sheeting thickness. If the effects of the first three variables versus the load capacity (as presented in Chapter 6) were examined, a linear relationship between the load capacity versus those variables could be clearly noted. The general form of the linear relationship can be expressed in Equation 7.18, where x stands for a variable, A and B are constant and intercept respectively.

$$P = A\,x + B \qquad \text{Eq. 7.18}$$

As shown in Figure 7.7, the relationship between the fourth variable (i.e. sheeting thickness) and the load capacity is assumed to be non-linear. If the non-linear assumption was to be drawn, then Equation 7.19 is the ideal form. However, it was decided to apply the linear assumption instead, without introducing further complexity into the final equation. Thus, the relationship between the sheeting thickness and the load capacity can be established through Equation 7.18.

$$P = A\,t_s^2 + B\,t_s + C \qquad \text{Eq. 7.19}$$

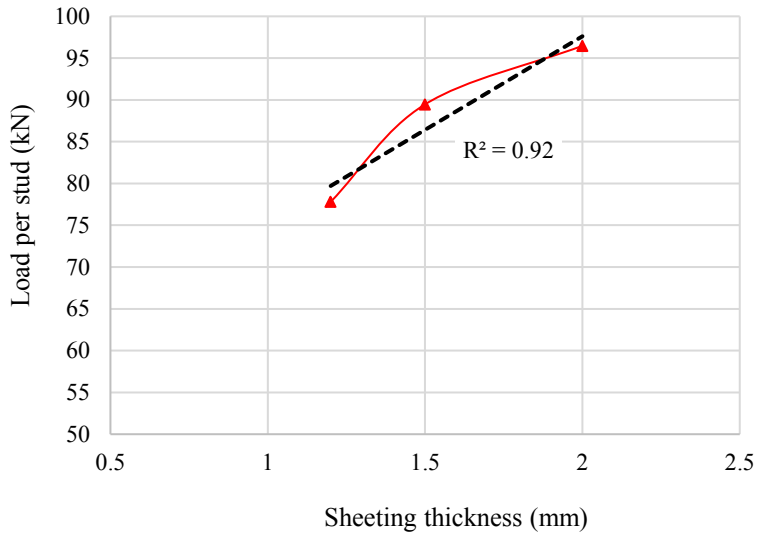


Figure 7.7 Relationship between the load capacity and sheeting thickness

The last variable, not yet considered, is the effect of the rib geometry. Normally, the ratio of the rib width to the rib height ($b_o/h_p$) is used for this purpose as seen in the former design equations. However, the findings in the previous chapter revealed that it was not possible to draw a steady correlation between narrow and wide ribbed decks through their rib deck ratios. If the rib deck ratio is included in the regression analysis, the analysis is highly expected to yield formula with inaccurate predictions. Therefore, the rib deck ratio was excluded from the analysis and replaced by the effective cross-sectional area of the concrete ($A_c$) as this was found to provide a much better demonstration to the effect of steel deck geometry. From the observation in section 6.5.2, the linear assumption embodied in Equation 7.18 can also express the relationship between the load capacity and the effective cross-sectional area of the concrete.

By substituting each independent variable in Equation 7.18, and adding all of them together, Equation 7.20 was obtained.

$$P_S = A\, f_{ck} + B\, A_s + C\, l_s + D\, t_s + E\, A_c + F \qquad \text{Eq. 7.20}$$

Where A, B, C, D, E, and F are constants to be determined. The least square regression analysis was conducted by the Add-in Solver which is available in Microsoft Excel. The test results of the 76 push-out specimens with single stud configuration were used for the regression analysis. As a result, Equation 7.21 was achieved which is the final form of the

equation of predicting the shear capacity of stud placed in parallel steel decks and arranged in a single row. The regression analysis gave a coefficient of correlation ($R^2$) of 0.975; the predicted strengths were then compared to the observed values to see how close the correlation is. The mean of the observed strengths to the predicted results and the coefficient of variation were 1.00 and 3.14% respectively, whilst the scatter in results lied within $\pm$5%. Figure 7.8 shows the relationship between the predicted strengths and the observed values associated with the best linear fit method. Details of the predicted strengths using the regression analysis are given in Appendix B (Table B.1).

$$P_S = 1.036\, f_{ck} + 0.154\, A_s + 0.162\, l_s + 26.144\, t_s + 0.001\, A_c - 57.504 \qquad \text{Eq. 7.21}$$

where:

$P_S$ = Shear capacity per stud placed in parallel steel deck (kN)

$f_{ck}$ = Characteristic cylinder strength of concrete (MPa)

$A_s$ = Cross-sectional area of headed stud ($mm^2$)

$l_s$ = Longitudinal stud spacing (mm), $3d \leq l_s \leq 8d$

$t_s$ = Sheeting thickness of steel decking (mm)

$A_c$ = Effective cross-sectional area of concrete ($mm^2$)

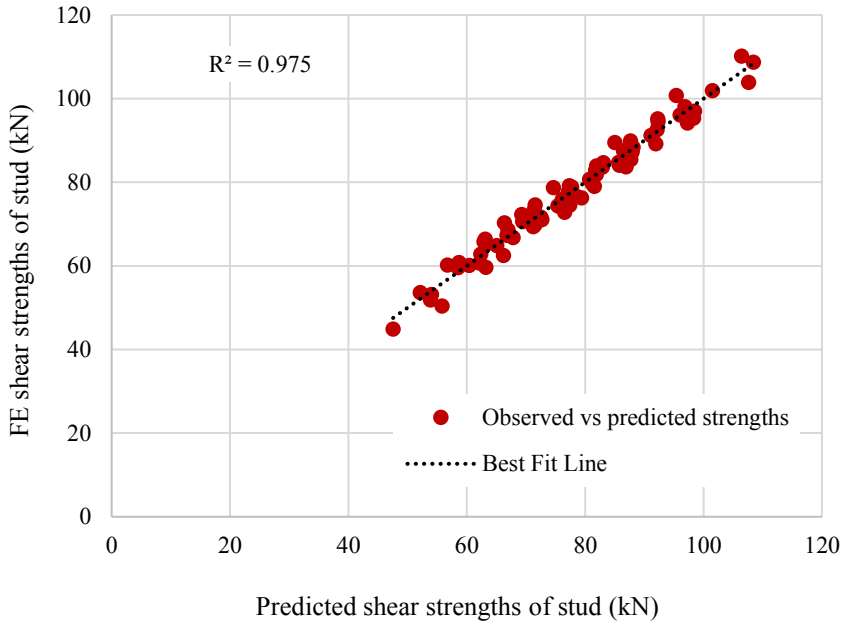


Figure 7.8 FE strengths versus predicted strengths using Eq. 7.21 (Single stud configuration)

### 7.8.2 Equation development: Two studs per row

The test results of the 60 push-out specimens with two studs per row were used to develop a relevant equation for predicting the shear capacity of the stud. The least square regression analysis method was also used. Using the same procedure applied to the specimens with single stud per row, the variables considered in this case were the concrete compressive strength, the diameter of the headed stud, longitudinal stud spacing, sheeting thickness, and the effective cross-sectional area of concrete. It is important to mention that the variable of the transverse stud spacing was not involved in the regression analysis since only one transverse spacing was considered in the parametric stud (i.e. 4*d*).

It was felt redundant to investigate the effect of the transverse stud spacing because Gnanasambandam (1995) and Wu (1998) found that the change in the transverse spacing from 3*d* to 6*d* gave insignificant influence on the shear capacity of the stud. It was then suggested that the transverse spacing of 4*d* is the ideal arrangement to put the headed studs into their best use, agreeing with what it is recommended in the Eurocode 4 provisions as

well. Based on this observation, the variable of the transverse stud spacing was also neglected in both Gnanasambandam's and Wu's equations (see Eq. 7.5 and Eq. 7.17).

By substituting each independent variable in Equation 7.18, and adding all of them together, Equation 7.22 was obtained.

$$P_D = A\, f_{ck} + B\, A_s + C\, l_s + D\, t_s + E\, A_c + F \qquad \text{Eq. 7.22}$$

The regression analysis yielded Equation 7.23 which is the final form of the equation of predicting the shear capacity of stud placed in parallel steel decks and arranged in two rows. The regression analysis gave a coefficient of correlation ($R^2$) of 0.975, the mean of the observed strengths to the predicted results and the coefficient of variation were 1.00 and 3.47% respectively, and the scatter in results lied within $\pm$5.5%. Figure 7.9 shows the relationship between the predicted strengths and the observed values associated with the best linear fit method. Details of the predicted strengths using the regression analysis are given in Appendix B (Table B.2).

$$P_D = 1.106\, f_{ck} + 0.147\, A_s + 0.172\, l_s + 29.488\, t_s + 0.001\, A_c - 62.085 \qquad \text{Eq. 7.23}$$

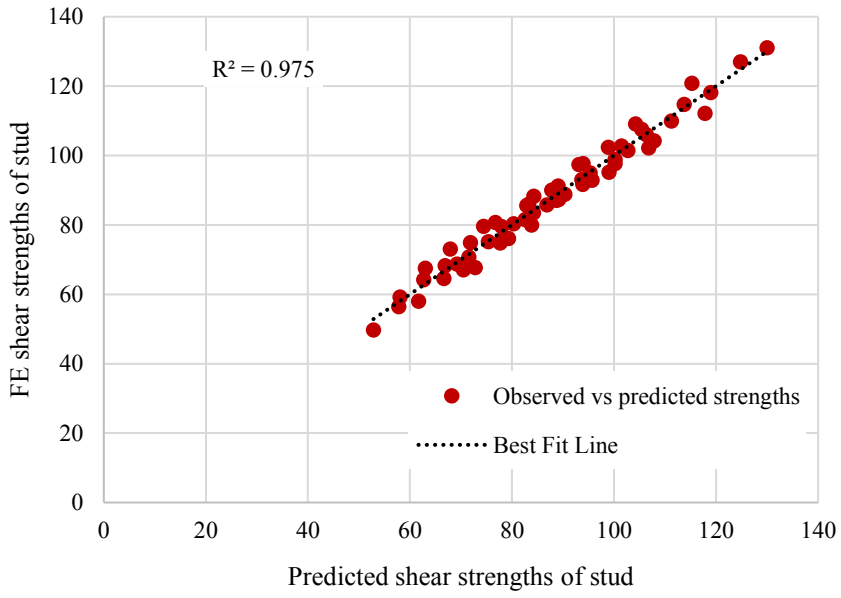


Figure 7.9 FE strengths versus predicted strengths using Eq. 7.23 (Double stud configuration)

## 7.9 Evaluation of the new developed equations

The reliability of both equations yielded from the regression analysis was evaluated against the ultimate load per stud obtained from many previous push-off tests. The evaluation was also assessed with the ultimate load per stud predicted by the equations from the EC4, ANSI/AISC 360-2016, Gnanasambandam (1995), Johnson and Yuan (1998b), and Wu (1998). This was meant to see whether the equations developed from the regression analysis work as effectively as the other existing equations or even better. Due to the limit of research done on the composite beam with parallel steel decks, the comparison was limited to the results taken from a few numbers of studies, yet some research had to be excluded for not meeting some conditions.

For instance, it was not possible to consider the work done by Robinson (1988) where the push-off tests only had one stud per connection (i.e. one headed stud embedded in the concrete slab). This arrangement is not common neither in experiments nor construction, because the longitudinal stud spacing would not exist in this case and that it is essential to examine its effect on the shear capacity of the stud. More importantly, most of the equations to be considered now involve the variable of the longitudinal stud spacing, if this term was equal to zero, the equations would provide unreasonable predictions. The exclusion was also imposed on the five push-off tests conducted by Jayas and Hosain (1988) for being performed only with a diameter of the stud of 13 mm. This type of headed stud is no longer used in practice, besides the developed equations in this study were formed based on the most common sizes used nowadays: 19 and 22 mm.

### 7.9.1 Push-off tests with single stud arrangement

The efficiency of Equation 7.21 was validated against some previous experiments as illustrated in Table 7.3. The process also included predicted strengths obtained from some existing design equations as mentioned earlier. Unfortunately, the number of push-off specimens to be examined are only four, and those were conducted by Gnanasambandam (1995). Figure 7.10 shows the details of the steel decking. The literature lacks any further research focusing on the single stud arrangement in parallel steel deck. Although research on composite beams with parallel profiled decking was recently done by Chen et al. (2016), the push test arrangement only had one stud per connection, besides the scope of research was

related to elevated temperatures. Nevertheless, the evaluation even with a few samples is still important to check if the validity of the proposed equation is satisfying.

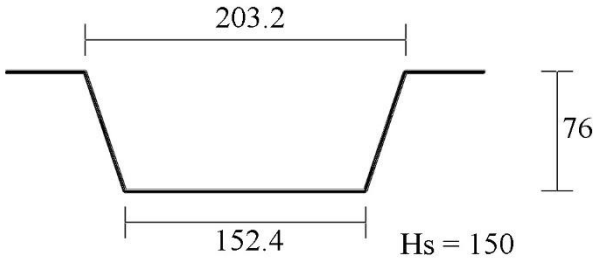


Figure 7.10 Details of the steel decking (All dimensions are in mm)

Referring to Table 7.3, the European code and American specification did not consider some crucial parameters such as the rib geometry ratio and longitudinal stud spacing. As a result, the predicted strengths remained constant despite the change in the studs' spacing. This necessitates that the existing rules in the EC4 and ANSI/AISC should be recalibrated for better predictions and more flexibility regarding rib geometry effects, and studs' layout within the ribs.

The comparison also revealed that Equation 7.6 proposed by Johnson and Yuan (1998b) for splitting failure gave undesirable predictions although the compared specimens ended with the same failure mode. This suggests that the developed equation by Johnson and Yuan (1998b) is unlikely to be applicable even with such specimens having wide rib geometries and depths not in excess of 80 mm. It was also interesting to notice that Equation 7.6 does not consider the effect of the longitudinal stud spacing. It should be mentioned that Equation 7.9 was also verified for the purpose of study despite being theoretically inapplicable due to the failure mode mismatch. The comparison showed that the predicted strengths were too way overrated, and the use of Equation 7.9 was even worse than Equation 7.6.

From Figure 7.11, the predicted strengths obtained from Equation 7.21 appeared to be in a very good agreement with the experimental values. The trend in Figure 7.11 is that the accuracy in results lies within ±10%. The accuracy of the equation proposed in this study is obviously as effective as those proposed by Gnanasambandam (1995) and Wu (1998). But still, Equation 7.21 has more advantage than any other equation whereas various rib geometries from narrow to wide are covered as discussed before. The mean ratio of the

predicted strengths to the experimental values and the coefficient of variation were 1.01 and 4.23% respectively, with a minimal scatter in results lied in ±6%.

With this accuracy, it proves that the new rule for representing the geometry effect of the ribbed decks through the effective cross-sectional area of concrete is workable. The term ($A_c$) introduced in Equation 7.21 is said to be an effective replacement to the term ($b_o/h_p$) since the latter was proven to misrepresent the correlation between the narrow and wide ribbed decks. Thus, it can be concluded that Equation 7.21 can be used for future design purposes to predict the shear capacity of the stud in parallel decking and arranged in one row.

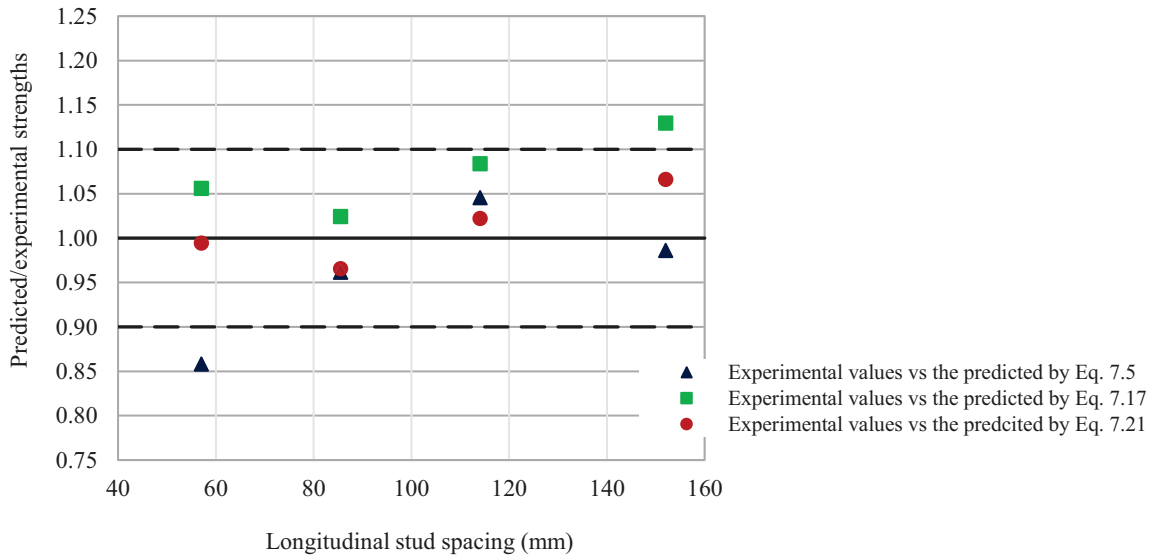


Figure 7.11 Predicted strengths versus experimental values for push-off tests with single stud per row

Table 7.3 Comparison of shear capacity of headed stud obtained from experiments and design equations for push-off tests with parallel decking and single stud per row

| Test | $f_c$ (MPa) | Steel decking details | | | | | Stud details | | Exp. Load per stud P (kN) | $P_S$ (kN) | $P_{EC4}$ (kN) | $P_{AIC}$ (kN) | $P_G$ (kN) | $P_{Yuan-S}$ (kN) | $P_{Yuan-P}$ (kN) | $P_W$ | $P_S/P$ | $P_{EC4}/P$ | $P_{AISC}/P$ | $P_G/P$ | $P_{Yuan-S}/P$ | $P_{Yuan-P}/P$ | $P_W/P$ |
|---|---|---|---|---|---|---|---|---|---|---|---|---|---|---|---|---|---|---|---|---|---|---|---|
| | | $b_o$ | $h_p$ | $b_o/h_p$ | $A_c$ ($mm^2$) | $t_s$ | $d \times h_{sc}$ | $l_s$ (mm) | | | | | | | | | | | | | | | |
| F41 | 26.4 | 177.8 | 76 | 2.33 | 28850 | 1.0 | 19 × 125 | 57 | 67.3 | 66.9 | 86.55 | 95.7 | 57.8 | 134.0 | 257.2 | 71.1 | 0.99 | 1.29 | 1.42 | 0.86 | 1.99 | 3.82 | 1.06 |
| F42 | 26.4 | 177.8 | 76 | 2.33 | 28850 | 1.0 | 19 × 125 | 85.5 | 74.1 | 71.5 | 86.55 | 95.7 | 71.3 | 134.0 | 288.5 | 75.9 | 0.97 | 1.17 | 1.29 | 0.96 | 1.81 | 3.89 | 1.02 |
| F43 | 26.4 | 177.8 | 76 | 2.33 | 28850 | 1.0 | 19 × 125 | 114 | 74.5 | 76.2 | 86.55 | 95.7 | 77.9 | 134.0 | 320.3 | 80.7 | 1.02 | 1.16 | 1.28 | 1.05 | 1.80 | 4.30 | 1.08 |
| F44 | 26.4 | 177.8 | 76 | 2.33 | 28850 | 1.0 | 19 × 125 | 152 | 77.2 | 82.3 | 86.55 | 95.7 | 76.1 | 134.0 | 369.2 | 87.2 | 1.07 | 1.12 | 1.24 | 0.99 | 1.74 | 4.78 | 1.13 |
| Mean | | | | | | | | | | | | | | | | | 1.01 | 1.18 | 1.31 | 0.96 | 1.83 | 4.20 | 1.07 |
| SD | | | | | | | | | | | | | | | | | 0.04 | 0.07 | 0.08 | 0.08 | 0.11 | 0.44 | 0.04 |
| CoV (%) | | | | | | | | | | | | | | | | | 4.23 | 5.99 | 5.99 | 8.12 | 5.99 | 10.53 | 4.14 |

### 7.9.2 Push-off tests with double stud arrangement

The applicability of Equation 7.23 was verified through many previous experiments done by Gnanasambandam (1995), Johnson Yuan (1998a), and Wu (1998). Details of the steel decks are shown in Figure 7.12. All the specimens in this comparison had headed studs placed at different transverse spacings varying from approximately 3*d* to 6*d*. It was interesting to examine the efficiency of Equation 7.23 with some tests featuring small headed studs of 16 mm. The comparison between the predicted and experimental values is presented in Tables 7.4 to 7.6 and Figures 7.13 to 7.15.

Considering the mean ratio of predicted over observed strengths along with the coefficient of variation, it is obvious that Equation 7.23 predict the results much better than the EC4 and ANSI/AISC. Again, the deficiency in both design codes is because some important parameters are not recognised such as the rib geometry, the longitudinal stud spacing, and the number of studs per row. Thus, the predicted strengths were achieved with a substantial deviation from the observed values. This is another observation that points out the necessity to have both existing rules revised for the shear capacity of the headed stud in parallel steel decks.

The undesirable predictions with a coefficient of variation greater than 25% were still associated with the developed equations by Johnson and Yuan (1998b) when they were applied to experiments done by different authors (see Table 7.4). The use of one of those equations (i.e. Eq. 7.6) was found only reliable on the tests performed by the same authors (see Table 7.5). This indicates that the effectiveness of the analytical model developed by Johnson and Yuan (1998b) is restricted to some cases. For the same table, the comparison showed that Equation 7.23 achieved an accuracy with a coefficient of variation of 5.38% compared to 7.53% obtained from Equation 7.6. The developed equation in this research was able to provide very good predictions to specimens featuring different rib geometries, and transverse/longitudinal stud spacings. The modern equation worked as effectively as Equation 7.6. With its simplicity and no preconditions in use, Equation 7.23 has more advantages than Equation 7.6.

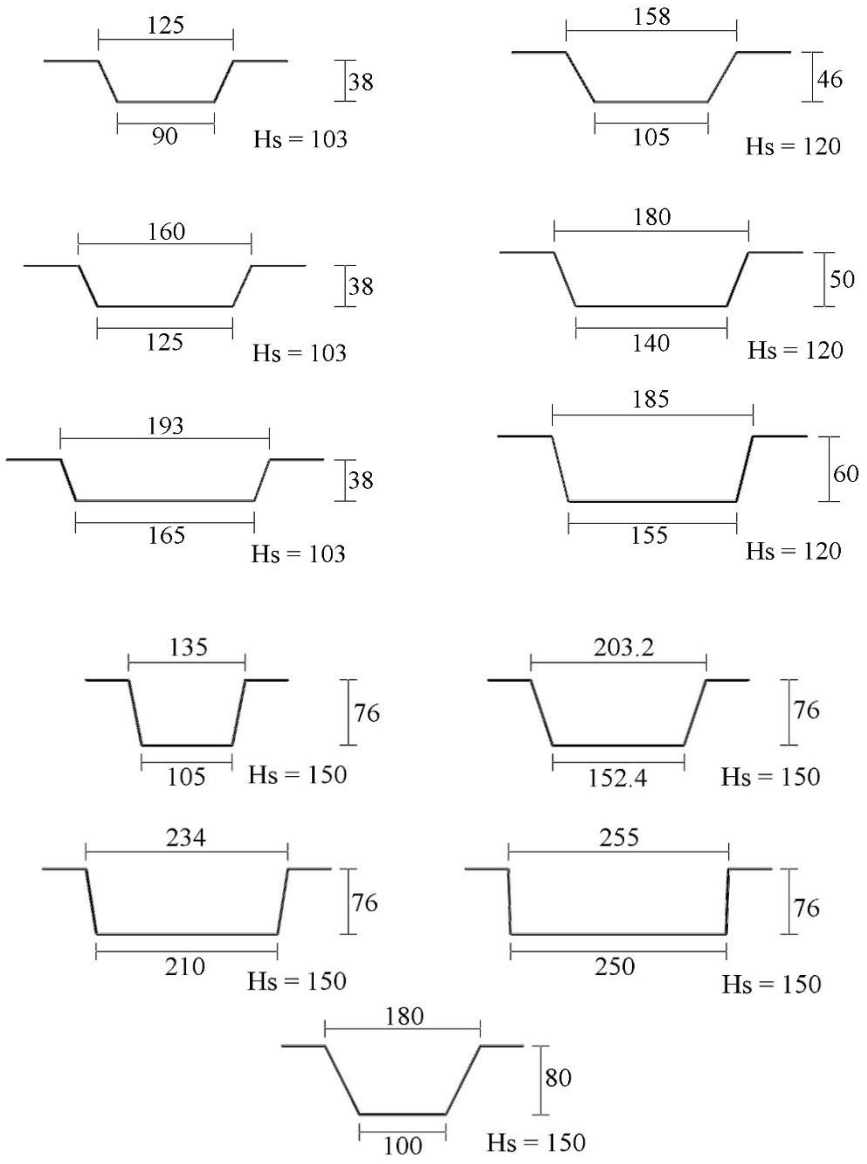


Figure 7.12 Details of the steel decks investigated (All dimensions are in mm)

Referring to Tables 7.4 and 7.6, the shear capacity of headed studs obtained from experiments were well predicted by Equation 7.23. The accuracy of the modern equation appeared to be as effective as those equations proposed by Gnanasambandam and Wu, or even better in some cases. The mean ratio of the predicted strengths to the observed values was very close to 1.00, and the coefficient of variations was within the lowest values corresponding to 7.96% and 4.64% in Tables 7.4 and 7.6 respectively. The accuracy in results is due to the fact that Equation 7.23 takes into account the most influential factors on the shear capacity of headed stud including the longitudinal stud spacing, concrete strength, and cross-sectional area of the stud. More importantly, the term ($A_c$) which is introduced in Equation 7.23 worked as an

effective representative of the rib geometry after being replaced over the term ($b_o/h_p$). This is another proof that the correlation between the narrow and wide ribbed decks is likely to be addressed by the new concept of the effective cross-sectional area of concrete. In conclusion, Equation 7.23 is adequate to be used for future design purposes to predict the shear capacity of the stud in parallel decking and arranged in two rows.

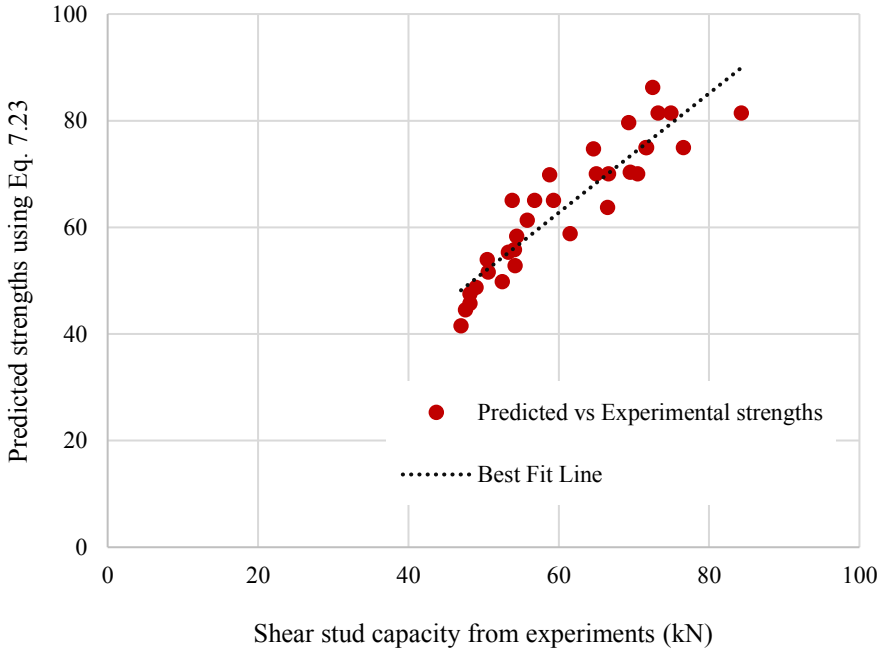


Figure 7.13 Comparison between predicted strengths using Eq. 7.23 and experimental results taken from Gnanasambandam (1995)

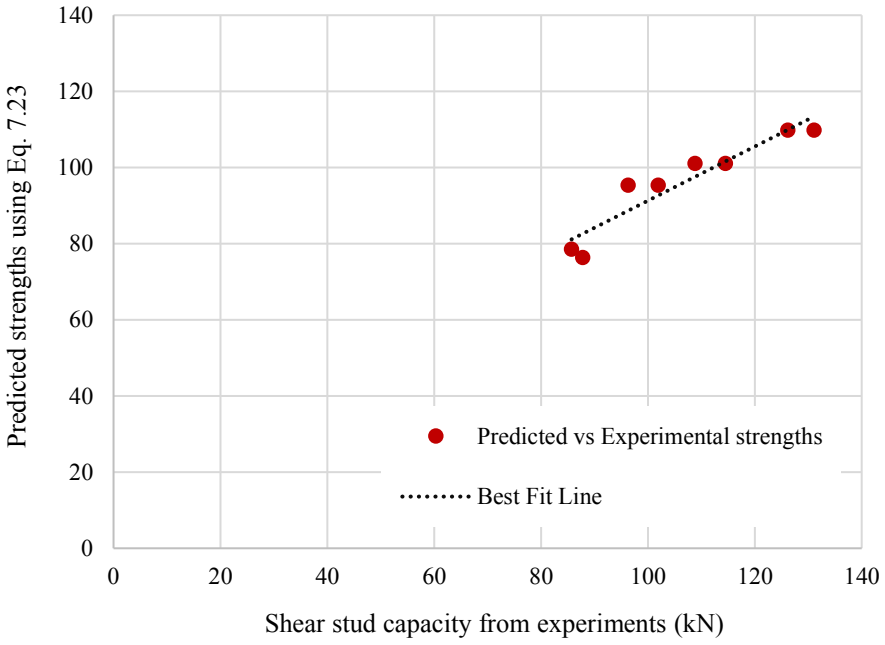


Figure 7.14 Comparison between predicted strengths using Eq. 7.23 and experimental results taken from Johnson Yuan (1998a)

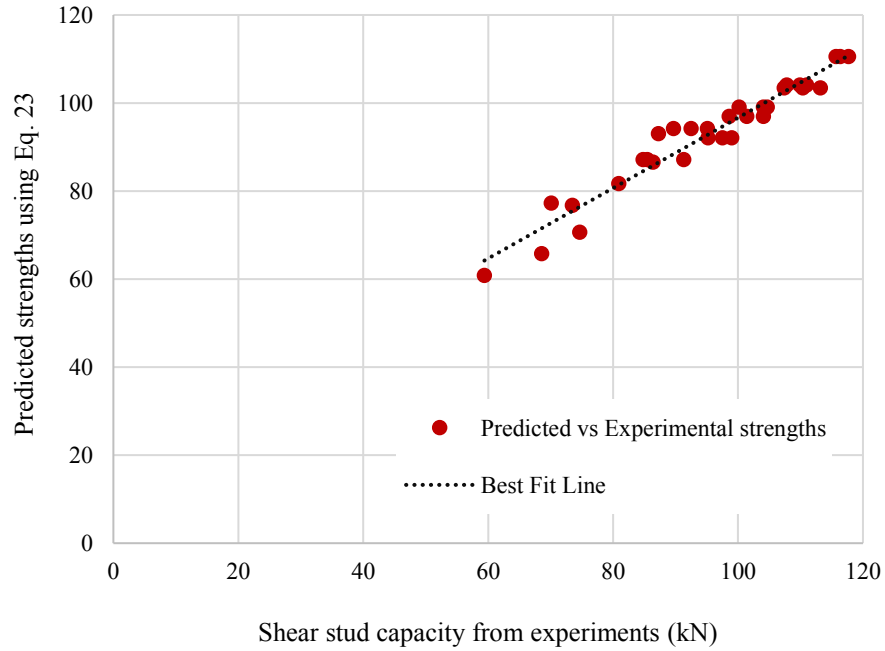


Figure 7.15 Comparison between predicted strengths using Eq. 7.23 and experimental results taken from Wu (1998)

Table 7.4 Comparison of shear capacity of headed stud obtained from experiments and design equations for push-off tests with parallel decking and double stud per row

| Test* | $f_c$ (MPa) | Steel decking details | | | | | Stud details | | | Exp. Load per stud P (kN) | $P_D$ (kN) | $P_{EC4}$ (kN) | $P_{AISC}$ (kN) | $P_G$ (kN) | $P_{Yuan-S}$ (kN) | $P_{Yuan-P}$ (kN) | $P_W$ | $P_D/P$ | $P_{EC4}/P$ | $P_{AISC}/P$ | $P_G/P$ | $P_{Yuan-S}/P$ | $P_{Yuan-P}/P$ | $P_W/P$ |
|---|---|---|---|---|---|---|---|---|---|---|---|---|---|---|---|---|---|---|---|---|---|---|---|---|
| | | $b_o$ | $h_p$ | $b_o/h_p$ | $A_c$ (mm$^2$) | $t_s$ | $d \times h_{sc}$ | $l_s$ (mm) | $S_t$ | | | | | | | | | | | | | | | |
| H11 | 23.5 | 113.2 | 38 | 2.98 | 12210 | 0.76 | 16 × 76 | 48 | 64 | 47.0 | 41.5 | 63.4 | 67.9 | 38.1 | 69.1 | 93.8 | 37.5 | 0.88 | 1.35 | 1.45 | 0.81 | 1.47 | 2.00 | 0.80 |
| H12 | 23.5 | 113.2 | 38 | 2.98 | 12210 | 0.76 | 16 × 76 | 72 | 64 | 48.2 | 45.7 | 63.4 | 67.9 | 47.1 | 69.1 | 104.1 | 39.8 | 0.95 | 1.32 | 1.41 | 0.98 | 1.43 | 2.16 | 0.83 |
| H13 | 23.5 | 113.2 | 38 | 2.98 | 12210 | 0.76 | 16 × 76 | 96 | 64 | 52.5 | 49.8 | 63.4 | 67.9 | 51.6 | 69.1 | 115.4 | 42.2 | 0.95 | 1.21 | 1.29 | 0.98 | 1.32 | 2.20 | 0.80 |
| H14 | 23.5 | 113.2 | 38 | 2.98 | 12210 | 0.76 | 16 × 76 | 128 | 64 | 53.3 | 55.3 | 63.4 | 67.9 | 50.4 | 69.1 | 130.8 | 45.3 | 1.04 | 1.19 | 1.27 | 0.95 | 1.30 | 2.45 | 0.85 |
| H21 | 23.5 | 150.5 | 38 | 3.96 | 15815 | 0.76 | 16 × 76 | 48 | 64 | 47.6 | 44.5 | 63.4 | 67.9 | 40.2 | 51.4 | 113.3 | 42.2 | 0.93 | 1.33 | 1.42 | 0.84 | 1.08 | 2.38 | 0.89 |
| H22 | 23.5 | 150.5 | 38 | 3.96 | 15815 | 0.76 | 16 × 76 | 72 | 64 | 49.0 | 48.7 | 63.4 | 67.9 | 49.2 | 51.4 | 127.9 | 44.6 | 0.99 | 1.29 | 1.39 | 1.00 | 1.05 | 2.61 | 0.91 |
| H23 | 23.5 | 150.5 | 38 | 3.96 | 15815 | 0.76 | 16 × 76 | 96 | 64 | 54.2 | 52.8 | 63.4 | 67.9 | 53.7 | 51.4 | 142.2 | 46.9 | 0.97 | 1.17 | 1.25 | 0.99 | 0.95 | 2.63 | 0.87 |
| H24 | 23.5 | 150.5 | 38 | 3.96 | 15815 | 0.76 | 16 × 76 | 128 | 64 | 54.4 | 58.3 | 63.4 | 67.9 | 52.5 | 51.4 | 159.2 | 50.0 | 1.07 | 1.16 | 1.25 | 0.96 | 0.95 | 2.92 | 0.92 |
| H31 | 23.5 | 189.0 | 38 | 4.97 | 19347 | 0.76 | 16 × 76 | 48 | 64 | 48.2 | 47.5 | 63.4 | 67.9 | 42.3 | 37.9 | 145.2 | 47.1 | 0.99 | 1.32 | 1.41 | 0.88 | 0.79 | 3.01 | 0.98 |
| H32 | 23.5 | 189.0 | 38 | 4.97 | 19347 | 0.76 | 16 × 76 | 72 | 64 | 50.6 | 51.6 | 63.4 | 67.9 | 51.4 | 37.9 | 162.5 | 49.4 | 1.02 | 1.25 | 1.34 | 1.02 | 0.75 | 3.21 | 0.98 |
| H33 | 23.5 | 189.0 | 38 | 4.97 | 19347 | 0.76 | 16 × 76 | 96 | 64 | 54.1 | 55.8 | 63.4 | 67.9 | 55.8 | 37.9 | 182.3 | 51.8 | 1.03 | 1.17 | 1.26 | 1.03 | 0.70 | 3.37 | 0.96 |
| H34 | 23.5 | 189.0 | 38 | 4.97 | 19347 | 0.76 | 16 × 76 | 128 | 64 | 55.8 | 61.3 | 63.4 | 67.9 | 54.6 | 37.9 | 207.1 | 54.9 | 1.10 | 1.14 | 1.22 | 0.98 | 0.68 | 3.71 | 0.98 |
| F21 | 26.4 | 177.8 | 76 | 2.33 | 28550 | 1.0 | 19 × 125 | 57 | 76 | 56.8 | 65.0 | 86.6 | 95.7 | 57.8 | 143.4 | 221.5 | 71.1 | 1.15 | 1.52 | 1.68 | 1.02 | 2.52 | 3.90 | 1.25 |
| F22 | 26.4 | 177.8 | 76 | 2.33 | 28550 | 1.0 | 19 × 125 | 85.5 | 76 | 66.6 | 70.0 | 86.6 | 95.7 | 71.3 | 143.4 | 246.1 | 75.9 | 1.05 | 1.30 | 1.44 | 1.07 | 2.15 | 3.70 | 1.14 |
| F23 | 26.4 | 177.8 | 76 | 2.33 | 28550 | 1.0 | 19 × 125 | 114 | 76 | 71.7 | 74.9 | 86.6 | 95.7 | 77.9 | 143.4 | 275.1 | 80.7 | 1.04 | 1.21 | 1.33 | 1.09 | 2.00 | 3.84 | 1.13 |
| F24 | 26.4 | 177.8 | 76 | 2.33 | 28550 | 1.0 | 19 × 125 | 152 | 76 | 74.9 | 81.4 | 86.6 | 95.7 | 76.1 | 143.4 | 306.7 | 87.2 | 1.09 | 1.16 | 1.28 | 1.02 | 1.91 | 4.09 | 1.16 |
| G11 | 23.5 | 120.0 | 76 | 1.58 | 19110 | 1.0 | 19 × 125 | 57 | 76 | 50.5 | 53.9 | 54.6 | 95.7 | 51.4 | 121.4 | 151.7 | 60.0 | 1.07 | 1.08 | 1.90 | 1.02 | 2.40 | 3.00 | 1.19 |
| G12 | 23.5 | 120.0 | 76 | 1.58 | 19110 | 1.0 | 19 × 125 | 85.5 | 76 | 61.5 | 58.8 | 54.6 | 95.7 | 64.1 | 121.4 | 166.1 | 64.5 | 0.96 | 0.89 | 1.56 | 1.04 | 1.97 | 2.70 | 1.05 |

Table 7.4 (Continued)

| Test* | $f_c$ (MPa) | Steel decking details | | | | | Stud details | | | Exp. Load per stud P (kN) | $P_D$ (kN) | $P_{EC4}$ (kN) | $P_{AISC}$ (kN) | $P_G$ (kN) | $P_{Yuan}$-S (kN) | $P_{Yuan}$-P (kN) | $P_W$ | $P_D/P$ | $P_{EC4}/P$ | $P_{AISC}/P$ | $P_G/P$ | $P_{Yuan}$-S/P | $P_{Yuan}$-P/P | $P_W/P$ |
|---|---|---|---|---|---|---|---|---|---|---|---|---|---|---|---|---|---|---|---|---|---|---|---|---|
| | | $b_o$ | $h_p$ | $b_o/h_p$ | $A_c$ (mm$^2$) | $t_s$ | $d \times h_{sc}$ | $l_s$ (mm) | $S_t$ | | | | | | | | | | | | | | | |
| G13 | 23.5 | 120.0 | 76 | 1.58 | 19110 | 1.0 | 19 × 125 | 114 | 76 | 66.5 | 63.7 | 54.6 | 95.7 | 70.4 | 121.4 | 181.8 | 69.1 | 0.96 | 0.82 | 1.44 | 1.06 | 1.82 | 2.73 | 1.04 |
| G14 | 23.5 | 120.0 | 76 | 1.58 | 19110 | 1.0 | 19 × 125 | 152 | 76 | 69.5 | 70.3 | 54.6 | 95.7 | 68.7 | 121.4 | 203.4 | 75.2 | 1.01 | 0.79 | 1.38 | 0.99 | 1.75 | 2.93 | 1.08 |
| G21 | 23.5 | 252.5 | 76 | 3.32 | 38060 | 1.0 | 19 × 125 | 57 | 76 | 58.8 | 69.8 | 89.4 | 95.7 | 58.6 | 160.5 | 305.3 | 76.4 | 1.19 | 1.52 | 1.63 | 1.00 | 2.73 | 5.19 | 1.30 |
| G22 | 23.5 | 252.5 | 76 | 3.32 | 38060 | 1.0 | 19 × 125 | 85.5 | 76 | 64.6 | 74.7 | 89.4 | 95.7 | 71.3 | 160.5 | 335.1 | 81.0 | 1.16 | 1.38 | 1.48 | 1.10 | 2.48 | 5.19 | 1.25 |
| G23 | 23.5 | 252.5 | 76 | 3.32 | 38060 | 1.0 | 19 × 125 | 114 | 76 | 69.3 | 79.6 | 89.4 | 95.7 | 77.6 | 160.5 | 370.2 | 85.5 | 1.15 | 1.29 | 1.38 | 1.12 | 2.32 | 5.34 | 1.23 |
| G24 | 23.5 | 252.5 | 76 | 3.32 | 38060 | 1.0 | 19 × 125 | 152 | 76 | 72.5 | 86.2 | 89.4 | 95.7 | 75.9 | 160.5 | 420.2 | 91.6 | 1.19 | 1.23 | 1.32 | 1.05 | 2.21 | 5.80 | 1.26 |
| F11 | 26.4 | 177.8 | 76 | 2.33 | 28550 | 1.0 | 19 × 125 | 57 | 57 | 59.3 | 65.0 | 86.6 | 95.7 | 57.8 | 144.8 | 229.9 | 71.1 | 1.10 | 1.46 | 1.61 | 0.97 | 2.44 | 3.88 | 1.20 |
| F12 | 26.4 | 177.8 | 76 | 2.33 | 28550 | 1.0 | 19 × 125 | 85.5 | 57 | 70.5 | 70.0 | 86.6 | 95.7 | 71.3 | 144.8 | 256.0 | 75.9 | 0.99 | 1.23 | 1.36 | 1.01 | 2.05 | 3.63 | 1.08 |
| F13 | 26.4 | 177.8 | 76 | 2.33 | 28550 | 1.0 | 19 × 125 | 114 | 57 | 76.6 | 74.9 | 86.6 | 95.7 | 77.9 | 144.8 | 286.1 | 80.7 | 0.98 | 1.13 | 1.25 | 1.02 | 1.89 | 3.74 | 1.05 |
| F14 | 26.4 | 177.8 | 76 | 2.33 | 28550 | 1.0 | 19 × 125 | 152 | 57 | 84.3 | 81.4 | 86.6 | 95.7 | 76.1 | 144.8 | 326.1 | 87.2 | 0.97 | 1.03 | 1.14 | 0.90 | 1.72 | 3.87 | 1.03 |
| F31 | 26.4 | 177.8 | 76 | 2.33 | 28550 | 1.0 | 19 × 125 | 57 | 95 | 53.8 | 65.0 | 86.6 | 95.7 | 57.8 | 130.0 | 214.3 | 71.1 | 1.21 | 1.61 | 1.78 | 1.07 | 2.42 | 3.98 | 1.32 |
| F32 | 26.4 | 177.8 | 76 | 2.33 | 28550 | 1.0 | 19 × 125 | 85.5 | 95 | 65.0 | 70.0 | 86.6 | 95.7 | 71.3 | 130.0 | 237.7 | 75.9 | 1.08 | 1.33 | 1.47 | 1.10 | 2.00 | 3.66 | 1.17 |
| F33 | 26.4 | 177.8 | 76 | 2.33 | 28550 | 1.0 | 19 × 125 | 114 | 95 | 71.6 | 74.9 | 86.6 | 95.7 | 77.9 | 130.0 | 263.7 | 80.7 | 1.05 | 1.21 | 1.34 | 1.09 | 1.81 | 3.68 | 1.13 |
| F34 | 26.4 | 177.8 | 76 | 2.33 | 28550 | 1.0 | 19 × 125 | 152 | 95 | 73.2 | 81.4 | 86.6 | 95.7 | 76.1 | 130.0 | 289.9 | 87.2 | 1.11 | 1.18 | 1.31 | 1.04 | 1.78 | 3.96 | 1.19 |
| Mean | | | | | | | | | | | | | | | | | | 1.04 | 1.23 | 1.41 | 1.01 | 1.71 | 3.48 | 1.06 |
| SD | | | | | | | | | | | | | | | | | | 0.08 | 0.18 | 0.17 | 0.07 | 0.61 | 0.95 | 0.15 |
| CoV (%) | | | | | | | | | | | | | | | | | | 7.96 | 14.91 | 11.93 | 7.16 | 35.40 | 27.31 | 14.52 |

* Push-off tests done by Gnanasambandam (1995)

Table 7.5 Comparison of shear capacity of headed stud obtained from experiments and design equations for push-off tests with parallel decking and double stud per row

| Test* | $f_c$ (MPa) | Steel decking details | | | | | Stud details | | | Exp. Load per stud P (kN) | $P_D$ (kN) | $P_{EC4}$ (kN) | $P_{AISC}$ (kN) | $P_G$ (kN) | $P_{Yuan-S}$ (kN) | $P_{Yuan-P}$ (kN) | $P_W$ | $P_D/P$ | $P_{EC4}/P$ | $P_{AISC}/P$ | $P_G/P$ | $P_{Yuan-S}/P$ | $P_{Yuan-P}/P$ | $P_W/P$ |
|---|---|---|---|---|---|---|---|---|---|---|---|---|---|---|---|---|---|---|---|---|---|---|---|---|
| | | $b_o$ | $h_p$ | $b_o/h_p$ | $A_c$ ($mm^2$) | $t_s$ | $d \times h_{sc}$ | $l_s$ (mm) | $S_t$ | | | | | | | | | | | | | | | |
| G9-1 | 28.6 | 140 | 80 | 1.75 | 23800 | 1.2 | 19 × 125 | 250 | 64.6 | 131.1 | 109.8 | 59.6 | 95.7 | 13.4 | 106.8 | N/A | 102.1 | 0.84 | 0.45 | 0.73 | 0.10 | 0.81 | N/A | 0.78 |
| G9-2 | 28.6 | 140 | 80 | 1.75 | 23800 | 1.2 | 19 × 125 | 250 | 64.6 | 126.2 | 109.8 | 59.6 | 95.7 | 13.4 | 106.8 | N/A | 102.1 | 0.87 | 0.47 | 0.76 | 0.11 | 0.85 | N/A | 0.81 |
| G15-1 | 30.2 | 132 | 46 | 2.87 | 17741 | 1.0 | 19 × 95 | 220 | 64.6 | 101.9 | 95.4 | 102.1 | 95.7 | 44.9 | 99.1 | N/A | 84.7 | 0.94 | 1.00 | 0.94 | 0.44 | 0.97 | N/A | 0.83 |
| G15-2 | 30.2 | 132 | 46 | 2.87 | 17741 | 1.0 | 19 × 95 | 220 | 64.6 | 96.3 | 95.4 | 102.1 | 95.7 | 44.9 | 99.1 | N/A | 84.7 | 0.99 | 1.06 | 0.99 | 0.47 | 1.03 | N/A | 0.88 |
| G16-1 | 33.2 | 160 | 50 | 3.2 | 20600 | 1.0 | 19 × 95 | 220 | 85.5 | 108.8 | 101.1 | 102.1 | 95.7 | 48.2 | 105.0 | N/A | 91.6 | 0.93 | 0.94 | 0.88 | 0.44 | 0.97 | N/A | 0.84 |
| G16-2 | 33.2 | 160 | 50 | 3.2 | 20600 | 1.0 | 19 × 95 | 220 | 85.5 | 114.5 | 101.1 | 102.1 | 95.7 | 48.2 | 105.0 | N/A | 91.6 | 0.88 | 0.89 | 0.84 | 0.42 | 0.92 | N/A | 0.80 |
| G17-1 | 22.2 | 173 | 60 | 2.88 | 21300 | 1.2 | 19 × 95 | 110 | 100.7 | 87.8 | 76.4 | 86.3 | 95.7 | 70.3 | 81.6 | N/A | 59.6 | 0.87 | 0.98 | 1.09 | 0.80 | 0.93 | N/A | 0.68 |
| G17-2 | 24.2 | 173 | 60 | 2.88 | 21300 | 1.2 | 19 × 95 | 110 | 100.7 | 85.7 | 78.6 | 90.9 | 95.7 | 73.4 | 82.4 | N/A | 62.2 | 0.92 | 1.06 | 1.12 | 0.86 | 0.96 | N/A | 0.73 |
| Mean | | | | | | | | | | | | | | | | | | 0.90 | 0.86 | 0.92 | 0.45 | 0.93 | N/A | 0.79 |
| SD | | | | | | | | | | | | | | | | | | 0.05 | 0.25 | 0.14 | 0.27 | 0.07 | N/A | 0.06 |
| CoV (%) | | | | | | | | | | | | | | | | | | 5.38 | 29.12 | 15.64 | 60.50 | 7.53 | N/A | 8.17 |

* Push-off tests done by Johnson and Yuan (1998a)

Table 7.6 Comparison of shear capacity of headed stud obtained from experiments and design equations for push-off tests with parallel decking and double stud per row

| Test* | $f_c$ (MPa) | Steel decking details | | | | | Stud details | | | Exp. Load per stud P (kN) | $P_D$ (kN) | $P_{EC4}$ (kN) | $P_{AISC}$ (kN) | $P_G$ (kN) | $P_{Yuan-S}$ (kN) | $P_{Yuan-P}$ (kN) | $P_W$ | $P_D/P$ | $P_{EC4}/P$ | $P_{AISC}/P$ | $P_G/P$ | $P_{Yuan-S}/P$ | $P_{Yuan-P}/P$ | $P_W/P$ |
|---|---|---|---|---|---|---|---|---|---|---|---|---|---|---|---|---|---|---|---|---|---|---|---|---|
| | | $b_o$ | $h_p$ | $b_o/h_p$ | $A_c$ ($mm^2$) | $t_s$ | $d \times h_{sc}$ | $l_s$ (mm) | $S_t$ | | | | | | | | | | | | | | | |
| J11 | 23.4 | 120.0 | 76 | 1.58 | 19110 | 1.0 | 19 × 125 | 57 | 76 | 59.4 | 60.9 | 54.5 | 95.7 | 51.3 | 121.1 | 151.4 | 59.8 | 1.03 | 0.92 | 1.61 | 1.01 | 0.86 | 2.04 | 2.55 |
| J12 | 23.4 | 120.0 | 76 | 1.58 | 19110 | 1.0 | 19 × 125 | 85.5 | 76 | 68.6 | 65.8 | 54.5 | 95.7 | 64.0 | 121.1 | 165.8 | 64.4 | 0.96 | 0.79 | 1.40 | 0.94 | 0.93 | 1.77 | 2.42 |
| J13 | 23.4 | 120.0 | 76 | 1.58 | 19110 | 1.0 | 19 × 125 | 114 | 76 | 74.7 | 70.7 | 54.5 | 95.7 | 70.2 | 121.1 | 181.4 | 68.9 | 0.95 | 0.73 | 1.28 | 0.92 | 0.94 | 1.62 | 2.43 |
| J14 | 23.4 | 120.0 | 76 | 1.58 | 19110 | 1.0 | 19 × 125 | 152 | 76 | 70.1 | 77.3 | 54.5 | 95.7 | 68.6 | 121.1 | 152.6 | 75.0 | 1.10 | 0.78 | 1.37 | 1.07 | 0.98 | 1.73 | 2.18 |
| J21 | 23.4 | 120.0 | 76 | 3.32 | 38060 | 1.0 | 19 × 125 | 57 | 76 | 73.5 | 76.8 | 114.5 | 95.7 | 58.5 | 160.2 | 304.7 | 76.3 | 1.04 | 1.56 | 1.30 | 1.04 | 0.80 | 2.18 | 4.15 |
| J22 | 23.4 | 120.0 | 76 | 3.32 | 38060 | 1.0 | 19 × 125 | 85.5 | 76 | 80.9 | 81.7 | 114.5 | 95.7 | 71.2 | 160.2 | 334.3 | 80.8 | 1.01 | 1.42 | 1.18 | 1.00 | 0.88 | 1.98 | 4.13 |
| J23 | 23.4 | 120.0 | 76 | 3.32 | 38060 | 1.0 | 19 × 125 | 114 | 76 | 86.4 | 86.6 | 114.5 | 95.7 | 77.4 | 160.2 | 369.4 | 85.4 | 1.00 | 1.33 | 1.11 | 0.99 | 0.90 | 1.85 | 4.28 |
| J24 | 23.4 | 120.0 | 76 | 3.32 | 38060 | 1.0 | 19 × 125 | 152 | 76 | 87.3 | 93.1 | 114.5 | 95.7 | 75.8 | 160.2 | 440.9 | 91.4 | 1.07 | 1.31 | 1.10 | 1.05 | 0.87 | 1.83 | 5.05 |
| L11 | 40 | 177.8 | 76 | 2.33 | 28550 | 1.0 | 19 × 125 | 57 | 76 | 84.8 | 87.2 | 92.0 | 95.7 | 71.1 | 168.6 | 272.6 | 87.5 | 1.03 | 1.09 | 1.13 | 1.03 | 0.84 | 1.99 | 3.21 |
| L12 | 40 | 177.8 | 76 | 2.33 | 28550 | 1.0 | 19 × 125 | 85.5 | 76 | 99 | 92.1 | 92.0 | 95.7 | 87.7 | 168.6 | 302.9 | 93.4 | 0.93 | 0.93 | 0.97 | 0.94 | 0.89 | 1.70 | 3.06 |
| L13 | 40 | 177.8 | 76 | 2.33 | 28550 | 1.0 | 19 × 125 | 114 | 76 | 98.6 | 97.0 | 92.0 | 95.7 | 95.9 | 168.6 | 338.7 | 99.4 | 0.98 | 0.93 | 0.97 | 1.01 | 0.97 | 1.71 | 3.43 |
| L14 | 40 | 177.8 | 76 | 2.33 | 28550 | 1.0 | 19 × 125 | 152 | 76 | 107.4 | 103.5 | 92.0 | 95.7 | 93.7 | 168.6 | 356.1 | 107.3 | 0.96 | 0.86 | 0.89 | 1.00 | 0.87 | 1.57 | 3.32 |
| L21 | 40 | 177.8 | 76 | 2.33 | 28550 | 1.0 | 19 × 125 | 57 | 95 | 91.3 | 87.2 | 92.0 | 95.7 | 71.1 | 160.0 | 263.7 | 87.5 | 0.95 | 1.01 | 1.05 | 0.96 | 0.78 | 1.75 | 2.89 |
| L22 | 40 | 177.8 | 76 | 2.33 | 28550 | 1.0 | 19 × 125 | 85.5 | 95 | 97.5 | 92.1 | 92.0 | 95.7 | 87.7 | 160.0 | 292.6 | 93.4 | 0.94 | 0.94 | 0.98 | 0.96 | 0.90 | 1.64 | 3.00 |
| L23 | 40 | 177.8 | 76 | 2.33 | 28550 | 1.0 | 19 × 125 | 114 | 95 | 104.1 | 97.0 | 92.0 | 95.7 | 95.9 | 160.0 | 324.6 | 99.4 | 0.93 | 0.88 | 0.92 | 0.95 | 0.92 | 1.54 | 3.12 |
| L24 | 40 | 177.8 | 76 | 2.33 | 28550 | 1.0 | 19 × 125 | 152 | 95 | 110.4 | 103.5 | 92.0 | 95.7 | 93.7 | 160.0 | 319.8 | 107.3 | 0.94 | 0.83 | 0.87 | 0.97 | 0.85 | 1.45 | 2.90 |
| L31 | 40 | 177.8 | 76 | 2.33 | 28550 | 1.0 | 19 × 125 | 57 | 114 | 85.5 | 87.2 | 92.0 | 95.7 | 71.1 | 154.1 | 258.9 | 87.5 | 1.02 | 1.08 | 1.12 | 1.02 | 0.83 | 1.80 | 3.03 |
| L32 | 40 | 177.8 | 76 | 2.33 | 28550 | 1.0 | 19 × 125 | 85.5 | 114 | 95.2 | 92.1 | 92.0 | 95.7 | 87.7 | 154.1 | 286.8 | 93.4 | 0.97 | 0.97 | 1.01 | 0.98 | 0.92 | 1.62 | 3.01 |

Table 7.6 (Continued)

| Test* | $f_c$ (MPa) | Steel decking details | | | | | Stud details | | | Exp. Load per stud P (kN) | $P_D$ (kN) | $P_{EC4}$ (kN) | $P_{AISC}$ (kN) | $P_G$ (kN) | $P_{Yuan-S}$ (kN) | $P_{Yuan-P}$ (kN) | $P_W$ | $P_D/P$ | $P_{EC4}/P$ | $P_{AISC}/P$ | $P_G/P$ | $P_{Yuan-S}/P$ | $P_{Yuan-P}/P$ | $P_W/P$ |
|---|---|---|---|---|---|---|---|---|---|---|---|---|---|---|---|---|---|---|---|---|---|---|---|---|
| | | $b_o$ | $h_p$ | $b_o/h_p$ | $A_c$ (mm$^2$) | $t_s$ | $d \times h_{sc}$ | $l_s$ (mm) | $S_t$ | | | | | | | | | | | | | | | |
| L33 | 40 | 177.8 | 76 | 2.33 | 28550 | 1.0 | 19 × 125 | 114 | 114 | 101.4 | 97.0 | 92.0 | 95.7 | 95.9 | 154.1 | 310.5 | 99.4 | 0.96 | 0.91 | 0.94 | 0.98 | 0.95 | 1.52 | 3.06 |
| L34 | 40 | 177.8 | 76 | 2.33 | 28550 | 1.0 | 19 × 125 | 152 | 114 | 113.2 | 103.5 | 92.0 | 95.7 | 93.7 | 154.1 | 290.9 | 107.3 | 0.91 | 0.81 | 0.85 | 0.95 | 0.83 | 1.36 | 2.57 |
| M11 | 42.1 | 222.0 | 76 | 2.92 | 34218 | 1.0 | 19 × 125 | 57 | 76 | 89.7 | 94.2 | 102.1 | 95.7 | 76.2 | 197.3 | 352.7 | 97.2 | 1.05 | 1.14 | 1.07 | 1.08 | 0.85 | 2.20 | 3.93 |
| M12 | 42.1 | 222.0 | 76 | 2.92 | 34218 | 1.0 | 19 × 125 | 85.5 | 76 | 100.2 | 99.1 | 102.1 | 95.7 | 93.3 | 197.3 | 388.7 | 103.3 | 0.99 | 1.02 | 0.96 | 1.03 | 0.93 | 1.97 | 3.88 |
| M13 | 42.1 | 222.0 | 76 | 2.92 | 34218 | 1.0 | 19 × 125 | 114 | 76 | 107.8 | 104.1 | 102.1 | 95.7 | 101.6 | 197.3 | 431.2 | 109.4 | 0.97 | 0.95 | 0.89 | 1.02 | 0.94 | 1.83 | 4.00 |
| M14 | 42.1 | 222.0 | 76 | 2.92 | 34218 | 1.0 | 19 × 125 | 152 | 76 | 116.4 | 110.6 | 102.1 | 95.7 | 99.4 | 197.3 | 493.6 | 117.6 | 0.95 | 0.88 | 0.82 | 1.01 | 0.85 | 1.69 | 4.24 |
| M21 | 42.1 | 222.0 | 76 | 2.92 | 34218 | 1.0 | 19 × 125 | 57 | 95 | 95.1 | 94.2 | 102.1 | 95.7 | 76.2 | 186.6 | 339.4 | 97.2 | 0.99 | 1.07 | 1.01 | 1.02 | 0.80 | 1.96 | 3.57 |
| M22 | 42.1 | 222.0 | 76 | 2.92 | 34218 | 1.0 | 19 × 125 | 85.5 | 95 | 104.7 | 99.1 | 102.1 | 95.7 | 93.3 | 186.6 | 373.7 | 103.3 | 0.95 | 0.98 | 0.91 | 0.99 | 0.89 | 1.78 | 3.57 |
| M23 | 42.1 | 222.0 | 76 | 2.92 | 34218 | 1.0 | 19 × 125 | 114 | 95 | 109.9 | 104.1 | 102.1 | 95.7 | 101.6 | 186.6 | 414.8 | 109.4 | 0.95 | 0.93 | 0.87 | 1.00 | 0.92 | 1.70 | 3.77 |
| M24 | 42.1 | 222.0 | 76 | 2.92 | 34218 | 1.0 | 19 × 125 | 152 | 95 | 117.7 | 110.6 | 102.1 | 95.7 | 99.4 | 186.6 | 447.1 | 117.6 | 0.94 | 0.87 | 0.81 | 1.00 | 0.84 | 1.59 | 3.80 |
| M31 | 42.1 | 222.0 | 76 | 2.92 | 34218 | 1.0 | 19 × 125 | 57 | 114 | 92.5 | 94.2 | 102.1 | 95.7 | 76.2 | 176.4 | 326.8 | 97.2 | 1.02 | 1.10 | 1.03 | 1.05 | 0.82 | 1.91 | 3.53 |
| M32 | 42.1 | 222.0 | 76 | 2.92 | 34218 | 1.0 | 19 × 125 | 85.5 | 114 | 104.1 | 99.1 | 102.1 | 95.7 | 93.3 | 176.4 | 359.5 | 103.3 | 0.95 | 0.98 | 0.92 | 0.99 | 0.90 | 1.69 | 3.45 |
| M33 | 42.1 | 222.0 | 76 | 2.92 | 34218 | 1.0 | 19 × 125 | 114 | 114 | 111 | 104.1 | 102.1 | 95.7 | 101.6 | 176.4 | 400.5 | 109.4 | 0.94 | 0.92 | 0.86 | 0.99 | 0.92 | 1.59 | 3.61 |
| M34 | 42.1 | 222.0 | 76 | 2.92 | 34218 | 1.0 | 19 × 125 | 152 | 114 | 115.7 | 110.6 | 102.1 | 95.7 | 99.4 | 176.4 | 402.4 | 117.6 | 0.96 | 0.88 | 0.83 | 1.02 | 0.86 | 1.52 | 3.48 |
| Mean | | | | | | | | | | | | | | | | | | 0.98 | 0.99 | 1.03 | 1.00 | 0.88 | 1.75 | 3.39 |
| SD | | | | | | | | | | | | | | | | | | 0.05 | 0.19 | 0.19 | 0.04 | 0.05 | 0.20 | 0.64 |
| CoV (%) | | | | | | | | | | | | | | | | | | 4.64 | 18.86 | 18.43 | 3.82 | 5.81 | 11.50 | 18.88 |

* Push-off tests done by Wu (1998)

## 7.10 Conclusions

This chapter answered the question about the reliability of the existing design equations in predicting the shear capacity of headed stud placed in narrow and/or deep steel decks. The study revealed that all the design equations could not represent an accurate correlation between wide ribbed decks ($b_o/h_p \geq 1.5$) and those with narrow geometries and depths greater than 80 mm. It was found that all the existing design equations were developed based on the concept that the term ($b_o/h_p$) is in a direct relationship with the shear capacity of the stud. However, the findings from this research indicated that this concept could no longer be applicable with the existence of narrow ribbed decks ($b_o/h_p < 1.5$). Therefore, a new rule was needed to modify this concept besides introducing a new set of equations which provide more accurate results. The idea of the effective cross-sectional area of concrete ($A_c$) was assumed to replace the term ($b_o/h_p$) and see how effective this could be.

The numerical results obtained from 136 push-off tests were used to yield new formulae using the least square regression analysis method. The new equations covered a wide range of steel ribbed geometries including narrow sizes for the first time, and the correlation between narrow and wide steel decks was established through the term ($A_c$). The effectiveness of the developed equations was checked against many previous experiments. The comparison showed that the new equations worked as effectively as some design equations or even much better compared to others.

The significances of the new equations are that they represent the accurate correlation between narrow and wide ribbed decks using the effective cross-sectional area of concrete instead of the rib deck ratio. This enables to avoid any discrepancies in results and set the different ranges of rib sizes to be better covered. Moreover, the new equations differentiate between the single and double row of studs' configurations, unlike some existing design equations. This differentiation allows the shear connector resistance to be predicted more effectively. Lastly, the new equations consider some parameters which have been paid less attention to before including the sheeting thickness and the large diameter of the stud (i.e. cross-sectional area of the stud).

# Chapter 8 Conclusions and Recommendations

# Chapter 8

# Conclusions and Recommendations

## 8.1 General

The behaviour of headed stud connectors in composite beams with narrow and very deep steel decks was investigated in this research. Both secondary and primary composite beam systems were considered. The significant contribution of this research is that investigating the behaviour of composite beams with steel decks deeper than 80 mm for the first time. Critical examination was carried out on the existing design equations to see if the shear stud capacity is accurately predicted with the use of narrow ($b_o/h_p < 1.5$) and very deep decks. The necessity led to introduce new equations that provide better correlation with the test results. With high accuracy and ease of use, the new equations will enable the designers to confidently adopt them in the practice.

The research work was accomplished by modelling a vast number of 3-D push-off tests using ABAQUS/Explicit package. The applicability of the FE model regarding the best compromise between the accuracy and computational efficiency was achieved through a series of extensive validation. Afterwards, the research was split into two main parts according to the orientation of the steel deck. The most significant findings for each part are reported below.

### 8.1.1 Conclusions for the behaviour of headed stud in secondary composite beams

1. Results from the FE modelling showed that the shear stud capacity with narrow ($b_o/h_p < 1.5$) and very deep decks (i.e. 100 and 146 mm deep) was almost 65% of that obtained from the traditional steel decks (60-80 mm deep). The narrow geometry of very deep decks which offers relatively less concrete volume was the main reason behind that drastic difference.

2. It was realised that the behaviour of the headed stud was mainly affected by the concrete embedded within ribs. Therefore, new techniques were proposed to the push

test arrangement aiming at developing the strength and ductility of headed stud placed in very deep decks. That included placing studs in every alternative rib and reinforcing the concrete embedded within ribs by special wire-mesh bars layout. The first technique led the shear stud capacity to increase by an average of 20%. The use of the special wire-mesh bars was successful in suppressing the concrete damage. This resulted in an average of 24% increase in the load bearing capacity besides an upgrade in ductility as compared to the control case. These techniques would enhance the behaviour of the headed stud if they were implemented in practice.

3. The shear stud capacities obtained from the FE modelling with 100 and 146 mm deep decks were compared to the predicted strengths achieved from the existing design equations. The comparison showed that both EC4 and ANSI/AISC provisions did not account for narrow ribbed ($b_o/h_p \leq 1.5$) and very deep decks. As a result, big deviations up to 50% were found between the FE modelling and predicted strengths in most cases. New calibrations are required on both design codes to account for not only the narrow rib geometries but also the stud's position within ribs.

4. The comparison also showed that none of the current analytical methods developed by Johnson and Yuan (1998b), Konrad (2011), and Nellinger et al. (2018) had provided the desirable results. All methods were developed from tests with wide geometries and mid-deep of steel decks. Thus, the shear stud capacities obtained from narrow and very deep decks were inaccurately predicted. With no effective equation, it was necessary to propose new equations that account for steel decks deeper than 80 mm.

5. From a comprehensive parametric study that involved 240 push-off tests, new equations were developed using the regression analysis method. The developed equations accounted for each studs' layout (Central, Favourable, Unfavourable and Staggered) and covered for the first time a wide range of ribbed geometries including narrow and very deep decks especially for central stud position. The applicability of the developed equations was checked against many previous experiments. The comparison showed that the new equations were not only as effective as previous design equations but were also proven to be more valid. The accuracy in results

remained within ±10%. Besides the accuracy, the new equations are easy to use. This will help the designers to directly apply these equations in the practice.

### 8.1.2 Conclusions for the behaviour of headed stud in primary composite beams

1. Contrary to what was believed in the past, the FE modelling indicated that a bigger rib deck ratio ($b_o/h_p$) did not necessarily mean a higher shear connector resistance. Some tests with narrow ($b_o/h_p < 1.5$) and very deep decks revealed higher shear stud capacity than those with wide geometries. It was concluded that the correlation between narrow and wide ribbed decks regarding the shear connector resistance can not be addressed through the rib deck ratio.

2. A new concept was introduced to more accurately explain the correlation between narrow and wide ribbed decks. This was through the effective cross-sectional area of concrete. Tests with a large effective cross-sectional area of concrete showed more shear connector resistance than those with a small effective zone, despite the latter having bigger rib deck ratio. This finding was more justifiable to replace the old concept aligning with the rib deck ratio.

3. Checking the existing design equations showed that all equations addressed a direct relationship between the rib deck ratio and the shear connector resistance. As this concept was seen unworkable with narrow geometries, predicted strengths with such geometries were inaccurate. The EC4 greatly underestimated the shear stud capacities of tests having narrow rib geometry ($b_o/h_p < 1.5$) and steel decks in excess of 80 mm deep. The deviation in results was 60% in some cases. Similarly, the use of the American provisions resulted in undesirable predicted strengths giving a deviation of about 20%.

4. A remarkable deviation of up to 25% was seen between the FE results obtained from tests with narrow geometries and the predicted strengths calculated from the design equations developed by Gnanasambandam (1995) and Wu (1998). That deviation was because those equations were developed based on only wide ribbed decks. The highest scatter in results, however, was observed within the developed formulae by

Johnson and Yuan (1998b), as the shear stud capacities were overestimated by 5 times. Again, with no effective equation, new formulae were needed.

5. Using the results from the FE modelling with 136 push-off tests, new equations were developed by the regression analysis method. The new equations covered a wide range of steel ribbed geometries including narrow sizes, and the correlation between narrow and wide steel decks was established through the effective cross-sectional area of concrete. The effectiveness of the developed equations was checked against many previous experiments. The comparison showed that the new equations worked as effectively as some design equations or even much better compared to others.

6. The significance of the new equations is that they represent the accurate correlation between narrow and wide ribbed decks using the effective cross-sectional area of concrete instead of the rib deck ratio. This enables to avoid any discrepancies in results and set the different ranges of rib sizes to be better covered.

## 8.2 Recommendations for future work

This research work has opened up new areas for further studies. The performance of composite beams with very deep decks can be extended to involve the following suggestions:

1. Performing a full-scale test to explore the behaviour of composite beams with very deep decks. The results are fundamental to correlate between the large-scale test and small-scale push-off tests regarding the load-slip capacity.

2. Extending the present research to involve the light-weight concrete or steel fibre reinforced concrete for both secondary and primary composite beams.

3. There are limited studies accounting for the seismic effect. Further studies are needed on this area especially with steel decks deeper than 80 mm.

4. The work carried out in this research can be extended to study the behaviour of headed stud connectors at elevated temperatures. The test results can be used to

evaluate the accuracy of available fire design codes at predicting the shear stud capacity with narrow and deep decks under fire hazard.

## 8.3 Contributions to knowledge and limitations

The significance of this research is that it studied the influence of narrow and deep geometries of steel decks on the behaviour of composite beams. The literature has been enriched with such topic that received almost no attention in the past. With no relevant guidance, the existing design/theoretical equations had to be evaluated in order to decide whether those equations are effective at predicting the shear stud capacity with narrow and deep deck geometries, or new formulae are needed. As the results were in the favour of formulating new equations, the current research accomplished this objective and has filled a crucial knowledge gap where the designers can rely on the new proposed equations to achieve more accurate results. However, the validation of some new equations was limited to few experiments. Hence, the scope of research on composite beams can involve further studies on some parameters including unfavourable and staggered studs in case of the secondary composite beams and single stud per row in case of the primary composite beams.

The work herein was limited to the finite element analysis. The challenge was to introduce a robust model that is capable of capturing the load-slip behaviour and the failure mode of the headed shear connector with high accuracy. ABAQUS/Explicit package was chosen for that task where the concrete material was identified via the Concrete Damage Plasticity (CDP) method. Sensitivity analysis was undertaken on the mesh size, mass scaling factor and loading rate. Wide range of steel deck geometries, headed stud's layout and slab reinforcement were part of the extensive validation. Eventually, the best model was selected based on the reasonable compromise between the accuracy and the computational analysis, enabling afterwards for investigating the behaviour of headed stud with narrow and deep decks in detail. Nevertheless, the numerical work herein could be more credited if accompanied with experiments in future.

# References

## References

ABAQUS Documentation (2014) *ABAQUS User's Manual*. Version 6.14, Hibbitt, Karlsson and Sorenson, USA.

American Institute of Steel Construction (1999) *Load and Resistance Factor Design Specification for Structural Steel Building*. Chicago, Illinois.

American Institute of Steel Construction 360-16 (2016) *Specification for Structural Steel Buildings*. Chicago, Illinois.

Bradford, M. A., Filonov. A., Hogan, T. J., Uy, B., and Ranzi G. (2006) "Strength and ductility of shear connection in composite T-beams with trapezoidal steel decking", *The Eight International Conference on Steel, Space and Composite Structures*, Kuala Lumpur, Malaysia, pp. 15-26.

BS EN 1992-1-1, Eurocode 2: 2004. *Design of Concrete Structures: Part 1-1: General Rules and Rules for Buildings*. London: British Standard Institution.

BS EN 1994-1-1, Eurocode 4: 2004. *Design of Composite Steel and Concrete Structures: Part 1-1: General Rules and Rules for Buildings*. London: British Standard Institution.

BS5950, Part 3.1: 1990. Structural use of steelwork in buildings. British Standards Institution, London.

Canadian Standards Association (1994) *Steel Structures for Building-limit States Design: CAN/CSA-S16.1-94*. Rexdale, Ontario.

Chan, T., W., K., Rezansoff, T. and Hosain, M., U. (1986) "Behaviour of headed shear stubs in stub-girder stub-assemblages", *Canadian Journal of Civil Engineering*, 13(1), pp. 106-115.

Chen, L.Z., Ranzi, G., Jiang, S.C., Tahmasebinia, F. and Li, G.Q. (2016) "Performance and design of shear connectors in composite beams with parallel profiled sheeting at elevated temperatures", *International Journal of Steel Structures*, 16(1), pp. 217-229.

Chen, L.Z., Ranzi, G., Jiang, S.C., Tahmasebinia, F. and Li, G.Q. (2015) "Behaviour and design of shear connectors in composite slabs at elevated temperatures", *Journal of Constructional Steel Research*, 115, pp. 387-397.

Cifuentes, H. and Medina, F. (2013) "Experimental study on shear bond behaviour of composite slabs according to Eurocode 4", *Journal of Constructional Steel Research*, 82, pp. 99-110.

Colaco, J., P. (1972) "A stub-girder system for high-rise buildings", *Engineering Journal, AISC*, 9(3), pp. 89-95.

Cornelissen, H., A., W., Hordijk, D., A. and Reinhardt, H., W. (1986) "Experimental determination of crack softening characteristics of normalwieght and lightweight concrete", *Heron*, 31(2), pp. 45-56.

Easterling, W., S., Gibbings, D., R. and Murry, T., M. (1993) "Strength of shear studs in steel deck on composite beams and joists", *Engineering Journal, AISC*, 30(2), pp. 44-55.

Ellobody, E. and Young, B. (2006) "Performance of shear connection in composite beams with profiled steel sheeting", *Journal of Constructional Steel Research*, 62(7), pp. 682-694.

Ernest, S., Bridge, R., Q. and Wheeler, A. (2010) "Correlation of beam tests with pushout tests in steel-concrete composite beams", *Journal of Structural Engineering, ASCE*, 136(2), pp. 183-192.

Fisher, J., W. (1970) "Design of composite beams with formed metal deck", *Engineering Journal, AISC,* 7(3), pp. 88-96.

Gnanasambandam, C. (1995) *Headed stud connectors in solid slabs and slabs with wide ribbed metal deck*. M.Sc. Dissertation. University of Saskatchewan, Saskatoon, Canada.

Grant, J., A., Fisher, J., W. and Slutter, R., G. (1977) "Composite beams with formed steel deck", *Engineering Journal, AISC*, 14(1), pp. 24-43.

Hawkins, N., M. and Mitchell, D. (1984) "Seismic response of composite shear connections", *Journal of Structural Engineering, ASCE*, 110(9), pp. 2120-2136.

Hicks, S. (2007) "Strength and ductility of headed stud connectors welded in modern profiled steel sheeting", *The Structural Engineer*, 85(10), pp. 32-38.

Hicks, S., J. and Smith, A, L. (2014) "Stud shear connectors in composite beams that support slabs with profiled steel sheeting", *Structural Engineering International*, 24(2), pp. 246-253.

Hillerborg, A. (1985) "The theoretical basis of a method to determine the fracture energy $G_f$ of concrete", *Materials and Structures*, 18(4), pp. 291-296.

Hillerborg, A., Modeer, M. and Petersson, P., E. (1976) "Analysis of crack formation and crack growth in concrete by means of fracture mechanics and finite elements", *Cement and Concrete Research*, 6(6), pp. 773-781.

Jayas, B., S. and Hosain, M., U. (1988) "Behaviour of headed studs in composite beams: push-out tests", *Canadian Journal of Civil Engineering*, 15(2), pp. 240-253.

Jayas, B., S. and Hosain, M., U. (1989) "Behaviour of headed studs in composite beams: full-size tests" *Canadian Journal of Civil Engineering*, 16(5), pp.712-724.

Johnson R., P. and Yuan, H. (1998a) "Existing rules and new tests for stud shear connectors in troughs of profiled sheeting", *Proceeding of the Institution of Civil Engineers, Structures and Buildings*, 128(3), pp. 244-251.

Johnson R., P. and Yuan, H. (1998b) "Models and design rules for stud shear connectors in troughs of profiled sheeting", *Proceeding of the Institution of Civil Engineers, Structures and Buildings*, 128(3), pp. 252-263.

Katwal, U. Tao, Z. and Hassan, M.K. (2018) "Finite element modelling of steel-concrete composite beams with profiled steel sheeting", *Journal of Constructional Steel Research*, 146, pp. 1-15.

Kim, B., Wright, H., D. and Cairns, R. (2001) "The behaviour of through-deck welded shear connectors: an experimental and numerical study", *Journal of Constructional Steel Research*, 57(12), pp. 1359-1380.

Kingspan (2011) *Kingspan Multideck Technical Handbook*. Available at: https://www.kingspan.com/gb/en-gb/products/structural-steel-solutions/structural-steel-products/multideck. (Accessed: 30/09/2018).

Kmiecik, P. and Kaminski, M. (2011) "Modelling of reinforced concrete structures and composite structures with concrete strength degradation taken into consideration", *Archives of Civil and Mechanical Engineering*, 6(3), pp. 623-636.

Konrad M. (2011) *Structural Behaviour of Headed Studs with trapezoidal Profiled Sheeting*. PhD thesis. University of Stuttgart, Stuttgart, Germany (in German).

Kullman, R., B. and Hosain M., U. (1985) "Shear capacity of stub-girders: full scale tests", *Journal of Structural Engineering, ASCE*, 3(1), pp. 56-75.

Lam, D. and El-Lobody, E. (2005) "Behaviour of headed stud shear connectors in composite beam", *Journal of Structural Engineering, ASCE*, 131(1), pp. 96-107.

Lawson, R., M. (1992) "Shear Connection in Composite Beams", *Proceeding in Composite Construction in Steel and Concrete II, ASCE*, 14-19 June 1992, Potosi, Missouri: American Society of Civil Engineer, pp. 81-97.

Lloyd, R., M. and Wright, H., D. (1990) "Shear connection between composite slabs and steel beams", *Journal of Constructional Steel Research*, 15(4), pp. 255-285.

Lyons, J., C., Easterling, S., W. and Murry, T., M. (1996) "Strength of headed shear studs in cold-formed steel deck" Proceeding in the 13th International Specialty Conference on Cold-Formed Steel Structures, 17-18 October 1996, St. Louis, Missouri, USA, pp. 403-414.

MC 10. *CEB-FIP Model Code 2010*. Switzerland: The International Federation for Structural Concrete; 2012.

Mirza, O. and Uy, B. (2009) "Behaviour of headed stud shear connector for composite steel-concrete beams at elevated temperatures", *Journal of Constructional Steel Research*, 65(33), pp. 662-674.

Mirza, O. and Uy, B. (2010) "Effects of the combination of axial shear loading on the behaviour of headed stud steel anchors", *Engineering Structures*, 32(1), pp. 93-105.

Mottram, J., T. and Johnson, R., P. (1990) "Push tests on studs welded through profiled steel sheeting", *The Structural Engineer*, 68(10), pp. 187-193.

Nellinger, S., Eggert, F., Kuhlmann, U., Odenbreit, C. and Obiala, R. (2018) "Short-span composite beam tests to evaluate stud resistances", *Proceeding of the Institution of Civil Engineers, Structures and Building*, 171(1), pp.17-28.

Nellinger, S., Odenbreit, C., Obiala, R. and Lawson, M. (2017) "Influence of transverse loading onto push-out tests with deep steel decking", *Journal of Constructional Steel Research*, 128(1), pp. 335-353.

Nguyen, H., T. and Kim, S., E. (2009) "Finite element modeling of push-out tests for large stud shear connectors", *Journal of Constructional Steel Research*, 65(10-11), pp. 1909-1920.

Nie, J., Cai, C., S. and Wang, T. (2005) "Stiffness and Capacity of Steel-Concrete Composite Beams with Profiled Sheeting", *Journal of Engineering Structures*, 27(7), pp. 1074-1085.

Oehlers, D., J. and Johnson, R. P. (1987) "The strength of stud shear connections in composite beams", *The structural Engineer*, 65(2), pp. 44-48.

Ollgaard, J., G., Slutter, R. G. and Fisher, J., W. (1971) "Shear strength of stud connectors in lightweight and normal-weight concrete", *Engineering Journal, AISC*, 8(2), pp. 55-64.

Patrick, M. (2000) "Experimental investigation and design of longitudinal shear reinforcement in composite edge beams", *Progress in Structural Engineering and Materials*, 2(2), pp. 196-217.

Qureshi, J. (2010) *Finite Element Modelling of Steel-Concrete Composite Structures*. PhD Thesis. School of Civil Engineering, The University of Leeds, Leeds.

Qureshi, J. and Lam, D. (2012) "Behaviour of headed shear stud in composite beams with profiled metal decking", *Advanced in Structural Engineering*, 15(9), pp. 1547-1558.

Qureshi, J., Lam, D., and Ye, J. (2011) "Effect of shear connector spacing and layout on the shear connector capacity in composite beams", *Journal of Constructional Steel Research*, 67(4), pp. 706-719.

Qureshi, J., Lam, D., and Ye, J. (2011) "The influence of profiled sheeting thickness and shear connector's position on strength and ductility of headed shear connector", *Engineering Structures*, 33(5), pp. 1643-1656.

R.M. Lawson, (1997) "Shear connection in composite beams-influence of steel deck shape", *Proceeding in Engineering Foundation Conference, Composite Construction in Steel and Concrete III*, ASCE, pp. 312-324.

Rambo-Roddenberry, M. D. (2002) *Behaviour and strength of welded stud shear connector*. PhD Thesis. Virginia Polytechnic and State University, Blacksburg, Virginia, USA.

Robinson, H. (1967) "Tests on composite beams with cellular deck", Journal of the Structural Division, ASCE, 93(4), pp. 139-164.

Robinson, H. (1988) "Multiple stud shear connections in deep ribbed metal deck", *Canadian Journal of Civil Engineering*, 15(4), pp. 553-569.

Smith, A., L. and Couchman, G., H. (2010) "Strength and ductility of headed stud shear connectors in profiled sheeting", *Journal of Constructional Steel Research*, 66(6), pp. 748-754.

TATA Steel (2016) *Composite floor decking design and technical information*. Available at: https://www.tatasteelconstruction.com/en_GB/Products/structural-buildings-and-bridges/Composite-floor-deck. (Accessed: 30/09/2018).

Wang, A.J. (2011) "Numerical studies on shear connectors in push-out tests under elevated temperatures", *Structural Engineering and Mechanics*, 39(3), pp. 317-338.

Wu, H. (1998) *Headed stud shear connectors in full-size composite beams with wide ribbed metal deck*. M.Sc. Dissertation. University of Saskatchewan, Saskatoon, Canada.

# Appendix A Regression analysis for tests results with transverse steel decks

Table A.1 Regression analysis for test results with single-central stud position

| Test parameter | Concrete strength $f_c$ (MPa) | Steel decking details | | | Headed stud details | | FE load (Measured) (kN) | Predicted load (kN) | SSE* |
|---|---|---|---|---|---|---|---|---|---|
| | | $b_o$ (mm) | $h_p$ (mm) | $b_o/h_p$ | $d \times h_{sc}$ (mm) | $h_{sc}/h_p$ | | | |
| 50 mm steel deck | 12 | 160 | 50 | 3.20 | 19 × 95 | 1.9 | 62.1 | 64.5 | 0.001335 |
| | 20 | 160 | 50 | 3.20 | 19 × 95 | 1.9 | 80.3 | 75.4 | 0.001454 |
| | 30 | 160 | 50 | 3.20 | 19 × 95 | 1.9 | 99.2 | 89.0 | 0.000025 |
| | 40 | 160 | 50 | 3.20 | 19 × 95 | 1.9 | 115.6 | 102.6 | 0.000529 |
| | 12 | 160 | 50 | 3.20 | 22 × 95 | 1.9 | 77.0 | 76.7 | 0.000014 |
| | 20 | 160 | 50 | 3.20 | 22 × 95 | 1.9 | 99.1 | 87.6 | 0.000162 |
| | 30 | 160 | 50 | 3.20 | 22 × 95 | 1.9 | 117.9 | 101.2 | 0.003524 |
| | 40 | 160 | 50 | 3.20 | 22 × 95 | 1.9 | 130.3 | 114.9 | 0.002962 |
| 60 mm steel deck | 12 | 154.5 | 60 | 2.58 | 19 × 100 | 1.6 | 59.1 | 61.0 | 0.000957 |
| | 20 | 154.5 | 60 | 2.58 | 19 × 100 | 1.6 | 76.2 | 71.9 | 0.002107 |
| | 30 | 154.5 | 60 | 2.58 | 19 × 100 | 1.6 | 94.4 | 85.5 | 0.000018 |
| | 40 | 154.5 | 60 | 2.58 | 19 × 100 | 1.6 | 111.7 | 99.1 | 0.000164 |
| | 12 | 154.5 | 60 | 2.58 | 22 × 100 | 1.6 | 72.5 | 73.2 | 0.000112 |
| | 20 | 154.5 | 60 | 2.58 | 22 × 100 | 1.6 | 93.1 | 84.1 | 0.001133 |
| | 30 | 154.5 | 60 | 2.58 | 22 × 100 | 1.6 | 111.2 | 97.8 | 0.000002 |
| | 40 | 154.5 | 60 | 2.58 | 22 × 100 | 1.6 | 126.1 | 111.4 | 0.000118 |
| 76 mm steel deck | 12 | 152.5 | 76 | 2.00 | 19 × 116 | 1.5 | 56.8 | 56.7 | 0.000004 |
| | 20 | 152.5 | 76 | 2.00 | 19 × 116 | 1.5 | 73.3 | 67.6 | 0.000144 |
| | 30 | 152.5 | 76 | 2.00 | 19 × 116 | 1.5 | 89.7 | 81.2 | 0.000006 |
| | 40 | 152.5 | 76 | 2.00 | 19 × 116 | 1.5 | 103.6 | 94.9 | 0.011604 |
| | 12 | 152.5 | 76 | 2.00 | 22 × 116 | 1.5 | 68.5 | 69.0 | 0.000044 |
| | 20 | 152.5 | 76 | 2.00 | 22 × 116 | 1.5 | 88.5 | 79.9 | 0.000295 |
| | 30 | 152.5 | 76 | 2.00 | 22 × 116 | 1.5 | 105.7 | 93.5 | 0.001908 |
| | 40 | 152.5 | 76 | 2.00 | 22 × 116 | 1.5 | 117.0 | 107.1 | 0.000832 |
| 80 mm steel deck | 12 | 135.5 | 80 | 1.69 | 19 × 125 | 1.6 | 54.2 | 54.1 | 0.000002 |
| | 20 | 135.5 | 80 | 1.69 | 19 × 125 | 1.6 | 69.2 | 65.0 | 0.001080 |
| | 30 | 135.5 | 80 | 1.69 | 19 × 125 | 1.6 | 84.6 | 78.7 | 0.000208 |

| | | | | | | | | | |
|---|---|---|---|---|---|---|---|---|---|
| | 40 | 135.5 | 80 | 1.69 | 19 × 125 | 1.6 | 98.8 | 92.3 | 0.000292 |
| | 12 | 135.5 | 80 | 1.69 | 22 × 125 | 1.6 | 65.4 | 66.4 | 0.000239 |
| | 20 | 135.5 | 80 | 1.69 | 22 × 125 | 1.6 | 83.6 | 77.3 | 0.000085 |
| | 30 | 135.5 | 80 | 1.69 | 22 × 125 | 1.6 | 99.6 | 90.9 | 0.000001 |
| | 40 | 135.5 | 80 | 1.69 | 22 × 125 | 1.6 | 111.6 | 104.5 | 0.000195 |
| 100 mm steel deck | 12 | 100 | 100 | 1.00 | 19 × 140 | 1.4 | 50.2 | 48.0 | 0.002081 |
| | 20 | 100 | 100 | 1.00 | 19 × 140 | 1.4 | 59.3 | 58.9 | 0.000043 |
| | 30 | 100 | 100 | 1.00 | 19 × 140 | 1.4 | 70.7 | 72.5 | 0.000644 |
| | 40 | 100 | 100 | 1.00 | 19 × 140 | 1.4 | 82.5 | 86.2 | 0.001814 |
| | 12 | 100 | 100 | 1.00 | 22 × 140 | 1.4 | 60.1 | 60.3 | 0.000008 |
| | 20 | 100 | 100 | 1.00 | 22 × 140 | 1.4 | 71.2 | 71.2 | 0.000000 |
| | 30 | 100 | 100 | 1.00 | 22 × 140 | 1.4 | 82.9 | 84.8 | 0.000502 |
| | 40 | 100 | 100 | 1.00 | 22 × 140 | 1.4 | 92.9 | 98.4 | 0.003154 |
| 146 mm steel deck | 12 | 134 | 146 | 0.67 | 19 × 195 | 1.3 | 48.1 | 45.4 | 0.003526 |
| | 20 | 134 | 146 | 0.67 | 19 × 195 | 1.3 | 57.2 | 56.3 | 0.000252 |
| | 30 | 134 | 146 | 0.67 | 19 × 195 | 1.3 | 68.6 | 69.9 | 0.000365 |
| | 40 | 134 | 146 | 0.67 | 19 × 195 | 1.3 | 79.1 | 83.6 | 0.002854 |
| | 12 | 134 | 146 | 0.67 | 22 × 195 | 1.3 | 58.0 | 57.7 | 0.000034 |
| | 20 | 134 | 146 | 0.67 | 22 × 195 | 1.3 | 69.1 | 68.6 | 0.000061 |
| | 30 | 134 | 146 | 0.67 | 22 × 195 | 1.3 | 80.8 | 82.2 | 0.000287 |
| | 40 | 134 | 146 | 0.67 | 22 × 195 | 1.3 | 90.8 | 95.8 | 0.002747 |
| Sum (Σ) | | | | | | | | | 0.049923 |

$P_C = A\,f_{ck} + B\,A_s + C\,(h_{sc}/h_p) + D\,(b_o/h_p)^2 + E\,(b_o/h_p) + F$

A = 1.472 B = 0.140 C = 24.978 D = -3.670 E = 16.412 F = -57.577

* SSE = [(Predicted – Measured) / Predicted]$^2$

Table A.2 Regression analysis for test results with single-favourable stud position

| Test parameter | Concrete strength $f_c$ (MPa) | Steel decking details | | | Headed stud details | | FE load (Measured) (kN) | Predicted load (kN) | SSE* |
|---|---|---|---|---|---|---|---|---|---|
| | | $b_o$ (mm) | $h_p$ (mm) | $b_o/h_p$ | $d \times h_{sc}$ (mm) | $h_{sc}/h_p$ | | | |
| 50 mm steel deck | 12 | 160 | 50 | 3.2 | 19 × 95 | 1.9 | 67.1 | 69.4 | 0.001073 |
| | 20 | 160 | 50 | 3.2 | 19 × 95 | 1.9 | 87.5 | 87.0 | 0.000037 |
| | 30 | 160 | 50 | 3.2 | 19 × 95 | 1.9 | 108.1 | 109.0 | 0.000064 |
| | 40 | 160 | 50 | 3.2 | 19 × 95 | 1.9 | 126.5 | 131.0 | 0.001164 |
| | 12 | 160 | 50 | 3.2 | 22 × 95 | 1.9 | 80.5 | 78.2 | 0.000840 |
| | 20 | 160 | 50 | 3.2 | 22 × 95 | 1.9 | 105.0 | 95.8 | 0.009154 |
| | 30 | 160 | 50 | 3.2 | 22 × 95 | 1.9 | 129.8 | 117.8 | 0.010320 |
| | 40 | 160 | 50 | 3.2 | 22 × 95 | 1.9 | 151.9 | 139.8 | 0.007453 |
| 60 mm steel deck | 12 | 154.5 | 60 | 2.58 | 19 × 100 | 1.6 | 63.8 | 77.8 | 0.032305 |
| | 20 | 154.5 | 60 | 2.58 | 19 × 100 | 1.6 | 83.1 | 95.4 | 0.016573 |
| | 30 | 154.5 | 60 | 2.58 | 19 × 100 | 1.6 | 102.9 | 117.4 | 0.015213 |
| | 40 | 154.5 | 60 | 2.58 | 19 × 100 | 1.6 | 122.3 | 139.4 | 0.015010 |
| | 12 | 154.5 | 60 | 2.58 | 22 × 100 | 1.6 | 76.6 | 75.2 | 0.000329 |
| | 20 | 154.5 | 60 | 2.58 | 22 × 100 | 1.6 | 99.7 | 92.8 | 0.005470 |
| | 30 | 154.5 | 60 | 2.58 | 22 × 100 | 1.6 | 123.5 | 114.8 | 0.005697 |
| | 40 | 154.5 | 60 | 2.58 | 22 × 100 | 1.6 | 146.8 | 136.8 | 0.005308 |
| 76 mm steel deck | 12 | 152.5 | 76 | 2.00 | 19 × 116 | 1.5 | 61.9 | 61.4 | 0.000063 |
| | 20 | 152.5 | 76 | 2.00 | 19 × 116 | 1.5 | 80.3 | 79.0 | 0.000266 |
| | 30 | 152.5 | 76 | 2.00 | 19 × 116 | 1.5 | 98.2 | 101.0 | 0.000774 |
| | 40 | 152.5 | 76 | 2.00 | 19 × 116 | 1.5 | 113.4 | 123.0 | 0.006102 |
| | 12 | 152.5 | 76 | 2.00 | 22 × 116 | 1.5 | 74.3 | 70.3 | 0.003282 |
| | 20 | 152.5 | 76 | 2.00 | 22 × 116 | 1.5 | 96.3 | 87.9 | 0.009198 |
| | 30 | 152.5 | 76 | 2.00 | 22 × 116 | 1.5 | 117.9 | 109.9 | 0.005340 |
| | 40 | 152.5 | 76 | 2.00 | 22 × 116 | 1.5 | 136.1 | 131.9 | 0.001029 |
| 80 mm steel deck | 12 | 135.5 | 80 | 1.69 | 19 × 125 | 1.6 | 59.1 | 69.8 | 0.023578 |
| | 20 | 135.5 | 80 | 1.69 | 19 × 125 | 1.6 | 75.4 | 87.4 | 0.018905 |
| | 30 | 135.5 | 80 | 1.69 | 19 × 125 | 1.6 | 95.2 | 109.4 | 0.016886 |
| | 40 | 135.5 | 80 | 1.69 | 19 × 125 | 1.6 | 110.7 | 131.4 | 0.024851 |

| | | | | | | | | | |
|---|---|---|---|---|---|---|---|---|---|
| | 12 | 135.5 | 80 | 1.69 | 22 × 125 | 1.6 | 70.9 | 67.3 | 0.002901 |
| | 20 | 135.5 | 80 | 1.69 | 22 × 125 | 1.6 | 92.5 | 84.9 | 0.008070 |
| | 30 | 135.5 | 80 | 1.69 | 22 × 125 | 1.6 | 114.7 | 106.9 | 0.005363 |
| | 40 | 135.5 | 80 | 1.69 | 22 × 125 | 1.6 | 129.2 | 128.9 | 0.000006 |
| Sum (Σ) | | | | | | | | | 0.252624 |
| $P_F = A f_{ck} + B A_s + C (h_{sc}/h_p) + D (b_o/h_p) + E$<br><br>A = 2.273 B = 0.201 C = 11.250 D = - 5.007 E = - 24.7 | | | | | | | | | |

* SSE = [(Predicted – Measured) / Predicted]$^2$

Table A.3 Regression analysis for test results with single-unfavourable stud position

| Test parameter | Concrete strength $f_c$ (MPa) | Steel decking details | | | Headed stud details | | FE load (Measured) (kN) | Predicted load (kN) | SSE* |
|---|---|---|---|---|---|---|---|---|---|
| | | $b_o$ (mm) | $h_p$ (mm) | $b_o/h_p$ | $d \times h_{sc}$ (mm) | $h_{sc}/h_p$ | | | |
| 50 mm steel deck | 12 | 160 | 50 | 3.2 | 19 × 95 | 1.9 | 61.7 | 69.9 | 0.013901 |
| | 20 | 160 | 50 | 3.2 | 19 × 95 | 1.9 | 77.0 | 80.4 | 0.001815 |
| | 30 | 160 | 50 | 3.2 | 19 × 95 | 1.9 | 90.8 | 93.5 | 0.000849 |
| | 40 | 160 | 50 | 3.2 | 19 × 95 | 1.9 | 101.2 | 106.6 | 0.002588 |
| | 12 | 160 | 50 | 3.2 | 22 × 95 | 1.9 | 74.0 | 73.1 | 0.000163 |
| | 20 | 160 | 50 | 3.2 | 22 × 95 | 1.9 | 92.4 | 83.5 | 0.011234 |
| | 30 | 160 | 50 | 3.2 | 22 × 95 | 1.9 | 109.0 | 96.6 | 0.016346 |
| | 40 | 160 | 50 | 3.2 | 22 × 95 | 1.9 | 121.5 | 109.7 | 0.011478 |
| 60 mm steel deck | 12 | 154.5 | 60 | 2.58 | 19 × 100 | 1.6 | 58.7 | 72.7 | 0.037109 |
| | 20 | 154.5 | 60 | 2.58 | 19 × 100 | 1.6 | 73.1 | 83.2 | 0.014698 |
| | 30 | 154.5 | 60 | 2.58 | 19 × 100 | 1.6 | 86.4 | 96.3 | 0.010538 |
| | 40 | 154.5 | 60 | 2.58 | 19 × 100 | 1.6 | 97.8 | 109.4 | 0.011213 |
| | 12 | 154.5 | 60 | 2.58 | 22 × 100 | 1.6 | 70.5 | 69.7 | 0.000125 |
| | 20 | 154.5 | 60 | 2.58 | 22 × 100 | 1.6 | 87.7 | 80.2 | 0.008747 |
| | 30 | 154.5 | 60 | 2.58 | 22 × 100 | 1.6 | 103.7 | 93.3 | 0.012430 |
| | 40 | 154.5 | 60 | 2.58 | 22 × 100 | 1.6 | 117.4 | 106.4 | 0.010695 |
| 76 mm steel deck | 12 | 152.5 | 76 | 2.00 | 19 × 116 | 1.5 | 54.6 | 54.0 | 0.000137 |
| | 20 | 152.5 | 76 | 2.00 | 19 × 116 | 1.5 | 64.5 | 64.4 | 0.000001 |
| | 30 | 152.5 | 76 | 2.00 | 19 × 116 | 1.5 | 75.4 | 77.5 | 0.000766 |
| | 40 | 152.5 | 76 | 2.00 | 19 × 116 | 1.5 | 82.9 | 90.6 | 0.007301 |
| | 12 | 152.5 | 76 | 2.00 | 22 × 116 | 1.5 | 65.5 | 57.1 | 0.021715 |
| | 20 | 152.5 | 76 | 2.00 | 22 × 116 | 1.5 | 77.4 | 67.6 | 0.021181 |
| | 30 | 152.5 | 76 | 2.00 | 22 × 116 | 1.5 | 90.5 | 80.7 | 0.014864 |
| | 40 | 152.5 | 76 | 2.00 | 22 × 116 | 1.5 | 99.5 | 93.8 | 0.003742 |
| 80 mm steel deck | 12 | 135.5 | 80 | 1.69 | 19 × 125 | 1.6 | 49.4 | 56.7 | 0.016685 |
| | 20 | 135.5 | 80 | 1.69 | 19 × 125 | 1.6 | 54.8 | 67.2 | 0.034079 |
| | 30 | 135.5 | 80 | 1.69 | 19 × 125 | 1.6 | 64.1 | 80.3 | 0.040722 |
| | 40 | 135.5 | 80 | 1.69 | 19 × 125 | 1.6 | 75.5 | 93.4 | 0.036743 |

| | | | | | | | | | |
|---|---|---|---|---|---|---|---|---|---|
| | 12 | 135.5 | 80 | 1.69 | 22 × 125 | 1.6 | 55.7 | 53.7 | 0.001328 |
| | 20 | 135.5 | 80 | 1.69 | 22 × 125 | 1.6 | 65.8 | 64.2 | 0.000605 |
| | 30 | 135.5 | 80 | 1.69 | 22 × 125 | 1.6 | 76.9 | 77.3 | 0.000029 |
| | 40 | 135.5 | 80 | 1.69 | 22 × 125 | 1.6 | 90.6 | 90.4 | 0.000004 |
| Sum (Σ) | | | | | | | | | 0.363831 |
| $P_U = A\,f_{ck} + B\,A_s + C\,(h_{sc}/h_p) + D\,(b_o/h_p) + E$<br><br>A = 1.339 B = 0.149 C = 27.571 D = 8.179 E = - 70.027 | | | | | | | | | |

* SSE = $[(\text{Predicted} - \text{Measured}) / \text{Predicted}]^2$

# Appendix B Regression analysis for tests results with parallel steel decks

Table B.1 Regression analysis for test results with single stud per row

| Test | Concrete strength $f_c$ (MPa) | Steel decking details | | | | Effective shear area $A_c$ (mm$^2$) | Headed stud details | | FE load (Measured) (kN) | Predicted load (kN) | SSE |
|---|---|---|---|---|---|---|---|---|---|---|---|
| | | $b_o$ (mm) | $h_p$ (mm) | $b_o/h_p$ | $t_s$ (mm) | | $d \times h_{sc}$ (mm) | $l_s$ (mm) | | | |
| A11 | 12 | 97.5 | 146 | 0.67 | 1.2 | 23481 | 19 × 195 | 57 | 51.9 | 53.9 | 0.001383 |
| A12 | 12 | 97.5 | 146 | 0.67 | 1.2 | 23481 | 19 × 195 | 85.5 | 59.6 | 58.5 | 0.000341 |
| A13 | 12 | 97.5 | 146 | 0.67 | 1.2 | 23481 | 19 × 195 | 114 | 66.4 | 63.1 | 0.002677 |
| A14 | 12 | 97.5 | 146 | 0.67 | 1.2 | 23481 | 19 × 195 | 152 | 72.3 | 69.3 | 0.001892 |
| A21 | 20 | 97.5 | 146 | 0.67 | 1.2 | 23481 | 19 × 195 | 57 | 60.7 | 62.2 | 0.000579 |
| A22 | 20 | 97.5 | 146 | 0.67 | 1.2 | 23481 | 19 × 195 | 85.5 | 67.3 | 66.8 | 0.000054 |
| A23 | 20 | 97.5 | 146 | 0.67 | 1.2 | 23481 | 19 × 195 | 114 | 73.4 | 71.4 | 0.000764 |
| A24 | 20 | 97.5 | 146 | 0.67 | 1.2 | 23481 | 19 × 195 | 152 | 77.1 | 77.6 | 0.000038 |
| A31 | 30 | 97.5 | 146 | 0.67 | 1.2 | 23481 | 19 × 195 | 57 | 71.5 | 72.6 | 0.000214 |
| A32 | 30 | 97.5 | 146 | 0.67 | 1.2 | 23481 | 19 × 195 | 85.5 | 77.8 | 77.2 | 0.000066 |
| A33 | 30 | 97.5 | 146 | 0.67 | 1.2 | 23481 | 19 × 195 | 114 | 82.9 | 81.8 | 0.000184 |
| A34 | 30 | 97.5 | 146 | 0.67 | 1.2 | 23481 | 19 × 195 | 152 | 87.2 | 87.9 | 0.000071 |
| A41 | 40 | 97.5 | 146 | 0.67 | 1.2 | 23481 | 19 × 195 | 57 | 83.6 | 82.9 | 0.000066 |
| A42 | 40 | 97.5 | 146 | 0.67 | 1.2 | 23481 | 19 × 195 | 85.5 | 88.4 | 87.5 | 0.000097 |
| A43 | 40 | 97.5 | 146 | 0.67 | 1.2 | 23481 | 19 × 195 | 114 | 92.6 | 92.2 | 0.000023 |
| A44 | 40 | 97.5 | 146 | 0.67 | 1.2 | 23481 | 19 × 195 | 152 | 95.3 | 98.3 | 0.000936 |
| B11 | 12 | 167.5 | 146 | 1.15 | 1.2 | 38531 | 19 × 195 | 57 | 59.7 | 63.2 | 0.003142 |
| B12 | 12 | 167.5 | 146 | 1.15 | 1.2 | 38531 | 19 × 195 | 85.5 | 66.8 | 67.9 | 0.000244 |
| B13 | 12 | 167.5 | 146 | 1.15 | 1.2 | 38531 | 19 × 195 | 114 | 71.7 | 72.5 | 0.000114 |
| B14 | 12 | 167.5 | 146 | 1.15 | 1.2 | 38531 | 19 × 195 | 152 | 76.6 | 78.6 | 0.000665 |
| B21 | 20 | 167.5 | 146 | 1.15 | 1.2 | 38531 | 19 × 195 | 57 | 69.8 | 71.5 | 0.000589 |
| B22 | 20 | 167.5 | 146 | 1.15 | 1.2 | 38531 | 19 × 195 | 85.5 | 76 | 76.2 | 0.000004 |
| B23 | 20 | 167.5 | 146 | 1.15 | 1.2 | 38531 | 19 × 195 | 114 | 80.7 | 80.8 | 0.000001 |
| B24 | 20 | 167.5 | 146 | 1.15 | 1.2 | 38531 | 19 × 195 | 152 | 83.7 | 86.9 | 0.001371 |
| B31 | 30 | 167.5 | 146 | 1.15 | 1.2 | 38531 | 19 × 195 | 57 | 81.9 | 81.9 | 0.000000 |
| B32 | 30 | 167.5 | 146 | 1.15 | 1.2 | 38531 | 19 × 195 | 85.5 | 87.5 | 86.5 | 0.000129 |
| B33 | 30 | 167.5 | 146 | 1.15 | 1.2 | 38531 | 19 × 195 | 114 | 91.2 | 91.1 | 0.000001 |

| | | | | | | | | | | | |
|---|---|---|---|---|---|---|---|---|---|---|---|
| B34 | 30 | 167.5 | 146 | 1.15 | 1.2 | 38531 | 19 × 195 | 152 | 94.2 | 97.3 | 0.001005 |
| B41 | 40 | 167.5 | 146 | 1.15 | 1.2 | 38531 | 19 × 195 | 57 | 95.2 | 92.3 | 0.001011 |
| B42 | 40 | 167.5 | 146 | 1.15 | 1.2 | 38531 | 19 × 195 | 85.5 | 98.1 | 96.9 | 0.000158 |
| B43 | 40 | 167.5 | 146 | 1.15 | 1.2 | 38531 | 19 × 195 | 114 | 101.9 | 101.5 | 0.000016 |
| B44 | 40 | 167.5 | 146 | 1.15 | 1.2 | 38531 | 19 × 195 | 152 | 103.9 | 107.6 | 0.001212 |
| C12 | 12 | 150 | 76 | 1.97 | 1.2 | 23738 | 19 × 125 | 57 | 53.2 | 54.1 | 0.000255 |
| C12 | 12 | 150 | 76 | 1.97 | 1.2 | 23738 | 19 × 125 | 85.5 | 60.8 | 58.7 | 0.001307 |
| C13 | 12 | 150 | 76 | 1.97 | 1.2 | 23738 | 19 × 125 | 114 | 65.2 | 63.3 | 0.000908 |
| C14 | 12 | 150 | 76 | 1.97 | 1.2 | 23738 | 19 × 125 | 152 | 70.6 | 69.4 | 0.000276 |
| C21 | 20 | 150 | 76 | 1.97 | 1.2 | 23738 | 19 × 125 | 57 | 62.8 | 62.4 | 0.000051 |
| C22 | 20 | 150 | 76 | 1.97 | 1.2 | 23738 | 19 × 125 | 85.5 | 68.6 | 67.0 | 0.000592 |
| C23 | 20 | 150 | 76 | 1.97 | 1.2 | 23738 | 19 × 125 | 114 | 74.6 | 71.6 | 0.001774 |
| C24 | 20 | 150 | 76 | 1.97 | 1.2 | 23738 | 19 × 125 | 152 | 78.9 | 77.7 | 0.000224 |
| C31 | 30 | 150 | 76 | 1.97 | 1.2 | 23738 | 19 × 125 | 57 | 71.1 | 72.7 | 0.000496 |
| C32 | 30 | 150 | 76 | 1.97 | 1.2 | 23738 | 19 × 125 | 85.5 | 79.2 | 77.3 | 0.000582 |
| C33 | 30 | 150 | 76 | 1.97 | 1.2 | 23738 | 19 × 125 | 114 | 83.9 | 81.9 | 0.000567 |
| C34 | 30 | 150 | 76 | 1.97 | 1.2 | 23738 | 19 × 125 | 152 | 88.4 | 88.1 | 0.000011 |
| C41 | 40 | 150 | 76 | 1.97 | 1.2 | 23738 | 19 × 125 | 57 | 84.7 | 83.1 | 0.000378 |
| C42 | 40 | 150 | 76 | 1.97 | 1.2 | 23738 | 19 × 125 | 85.5 | 89.9 | 87.7 | 0.000630 |
| C43 | 40 | 150 | 76 | 1.97 | 1.2 | 23738 | 19 × 125 | 114 | 94.6 | 92.3 | 0.000613 |
| C44 | 40 | 150 | 76 | 1.97 | 1.2 | 23738 | 19 × 125 | 152 | 97 | 98.5 | 0.000222 |
| D12 | 12 | 79.3 | 76 | 1.04 | 1.2 | 13238 | 19 × 125 | 57 | 44.9 | 47.5 | 0.003100 |
| D12 | 12 | 79.3 | 76 | 1.04 | 1.2 | 13238 | 19 × 125 | 85.5 | 53.6 | 52.2 | 0.000760 |
| D13 | 12 | 79.3 | 76 | 1.04 | 1.2 | 13238 | 19 × 125 | 114 | 60.2 | 56.8 | 0.003636 |
| D14 | 12 | 79.3 | 76 | 1.04 | 1.2 | 13238 | 19 × 125 | 152 | 65.8 | 62.9 | 0.002081 |
| D21 | 20 | 79.3 | 76 | 1.04 | 1.2 | 13238 | 19 × 125 | 57 | 50.4 | 55.8 | 0.009487 |
| D22 | 20 | 79.3 | 76 | 1.04 | 1.2 | 13238 | 19 × 125 | 85.5 | 60.1 | 60.5 | 0.000034 |
| D23 | 20 | 79.3 | 76 | 1.04 | 1.2 | 13238 | 19 × 125 | 114 | 64.9 | 65.1 | 0.000007 |
| D24 | 20 | 79.3 | 76 | 1.04 | 1.2 | 13238 | 19 × 125 | 152 | 69.4 | 71.2 | 0.000654 |
| D31 | 30 | 79.3 | 76 | 1.04 | 1.2 | 13238 | 19 × 125 | 57 | 62.5 | 66.2 | 0.003129 |
| D32 | 30 | 79.3 | 76 | 1.04 | 1.2 | 13238 | 19 × 125 | 85.5 | 70.7 | 70.8 | 0.000003 |
| D33 | 30 | 79.3 | 76 | 1.04 | 1.2 | 13238 | 19 × 125 | 114 | 74.4 | 75.4 | 0.000187 |

| | | | | | | | | | | | |
|---|---|---|---|---|---|---|---|---|---|---|---|
| D34 | 30 | 79.3 | 76 | 1.04 | 1.2 | 13238 | 19 × 125 | 152 | 79 | 81.6 | 0.001004 |
| D41 | 40 | 79.3 | 76 | 1.04 | 1.2 | 13238 | 19 × 125 | 57 | 72.8 | 76.6 | 0.002421 |
| D42 | 40 | 79.3 | 76 | 1.04 | 1.2 | 13238 | 19 × 125 | 85.5 | 79.7 | 81.2 | 0.000333 |
| D43 | 40 | 79.3 | 76 | 1.04 | 1.2 | 13238 | 19 × 125 | 114 | 84.1 | 85.8 | 0.000391 |
| D44 | 40 | 79.3 | 76 | 1.04 | 1.2 | 13238 | 19 × 125 | 152 | 89.2 | 91.9 | 0.000894 |
| H11 | 12 | 97.5 | 146 | 0.67 | 1.5 | 23481 | 19 × 195 | 85.5 | 70.3 | 66.4 | 0.003521 |
| H12 | 20 | 97.5 | 146 | 0.67 | 1.5 | 23481 | 19 × 195 | 85.5 | 78.7 | 74.7 | 0.002937 |
| H13 | 30 | 97.5 | 146 | 0.67 | 1.5 | 23481 | 19 × 195 | 85.5 | 89.5 | 85.0 | 0.002779 |
| H14 | 40 | 97.5 | 146 | 0.67 | 1.5 | 23481 | 19 × 195 | 85.5 | 100.8 | 95.4 | 0.003225 |
| I11 | 12 | 97.5 | 146 | 0.67 | 2.0 | 23481 | 19 × 195 | 85.5 | 76.3 | 79.4 | 0.001557 |
| I12 | 20 | 97.5 | 146 | 0.67 | 2.0 | 23481 | 19 × 195 | 85.5 | 85.5 | 87.7 | 0.000644 |
| I13 | 30 | 97.5 | 146 | 0.67 | 2.0 | 23481 | 19 × 195 | 85.5 | 96.5 | 98.1 | 0.000263 |
| I14 | 40 | 97.5 | 146 | 0.67 | 2.0 | 23481 | 19 × 195 | 85.5 | 108.7 | 108.5 | 0.000005 |
| L11 | 12 | 97.5 | 146 | 0.67 | 1.2 | 23481 | 22 × 195 | 100 | 74.5 | 77.4 | 0.001411 |
| L12 | 20 | 97.5 | 146 | 0.67 | 1.2 | 23481 | 22 × 195 | 100 | 84.8 | 85.7 | 0.000110 |
| L13 | 30 | 97.5 | 146 | 0.67 | 1.2 | 23481 | 22 × 195 | 100 | 96.1 | 96.1 | 0.000000 |
| L14 | 40 | 97.5 | 146 | 0.67 | 1.2 | 23481 | 22 × 195 | 100 | 110.2 | 106.4 | 0.001256 |
| Sum (Σ) | | | | | | | | | | | 0.073763 |

$P_S = A\,f_{ck} + B\,A_s + C\,l_s + D\,t_s + E\,A_c + F$

A = 1.036 B = 0.154 C = 0.162 D = 26.144 E = 0.001 F = - 57.504

Table B.2 Regression analysis for test results with double studs per row

| Test | Concrete strength $f_c$ (MPa) | Steel decking details | | | | Effective shear area $A_c$ (mm$^2$) | Headed stud details | | FE load (Measured) (kN) | Predicted load (kN) | SSE |
|---|---|---|---|---|---|---|---|---|---|---|---|
| | | $b_o$ (mm) | $h_p$ (mm) | $b_o/h_p$ | $t_s$ (mm) | | $d \times h_{sc}$ (mm) | $l_s$ (mm) | | | |
| E11 | 12 | 167.5 | 146 | 1.15 | 1.2 | 38531 | 19 × 195 | 57 | 67.1 | 70.5 | 0.002267 |
| E12 | 12 | 167.5 | 146 | 1.15 | 1.2 | 38531 | 19 × 195 | 85.5 | 75.2 | 75.4 | 0.000005 |
| E13 | 12 | 167.5 | 146 | 1.15 | 1.2 | 38531 | 19 × 195 | 114 | 80.4 | 80.3 | 0.000002 |
| E14 | 12 | 167.5 | 146 | 1.15 | 1.2 | 38531 | 19 × 195 | 152 | 85.8 | 86.8 | 0.000139 |
| E21 | 20 | 167.5 | 146 | 1.15 | 1.2 | 38531 | 19 × 195 | 57 | 76.1 | 79.3 | 0.001632 |
| E22 | 20 | 167.5 | 146 | 1.15 | 1.2 | 38531 | 19 × 195 | 85.5 | 83.5 | 84.2 | 0.000072 |
| E23 | 20 | 167.5 | 146 | 1.15 | 1.2 | 38531 | 19 × 195 | 114 | 88.8 | 89.1 | 0.000013 |
| E24 | 20 | 167.5 | 146 | 1.15 | 1.2 | 38531 | 19 × 195 | 152 | 92.9 | 95.7 | 0.000840 |
| E31 | 30 | 167.5 | 146 | 1.15 | 1.2 | 38531 | 19 × 195 | 57 | 88.8 | 90.4 | 0.000300 |
| E32 | 30 | 167.5 | 146 | 1.15 | 1.2 | 38531 | 19 × 195 | 85.5 | 95 | 95.3 | 0.000008 |
| E33 | 30 | 167.5 | 146 | 1.15 | 1.2 | 38531 | 19 × 195 | 114 | 98.9 | 100.2 | 0.000165 |
| E34 | 30 | 167.5 | 146 | 1.15 | 1.2 | 38531 | 19 × 195 | 152 | 102.2 | 106.7 | 0.001804 |
| E41 | 40 | 167.5 | 146 | 1.15 | 1.2 | 38531 | 19 × 195 | 57 | 102.8 | 101.4 | 0.000184 |
| E42 | 40 | 167.5 | 146 | 1.15 | 1.2 | 38531 | 19 × 195 | 85.5 | 106 | 106.3 | 0.000010 |
| E43 | 40 | 167.5 | 146 | 1.15 | 1.2 | 38531 | 19 × 195 | 114 | 110 | 111.2 | 0.000125 |
| E44 | 40 | 167.5 | 146 | 1.15 | 1.2 | 38531 | 19 × 195 | 152 | 112.2 | 117.8 | 0.002255 |
| F11 | 12 | 150 | 76 | 1.97 | 1.2 | 23738 | 19 × 125 | 57 | 59.2 | 58.1 | 0.000388 |
| F12 | 12 | 150 | 76 | 1.97 | 1.2 | 23738 | 19 × 125 | 85.5 | 67.5 | 63.0 | 0.005181 |
| F13 | 12 | 150 | 76 | 1.97 | 1.2 | 23738 | 19 × 125 | 114 | 73.1 | 67.9 | 0.005918 |
| F14 | 12 | 150 | 76 | 1.97 | 1.2 | 23738 | 19 × 125 | 152 | 79.6 | 74.4 | 0.004833 |
| F21 | 20 | 150 | 76 | 1.97 | 1.2 | 23738 | 19 × 125 | 57 | 68.3 | 66.9 | 0.000435 |
| F22 | 20 | 150 | 76 | 1.97 | 1.2 | 23738 | 19 × 125 | 85.5 | 74.9 | 71.8 | 0.001844 |
| F23 | 20 | 150 | 76 | 1.97 | 1.2 | 23738 | 19 × 125 | 114 | 80.7 | 76.7 | 0.002682 |
| F24 | 20 | 150 | 76 | 1.97 | 1.2 | 23738 | 19 × 125 | 152 | 86 | 83.3 | 0.001071 |
| F31 | 30 | 150 | 76 | 1.97 | 1.2 | 23738 | 19 × 125 | 57 | 79.5 | 78.0 | 0.000387 |
| F32 | 30 | 150 | 76 | 1.97 | 1.2 | 23738 | 19 × 125 | 85.5 | 85.6 | 82.9 | 0.001080 |
| F33 | 30 | 150 | 76 | 1.97 | 1.2 | 23738 | 19 × 125 | 114 | 90 | 87.8 | 0.000635 |
| F34 | 30 | 150 | 76 | 1.97 | 1.2 | 23738 | 19 × 125 | 152 | 93.3 | 94.3 | 0.000120 |

| | | | | | | | | | | | |
|---|---|---|---|---|---|---|---|---|---|---|---|
| F41 | 40 | 150 | 76 | 1.97 | 1.2 | 23738 | 19 × 125 | 57 | 91.2 | 89.0 | 0.000596 |
| F42 | 40 | 150 | 76 | 1.97 | 1.2 | 23738 | 19 × 125 | 85.5 | 97.7 | 93.9 | 0.001604 |
| F43 | 40 | 150 | 76 | 1.97 | 1.2 | 23738 | 19 × 125 | 114 | 102.4 | 98.8 | 0.001291 |
| F44 | 40 | 150 | 76 | 1.97 | 1.2 | 23738 | 19 × 125 | 152 | 107.6 | 105.4 | 0.000437 |
| G11 | 12 | 141 | 60 | 2.35 | 1.2 | 17520 | 19 × 100 | 57 | 49.7 | 52.8 | 0.003543 |
| G12 | 12 | 141 | 60 | 2.35 | 1.2 | 17520 | 19 × 100 | 85.5 | 56.5 | 57.8 | 0.000473 |
| G13 | 12 | 141 | 60 | 2.35 | 1.2 | 17520 | 19 × 100 | 114 | 64.2 | 62.7 | 0.000598 |
| G14 | 12 | 141 | 60 | 2.35 | 1.2 | 17520 | 19 × 100 | 152 | 68.7 | 69.2 | 0.000055 |
| G21 | 20 | 141 | 60 | 2.35 | 1.2 | 17520 | 19 × 100 | 57 | 58 | 61.7 | 0.003585 |
| G22 | 20 | 141 | 60 | 2.35 | 1.2 | 17520 | 19 × 100 | 85.5 | 64.6 | 66.6 | 0.000906 |
| G23 | 20 | 141 | 60 | 2.35 | 1.2 | 17520 | 19 × 100 | 114 | 70.8 | 71.5 | 0.000100 |
| G24 | 20 | 141 | 60 | 2.35 | 1.2 | 17520 | 19 × 100 | 152 | 75.7 | 78.1 | 0.000916 |
| G31 | 30 | 141 | 60 | 2.35 | 1.2 | 17520 | 19 × 100 | 57 | 67.7 | 72.8 | 0.004827 |
| G32 | 30 | 141 | 60 | 2.35 | 1.2 | 17520 | 19 × 100 | 85.5 | 74.8 | 77.7 | 0.001361 |
| G33 | 30 | 141 | 60 | 2.35 | 1.2 | 17520 | 19 × 100 | 114 | 81.6 | 82.6 | 0.000140 |
| G34 | 30 | 141 | 60 | 2.35 | 1.2 | 17520 | 19 × 100 | 152 | 87.4 | 89.1 | 0.000374 |
| G41 | 40 | 141 | 60 | 2.35 | 1.2 | 17520 | 19 × 100 | 57 | 80 | 83.8 | 0.002072 |
| G42 | 40 | 141 | 60 | 2.35 | 1.2 | 17520 | 19 × 100 | 85.5 | 87.1 | 88.7 | 0.000336 |
| G43 | 40 | 141 | 60 | 2.35 | 1.2 | 17520 | 19 × 100 | 114 | 93.1 | 93.6 | 0.000033 |
| G44 | 40 | 141 | 60 | 2.35 | 1.2 | 17520 | 19 × 100 | 152 | 97.7 | 100.2 | 0.000615 |
| J11 | 12 | 167.5 | 146 | 1.15 | 1.5 | 38531 | 19 × 195 | 85.5 | 88.3 | 84.3 | 0.002295 |
| J12 | 20 | 167.5 | 146 | 1.15 | 1.5 | 38531 | 19 × 195 | 85.5 | 97.4 | 93.1 | 0.002121 |
| J13 | 30 | 167.5 | 146 | 1.15 | 1.5 | 38531 | 19 × 195 | 85.5 | 109.1 | 104.2 | 0.002237 |
| J14 | 40 | 167.5 | 146 | 1.15 | 1.5 | 38531 | 19 × 195 | 85.5 | 120.8 | 115.2 | 0.002334 |
| K11 | 12 | 167.5 | 146 | 1.15 | 2.0 | 38531 | 19 × 195 | 85.5 | 95.2 | 99.0 | 0.001479 |
| K12 | 20 | 167.5 | 146 | 1.15 | 2.0 | 38531 | 19 × 195 | 85.5 | 104.2 | 107.9 | 0.001149 |
| K13 | 30 | 167.5 | 146 | 1.15 | 2.0 | 38531 | 19 × 195 | 85.5 | 118.2 | 118.9 | 0.000036 |
| K14 | 40 | 167.5 | 146 | 1.15 | 2.0 | 38531 | 19 × 195 | 85.5 | 131.1 | 130.0 | 0.000075 |
| M11 | 12 | 167.5 | 146 | 1.15 | 1.2 | 38531 | 22 × 195 | 100 | 91.7 | 93.8 | 0.000510 |
| M12 | 20 | 167.5 | 146 | 1.15 | 1.2 | 38531 | 22 × 195 | 100 | 101.5 | 102.7 | 0.000129 |
| M13 | 30 | 167.5 | 146 | 1.15 | 1.2 | 38531 | 22 × 195 | 100 | 114.8 | 113.7 | 0.000089 |
| M14 | 40 | 167.5 | 146 | 1.15 | 1.2 | 38531 | 22 × 195 | 100 | 127 | 124.8 | 0.000314 |

| Sum (Σ) | 0.071025 |
|---|---|
| $P_D = A f_{ck} + B A_s + C l_s + D t_s + E A_c + F$<br><br>A = 1.106 B = 0.147 C = 0.172 D = 29.488 E = 0.001 F = - 62.085 | |

# Author's Publications

## Journal Papers

Albarram, A., Qureshi, J. and Abbas A. (2018) "Effect of rib geometry in steel-concrete composite beams with deep profiled sheeting" *International Journal of Steel Structures*. (Under Review).

## Conference Articles

Albarram, A., Qureshi, J. and Abbas A. (2018) "Behaviour of composite beams with narrow and wide parallel ribbed steel decking", *Proceeding of 114th The IRES International Conference*, London, UK, 7-8 May, pp. 1-11.

Albarram, A., Qureshi, J. and Abbas, A. (2017) "Developing the strength and ductility of shear stud connection in deep profiled decking", *Proceeding of the 2017 World Congress on Advances in Structural Engineering and Mechanics*, Ilsan, South Korea, 28 Aug. – 1 Sep., pp. 1-12.

Albarram, A., Qureshi, J. and Abbas, A. (2017) "Effect of large stud shear connectors on the behaviour of composite beams with 146 mm deep decking", *Proceeding of the 3rd International Conference on Structural Architectural and Civil Engineering*, Pattaya, Thailand, 8-9 Jul., pp. 99-103.

Albarram, A., Qureshi, J. and Abbas, A. (2017) "Behaviour of steel-concrete composite beams with deep profiled sheeting", *Proceeding of the 19th Young Researcher's Conference*, The Institution of Structural Engineers, London, UK, 5 Apr., pp. 20-21.

## Poster presentation

Albarram, A., Qureshi, J. and Abbas A. (2016) "The influence of profiled sheeting depth on the behaviour of composite beams" *University of East London Research Conference*, 29 Jun., (winning the first prize for best poster presentation).

Albarram, A. (2018) "Are the design codes safe for the composite floor system?", *Three Minute Thesis Competition at the University of East London*, (Finalist Stage).